Defining the anti-cancer role and elucidating the mechanism behind the selective anti-cancer ability of the plant derived flavonoid eriodictyol

THESIS SUBMITTED FOR THE DEGREE OF

DOCTOR OF PHILOSOPHY

IN

SCIENCE

BY

SHIBJYOTI DEBNATH

INDEX No.: 03/16/Life. Sc./24

DEPARTMENT OF LIFE SCIENCE AND BIOTECHNOLOGY

JADAVPUR UNIVERSITY

2022

Dedicated to

My family

CERTIFICATE FROM THE SUPERVISOR

This is to certify that the thesis entitled "**Defining the anti-cancer role and elucidating the mechanism behind the selective anti-cancer ability of the plant derived flavonoid eriodictyol**" submitted by Sri Shibjyoti Debnath who got his name registered on 13/01/2016 for the reward of Ph.D. (Science) degree of Jadavpur University, is absolutely based upon his own work under the supervision of **Prof. Kaushik Biswas** and that neither this thesis nor any part of it has been submitted for either any degree/diploma or any other academic award anywhere before.

Kaushik Biswas
.....

12-07-2022
.....

Kaushik Biswas, Ph.D
Professor
Div. of Molecular Medicine
Bose Institute
EN 80, Salt Lake, Sector V
Kolkata-700091, INDIA

(Signature of the Supervisor date with official seal)

ACKNOWLEDGEMENTS

"I don't need to know everything; I just need to know where to find it, when I need it."

This sums up the journey of my last 8 years of Ph.D. Although it has been a long struggle but definitely an exciting one. It gives me immense pleasure to acknowledge the people who were there through this journey.

I would like to start by acknowledging my supervisor Prof. Kaushik Biswas for his insightful suggestions and support throughout my Ph.D. study. I am thankful for his immense patience and motivation and providing me with all the resources for my research and his guidance during my research work and thesis writing.

I would like to thank my labmates Manjari di, Barun da, Avisek da, Pravat da, Dipanwita di, Tarun, Abhisek, Elora, Subha, Sounak, Sanchari & Aishwarya for making my stay at the lab full of memories.

We all need reliable people for this long journey and I am lucky to find my gems and friends for life during this ride. A thank you is a small word for you all for being there for me, Riya, Debarghya, Sudip and Guddi. I feel happy to share my tears and laughter with you all. Without you all this journey would have never been completed. Thank you all for listening and living with me during all the lows and highs and still loving me and being my friends.

A well-deserved thank you to my love Ananya for being there always for me and supporting me through thick and thin.

My heart-felt thanks to my didibhai and Bubai da for their unconditional support in my life.

This cannot end without thanking the two most important people in my life, Maa and Baba. This journey couldn't have started or ended without their support. This thesis equally belongs to them as much to me. Thank you both for believing in me and supporting me and always loving me and caring for me.

Shibjyoti Debnath

ABSTRACT

Index no.: 03/16/Life. Sc./24

Title: Defining the anti-cancer role and elucidating the mechanism behind the selective anti-cancer ability of the plant derived flavonoid eriodictyol.

Submitted by: Shibjyoti Debnath

Anti-inflammatory flavonoid Eriodictyol displays selective cytotoxicity towards cancer cells compared to normal cells. Investigation of this phenomenon at the molecular level revealed that Eriodictyol significantly upregulated TNFR1 expression in tumor cells (HeLa and SK-RC-45) while normal cells (HEK and NKE) displayed negligible TNFR1 expression irrespective of absence or presence of Eriodictyol. Detailed mechanistic study revealed that Eriodictyol induced apoptosis through expression of the pro-apoptotic components, namely TNFR1, FADD and TRADD in cancer cells. In addition, CRISPR/Cas9 mediated knockout of TNFR1 was also found to completely abrogate apoptosis in HeLa cells in response to Eriodictyol. Finally, *in vivo* data demonstrated that Eriodictyol impedes tumor growth, progression and metastasis in mice implanted with 4T1 breast cancer cells. Thus, our study has identified Eriodictyol as a compound with high selectivity index towards cancer cells through a novel anti-tumor mechanism and suggest that it can be further explored for its potential to be used in cancer therapeutics.

Submitted by: Shibjyoti Debnath

The thesis has been divided into three chapters -

Chapter 1 Screening and identification of anti-inflammatory polyphenols as potent anti-cancer agents-Identification of Eriodictyol as a selective cytotoxic agent.

Chapter Defining the anti-cancer role of Eriodictyol, and delineating the mechanism of its selective cytotoxicity.

Chapter 3 Assessment of the role of Eriodictyol in prevention of cancer progression and metastasis in *in vivo* syngeneic mice tumour model.

Therefore, my research work dissected *the detailed molecular mechanism behind the selective cytotoxicity of Eriodictyol towards cancer cell lines. We have shown how TNFR1 plays an important role in Eriodictyol mediated apoptosis selectively in cancer cells.*

Shibjyoti Debnath
12/7/2022

Kaushik Biswas 12/07/2022
Kaushik Biswas, Ph.D
Professor
Div. of Molecular Medicine
Bose Institute
EN 80, Salt Lake, Sector V
Kolkata-700091, INDIA

CONTENTS

Page No.

SYNOPSIS

Epidemiologic and clinical studies indicate a strong relationship between chronic inflammation and cancer. So, we wondered whether flavonoids by virtue of being anti-inflammatory could also be anti-cancer. This led us to screen a panel of flavonoids for anti-inflammatory activity in an *in vitro* environment. For this we selected 12 compounds from plant sources that belong to both flavonoids and non-flavonoid polyphenols. Individual compounds were studied to determine their anti-inflammatory potential using *in vitro* cell culture techniques utilizing PMA (Phorbol myristate acetate) treated THP-1 monocytic cell line induced with LPS (Lipopolysaccharide) to mimic inflammatory conditions in the presence or absence of the test substance, followed by assay for inflammatory mediators such as TNF-α, IL-6, MCP-1, and IL-8 at messenger RNA levels. We discovered that Eriodictyol has potent anti-inflammatory activity among these compounds. A detailed literature search revealed only a few studies on its possible selective anti-cancer activity exist, with even fewer data regarding its mechanism of anti-cancer activity. Therefore, we investigated the mechanism of its selective cytotoxicity. We found out that Eriodictyol exhibited significant selective cytotoxicity in a number of cancer cells as compared to normal cells, by restricting proliferation to the G2/M phase. Furthermore, when compared to untransformed WI-38 and NKE cell lines, Eriodictyol induced significant apoptosis in HeLa, MCF-7, and HCT-116 cell lines (human cancer cells), as well as 4T1 and CT-26 cell lines (mouse cancer cells). Furthermore, molecular analysis revealed that Eriodictyol induced apoptosis in HeLa cells by upregulating the expression of pro-apoptotic components of the Death Inducing Signaling Complex (DISC), namely TNFR1, FADD, and TRADD. Furthermore, TNFR1 knockout via CRISPR/Cas9 blocked Eriodictyol-dependent apoptosis in HeLa cells, confirming that Eriodictyol-mediated apoptosis is TNFR1-dependent. While normal cells (HEK and NKE) showed no visible TNFR1 expression or upregulated TNFR1 in response to Eriodictyol, tumor cells (HeLa) exhibited elevated TNFR1 expression and dramatically upregulated the same in response to Eriodictyol, explaining the possible underlying selectivity of Eriodictyol's anti-cancer activity. Finally, an *in vivo* tumor model in mice implanted with 4T1 breast cancer cells revealed that Eriodictyol inhibits tumor development, proliferation, and metastasis while having no adverse effects. Thus, our research has revealed Eriodictyol as a compound with a high selectivity for cancer cells, which could be explored further for possible applications in cancer therapies.

General Introduction

A. The origin of the term "cancer"

The ancient Greek doctor Hippocrates, known as the "Father of Medicine," is credited with coining the term cancer. He referred “Carcinos” and carcinoma to describe non-ulcer forming traumas and ulcer framing tumors, respectively. Celsus (28-50 BC) the Roman specialist later made an interpretation of the Greek expression into malignancy, the Latin word for “Crab”. Another Greek doctor, Galen (130-200 AD), utilized the word "Oncos” (Greek for swelling) to depict disease cells. While Hippocrates and Celsus' crab analogy is still used to portray threatening tumors, the expression of Galen is currently utilized by oncologists [1-3].

B. What exactly is cancer?

Cancer is a spectrum of disorders characterized by uncontrollable cell proliferation with the ability to infiltrate or spread to other parts of the body [4]. They frequently create a malignant cell mass or lump known as a neoplasm or tumor[5].

C. Stages of Tumor Progression

The progression from benign to malignant tumor involves multiple steps known as malignant progression[6].

- Cancers follows a stepwise fashion:
  - **Hyperplasia** – normal appearance but uncontrollable cell division
  - **Dysplasia** - Both the tumor cells and the tissue appear aberrant.
  - **Carcinoma *in situ*** - Carcinoma *in situ* (CIS) refers to a group of abnormal cells that can only be found in the location where they first formed in the body. These abnormal cells have the potential to develop into cancer and spread to nearby normal tissue.
  - **Malignant Cancer** - The tumor has started to infect surrounding or distant tissues.
- **Benign tumors** remain localized and do not invade other tissues.

D. Grades of Cancer

The grade of a malignancy reflects how aberrant the cancer cells and tissue appear under a microscope in comparison to healthy cells. Low grade tumors are cancer cells that resemble healthy cells and tissue in appearance and organization. These tumors are highly differentiated. Lower grade tumors are less aggressive and often have a better prognosis. The greater the grade

of cancer, the more aberrant the cells appear and arrange themselves. Cancer cells with higher grades are more aggressive. They are referred to be undifferentiated or weakly differentiated. Some cancers have their own grading system for tumors. Many others have a conventional grade scale of 1-4 [7].

- **Grade 1:** Tumor cells and tissue resemble healthy cells and tissue the most. These are known as well-differentiated tumors and are classified as low grade.
- **Grade 2:** The cells and tissue are somewhat aberrant and are referred to as moderately differentiated. These are tumors of moderate grade.
- **Grade 3:** Cancer cells and tissue appear to be exceedingly aberrant. Because they no longer have an architectural framework or pattern, these tumors are deemed poorly differentiated. Grade 3 tumors are classified as high grade.
- **Grade 4:** The cells in these undifferentiated tumors are the most aberrant. These are the most severe tumors, and they often grow and spread rapidly than lower grade tumors.

E. Types of cancer based on cell of origin

i. Carcinomas

Carcinomas begin in the epithelial tissues and spread to other tissues. These function as the body's skin on the outside [8].

Each type of epithelial cells, can grow into a different type of carcinoma.

Squamous cell carcinoma

Squamous cell carcinoma begins in the cells of the squamous epidermis.

Adenocarcinoma

Adenocarcinomas occur in adenomatous cells, which are glandular cells. Fluids are produced by glandular cells for moisture.

Transitional cell carcinoma

Transitional cells are cells that can stretch when an organ grows in size. They generate transitional epithelium, which is a type of tissue. The bladder lining is one example. Transitional cell carcinoma refers to cancers that arise in these cells.

Basal cell carcinoma

The deepest layer of skin cells is lined by basal cells. Basal cell carcinomas are cancers that begin in these cells.

ii. Sarcomas

Sarcomas develop in connective tissues, which are the body's supporting structures. Connective tissues include tissues that support organs like bone and cartilage. Sarcomas are far more uncommon than carcinomas. They are typically classified into two categories.:

- bone sarcomas (osteosarcoma)
- soft tissue sarcomas

Bone sarcomas

Bone cells give rise to bone sarcoma.

Soft tissue sarcomas

Soft tissue sarcomas develop from cartilage or muscle.

Cartilage

Chondrosarcoma is a type of cartilage cancer.

Muscle

Rhabdomyosarcoma and leiomyosarcoma are cancers of the muscle cells.

iii. Leukaemias

Leukaemia is a disease that causes the bone marrow to create an excessively large amount of white blood cells. Blood cells do not function correctly because they are not fully developed. In the blood, aberrant cells multiply. There are different types of leukaemia.

Lymphomas and myeloma

Lymphomas and myeloma are malignancies of the lymphatic system. The lymphatic network is a combination of tubes and glands throughout the body that filter biological fluids and fight illness.

Lymphomas

Lymphomas are cancerous tumors that grow from lymphatic system cells. Lymphoma can grow practically any place in the body since the lymphatic system runs throughout it. The aberrant cells start to amass in the lymph nodes and other organs like the bone marrow and spleen. They can later develop into tumors.

iv. Myeloma

It is a type of cancer that originates in the plasma cells. Plasma cells are produced in bone marrow.

Brain and spinal cord cancers

Glioma (brain tumor) caused by glial cells. Non-cancerous (benign) brain or spinal cord tumors grow relatively slowly. Others are malignant, with a predisposition to develop and spread.

F. Cause of cancer

Carcinogens, or substances that cause cancer, were identified through research in animals as well as epidemiological analyses of cancer rates in human communities (e.g., cigarette smokers have a greater incidence of lung cancer) [9, 10]. Based on the mechanism of cancer causation, all carcinogenic chemicals can be classed as genotoxic or nongenotoxic carcinogens. Genotoxic carcinogens are substances that interact with DNA to produce DNA damage or to generate covalent DNA adducts, resulting in mutations and genetic abnormalities. Nongenotoxic carcinogens, on the other hand, are substances that promote tumor growth by pathways other than direct DNA destruction.

Since, the process of carcinogenesis is extremely complex and multi-factorial, speaking of a single cause behind any cancer seems unduly simplistic. Cancer, on the other hand, has been linked to a range of causes in both animals and humans, including radiation and viruses [11].

i. Chemical Carcinogens

Cigarette smoke is a significant carcinogen. Cigarette smoke including nicotine, can contain components such as polycyclic aromatic hydrocarbons, aza-arenes, N-nitrosamines, aromatic amines, aldehydes, and other organic and inorganic chemicals generated by combustion, distillation, pyrolysis, and pyrosynthesis [12]. The majority of these are known carcinogens including nitrosamine, benzene, benzopyrenes, carbon monoxide, and heavy metals including lead, arsenic, mercury, aluminium, nickel, cadmium, and so on [13]. Pesticides, insecticides, herbicides, rodenticides, insect repellents, animal repellents, disinfectants, and other chemicals, such as DDT, BHC, Chlordane, Toxaphene, Aldrin, Malathion, Linden, and others, contain carcinogens [14].

Carcinogens are also found in food preservatives, artificial sweeteners, and food dyes [15]. For example, butylated hydoxytoluene, a food additive, has been linked to liver cancer, while aspartame, an artificial sweetener, has been linked to brain tumors. Similarly, exposure to other environmental carcinogens such as inorganic arsenic compound and vinyl chlorides, which are components of asbestos and PVC plastics, respectively, causes skin and lung cancer.

ii. Physical Carcinogens

X-ray, gamma-ray, particle radiation, EMF radiation, and UV radiation are also carcinogenic, operating by physically rupturing DNA [16]. The Chernobyl disaster's leukaemia and radiation-related mortality, as well as the prevalence of thyroid cancer, demonstrate the effects of physical carcinogens on human life [17].

iii. Oncovirus

Oncoviruses are cancer-causing viruses that can have a DNA or RNA genome. They account for a small percentage of all cancers and can be recognized by simple blood tests, prevented with immunization and treated with antiviral drugs [18]. The viruses are classified into two types: DNA tumor viruses and RNA tumor viruses. After infecting animal cells, RNA viruses or retroviruses create numerous DNA copies of their viral RNA and insert them into the host genome. Oncogenes contained in the integrated viral genome confer replicative capability to the host cell, altering it. The most common examples are the Human Papilloma Virus (HPV) which cause cervical cancer and the Epstein Barr virus causing Burkitt's lymphoma, a common disease in African countries [19].

Virus	Malignancy
Epstein Barr	Nasopharyngial carcinoma
Epstein Barr	Burkitt's lymphoma and testicular tumor
Hepatitis B Hepatitis C	Hepatocellular carcinoma
HIV	Non- Hodgkin's-lymphoma, Kaposi's sarcoma, ca cervix, ca anus
HPV (human papilloma virus)	Ca cervix and anal cancer
Human herpes virus 8 (HHV8)	Kaposi's sarcoma, multiple myeloma

Table 1. Different malignancies caused by viruses [20]

iv. Genetic Factors

Somatic mutations frequently alter the number and structure of genes and chromosomes in cancer cells. Translocations and inversions of chromosomes, as well as point mutations within genes, are common in cancer cells. These mutations result in altered gene expression resulting in mutant proteins with either a loss-of-function, and less frequently gain-of-function. The application of Karyotyping led to the breakthrough discovery of the Philadelphia chromosome (translocation of chromosome 22 to chromosome 9) in chronic myeloid leukaemia (CML) [21]

and similarly translocation of chromosome 8 to chromosome 14 in Burkitt's lymphoma [22], which were two of the few remarkable scientific triumphs over cancer that helped in the understanding of the genetic roots of the disease and also the lives of millions of individuals who could now be diagnosed with these cancers at early stages. Disorders such as familial Retinoblastoma (Rb), familial adenomatous polyposis (APC), multiple endocrine neoplasia, and breast carcinoma were linked to an increased risk in persons with a family history of such malignancy [23-25].

v. Oncogenes & Tumor-suppressor genes

Oncogenes are genes that promote tumor development by increasing their activity, whereas tumor suppressor genes are those that inhibit the activity of tumor-supporting genes. If the tumor suppressor gene BRCA 1 is mutated, people with a family history of breast-ovarian cancer syndrome are more likely to get breast cancer. In human cancers, oncogenes such as NRAS, KRAS, and MYC are frequently activated[20]. In almost 30% of all cancers, the Ras gene is mutated, whereby it becomes a constitutively active leading to uncontrolled proliferation and growth [26]. The tumor suppressor gene TP53 encodes the protein p53, which directly participates in DNA repair to prevent oncogenesis or trigger apoptosis [27]. Nearly half of all human malignancies have a loss of function mutation in the p53 gene [28], earning it the title "guardian of the genome."

G. Hallmarks of cancer

The development of all kinds of human cancer is governed by a common set of rules. These properties contribute to the transformation of normal cells into cancer cells. The eight cancer hallmarks tumorthat define the carcinogenesis (Fig. 1) are [29] :

- Sustaining proliferative signaling
- Resisting cell death
- Evading growth suppressors
- Inducing angiogenesis
- Enabling replicative immortality
- Activating invasion and metastasis (Fig. 2)
- Avoiding immune destruction
- Deregulating cellular energetics

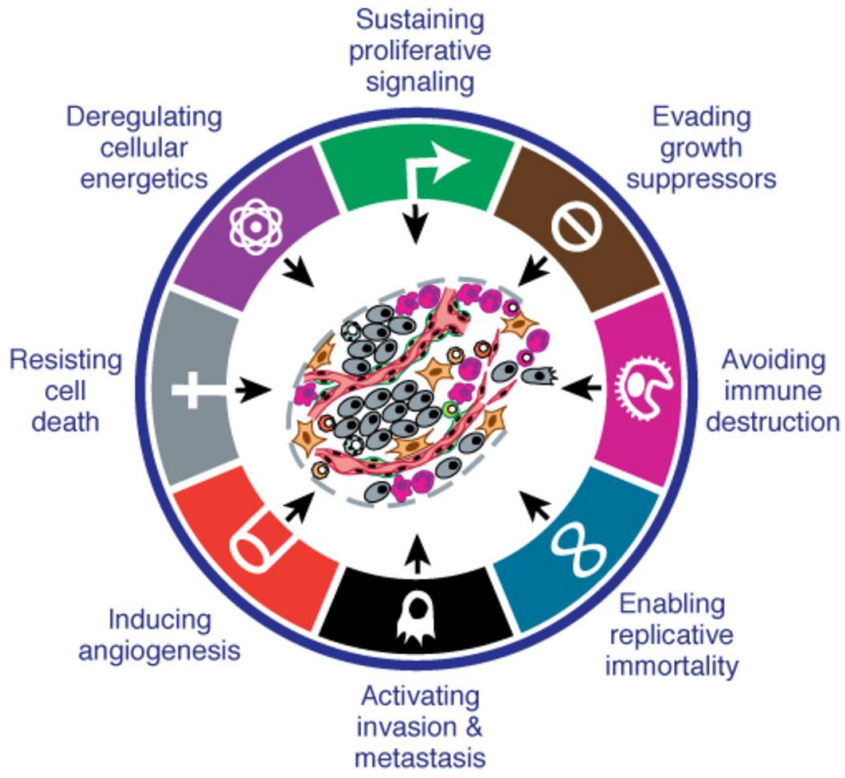

Figure 1 ***The eight hallmarks of cancer.*** Source **"Hallmarks of Cancer: The Next Generation"** (Cell: 2011)

1. Self-sufficiency in growth signals

Normal cells need mitotic signals to grow, and then they can transform from an inactive state to an active proliferative state. These signals are carried by transmembrane receptors that bind to signal molecules such as growth factors and extracellular matrix components. Many oncogenes that influence cell behavior imitate natural growth signals in some way. Intracellular tyrosine kinase domains that create MITOGENIC SIGNALS are commonly found in growth factors that attach to cell surface receptors [30]. Constitutive activation of signaling circuits is typically induced by activated growth factor receptors, according to somatic mutations identified in certain human cancers (such as mutant B-Raf melanoma)[30, 31].

2. Insensitivity to anti-growth signaling

Cancer cells overcome a powerful program that regulates cell proliferation in a negative way[32]. Most of these programs rely on the behavior of tumor suppressor genes[33]. Multi-term growth signals act within normal tissue to maintain tissue cell arrest and homeostasis. These signals include both availability of growth inhibitors and extracellular matrix as well as factors detected on nearby cell surfaces. Like their positively acting counterparts, these growth-suppressing signals are generated by receptors on the transmembrane cell surface that are

bound to intracellular signal circuits. A variety of strategies were used by cancer cells to develop resistance to cell apoptosis. The tumor suppressor gene p53 is clearly associated with the most common loss of proapoptotic regulators caused by mutations. Functional deactivation of the p53 protein, which has been observed in more than half of all human cancers, destroys DNA damage sensor that can activate the apoptosis cascade [34].

3. Evading and resisting cell death

The apoptosis mechanism is present in the body in nearly all kinds of cells and acts as a counter-operative strategy against uncontrolled cell proliferation. The detection and identification of Bcl-2's antiapoptotic behavior paved the way towards understanding regulation of apoptosis, the upstream regulators and downstream effectors. The regulation can be divided into two main pathways, one being extrinsic, which receives and processes extracellular signals, and another intrinsic pathway, which detects signal-inducing internal death and engages effectors, such as the Cysteine Aspartyl Proteases (Caspases) that facilitate death[35]. The extrinsic pathway activates effector caspase 8 while caspase 9 is activated by the intrinsic pathway. Consequently, the caspases trigger cell death by inducing proteolysis, disassembling cellular organelles, assembling them into membrane bound apoptotic bodies, and subsequent removal by adjacent phagocytic cells. The Bcl-2 protein family contains both pro- and anti-apoptotic proteins that act as apoptotic triggers, sending signals of cell death or survival. Bcl-2 and its family members (Bcl-xL, Bcl-w, and Mcl-1) control apoptosis by binding to and inhibiting the pro-apoptotic Bax and Bak proteins. Once activated Bax and Bak oligomerize and form pores in the mitochondrial membrane, resulting in the release of cytochrome c, which activates the intrinsic apoptotic effector pathway [35]. While apoptosis may be activated by various signaling molecules, its activation by tumor suppressor p53 is by far the most notable. It was established that loss of function mutation of p53 is the most profound among several ways through which tumor cells evade apoptosis. Nearly one third of all tumors have tumor suppressor protein p53 mutation, down-regulation or other functional alterations. In addition, cancer cells gain similar capacity to evade death by up-regulating anti-apoptotic proteins, down-regulating proapoptotic proteins, or by increasing the signaling of survival molecules, or even by short-circuiting the signals inducing extrinsic death.

4. Enabling replicative immortality

Cancer cells must be able to replicate indefinitely in order to form macroscopic tumors. This ability contrasts sharply with the activity of most normal cell lines in the body, which can only go through a limited number of cell growth-and-division cycles in a succession. This is accomplished by preventing senescence and crisis leading to cell death. Telomeres covering the proximities of chromosomes are essential to the unlimited proliferation capability[36]. Telomeres, which are made up of distinct tandem hexanucleotide repeats, eventually shorten with every cell division in cultured non-immortalized cells, resulting in end-to-end chromosome fusions and dicentric chromosomes whose resolution contributes to karyotype scrambling. As a result, the lifetime of a cell's telomeric DNA determines how many generations of cells its progeny will pass through until telomeres are entirely damaged and lose their protective capabilities, triggering crisis entry [37]. Telomerase is an enzyme which is found to be frequently over-expressed in several cancers [38, 39], which adds TTAGGG repeats at the end of telomeres and prevent telomere shortening, thereby enabling cancer cells to gain replicative immortality.

5. Inducing angiogenesis

The cancer's "angiogenesis switch" is virtually always set to light up and continuously sprout new blood vessels, which aid in the expansion of the tumor. Vascular Endothelial Growth Factor-A (VEGF-A) and Thrombospondin-1 (TSP-1) are well-known angiogenesis inducers.[40]. VEGF, angiopoietin, and FGF signals are linked to a network of signal transduction pathways involving ligands for endothelial cell-expressed signaling receptors (e.g., Notch Robo and Eph-A / B). In general, blood vessels created within tumors are abnormal due to an imbalanced mixture of chronically activated angiogenesis and leaky vessels and inappropriate endothelial cell proliferation rates. Various bone marrow-derived cells contribute to tumor angiogenesis, including macrophages, mast cells and bone marrow ancestors. These cells penetrate the premalignant lesions and the tumors that have been made and gather at the edges of these lesions [41].

6. Reprogramming energy metabolism

Instead of converting glucose into CO_2, H_2O, and heat, cancer cells use a glycolytic pathway to break down glucose into cytoplasmic lactate from pyruvate(aerobic or Warburg effect) [42]. This is in contrast to normal cells where pyruvate is converted to CO_2 through oxidative

phosphorylation in the mitochondria. The lower energy output for this route is balanced to increase glucose uptake. In hypoxic conditions present in some tumors, this dependence on glycolysis can be further emphasized. The hypoxia response mechanism works in a variety of ways to increase the activity of glucose transporters and other enzymes in the glycolysis pathway. Because glycolysis is increasing, it can be diverted to a variety of biosynthetic pathways, including those that create nucleotide and amino acid intermediates. This really boosts the manufacture of polymers and organelles required for the formation of new cells. Cancer cells in hypoxia use glucose as fuel and excrete lactic acid as waste. It is preferentially utilized as an imported fuel (LACTATE SHUTTLE) [43].

7. Activating invasion and metastasis

Invasion and metastasis are closely related and are described as a capacity of cancer cells to escape from a tumor mass, enter circulation and colonize at a new location where space and nutrients are not initially restricted [44] as described in Fig. 2. Tumor cells with metastatic capabilities display improvements in cell adhesion molecules from a variety of cells. N-cadherin is upregulated while E-cadherin is downregulated during EMT in cancers and this "cadherin switch" is associated with enhanced migratory and invasive traits, which caused inferior patient survival rate [45, 46]. E-cadherin junctions form the stable adherens junction and enable strong cell–cell contact. As p120 catenin and β-catenin are strongly bound to the E-cadherin complex, they are not available to activate Wnt/β-catenin pathway and P13K pathway [47]. N-cadherin junction enables the stabilization of fibroblast growth factor receptor (FGFR) which leads to activation of MAPK/ERK pathway and activates the PI3K pathway in association with PDGFR to enhance cell survival and migration [48]. E-Cadherin, the cell-to -cell adhesion molecule of epithelial cells, is extensively down-regulated after carcinoma transformation and inhibits the transmission of anti-growth signaling circuits, such as the transcription factors Lef / Tcf [49]. Within invasive carcinoma the cell adhesion molecules associated with embryonic and inflammatory processes such as N-cadherin and vimentins are upregulated. All of these changes are a typical hallmark of cancer cells undergoing invasion-metastasis cascade that starts with local invasion, intravasation into nearby circulatory vessels, movement through vessels followed by escape from the lumina of these vessels, forming a small nodule of cancer cells and subsequent growth into macroscopic tumor known as colonization. Available research suggests the activation of a developmental regulatory system in cancer cells called the epithelial-mesenchymal transition (EMT) imparts metastatic

capability. EMT is regulated by a collection of pleiotropically active transcription factors known

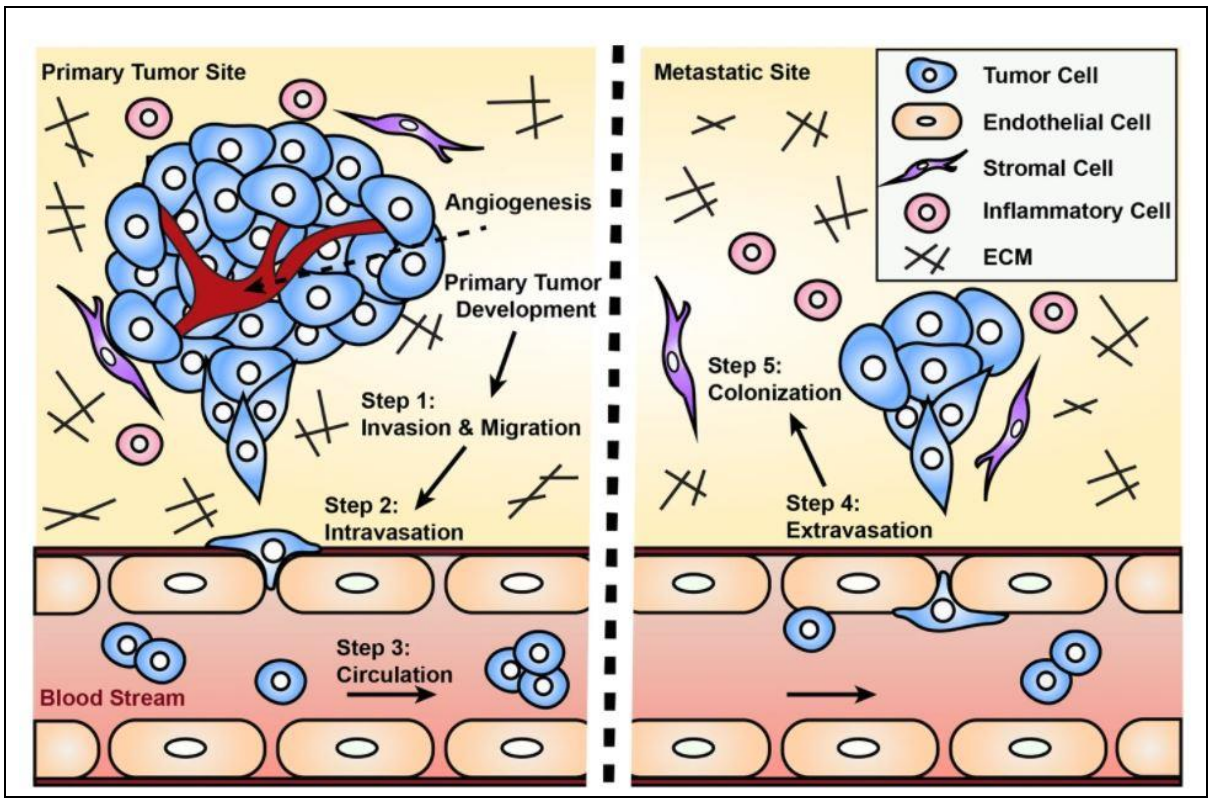

Figure 2 ***Metastatic Cascade.*** A schematic illustrating the key processes in metastasis. Step 1: Cancer cells infiltrate the basement membrane and spread throughout the tumor stroma; Step 2: intravasation in vasculature; Step 3: Tumor cells infiltrate the body by adhering to blood arteries near secondary locations; step 4: endothelial barrier extravasation; and step 5: colonization in a remote desired organ. Reproduced from Precision oncology "**Engineered models to parse apart the metastatic cascade**"

as Snail, Slug, Twist, and Zeb1/2, which are shown to be involved in growth processes. Some of these transcription factors are responsible for the loss of adhesion junctions, conversion from epithelial to mesenchymal morphology in neoplastic cells, the production and secretion of extracellular matrix degrading enzymes and the effect of apoptosis resistance [50]. In addition, the neoplastic stromal cells contribute by imparting invasive and metastatic capabilities to the tumorigenesis process in a heterotypic manner. For example, mesenchymal stromal cells secrete molecules of CCL5/RANTs in response to signals obtained from cancer cells which thus stimulate such cells' invasive actions. In addition, neighboring macrophages secrete matrix metalloproteases and cysteine cathepsin proteases which facilitate tumor cell invasion. These macrophages associated with tumors are often stimulated by cytokines released by cancer cells and in return provide certain growth factors that support intravasation and metastatic spread of cancer cells [51]. The final step of the metastatic process, that is colonization, is extremely

complex and is yet not clearly understood. Since, the EMT process is initiated by cancer cells in the primary tumor at a time much earlier than its dissemination, at least initially, it is most poorly adapted to the tissue microenvironment on which it landed. Accordingly, the cells develop new ways to thrive on the foreign tissue microenvironment immediately and effectively. Alternatively, their ability to colonize in the distant tissue as macroscopic tumors can take place in cells during initial primary tumor development prior to dissemination. As a result, the ability to colonize at a given spot may be developed as a result of selection pressure on disseminated cells to adapt to the milieu of alien tissues. Recent work indicates that the EMT program induced in cells during propagation could be responsible for attributing colonizing characteristics and self-sustaining abilities at the colonization site for clonal expansion [52].

8. Tumor promoting inflammation

Tumor-associated inflammatory response has the unexpected and paradoxical consequence of boosting tumorigenesis and growth, allowing early-stage neoplasms to develop hallmark capabilities [53]. Inflammation is caused by the introduction of biologically active molecules into the tumor microenvironment, such as growth variables that determine proliferation signals, survival factors that limit tissue damage, angiogenesis promoting factors, and extracellular matrix-modifying enzyme-inducing signals that foster neovascularization, invasion, and metastasis [54]. It may contribute to a number of characteristics that lead to the activation of programs that promote EMT and other characteristics. Importantly, inflammation can obviously encourage full-fledged cancer growth in early neoplasms and is visible in some cases at the early phases of tumor evolution. Furthermore, inflammatory cells that emit actively mutagenic chemicals against surrounding cancer cells, particularly reactive oxygen species, accelerate their genetic evolution and elevate them to a malignant state.

Moreover, chronic inflammatory mediators have pleiotropic effects on cancer development. On the one hand, chronic inflammation promotes carcinogenesis, malignant transformation, tumor development, invasion, and metastatic dissemination; on the other hand, chronic inflammation can also activate immune effector pathways, which may inhibit tumor growth [55]. Cancer and inflammation are linked through intrinsic and extrinsic mechanisms. Both routes lead to the activation of transcription factors including NF-kB, STAT-3, and HIF-1α, as well as the accumulation of tumorigenic factors in the tumor and microenvironment [56] . STAT-3 and NF-kB interact on various levels, promoting tumor-associated inflammation and suppressing anti-tumor immune responses. These elements also contribute to tumor

development, progression, and metastatic dissemination [57]. By influencing the production of tumor-promoting factors, IL-1b, IL-6, TNF-α, and PGHS-2 operate as essential mediators of an inflammatory environment [58]. As a result, inflammation aids cancer cells in acquiring the core properties of cancer hallmarks (Fig.3) [59].

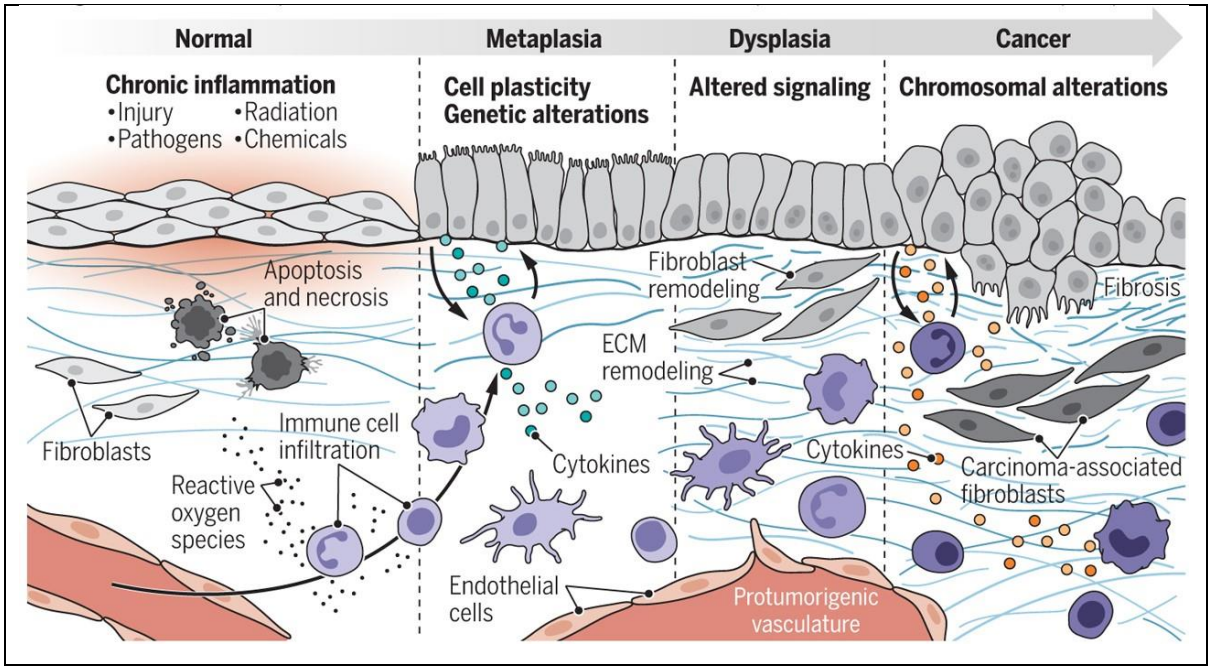

Figure 3 ***Chronic inflammation–associated cancer pathogenesis.*** Chronic inflammation–associated cancers (CIACs) progress through three stages of pathogenic evolution: metaplasia, dysplasia, and malignancy. Several changes occur in the tissue milieu during this period, including alterations in stromal cells (immune system, endothelium, and fibroblasts) and the matrix proteins (ECM). Source: Science perspective **"Stromal directives can control cancer"**

H. Inflammation linked cancer

1. Evidence from epidemiology and clinical studies

Clinical and epidemiological studies strongly suggested a possible correlation between inflammation and cancer [59]. Colorectal cancer was found to be substantially more likely when paired with inflammatory bowel illnesses such as ulcerative colitis [60] and Crohn's disease [61]. Furthermore, helicobacter pylori infection in the gastrointestinal system led to lymphoma. adenocarcinoma and mucosal-related lymphoma in the lymphoid tissue [62].

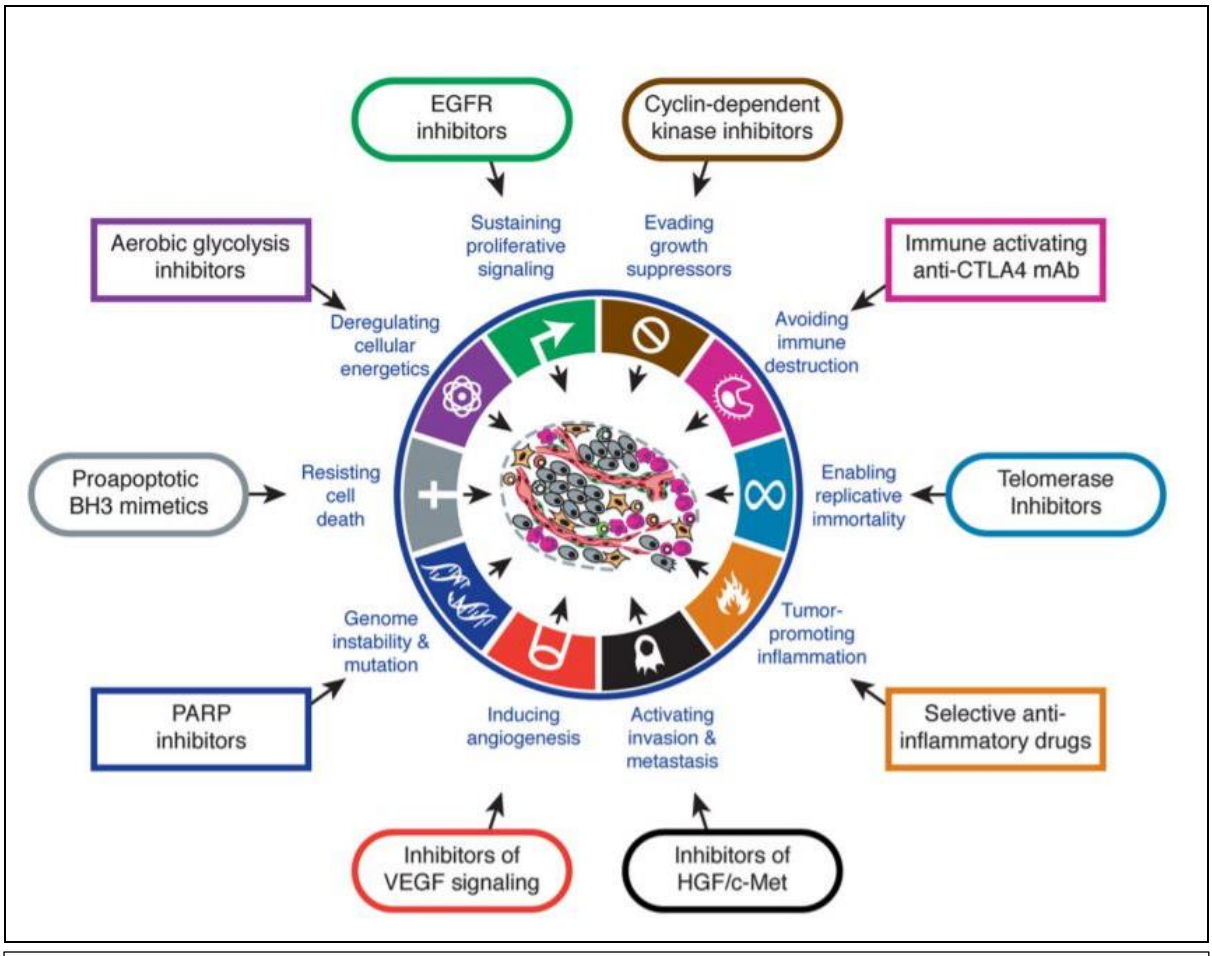

Figure 4 ***Therapeutic targeting of the hallmarks of cancer.*** Agents that inhibit each of the acquired characteristics required for tumorigenesis have been developed and are now in clinical studies or, in some cases, approved for use in the treatment of certain types of human cancer. Source **"Hallmarks of Cancer: The Next Generation" (Cell: 2011)**

Chronic hepatitis B and C infection increased the risk of developing hepatocellular carcinoma on another occasion [63]. Chronic inflammation/non-infectious agent could lead to cancer as well [64]. For example, there were evidences of strong associations between ulcer Marjolin's and carcinoma of the skin [65], asbestos and mesothelioma [66], silica, smoke cigarettes and bronchial cancer, chronic asthma/lung [67], sarcoidosis and lung cancer [68], ulcerated lichen planes and verrucous carcinomas [69]. The relationship between systemic inflammation and development of the tumor is thus supported by extensive evidences.

2. Mechanisms for the association between inflammation and cancer

It is well established that the presence of some chemokines, cytokines, and myeloid cell subsets in CRC was associated with a poor prognosis [70]. Furthermore, pre-clinical animal models using genetic engineering methods showed that inhibiting the inflammatory response prevented the growth and progression of tumors [71] depicted in Fig. 5. Tumor Elicited Inflammation

(TEI) is a process in which malignant cancer cells recruit immune cells to secrete inflammatory mediators for tumor growth and to modulate the microenvironment according to their needs [72]. The initial inflammatory stimulation in tumors that are not connected with mucosal interfaces may be sensing oncogenic transformation, apoptosis or oxygen deficiency [73].

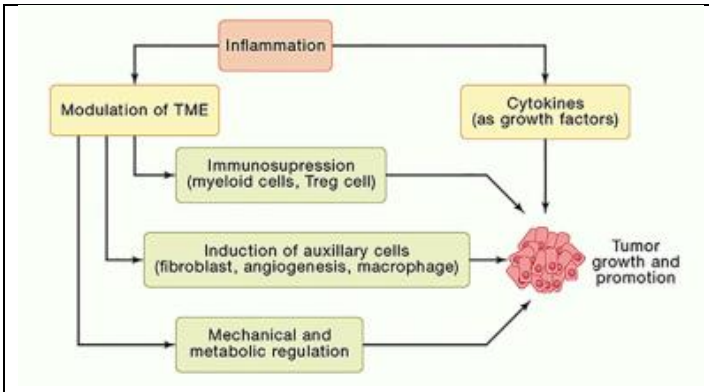

Figure 5 ***How Stroma Control Cancer*** Inflammatory ingredients generated by immune cells inside the TME, such as cytokines and growth factors, could affect pre-malignant and cancer cells. Source: Science perspective **"Stromal directives can control cancer"**

3. Cytokines and chemokines in cancer-related inflammation

TNF was found in small amounts in many malignant cells on a regular basis. Animal models showed that TNF-derived from malignant cells promoted the development and spread of syngeneic, xenogeneic, and cancerous tumors in the skin, ovary, pancreas, pleural cavity, and bowel [74]. TNF could play a direct role in oncogene activation, DNA damage, and EMT stimulation. This might explain, at least in part, TNF's ability to improve tumor cell metastatic activity, which was first observed in the 1990s and elucidated by Michael Karin's group in 2009. Many human tumors, both in malignant cells and other microenvironmental cells, contain TNF protein and are found in high plasma concentrations of advanced cancer patients [75]. In Stage 1 lung cancer, TNF expression was found to be a major contributor to an 11-gene signature of low prognosis [76].

IL-6 signalling imbalance causes a variety of inflammatory diseases [77]. In various cancer models, oncogenic Ras-mediated IL-6 enhanced tumor growth in both malignant and stromal cells, and linked to clinical malignancies, including multiple myeloma and hepatocellular carcinoma [78]. IL-6 acted as an autocrine or paracrine growth factor in certain malignancies, particularly those of hematologic origin; it inhibited apoptosis and signals via STAT3, which was activated in many malignancies via STAT3 [79]. In the tumor microenvironment, IL-6 activated genes that promote cell proliferation and angiogenesis [80].

IL-1 developed IL-17-producing CD+ T cells [81]. The IL-23/IL-17 axis was shown to facilitate skin carcinogenesis [82]. IL-1 plays a role in human cancer, particularly multiple

myeloma [83]. This axis was disrupted by proteasome inhibitors and thalidomide and lenalidomide causing cytokine inhibitors. Myeloma cells produce IL-1, which activates stromal cell production in the bone marrow, and in the process, this cytokine acts as a growth factor for myeloma cells.

Tumor-associated macrophages (TAMs) are the primary cells that produce cytokines, chemokines, growth factors, and stimulate the release of inhibitory immunological checkpoint proteins in T cells to generate an immunosuppressive tumor microenvironment (TME) [51, 84]. Tumor-associated macrophages (TAMs) are one of the most common forms of tumor-infiltrating immune cells and are divided into two functionally distinct subtypes: classically activated M1 macrophages and alternatively activated M2 macrophages [84]. The former typically performs anti-tumor functions such as directly mediating cytotoxicity and antibody-dependent cell-mediated cytotoxicity (ADCC) to kill tumor cells, whereas the latter can promote tumor cell occurrence and metastasis, inhibit T cell-mediated anti-tumor immune response, promote tumor angiogenesis, and lead to tumor progression [85, 86]. Because M1 and M2 macrophages are highly flexible, they can be changed into each other in response to changes in the tumor microenvironment or therapeutic treatments [87, 88]. TAM recruitment in tumors was long related to CCL2 (MCP-1) [83]. TAM survival and polarization of M2 macrophages are also aided by CC chemokines. CCL2 and its cognate receptor CCR2 were studied in prostate cancer mouse tumors in particular where data suggest that bone marrow endothelial cells are a major source of CCL2, and that an elevated secretion of CCL2 recruits prostate cancer epithelial cells to the bone microenvironment and regulates their proliferation rate [89, 90]. Hypoxia may trigger a form of cell death that leads to immune rejection of the tumor; CCL28 induction is a way to mitigate this by attracting immune suppressive and angiogenic T regulatory cells [89].

4. Other key players in inflammation

i. NF-kB

NF-kB is a crucial mediator of inflammatory development and controls the expression of a wide range of inflammatory molecules, such as cytokines and adhesion factors. As a major regulator, NF-kB is tightly controlled by multiple proteins, like the A20 zinc finger protein [91]. NF-kB activation plays a role in a variety of inflammatory diseases [92]. In both enterocytes and a mouse model of Crohn's disease, suppression of NF-kB reduced the inflammatory response. In intraepidermal inflammation, NF-kB induced neutrophil chemotaxis

[93]. Apoptosis and phagocytosis of inflammatory cells were also linked to NF-kB regulation [94]. These findings indicate that chronic inflammation is critically influenced by NF-kB.

ii. Inducible nitric oxide synthase (iNOS)

Overexpression of iNOS, an enzyme that catalyzes the formation of NO, was discovered in chronic inflammatory diseases and cancers of different forms [95]. A specific NOS inhibitor was revealed in a recent animal model study to halt the advancement of carcinogenic N-nitrosomethylbenzylamine-induced rat esophageal carcinogenesis [96]. NO is a crucial regulator of the inflammatory response as well as the progression of cancer. Because proinflammatory cytokines such as TNF-α and IL-1β, as well as NF-kB transactivation, activate iNOS, it might well be the link between inflammation and cancer [97]. Continuous NO synthesis during chronic inflammation can cause DNA damage [98]. Increased NO production can activate p53, however p53 mutations can cause cancer. NO may be involved in angiogenesis, leukocyte binding and infiltration, and metastasis [99].

iii. Cyclooxygenase-2 (COX-2)

Inflammatory cytokines such as IL-1α and TNF-α, and growth modulators such as EGF activate COX-2 [100]. Prostaglandins are the key inflammatory mediators generated by the COX-2 enzyme [101]. Prolonged use of nonsteroidal anti-inflammatory medications (NSAIDs) was related to a lower risk of a range of malignancies, since NSAIDs reduce COX-2 activity [102, 103]. Overexpressed COX-2 plays a role in cell proliferation, antiapoptotic intervention, angiogenesis, and metastasis formation [104, 105]. Cigarette smoke promotes the COX-2 pathway in human lung fibroblasts, suggesting a plausible explanation for smoking-induced inflammatory lung disorders [106].

iv. Hypoxia-inducible factor 1-alpha (HIF-1α)

Hypoxia in the inflammatory lesions is a normal occurrence due to metabolic changes during inflammation [107]. In addition, **HIF-1α** increases transcription of the VEGF, a powerful angiogenic factor promoting tumor growth and metastasis, as HIF-1 **α** is critical for tumor growth and metastases [108]. HIF-1**α** could contribute to the development of chronic inflammation that is susceptible to cancer [109]. It can activate pro-inflammatory cytokines (IL-1β, TNF-α, IL-6) in the microenvironment that can be controlled via NF-kB activation or

COX-2 induction [110]. HIF-1, however, can work as a promoter, speeding up the growth of inflammatory-related cancers [111].

A pictorial depiction of how chronic inflammation leads to cancer is described in Fig. 6

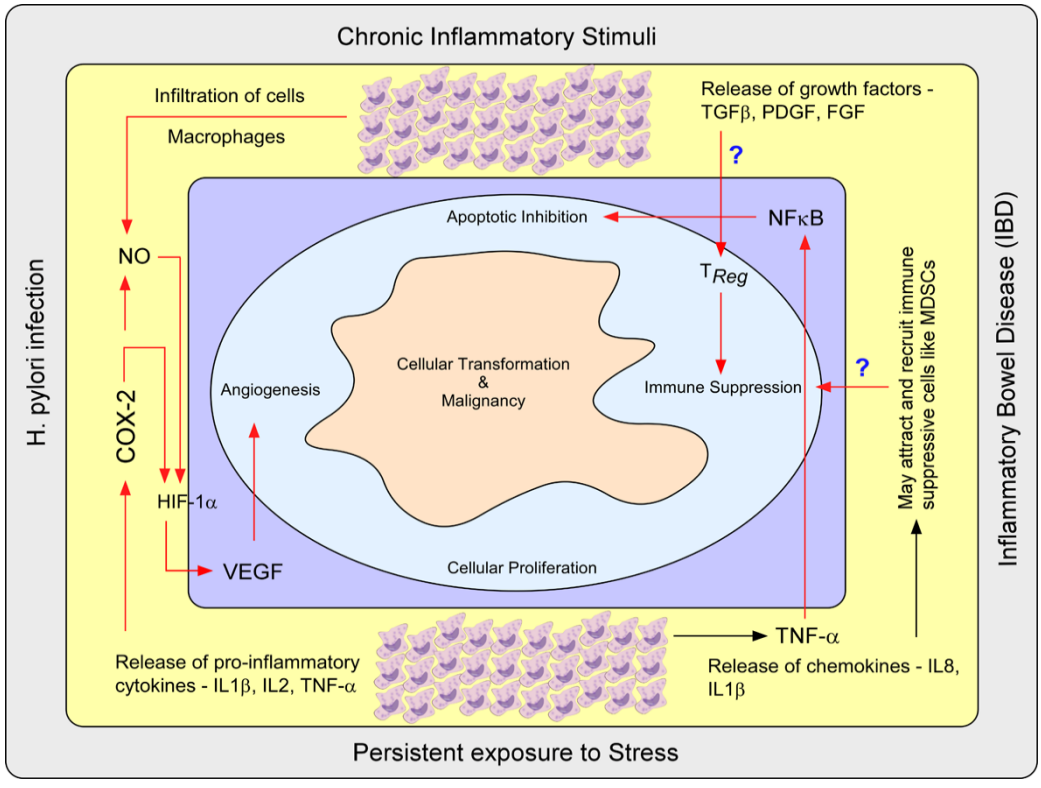

Figure 6 ***How chronic inflammation can lead to cancer.*** Chronic stress, H. pylori infection, and inflammatory bowel illness can all cause chronic inflammatory stimulation. Inflammatory signals can structure the Tumor Microenvironment to improve the infiltration, cellular proliferation, and particular functional areas of pro-tumorigenic cells within the TM.

I. Role of apoptosis in cancer: pathogenesis

Cell death has long been regarded to be a mechanism that needs to be by-passed for development of cancer. Although apoptosis suppression can cause cancer, cancerous cells are not always resistant to apoptosis [112]. Some forms of human tumors, in fact, are more prone to apoptosis than their normal tissue equivalents [113]. Contrary to popular belief, upregulation of apoptosis in cancerous tissue were linked to a higher death risk in some cancer types [114-116]. Finally, large levels of anti-apoptotic protein Bcl-2 was linked to a prognostic indicator in some cancers [113, 117]. Often it has been seen that apoptosis drives the cancer cells to look for new land suitable for their inhabitation. The difference between a malignant and a benign tumour is that the latter is

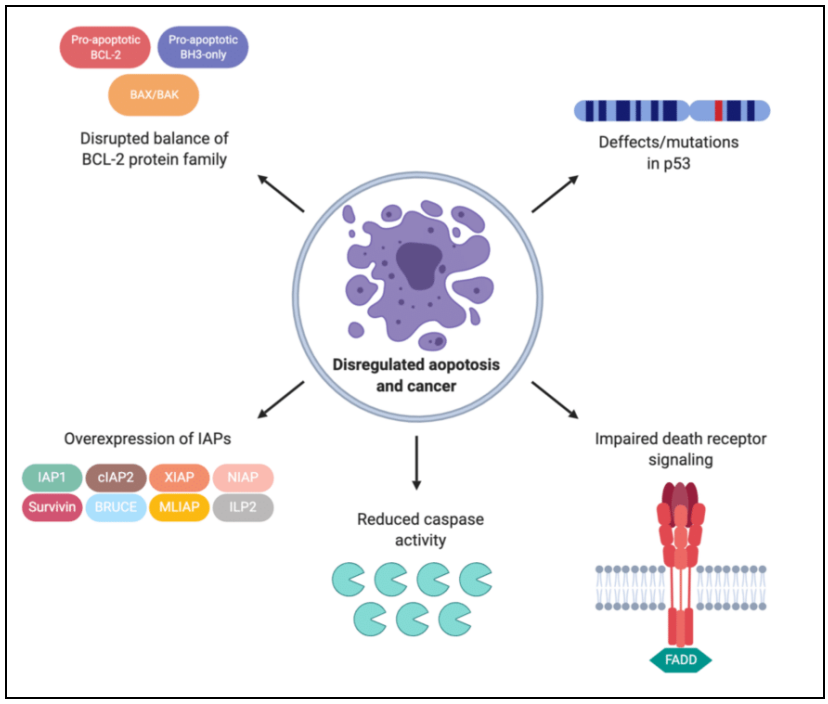

Figure 7 ***Mechanisms involved in apoptosis evasion and carcinogenesis.*** Different pathways of dysregulated apoptosis that leads to cancer.

better organized, has lower apoptosis and thus, does not have the drive to move. So, cancer cells are forced to leave that site of origin and move to better favorable condition (metastasis) [118].

Understanding the apoptosis process is crucial since it helps in the understanding of the consequences if, and when the apoptotic process gets disrupted. This, in particular, can help in the creation of drugs that target specific apoptotic markers or pathways. Caspases play an important role in the apoptosis process since they operate both as initiators and executors [119]. The intrinsic (or mitochondrial) and extrinsic (or death) routes of apoptosis are the two primary pathways (Figure 9). Both pathways eventually lead to a specific apoptosis route or action.

i. The extrinsic death receptor pathway

When death agonists attach to a death receptor, the extrinsic death receptor pathway is activated. While there are additional death receptors, the type 1 TNF receptor (TNFR1) and a related protein known as Fas (CD95) appear to be the most well-known, and its agonists are known as TNF and Fas ligands (FasL). TNF receptor-associated death domain (TRADD) and Fas-associated death domain (FADD) adaptor proteins, as well as cysteine proteases like caspase 8, are recruited to these death receptors' intracellular death domains. Then DISC and

pro-caspase 8 are activated. Caspase 8 is an apoptosis-inducing caspase that cleaves executioner caspases [120].

ii. The intrinsic pathway

As the term suggests, the intrinsic route begins within the cell. Internal drivers of mitochondrial pathway activation include irrevocable genetic damage and substantial oxidative stress [121]. Elevated mitochondrial permeability of pro-apoptotic chemicals such as cytochrome-c expelled into the cytoplasm induces this system to develop. This route is regulated by the Bcl-2 protein family, named after the BCL2 gene, which was discovered at the chromosomal breakpoint of the chromosome 18 to 14 translocation to non-Hodgkin follicular lymphoma. Pro-apoptotic proteins (e.g., Bax, Bak, Bad) and anti-apoptotic proteins (e.g., Bcl-Xs, Bid, Bik, Bim) are the two principal Bcl-2 protein groups (e.g., Bcl-2, Bcl-XL and Mcl-1). Apoptotic factors secreted into the cytoplasm include apoptosis inducing factor (AIF), Smac, IAP binding protein (DIABLO), and protein A (HtrA2). Caspase 3 is activated by cytoplasmic cytochrome c causing release of an apoptosome complex consisting of cytochrome c, Apaf-1, and caspase 9. By interacting to apoptosis protein inhibitors (IAPs) and disrupting their caspase-3 or -9 link, Smac/DIABLO or Omi/HtrA2 increases caspase activation [122].

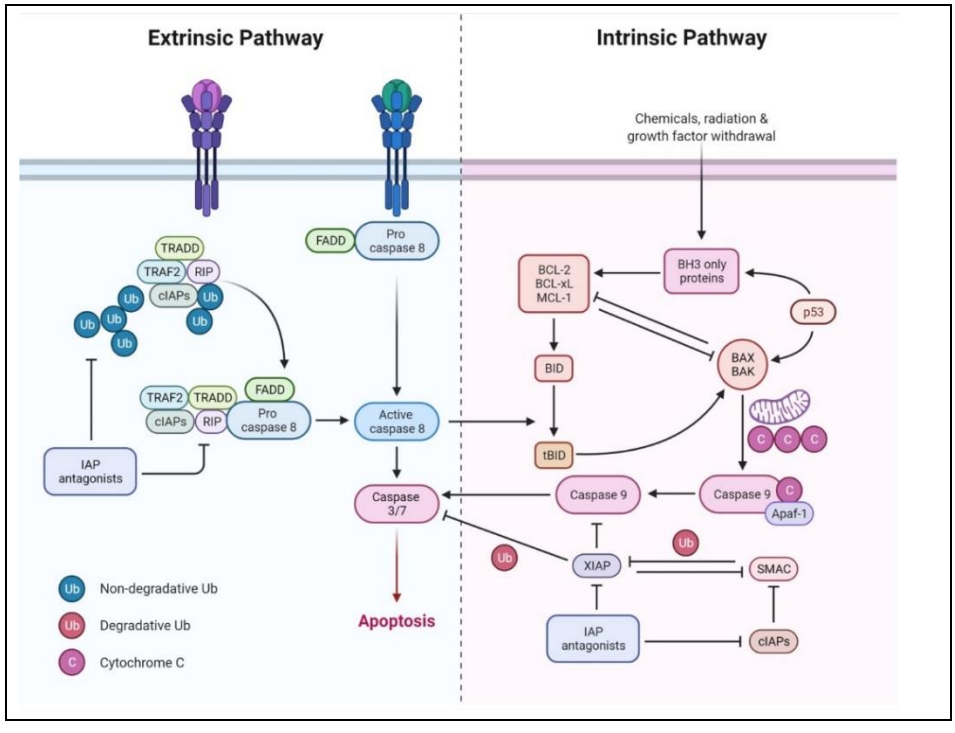

Figure 8 ***Extrinsic and Intrinsic pathway of apoptosis.*** TRAIL receptor (TRAILR) and FAS can activate induce caspases (caspase-8 and caspase-10) via oligomerization by adaptor proteins such as FAS-associated death domain protein in the extrinsic apoptotic pathway (FADD). When functional caspases-8 and -10 cleave and activate effector caspases-3 and -7, apoptosis occurs. The permeability of the mitochondrial outer membrane is required for the intrinsic (or mitochondrial) mechanism of apoptosis (MOMP). Anti-apoptotic BCL-2 family of proteins counteract this. MOMP, proteins from the mitochondrial intermembranous area, cytochrome c, are discharged into the cytosol. Cytochrome c reacts to apoptotic protease activating factor 1 (APAF1), causing apoptosomes to form and caspase-9 to be activated. Caspase-9 activation causes caspase-3 and caspase-7 engagement, resulting in apoptosis. SMAC release from mitochondria induces apoptosis by blocking the XIAP. Caspase-8 degrades the BH3-only protein BH3-interacting death module activator (BID), enabling the

J. Targeting apoptosis in cancer therapy

The plethora of literature indicates that apoptotic abnormalities demonstrate a role in carcinogenesis and several innovative apoptosis-targeting therapeutic techniques can be adopted. In a number of combination therapies with conventional antibody drugs, several of these new agents or therapeutic techniques have also been developed to improve widely available treatment methods [123].

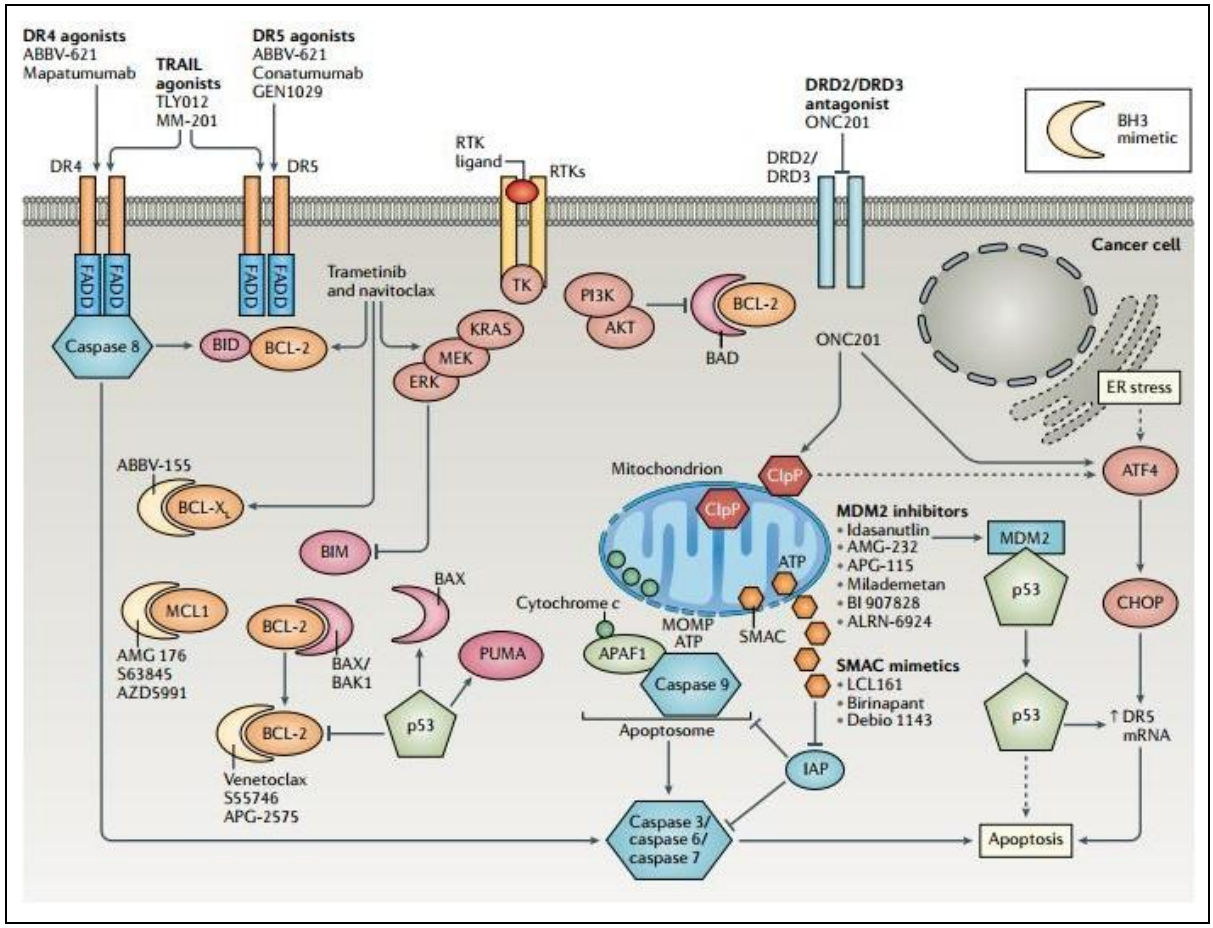

Figure 9 ***Therapeutic approaches targeting apoptosis pathways in cancer cells.*** BCL-2 proteins that inhibit apoptosis interact with BH3 mimics, activating BAX and BAK1. BCL-2, BCL-XL, and MCL1 inhibitor clinical trials have commenced. Antagonist antibodies, soluble ligands, recombinant TRAIL-IgG1 fusion proteins, and pegylated recombinant TRAIL can all activate death receptor 4 (DR4) and DR5. Because altering oncogenic signalling pathways increases apoptosis, treatment studies with combinations of MEK inhibitors and the dual BCL-2–BCL-XL inhibitor navitoclax are being done. Pro-survival pathways including AKT and MEK phosphorylate pro-apoptotic proteins like BAD and BIM, which prevents apoptosis. ONC201 is a medicine that activates ATF4 and induces DR5 overexpression and cell death via binding to the dopamine receptors DRD2 and DRD3, as well as the mitochondrial caseinolytic protease P (ClpP). SMAC analogues and IAP protein inhibitors are now being tested in clinical trials. Reproduced from **"Targeting apoptosis in cancer"** published in nature reviews (2020)

Yet, numerous confusing and troubling aspects remain unsolved, such as how conventional therapeutic options develop tumor resistance and if they should cause a high number of healthy cells to perish. If typical anticancer treatments were utilised, they would burn out both normal and cancer cells, resulting in horrific side effects and tumor resilience. However, if apoptosis-targeting medicines do work on a specific pathway or protein, it will be clinically useful. The majority of clinical trial drugs target numerous targets, including Bcl protein family inhibitors and pan-IAP inhibitors. Current research will focus on therapies that can elicit apoptosis preferentially in particular malignant cells [124, 125].

K. Anti-inflammatory activities of flavonoids: implications in cancer therapy

Flavonoids are a class of natural compounds with various phenolic structures. Fruits, vegetables, cereals, flowers, tea, bark, roots, and stems all contain flavonoids. These natural compounds have well-documented health benefits in humans. Flavonoids have a wide range of medical, pharmacological, and cosmetic uses due to their anti-oxidative, anti-inflammatory, anti-mutagenic, anti-carcinogenic, and cellular enzyme regulating properties. The chronic inflammatory process causes or worsens a significant number of non-infectious disorders. Most inflammatory processes underlying chronic illnesses, such as carcinogenesis, are said to be combated by flavonoids [126-128].

Flavonoids have chemo-preventive benefits in a preclinical model by preventing cancer growth, decreasing CSC formation, and relieving lung metastasis [129]. Hydroxysafflor yellow A reduces cancer metastasis by modulating the PI3K/AKT, MAPK/ERK, and STAT3 pathways—all of which are important CSC-associated inflammatory signaling cascades [130]. In another study, natural flavonoid Apigenin in combination with epigallocatechin-3-gallate drastically reduced the pro-inflammatory cytokines COX-2, iNOS, and TNF-α, as well as the

pro-angiogenic factors VEGF and eNOS, and caused apoptosis by boosting the Bax/Bcl-2 ratio *in vitro* [131, 132]. Another study discovered that Icaritin has anti-metastatic properties via lowering CXCR4 expression, which can help to prevent cancer progression [133]. Furthermore, Luteolin inhibit EMT and metastasis by targeting the integrin-modulated ILK/YAP pathway [134, 135]. Kaempferol and Naringenin inhibit angiogenesis and metastasis by inhibiting VEGF-induced oxidative stress and NF-kB signaling, as well as downregulating adhesion molecules including VCAM-1, ICAM-1, and E-selectin; these actions reduce the development of new blood capillaries in cancer tissue[136]. Finally, through the ERK/IL-6/STAT3 and Arg-1/iNOS/Nox2/NF-B/STAT3 signaling pathways, MDSC activation is implicated in chronic inflammation-related immunosuppression and CD4+/CD8+ T cell activation [137]. Silibinin inhibit MDSC-mediated immunosuppression, which is essential for cancer development and metastasis [138]. Quercetin also exert anti-inflammatory effects through regulating inhibition of pro-inflammatory immune cell COX-2, chemokines, transcription factors, and cytokines as well as PI3K/AKT and IKK/JNK inhibition [139, 140].

Isolated flavonoids in pre-clinical studies

Chronic inflammation predisposes cells to malignant transformation and promotes carcinogenesis at all stages. The anti-inflammatory and anti-cancer activities of flavonoids were studied in cancer research since the previous century. In DMBA-induced and TPA-promoted SENCAR mice (SENsitivity to CARcinogenesis) , GTPs (Green Tea polyphenols), silymarin, and apigenin reduced skin tumor promotion by lowering skin papilloma development. As previously noted, numerous signaling pathways, such as MAPK, AKT, mTOR, STAT3, and/or NF-kB, are connected with chronic inflammation and might potentially contribute to tumor promotion. As a result, research in the twenty-first century focus on the specific molecular processes and signaling pathways used by flavonoids to combat inflammation at distinct stages of carcinogenesis [141].

In BC3, BCBL1, and BC1 (primary effusion lymphoma cells infected by Kaposis's Sarcoma Herpes Virus), Quercetin suppressed the PI3K/AKT/mTOR, Wnt/β-Catenin, and STAT3 signaling pathways. Furthermore, Quercetin prevented tumor promotion by downregulating proinflammatory cytokines IL-6 and IL-10; pro-survival molecules downstream of PI3K/AKT/mTOR, Wnt/β-Catenin, and STAT3 such as c-FLIPL; and cell proliferation molecules such as cyclin D1 and cMyc [142]. Furthermore, Icaritin (Epimedium species) from a Chinese herbal medication suppressed proliferation and tumor development while inducing

apoptosis in K562 and primary chronic myeloid leukemia cells. In a mouse model, Icaritin affected chronic inflammatory signaling pathways such as MAPK/ERK/JNK and JAK2/STAT3/AKT by upregulating p-JNK and p-C-JUN and downregulating p-ERK, p-P38, JAK-2, p-JNK, p-STAT3, and p-AKT in a dose- and time-dependent manner [143]. Furthermore, Fisetin inhibited the production of inflammatory mediators and ICAM-1 in A549 lung adenocarcinoma cells during IL-1-induced inflammation. Additionally, Fisetin inhibited COX-2, PGE2, IL-8, CCL5, MCP-1, TNF-, and IL-6 as well as the NF-B and ERK1/2 signaling pathways in IL-1B-stimulated A549 cells, indicating that it might help inhibit tumor progression. In fact Fisetin triggered apoptosis in TU212 head and neck squamous cell carcinoma cells by boosting caspase-3 expression and activating the inflammatory PI3K/AKT/NF-kB signaling pathway [144]. Mechanistically, lower Ki67 levels and the inactivation of ERK1/2- and PI3K/AKT-regulated mTOR were linked to the reduction of TU212 cell proliferation and subsequent alterations in tumor volume and weight in nude mice following Fisetin administration [145]. The combination of Fisetin and Carnosic acid increased their anti-inflammatory actions against tumor promotion and targets multiple deregulated pathways associated with inflammation and cancer that include nuclear factor kappa B (NFκB), apoptotic related proteins and phosphatidylinositol-3-kinase (PI3 K)/Akt in human lung cancer cell lines HCC827 and H358 and their mouse xenografts [146]. Fisetin and Carnosic acid co-treatment increased apoptosis by upregulating caspase-3, Bax, and Bad, as well as the TRAIL death receptor, and downregulating the anti-apoptotic Bcl-2 and Bcl-xl proteins [147]. Interestingly, Luteolin suppressed glioma cell multiplication by inducing apoptosis in U251 and LN229 cells. The anti-inflammatory effects of Luteolin and the concomitant activation of MAPKs (JNK, ERK, and p38) and death receptors (FADD) that controlled apoptotic proteins, induced apoptosis in U251 and LN229 cells (caspase-8, caspase-3, and PARP). It was also observed that Luteolin increased cell autophagy by increasing LC3B II/I and decreasing p62. Furthermore, Luteolin lowered the expression of the STAT3 signaling pathway target genes Mcl-1, Survivin, and Bcl-xl, which reduced inflammation in gastric cancer cell lines SGC7901, SGC7901/DDP, HGC27, MGC803, BGC803, and BGC823. The disruption of HSP90-STAT3 binding, which enhanced SHP-1 interaction, mediated the inhibition of the STAT3 pathway following Luteolin administration. Luteolin's anti-cancer activity was demonstrated in SGC7901, SGC7901/DDP, and HGC27 murine xenograft models [148]. In addition, Luteolin and its derivative Apigenin demonstrated a synergistic impact *in vivo* on H358 murine xenografts and Lewis lung cancer. By inhibiting STAT3 phosphorylation, Luteolin and

Apigenin suppressed lung cancer cell proliferation, caused apoptosis, and reduced IFN-driven PD-L1 expression at inflammatory regions [149]. Apigenin decreased tumor development of HepG2 HCC by inhibiting cell proliferation and inducing apoptosis and autophagy via PI3K/AKT/mTOR pathway suppression due to its anti-inflammatory and antioxidant effects [150]. Furthermore, Apigenin reduced the phosphorylation of the signaling molecules Lyn, Syk, phospholipase C1, ERK, and JNK, as well as the production of the cytokines TNF-α, IL-4, IL-5, IL-6, IL-13, and COX-2 in RBL-2H3 rat leukemia cells, all of which increase inflammation and promote carcinogenesis [151]. Another research found that Apigenin suppressed IL-6 production and cell proliferation while promoting apoptosis in Eca-109 and Kyse-30 human esophageal cancer cells via activating PARP and caspase-8 [152]. Role of flavonoids in apoptotic pathway in cancer has been depicted in Fig. 11.

L. Role of flavonoids in DNA damage and repair

Natural substances of many categories are employed in cancer prevention and treatment [140]. Recent research has looked at the role of flavonoids derived from food in the protection of oxidative stress-related disorders such as cancer and cardiovascular disease. Many cellular, metabolic, and immunological mechanisms involved in cancer initiation and progression are regulated by flavonoids [153]. A number of studies have shown that flavonoids can preserve cellular DNA from damage as shown in Fig. 12.

Flavonoids have been hypothesized to form complexes with DNA and protect it from oxidative damage. The binding mechanisms of antioxidants to the DNA duplex are linked to their antioxidative potential [154]. FTIR and UV-Visible spectroscopy techniques were used to analyze the interactions of flavonoids quercetin, kaempferol, and delphinidin with DNA at the molecular level and discovered that delphinidin causes a stronger stabilizing effect on DNA duplex than quercetin and kaempferol [155]. Flavonoids such as hesperitin and naringenin bonded with and stabilized calf thymus DNA [156]. Quercetin, a flavonoid, has recently been shown to interact with human telomerase sequences and stabilize the G-quadruplex structure [157].

Anthocyanins were reported to have anticancer activity in oral squamous cell carcinoma [158]. These flavonoids induces apoptotic cell death by increasing DNA damage, ROS induction and mitochondrial depolarization. It also increases phosphorylation of γ-H2AX and DSBs, thus enforcing cancer cell to death. Diadzen is used for breast cancer also induces apoptosis in MCF-

7 and MDA-MB-231 breast cancer cells by inducing γ-H2AX, DNA damage, cell cycle arrest and p53 expression [159].

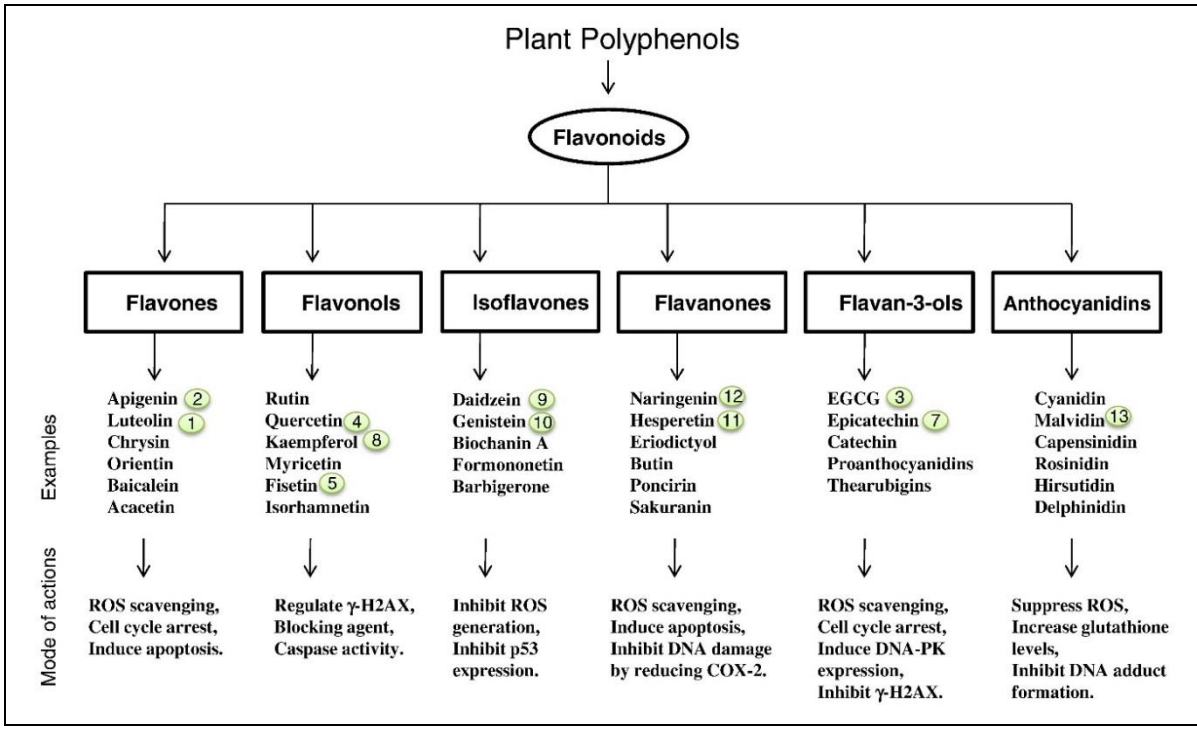

Figure 10 ***Classification of flavonoids.*** Flavonoids can be classified into six groups with different mode of action in each category. Source: "**Plant flavonoids in cancer chemoprevention: role in genome stability"** (JNB, George et al).

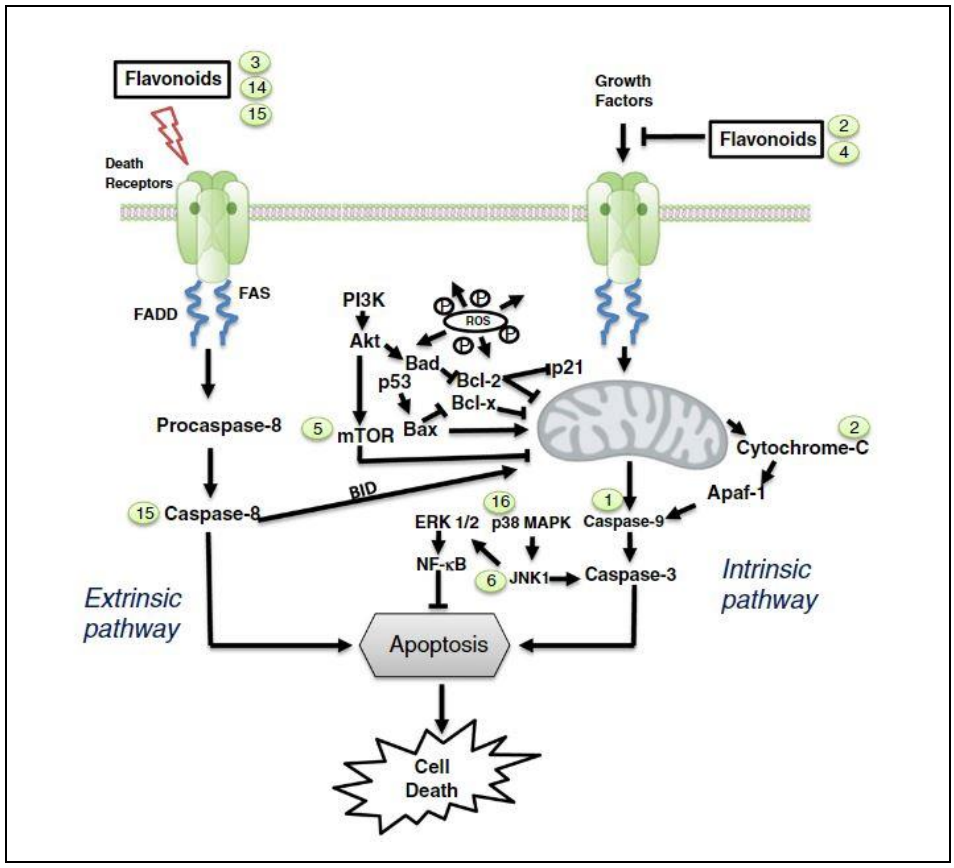

Figure 11 ***Flavonoids in apoptotic pathways in cancer cells are depicted schematically.*** Flavonoids' diverse mechanisms of action in extrinsic and intrinsic pathways. Source: "**Plant flavonoids in cancer chemoprevention: role in genome stability"** (JNB, George et al)

M. Limitations of flavonoids for clinical use

Flavonoids are 15C- ring structures containing 2 benzene rings linked by a 3C- chain (Fig. 15). They vary widely in structure (functional groups), categorization, molecular weight, glycosylation, and esterification. Owing to the presence of the polar -O- ring, as well as -OH groups, Flavonoids are poorly cell permeable limiting their bioavailability. In normal cells, these low concentrations of flavonoids have no influence on the cell cycle process. When supplied in large dosages, other substances such as 3-Hydroxyflavone, Luteolin, and Apigenin displayed considerable cytotoxicity with enhanced ROS production. The clinical use of flavonoids is restricted owing to significant challenges linked with their efficacious use, such as (1) the harvesting and recognition of flavonoids from their natural assets; (2) appearance of the effects of flavonoids in lessening the risk of developing cancer, in conjunction with the time and expense for scientific studies; and (3) numerous pk / pd obstacles (e.g., bioavailability) [160].

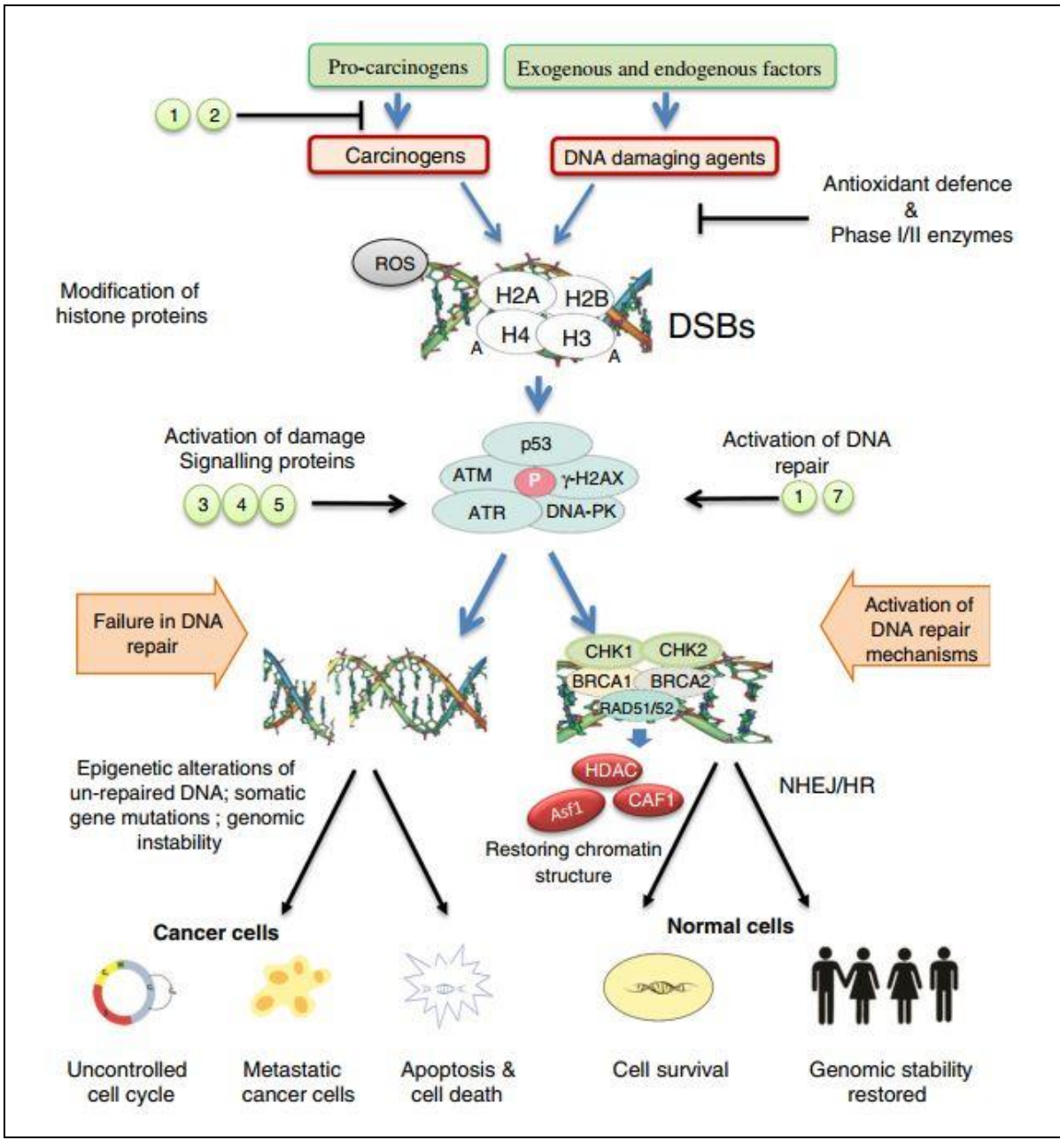

Figure 12 ***Mechanisms of DNA damage and repair by Flavonoids*.** DSBs can be caused by a variety of DNA-damaging agents, which are then followed by chromatin changes that activate damage signaling proteins and repair pathways. Flavonoids have the ability to control these effects by functioning as antioxidants, inducing antioxidant defense and phase I/II enzymes, inhibiting DNA damaging proteins, boosting repair mechanisms in normal cells, and restoring genomic integrity in normal cells. Failure of repair systems can lead to an unregulated cell cycle, somatic mutations (chromosomal abnormalities, telomerase shortening, etc.), and the creation of malignant tumors. Source: "**Plant flavonoids in cancer chemoprevention: role in genome stability"** (JNB, George et al)

N. A brief background study on Eriodictyol

i. What is Eriodictyol?

Eriodictyol is a tetrahydroxyflavanone, which is a flavanone with hydroxy groups replaced at positions 5, 7, 3', and 4'. It is a 3'-hydroxyflavanone and a tetrahydroxyflavanone [161]. Eriodictyol belongs to the flavanone group of flavonoids and can be found in citrus fruits and Chinese medicines. Its anti-inflammatory, antiallergenic, antibacterial, anticancer, and antioxidant activities have been reported [162].

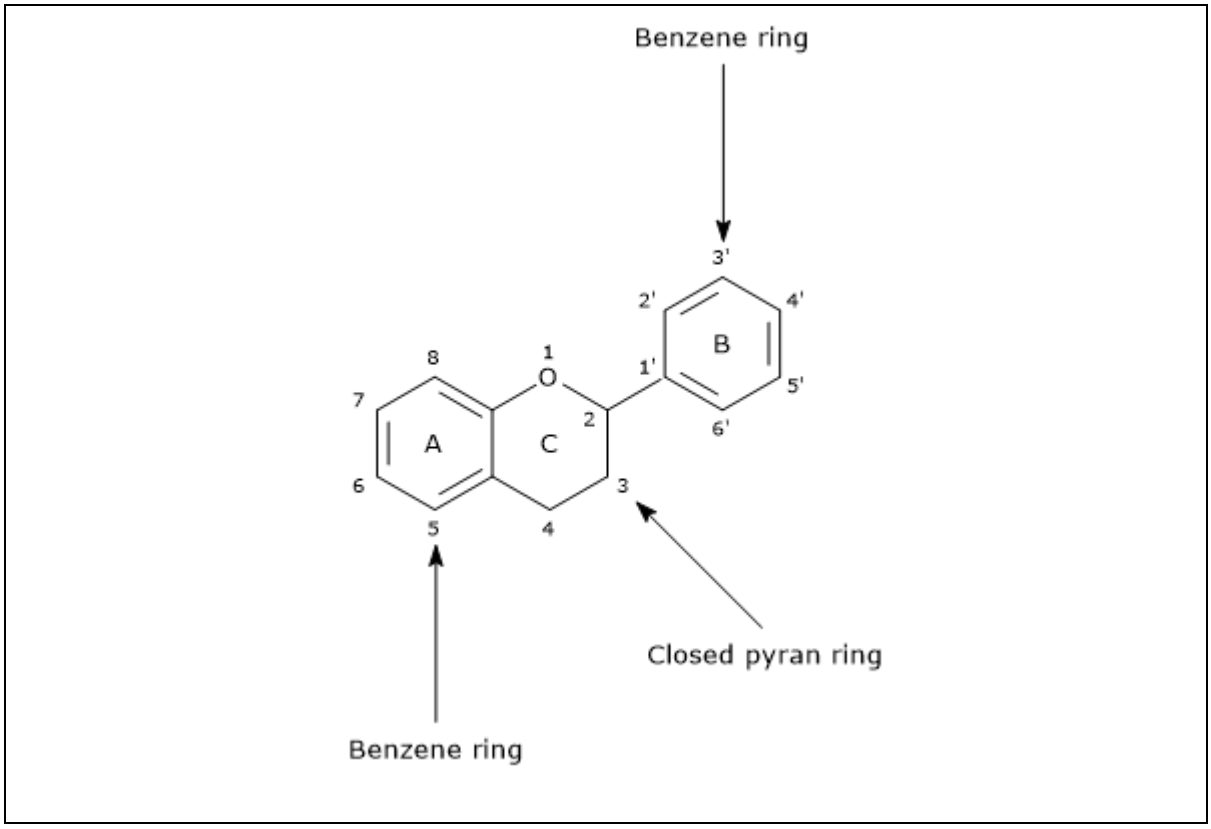

Figure 13: Flavonoid basic structure is a skeleton of **diphenylpropane**, namely, two benzene rings (ring A and B, see figure) linked by a three carbon chain that forms a closed pyran ring (heterocyclic ring containing oxygen, the C ring) with benzenic A ring. Therefore, their structure is also referred to as C6-C3-C6.

ii. Eriodictyol as anti-inflammatory agent

Tetra-hydroxy-flavanone, Eriodictyol has antioxidant and anti-inflammatory activities [163]. Eriodictyol is also capable of shielding the human epithelial pigment (ARPE-19) cells from oxidative stress [164]. In a mouse model of acute lung damage produced by lipopolysaccharide (LPS), Eriodictyol inhibited the production of cytokines (TNF-, IL-6, IL-1,) in macrophages through modulating the Nrf2 pathway [130]. Furthermore, Eriodictyol mitigated oxidative stress in lung tissues by decreasing the accumulation of H2O2, OH•, and MDA. In another in vivo study, Eriodictyol was found to reduce inflammation and oxidative stress, hence reducing cisplatin-induced kidney issues [165].

Furthermore, Eriodictyol therapy inhibited the formation of cisplatin-induced TNF-α and IL-1β in kidney tissues while increasing superoxide dismutase and glutathione peroxidase activities [166]. Cyclooxygenase-1 (COX-l), cyclooxygenase-2 (COX-2) and xanthine oxidase (XO) are all enzymes that play important roles in the pathophysiology of inflammatory disorders. Eriodictyol inhibited COX-1 and COX-2 activity by suppressing XO activity [167]. Furthermore, Eriodictyol reduces the synthesis of inducible nitric oxide synthase (iNOS) and cyclooxygenase-2 (COX-2) and also the increase of IL-1-induced prostaglandin E2 (PGE2) and nitric oxide synthase (NOS) [168]. Even Eriodictyol inhibited the induction of inflammatory cytokines and matrix metalloproteinases (MMPs) triggered by IL-1 activation. Furthermore, Eriodictyol pretreatment reduced IkBα degradation and p-p65 levels while increasing IL-1-stimulated heme oxygenase 1 (HO-1). Si-Nrf2 treatment significantly reduced Nrf2 and HO-1 expression in chondrocytes. Furthermore, si-Nrf2 transfection inhibited Eriodictyol's anti-inflammatory effects in chondrocytes. These studies indicate that Eriodictyol has anti-inflammatory action in chondrocytes activated by IL-1β. The effect of decreasing NF-kB was achieved by stimulation of the signal transduction pathway Nrf2 / HO-1.

iii. Eriodictyol as an anti-cancer agent

Eriodictyol demonstrate anti-proliferative effect in glioma cells (CHG-5 and U87MG) by blocking the signaling pathway for PI3K / Akt / NF-kB [169]. Eriodictyol suppresses tumor growth in nude mice. In addition, Eriodictyol blocked transactivation of RSK2-mediated ATF1 and transformation of JB6 Cl41 cells induced by the tumor promoter [170].

In addition, Eriodictyol amplifies the EGCG-induced activation of the 67-kDa laminin receptor (67LR) via nitric oxide synthase (NOS) / protein kinase B / protein kinase C delta, thereby significantly inducing apoptosis in *in vitro* and Balb/c model [171]. Molecular signalling pathways modulated by Eriodictyol is depicted in Fig. 14.

O. Why study Eriodictyol?

Some natural plant-based medications have limitations, such as adverse drug responses, toxicity, and safety, which restrict their therapeutic potential and necessitate improvement through medicinal chemistry [172-174]. Despite extensive testing of a wide range of natural plant-derived medicines, only a handful (such as Paclitaxel, Vinblastine, Camptothecin analogues, and others) have been approved for clinical use as potent anti-cancer chemotherapeutics [174]. However, due to the extensive biodiversity of the plants and

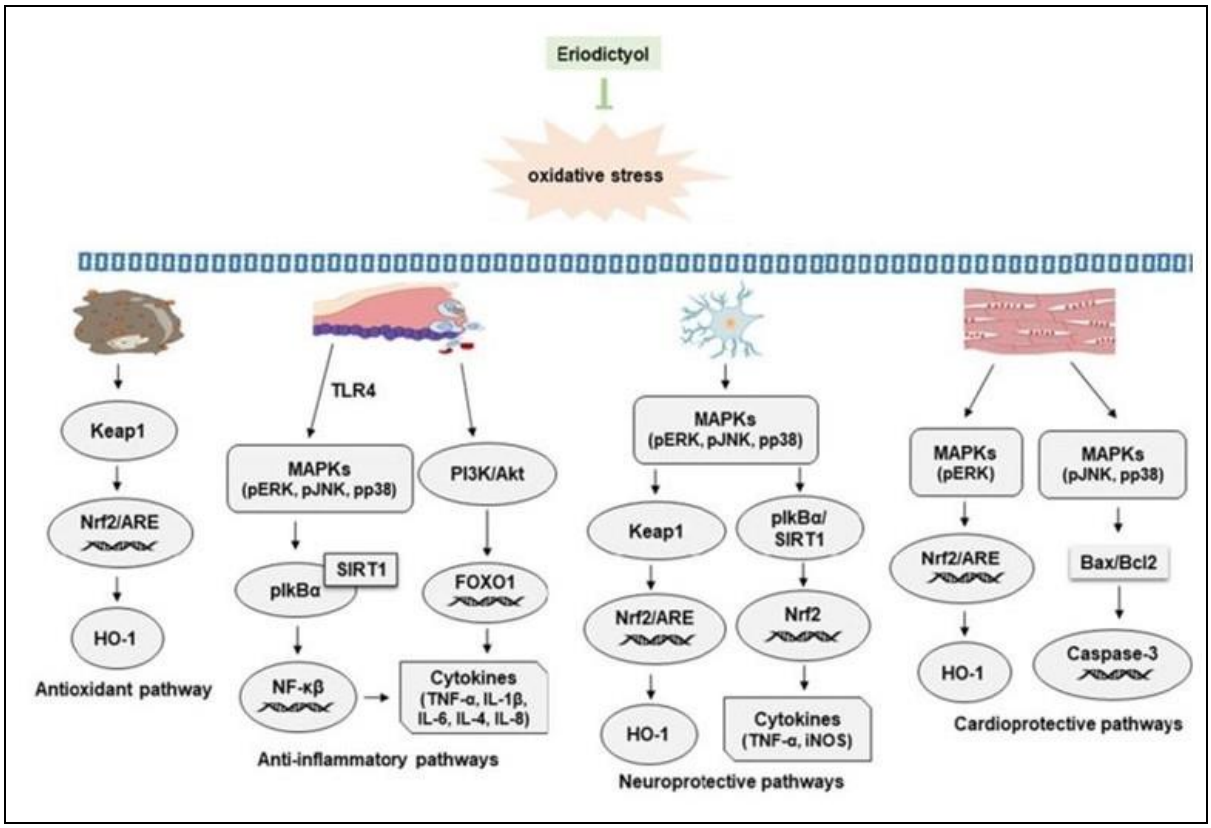

Figure 14 ***Molecular signaling pathways of Eriodictyol***. Eriodictyol has been demonstrated to benefit a variety of health issues associated with oxidative stress. Source: Archives of Pharmacal Research **"The Pharmacological and biological roles of Eriodictyol"**

numerous benefits of the plant-based natural agents (like the ease in availability, prominent efficacy, less toxicity, etc.), worldwide, they are under comprehensive research as promising scaffolds and leads for the development of more effective and selective anti-cancer agents for future therapeutic implication. Eriodictyol, a flavonoid is well-known for its anti-inflammatory and anti-oxidant properties [175]. Literature suggests that Eriodictyol abrogates RSK2-ATF1 signaling thereby inhibiting EGF-triggered neoplastic transformation [176] and inducing tumor cell apoptosis in combination with epigallocatechin-3-gallate [177]. It has also been shown to induce selective cytotoxicity in cancer cells over normal cells, although, the mechanism of its selectivity towards cancer cells is unclear and demands further research [169, 178, 179]. This lacuna led us to propose a detailed investigation of its precise molecular mechanisms to delineate the cause for its high selectivity towards cancer cells.

References

1. Gao, S., et al., *Efficient Biosynthesis of (2S)-Eriodictyol from (2S)-Naringenin in Saccharomyces cerevisiae through a Combination of Promoter Adjustment and Directed Evolution.* ACS Synthetic Biology, 2020. **9**(12): p. 3288-3297.
2. Kardinal, C.G. and J.W. Yarbro, *A conceptual history of cancer.* Semin Oncol, 1979. **6**(4): p. 396-408.
3. Hajdu, S.I., *A note from history: landmarks in history of cancer, part 1.* Cancer, 2011. **117**(5): p. 1097-102.
4. Ashkenazi, A., *Targeting death and decoy receptors of the tumour-necrosis factor superfamily.* Nat Rev Cancer, 2002. **2**(6): p. 420-30.
5. El-Deiry, W.S., *Insights into cancer therapeutic design based on p53 and TRAIL receptor signaling.* Cell Death Differ, 2001. **8**(11): p. 1066-75.
6. U. S. National Institutes of Health, N.C.I.; Available from: https://training.seer.cancer.gov/.
7. Cowherd, S., *Tumor Staging and Grading: A Primer.* Methods in molecular biology (Clifton, N.J.), 2012. **823**: p. 1-18.
8. America, C.T.C.o.; Available from: https://www.cancercenter.com/carcinoma.
9. Auerbach, C., J.M. Robson, and J.G. Carr, *The Chemical Production of Mutations.* 1947. **105**(2723): p. 243-247.
10. Asthana, S., R.S. Patil, and S. Labani, *Tobacco-related cancers in India: A review of incidence reported from population-based cancer registries.* Indian journal of medical and paediatric oncology : official journal of Indian Society of Medical & Paediatric Oncology, 2016. **37**(3): p. 152-157.
11. Ames, B.N., *Identifying environmental chemicals causing mutations and cancer.* Science, 1979. **204**(4393): p. 587-93.
12. Adams, J.D., S.J. Lee, and D. Hoffmann, *Carcinogenic agents in cigarette smoke and the influence of nitrate on their formation.* Carcinogenesis, 1984. **5**(2): p. 221-3.
13. Adams, J.D., K.J. O'Mara-Adams, and D. Hoffmann, *Toxic and carcinogenic agents in undiluted mainstream smoke and sidestream smoke of different types of cigarettes.* Carcinogenesis, 1987. **8**(5): p. 729-31.
14. Dich, J., et al., *Pesticides and cancer.* Cancer Causes Control, 1997. **8**(3): p. 420-43.
15. National Research Council (US) Committee on Diet, N., and Cancer. Diet, Nutrition, and Cancer. Washington (DC): National Academies Press (US); 1982. THE CARCINOGENICITY OF FOOD ADDITIVES AND CONTAMINANTS. Available from: https://www.ncbi.nlm.nih.gov/books/NBK216646/.
16. *Radiation.* IARC Monogr Eval Carcinog Risks Hum, 2012. **100**(Pt D): p. 7-303.
17. Hatch, M., et al., *The Chernobyl disaster: cancer following the accident at the Chernobyl nuclear power plant.* Epidemiol Rev, 2005. **27**: p. 56-66.
18. Warowicka, A., et al., *[Oncogenic viruses and cancer]*. Postepy Biochem, 2020. **66**(4): p. 336-355.
19. Butt, A.Q. and S.M. Miggin, *Cancer and viruses: a double-edged sword.* Proteomics, 2012. **12**(13): p. 2127-38.
20. Willecke, K. and R. Schäfer, *Human oncogenes.* Hum Genet, 1984. **66**(2-3): p. 132-42.
21. Kang, Z.-J., et al., *The Philadelphia chromosome in leukemogenesis.* Chinese journal of cancer, 2016. **35**: p. 48-48.
22. Thomas, D.A., et al., *Burkitt lymphoma and atypical Burkitt or Burkitt-like lymphoma: should these be treated as different diseases?* Current hematologic malignancy reports, 2011. **6**(1): p. 58-66.

23. Witkiewicz, A.K. and E.S. Knudsen, *Retinoblastoma tumor suppressor pathway in breast cancer: prognosis, precision medicine, and therapeutic interventions.* Breast cancer research : BCR, 2014. **16**(3): p. 207-207.
24. Benson, J.R. and M. Baum, *Breast cancer, desmoid tumours, and familial adenomatous polyposis--a unifying hypothesis.* Lancet, 1993. **342**(8875): p. 848-50.
25. Jeong, Y.J., H.K. Oh, and J.G. Bong, *Multiple endocrine neoplasia type 1 associated with breast cancer: A case report and review of the literature.* Oncology letters, 2014. **8**(1): p. 230-234.
26. Gimple, R.C. and X. Wang, *RAS: Striking at the Core of the Oncogenic Circuitry.* 2019. **9**.
27. Aubrey, B.J., A. Strasser, and G.L. Kelly, *Tumor-Suppressor Functions of the TP53 Pathway.* Cold Spring Harbor perspectives in medicine, 2016. **6**(5): p. a026062.
28. Ozaki, T. and A. Nakagawara, *Role of p53 in Cell Death and Human Cancers.* Cancers, 2011. **3**(1): p. 994-1013.
29. Hanahan, D. and Robert A. Weinberg, *Hallmarks of Cancer: The Next Generation.* Cell, 2011. **144**(5): p. 646-674.
30. Ascierto, P.A., et al., *The role of BRAF V600 mutation in melanoma.* Journal of translational medicine, 2012. **10**: p. 85-85.
31. Lukashev, M.E. and Z. Werb, *ECM signalling: orchestrating cell behaviour and misbehaviour.* Trends Cell Biol, 1998. **8**(11): p. 437-41.
32. Amin, A.R.M.R., et al., *Evasion of anti-growth signaling: A key step in tumorigenesis and potential target for treatment and prophylaxis by natural compounds.* Seminars in cancer biology, 2015. **35 Suppl**: p. S55-S77.
33. Amin, A.R.M.R., et al., *Evasion of anti-growth signaling: A key step in tumorigenesis and potential target for treatment and prophylaxis by natural compounds.* Seminars in Cancer Biology, 2015. **35**: p. S55-S77.
34. Aubrey, B.J., et al., *How does p53 induce apoptosis and how does this relate to p53-mediated tumour suppression?* Cell Death & Differentiation, 2018. **25**(1): p. 104-113.
35. Fulda, S. and K.M. Debatin, *Extrinsic versus intrinsic apoptosis pathways in anticancer chemotherapy*. Oncogene, 2006. **25**(34): p. 4798-4811.
36. Fajkus, J., M. Dvorácková, and E. Sýkorová, *Analysis of telomeres and telomerase.* Methods Mol Biol, 2008. **463**: p. 267-96.
37. Trybek, T., et al., *Telomeres and telomerase in oncogenesis (Review).* Oncol Lett, 2020. **20**(2): p. 1015-1027.
38. Jafri, M.A., et al., *Roles of telomeres and telomerase in cancer, and advances in telomerase-targeted therapies.* Genome Med, 2016. **8**(1): p. 69.
39. Dratwa, M., et al., *TERT—Regulation and Roles in Cancer Formation.* 2020. **11**.
40. Kaur, S., et al., *Thrombospondin-1 inhibits VEGF receptor-2 signaling by disrupting its association with CD47.* J Biol Chem, 2010. **285**(50): p. 38923-32.
41. Nishida, N., et al., *Angiogenesis in cancer.* Vascular health and risk management, 2006. **2**(3): p. 213-219.
42. Liberti, M.V. and J.W. Locasale, *The Warburg Effect: How Does it Benefit Cancer Cells?* Trends in biochemical sciences, 2016. **41**(3): p. 211-218.
43. Al Tameemi, W., et al., *Hypoxia-Modified Cancer Cell Metabolism.* 2019. **7**(4).
44. Martin TA, Y.L., Sanders AJ, et al. Cancer Invasion and Metastasis: Molecular and Cellular Perspective. In: Madame Curie Bioscience Database [Internet]. Austin (TX): Landes Bioscience; 2000-2013. Available from: https://www.ncbi.nlm.nih.gov/books/NBK164700/.

45. Mrozik, K.M., et al., *N-cadherin in cancer metastasis, its emerging role in haematological malignancies and potential as a therapeutic target in cancer.* BMC Cancer, 2018. **18**(1): p. 939.
46. Araki, K., et al., *E/N-cadherin switch mediates cancer progression via TGF-β-induced epithelial-to-mesenchymal transition in extrahepatic cholangiocarcinoma.* Br J Cancer, 2011. **105**(12): p. 1885-93.
47. Gheldof, A. and G. Berx, *Cadherins and epithelial-to-mesenchymal transition.* Prog Mol Biol Transl Sci, 2013. **116**: p. 317-36.
48. Birchmeier, W. and J. Behrens, *Cadherin expression in carcinomas: role in the formation of cell junctions and the prevention of invasiveness.* Biochim Biophys Acta, 1994. **1198**(1): p. 11-26.
49. Gottardi, C.J., E. Wong, and B.M. Gumbiner, *E-cadherin suppresses cellular transformation by inhibiting beta-catenin signaling in an adhesion-independent manner.* J Cell Biol, 2001. **153**(5): p. 1049-60.
50. Glinsky, G.V., et al., *Apoptosis and metastasis: increased apoptosis resistance of metastatic cancer cells is associated with the profound deficiency of apoptosis execution mechanisms.* Cancer Letters, 1997. **115**(2): p. 185-193.
51. Lin, Y., J. Xu, and H. Lan, *Tumor-associated macrophages in tumor metastasis: biological roles and clinical therapeutic applications.* Journal of Hematology & Oncology, 2019. **12**(1): p. 76.
52. Pearson, G.W., *Control of Invasion by Epithelial-to-Mesenchymal Transition Programs during Metastasis.* Journal of clinical medicine, 2019. **8**(5): p. 646.
53. Coussens, L.M. and Z. Werb, *Inflammation and cancer.* Nature, 2002. **420**(6917): p. 860-867.
54. Grivennikov, S.I., F.R. Greten, and M. Karin, *Immunity, inflammation, and cancer.* Cell, 2010. **140**(6): p. 883-899.
55. Mantovani, A., et al., *Cancer-related inflammation.* Nature, 2008. **454**(7203): p. 436-444.
56. Meylan, E., et al., *Requirement for NF-κB signalling in a mouse model of lung adenocarcinoma.* Nature, 2009. **462**(7269): p. 104-107.
57. Mori, T., et al., *IL-1β and TNFα-initiated IL-6–STAT3 pathway is critical in mediating inflammatory cytokines and RANKL expression in inflammatory arthritis.* International Immunology, 2011. **23**(11): p. 701-712.
58. Greten, F.R. and S.I. Grivennikov, *Inflammation and Cancer: Triggers, Mechanisms, and Consequences.* Immunity, 2019. **51**(1): p. 27-41.
59. Colotta, F., et al., *Cancer-related inflammation, the seventh hallmark of cancer: links to genetic instability.* Carcinogenesis, 2009. **30**(7): p. 1073-81.
60. Lakatos, P.-L. and L. Lakatos, *Risk for colorectal cancer in ulcerative colitis: changes, causes and management strategies.* World journal of gastroenterology, 2008. **14**(25): p. 3937-3947.
61. Freeman, H.-J., *Colorectal cancer risk in Crohn's disease.* World journal of gastroenterology, 2008. **14**(12): p. 1810-1811.
62. Wroblewski, L.E., R.M. Peek, Jr., and K.T. Wilson, *Helicobacter pylori and gastric cancer: factors that modulate disease risk.* Clinical microbiology reviews, 2010. **23**(4): p. 713-739.
63. El-Serag, H.B., *Epidemiology of viral hepatitis and hepatocellular carcinoma.* Gastroenterology, 2012. **142**(6): p. 1264-1273.e1.
64. Singh, N., et al., *Inflammation and cancer.* Annals of African medicine, 2019. **18**(3): p. 121-126.

65. Pekarek, B., S. Buck, and L. Osher, *A Comprehensive Review on Marjolin's Ulcers: Diagnosis and Treatment.* The journal of the American College of Certified Wound Specialists, 2011. **3**(3): p. 60-64.
66. Noonan, C.W., *Environmental asbestos exposure and risk of mesothelioma.* Annals of translational medicine, 2017. **5**(11): p. 234-234.
67. Thomson, N.C., R. Chaudhuri, and E. Livingston, *Asthma and cigarette smoking.* 2004. **24**(5): p. 822-833.
68. Kim, J.J., et al., *Lung Cancer Associated with Sarcoidosis - A case report.* The Korean journal of thoracic and cardiovascular surgery, 2011. **44**(4): p. 301-303.
69. Mayron, R., et al., *Verrucous carcinoma arising in ulcerative lichen planus of the soles.* J Dermatol Surg Oncol, 1988. **14**(5): p. 547-51.
70. Itatani, Y., et al., *The Role of Chemokines in Promoting Colorectal Cancer Invasion/Metastasis.* International journal of molecular sciences, 2016. **17**(5): p. 643.
71. Luo, J.-L., et al., *Inhibition of NF-* κ*B in cancer cells converts inflammation- induced tumor growth mediated by TNF* α *to TRAIL-mediated tumor regression.* Cancer Cell, 2004. **6**(3): p. 297-305.
72. Wang, K. and M. Karin, *Tumor-Elicited Inflammation and Colorectal Cancer.* Adv Cancer Res, 2015. **128**: p. 173-96.
73. Taylor, C.T. and S.P. Colgan, *Regulation of immunity and inflammation by hypoxia in immunological niches.* Nature Reviews Immunology, 2017. **17**(12): p. 774-785.
74. Wang, X. and Y. Lin, *Tumor necrosis factor and cancer, buddies or foes?* Acta pharmacologica Sinica, 2008. **29**(11): p. 1275-1288.
75. Al Obeed, O.A., et al., *Increased expression of tumor necrosis factor-* α *is associated with advanced colorectal cancer stages.* World journal of gastroenterology, 2014. **20**(48): p. 18390-18396.
76. Nakayama, S., et al., *TNF-* α *receptor 1 expression predicts poor prognosis of diffuse large B-cell lymphoma, not otherwise specified.* Am J Surg Pathol, 2014. **38**(8): p. 1138-46.
77. Tanaka, T., M. Narazaki, and T. Kishimoto, *IL-6 in inflammation, immunity, and disease.* Cold Spring Harbor perspectives in biology, 2014. **6**(10): p. a016295-a016295.
78. Kumari, N., et al., *Role of interleukin-6 in cancer progression and therapeutic resistance.* Tumor Biology, 2016. **37**(9): p. 11553-11572.
79. Wei, L.-H., et al., *The anti-apoptotic role of interleukin-6 in human cervical cancer is mediated by up-regulation of Mcl-1 through a PI 3-K/Akt pathway.* Oncogene, 2001. **20**(41): p. 5799-5809.
80. Gopinathan, G., et al., *Interleukin-6 Stimulates Defective Angiogenesis.* Cancer research, 2015. **75**(15): p. 3098-3107.
81. Sha, Y. and S. Markovic-Plese, *Activated IL-1RI Signaling Pathway Induces Th17 Cell Differentiation via Interferon Regulatory Factor 4 Signaling in Patients with Relapsing-Remitting Multiple Sclerosis.* 2016. **7**(543).
82. Yan, J., M.J. Smyth, and M.W.L. Teng, *Interleukin (IL)-12 and IL-23 and Their Conflicting Roles in Cancer.* Cold Spring Harbor perspectives in biology, 2018. **10**(7): p. a028530.
83. Lust, J.A. and K.A. Donovan, *The role of interleukin-1 beta in the pathogenesis of multiple myeloma.* Hematol Oncol Clin North Am, 1999. **13**(6): p. 1117-25.
84. Pan, Y., et al., *Tumor-Associated Macrophages in Tumor Immunity.* Front Immunol, 2020. **11**: p. 583084.
85. Ley, K., *M1 Means Kill; M2 Means Heal.* The Journal of Immunology, 2017. **199**(7): p. 2191.

86. Martinez, F.O. and S. Gordon, *The M1 and M2 paradigm of macrophage activation: time for reassessment.* F1000Prime Rep, 2014. **6**: p. 13.
87. Sica, A. and A. Mantovani, *Macrophage plasticity and polarization: in vivo veritas.* J Clin Invest, 2012. **122**(3): p. 787-95.
88. Shapouri-Moghaddam, A., et al., *Macrophage plasticity, polarization, and function in health and disease.* Journal of Cellular Physiology, 2018. **233**(9): p. 6425-6440.
89. Loberg, R.D., et al., *CCL2 is a potent regulator of prostate cancer cell migration and proliferation.* Neoplasia (New York, N.Y.), 2006. **8**(7): p. 578-586.
90. Loberg, R.D., et al., *CCL2 is a potent regulator of prostate cancer cell migration and proliferation.* Neoplasia, 2006. **8**(7): p. 578-86.
91. Pujari, R., et al., *A20-mediated negative regulation of canonical NF-κB signaling pathway.* Immunologic Research, 2013. **57**(1): p. 166-171.
92. Liu, T., et al., *NF-κB signaling in inflammation.* Signal transduction and targeted therapy, 2017. **2**: p. 17023.
93. Mussbacher, M., et al., *Cell Type-Specific Roles of NF-κB Linking Inflammation and Thrombosis.* Frontiers in immunology, 2019. **10**: p. 85-85.
94. Szondy, Z., et al., *Anti-inflammatory Mechanisms Triggered by Apoptotic Cells during Their Clearance.* Frontiers in immunology, 2017. **8**: p. 909-909.
95. Nakazawa, H., et al., *iNOS as a Driver of Inflammation and Apoptosis in Mouse Skeletal Muscle after Burn Injury: Possible Involvement of Sirt1 S-Nitrosylation-Mediated Acetylation of p65 NF-κB and p53.* PloS one, 2017. **12**(1): p. e0170391-e0170391.
96. Chen, T., et al., *Chemopreventive effects of a selective nitric oxide synthase inhibitor on carcinogen-induced rat esophageal tumorigenesis.* Cancer Res, 2004. **64**(10): p. 3714-7.
97. Fonseca, S.G., et al., *TNF-alpha mediates the induction of nitric oxide synthase in macrophages but not in neutrophils in experimental cutaneous leishmaniasis.* Eur J Immunol, 2003. **33**(8): p. 2297-306.
98. Tripathi, P., et al., *The role of nitric oxide in inflammatory reactions.* FEMS Immunology & Medical Microbiology, 2007. **51**(3): p. 443-452.
99. Gallo, O., et al., *Role of nitric oxide in angiogenesis and tumor progression in head and neck cancer.* J Natl Cancer Inst, 1998. **90**(8): p. 587-96.
100. Font-Nieves, M., et al., *Induction of COX-2 enzyme and down-regulation of COX-1 expression by lipopolysaccharide (LPS) control prostaglandin E2 production in astrocytes.* J Biol Chem, 2012. **287**(9): p. 6454-68.
101. Muraoka, N., et al., *Role of cyclooxygenase-2-mediated prostaglandin E2-prostaglandin E receptor 4 signaling in cardiac reprogramming.* Nature Communications, 2019. **10**(1): p. 674.
102. FitzGerald, G.A., *COX-2 and beyond: approaches to prostaglandin inhibition in human disease.* Nature Reviews Drug Discovery, 2003. **2**(11): p. 879-890.
103. Pang, L.Y., E.A. Hurst, and D.J. Argyle, *Cyclooxygenase-2: A Role in Cancer Stem Cell Survival and Repopulation of Cancer Cells during Therapy.* Stem Cells Int, 2016. **2016**: p. 2048731.
104. Liu, B., L. Qu, and S. Yan, *Cyclooxygenase-2 promotes tumor growth and suppresses tumor immunity.* Cancer Cell International, 2015. **15**(1): p. 106.
105. Ghosh, N., et al., *COX-2 as a target for cancer chemotherapy.* Pharmacological Reports, 2010. **62**(2): p. 233-244.
106. Huang, R.Y. and G.G. Chen, *Cigarette smoking, cyclooxygenase-2 pathway and cancer.* Biochim Biophys Acta, 2011. **1815**(2): p. 158-69.
107. Eltzschig, H.K. and P. Carmeliet, *Hypoxia and inflammation.* The New England journal of medicine, 2011. **364**(7): p. 656-665.

108. Masoud, G.N. and W. Li, *HIF-1 α pathway: role, regulation and intervention for cancer therapy.* Acta Pharm Sin B, 2015. **5**(5): p. 378-89.
109. Balamurugan, K., *HIF-1 at the crossroads of hypoxia, inflammation, and cancer.* International Journal of Cancer, 2016. **138**(5): p. 1058-1066.
110. Imtiyaz, H.Z. and M.C. Simon, *Hypoxia-inducible factors as essential regulators of inflammation.* Curr Top Microbiol Immunol, 2010. **345**: p. 105-20.
111. Jun, J.C., et al., *Hypoxia-Inducible Factors and Cancer.* Current sleep medicine reports, 2017. **3**(1): p. 1-10.
112. Maxwell, S.A. and G.E. Davis, *Differential gene expression in p53-mediated apoptosis-resistant vs. apoptosis-sensitive tumor cell lines.* 2000. **97**(24): p. 13009-13014.
113. Lipponen, P., et al., *Apoptosis suppressing protein bcl-2 is expressed in well-differentiated breast carcinomas with favourable prognosis.* J Pathol, 1995. **177**(1): p. 49-55.
114. Wang, R.A., et al., *Apoptosis drives cancer cells proliferate and metastasize.* J Cell Mol Med, 2013. **17**(1): p. 205-11.
115. Lipponen, P., et al., *Apoptosis in breast cancer as related to histopathological characteristics and prognosis.* Eur J Cancer, 1994. **30a**(14): p. 2068-73.
116. Vaquero, J., et al., *Relationship between apoptosis and proliferation in secondary tumors of the brain.* Neuropathology, 2004. **24**(4): p. 302-5.
117. Pillai, K., et al., *Does the expression of BCL2 have prognostic significance in malignant peritoneal mesothelioma?* American journal of cancer research, 2013. **3**(3): p. 312-322.
118. Schuyer, M., et al., *Reduced expression of BAX is associated with poor prognosis in patients with epithelial ovarian cancer: a multifactorial analysis of TP53, p21, BAX and BCL-2.* British Journal of Cancer, 2001. **85**(9): p. 1359-1367.
119. Wang, R.-A., et al., *Apoptosis drives cancer cells proliferate and metastasize.* Journal of cellular and molecular medicine, 2013. **17**(1): p. 205-211.
120. Li, J. and J. Yuan, *Caspases in apoptosis and beyond.* Oncogene, 2008. **27**(48): p. 6194-6206.
121. Elmore, S., *Apoptosis: a review of programmed cell death.* Toxicologic pathology, 2007. **35**(4): p. 495-516.
122. Schimmer, A.D., *Inhibitor of apoptosis proteins: translating basic knowledge into clinical practice.* Cancer Res, 2004. **64**(20): p. 7183-90.
123. Galluzzi, L., O. Kepp, and G. Kroemer, *5 - Pathophysiology of Cancer Cell Death*, in *Abeloff's Clinical Oncology (Fifth Edition)*, J.E. Niederhuber, et al., Editors. 2014, Churchill Livingstone: Philadelphia. p. 69-77.e3.
124. Carneiro, B.A. and W.S. El-Deiry, *Targeting apoptosis in cancer therapy.* Nature Reviews Clinical Oncology, 2020. **17**(7): p. 395-417.
125. Khan, K.H., M. Blanco-Codesido, and L.R. Molife, *Cancer therapeutics: Targeting the apoptotic pathway.* Critical Reviews in Oncology/Hematology, 2014. **90**(3): p. 200-219.
126. Pfeffer, C.M. and A.T.K. Singh, *Apoptosis: A Target for Anticancer Therapy.* International journal of molecular sciences, 2018. **19**(2): p. 448.
127. Samec, M., et al., *Flavonoids Targeting HIF-1: Implications on Cancer Metabolism.* Cancers, 2021. **13**(1).
128. Liskova, A., et al., *Flavonoids in Cancer Metastasis.* 2020. **12**(6): p. 1498.
129. Abotaleb, M., et al., *Flavonoids in Cancer and Apoptosis.* 2019. **11**(1): p. 28.
130. Vuong, T., et al., *Role of a polyphenol-enriched preparation on chemoprevention of mammary carcinoma through cancer stem cells and inflammatory pathways modulation.* Journal of Translational Medicine, 2016. **14**(1): p. 13.
131. Jiang, M., et al., *Hydroxysafflor yellow A inhibited lipopolysaccharide-induced non-small cell lung cancer cell proliferation, migration, and invasion by suppressing the*

PI3K/AKT/mTOR and ERK/MAPK signaling pathways. Thoracic Cancer, 2019. **10**(6): p. 1319-1333.
132. Zhang, X., et al., *Systems pharmacology unravels the synergic target space and therapeutic potential of Rhodiola rosea L. for non-small cell lung cancer.* Phytomedicine, 2020. **79**: p. 153326.
133. Liang, Y.-C., et al., *Suppression of inducible cyclooxygenase and inducible nitric oxide synthase by apigenin and related flavonoids in mouse macrophages.* Carcinogenesis, 1999. **20**(10): p. 1945-1952.
134. Lim, R.Z.L., et al., *STAT-3 regulation of CXCR4 is necessary for the prenylflavonoid Icaritin to enhance mesenchymal stem cell proliferation, migration and osteogenic differentiation.* Biochim Biophys Acta Gen Subj, 2018. **1862**(7): p. 1680-1692.
135. Kim, B. and B. Park, *Baohuoside I Suppresses Invasion of Cervical and Breast Cancer Cells through the Downregulation of CXCR4 Chemokine Receptor Expression.* Biochemistry, 2014. **53**(48): p. 7562-7569.
136. Cao, D., et al., *Luteolin suppresses epithelial-mesenchymal transition and migration of triple-negative breast cancer cells by inhibiting YAP/TAZ activity.* Biomedicine & Pharmacotherapy, 2020. **129**: p. 110462.
137. Subbaraj, G.K., Y.S. Kumar, and L. Kulanthaivel, *Antiangiogenic role of natural flavonoids and their molecular mechanism: an update.* The Egyptian Journal of Internal Medicine, 2021. **33**(1): p. 29.
138. Shukla, K., et al., *Didymin by suppressing NF-κB activation prevents VEGF-induced angiogenesis in vitro and in vivo.* Vascular Pharmacology, 2019. **115**: p. 18-25.
139. Forghani, P., M.R. Khorramizadeh, and E.K. Waller, *Silibinin inhibits accumulation of myeloid-derived suppressor cells and tumor growth of murine breast cancer.* Cancer Med, 2014. **3**(2): p. 215-24.
140. Yahfoufi, N., et al., *The Immunomodulatory and Anti-Inflammatory Role of Polyphenols.* Nutrients, 2018. **10**(11).
141. Kopustinskiene, D.M., et al., *Flavonoids as Anticancer Agents.* Nutrients, 2020. **12**(2).
142. Katiyar, S.K., R. Agarwal, and H. Mukhtar, *Inhibition of both stage I and stage II skin tumor promotion in SENCAR mice by a polyphenolic fraction isolated from green tea: inhibition depends on the duration of polyphenol treatment.* Carcinogenesis, 1993. **14**(12): p. 2641-2643.
143. Granato, M., et al., *Quercetin induces apoptosis and autophagy in primary effusion lymphoma cells by inhibiting PI3K/AKT/mTOR and STAT3 signaling pathways.* The Journal of Nutritional Biochemistry, 2017. **41**: p. 124-136.
144. Zhu, J.f., et al., *Icaritin Shows Potent Anti-Leukemia Activity on Chronic Myeloid Leukemia In Vitro and In Vivo by Regulating MAPK/ERK/JNK and JAK2/STAT3 /AKT Signalings.* PLOS ONE, 2011. **6**(8): p. e23720.
145. Peng, H.-L., et al., *Fisetin inhibits the generation of inflammatory mediators in interleukin-1β -induced human lung epithelial cells by suppressing the NF-κB and ERK1/2 pathways.* International Immunopharmacology, 2018. **60**: p. 202-210.
146. Zhang, X.-J. and S.-S. Jia, *Fisetin inhibits laryngeal carcinoma through regulation of AKT/NF-κB/mTOR and ERK1/2 signaling pathways.* Biomedicine & Pharmacotherapy, 2016. **83**: p. 1164-1174.
147. Johnson, J.J., *Carnosol: a promising anti-cancer and anti-inflammatory agent.* Cancer Lett, 2011. **305**(1): p. 1-7.
148. Shi, B., et al., *Carnosic acid and fisetin combination therapy enhances inhibition of lung cancer through apoptosis induction.* Int J Oncol, 2017. **50**(6): p. 2123-2135.

149. Song, S., et al., *Luteolin selectively kills STAT3 highly activated gastric cancer cells through enhancing the binding of STAT3 to SHP-1.* Cell Death & Disease, 2017. **8**(2): p. e2612-e2612.
150. Jiang, Z.-B., et al., *Luteolin and its derivative apigenin suppress the inducible PD-L1 expression to improve anti-tumor immunity in KRAS-mutant lung cancer.* Cancer Letters, 2021. **515**: p. 36-48.
151. Yang, J., C. Pi, and G. Wang, *Inhibition of PI3K/Akt/mTOR pathway by apigenin induces apoptosis and autophagy in hepatocellular carcinoma cells.* Biomedicine & Pharmacotherapy, 2018. **103**: p. 699-707.
152. Park, C.-H., et al., *Effects of Apigenin on RBL-2H3, RAW264.7, and HaCaT Cells: Anti-Allergic, Anti-Inflammatory, and Skin-Protective Activities.* 2020. **21**(13): p. 4620.
153. Qiu, J.-G., et al., *Apigenin Inhibits IL-6 Transcription and Suppresses Esophageal Carcinogenesis.* 2019. **10**.
154. Abotaleb, M., et al., *Flavonoids in Cancer and Apoptosis.* Cancers (Basel), 2018. **11**(1).
155. Kanakis, C., et al., *An Overview of DNA and RNA Bindings to Antioxidant Flavonoids.* Cell biochemistry and biophysics, 2007. **49**: p. 29-36.
156. Kanakis, C.D., et al., *An overview of DNA and RNA bindings to antioxidant flavonoids.* Cell biochemistry and biophysics, 2007. **49**(1): p. 29-36.
157. Hegde, A.H., S.N. Prashanth, and J. Seetharamappa, *Interaction of antioxidant flavonoids with calf thymus DNA analyzed by spectroscopic and electrochemical methods.* J Pharm Biomed Anal, 2012. **63**: p. 40-6.
158. Tawani, A. and A. Kumar, *Structural Insight into the interaction of Flavonoids with Human Telomeric Sequence.* Scientific Reports, 2015. **5**(1): p. 17574.
159. Yue, E., et al., *Anthocyanin is involved in the activation of pyroptosis in oral squamous cell carcinoma.* Phytomedicine, 2019. **56**: p. 286-294.
160. Liu, X., et al., *Anti-breast cancer potential of daidzein in rodents.* Life Sci, 2012. **91**(11-12): p. 415-9.
161. Amawi, H., C.R. Ashby, Jr., and A.K. Tiwari, *Cancer chemoprevention through dietary flavonoids: what's limiting?* Chinese journal of cancer, 2017. **36**(1): p. 50-50.
162. Los, M., et al., *Activation and Caspase-mediated Inhibition of PARP: A Molecular Switch between Fibroblast Necrosis and Apoptosis in Death Receptor Signaling.* 2002. **13**(3): p. 978-988.
163. Shukla, R., et al., *Chapter 18 - Role of Flavonoids in Management of Inflammatory Disorders*, in *Bioactive Food as Dietary Interventions for Arthritis and Related Inflammatory Diseases (Second Edition)*, R.R. Watson and V.R. Preedy, Editors. 2019, Academic Press. p. 293-322.
164. Fortes Rossato, M., et al., *Eriodictyol: A flavonoid antagonist of the TRPV1 receptor with antioxidant activity.* Biochemical pharmacology, 2010. **81**: p. 544-51.
165. Johnson, J., P. Maher, and A. Hanneken, *The flavonoid, eriodictyol, induces long-term protection in ARPE-19 cells through its effects on Nrf2 activation and phase 2 gene expression.* Investigative ophthalmology & visual science, 2009. **50**(5): p. 2398-2406.
166. Li, C.Z., et al., *Eriodictyol attenuates cisplatin-induced kidney injury by inhibiting oxidative stress and inflammation.* Eur J Pharmacol, 2016. **772**: p. 124-30.
167. Mokdad-Bzeouich, I., et al., *Investigation of immunomodulatory and anti-inflammatory effects of eriodictyol through its cellular anti-oxidant activity.* Cell stress & chaperones, 2016. **21**(5): p. 773-781.
168. Calderón-Oliver, M. and E. Ponce-Alquicira, *Chapter 7 - Fruits: A Source of Polyphenols and Health Benefits*, in *Natural and Artificial Flavoring Agents and Food Dyes*, A.M. Grumezescu and A.M. Holban, Editors. 2018, Academic Press. p. 189-228.

169. Wang, Y., et al., *Eriodictyol inhibits IL-1β-induced inflammatory response in human osteoarthritis chondrocytes.* Biomedicine & Pharmacotherapy, 2018. **107**: p. 1128-1134.
170. Li, W., et al., *Eriodictyol Inhibits Proliferation, Metastasis and Induces Apoptosis of Glioma Cells via PI3K/Akt/NF-κB Signaling Pathway.* 2020. **11**(114).
171. Liu, K., et al., *Eriodictyol Inhibits RSK2-ATF1 Signaling and Suppresses EGF-induced Neoplastic Cell Transformation **.* Journal of Biological Chemistry, 2011. **286**(3): p. 2057-2066.
172. Kumazoe, M., et al., *Metabolic Profiling-based Data-mining for an Effective Chemical Combination to Induce Apoptosis of Cancer Cells.* Scientific Reports, 2015. **5**(1): p. 9474.
173. Tewari, D., P. Rawat, and P.K. Singh, *Adverse drug reactions of anticancer drugs derived from natural sources.* Food and Chemical Toxicology, 2019. **123**: p. 522-535.
174. Liu, Z.-B., et al., *Natural substances derived from herbs or plants are promising sources of anticancer agents against colorectal cancer via triggering apoptosis.* Journal of Pharmacy and Pharmacology, 2021: p. rgab130.
175. Ma, X. and Z. Wang, *Anticancer drug discovery in the future: an evolutionary perspective.* Drug Discovery Today, 2009. **14**(23): p. 1136-1142.
176. Lee, J.K., *Anti-inflammatory effects of eriodictyol in lipopolysaccharide-stimulated raw 264.7 murine macrophages.* Arch Pharm Res, 2011. **34**(4): p. 671-9.
177. Liu, K., et al., *Eriodictyol inhibits RSK2-ATF1 signaling and suppresses EGF-induced neoplastic cell transformation.* J Biol Chem, 2011. **286**(3): p. 2057-66.
178. Kumazoe, M., et al., *Metabolic profiling-based data-mining for an effective chemical combination to induce apoptosis of cancer cells.* Sci Rep, 2015. **5**: p. 9474.
179. Tang, L., et al., *Eriodictyol inhibits the growth of CNE1 human nasopharyngeal cancer growth by targeting MEK/ERK signalling pathway, inducing cellular autophagy and inhibition of cell migration and invasion.* J buon, 2020. **25**(5): p. 2389-2394.
180. Zhang, Y., R. Zhang, and H. Ni, *Eriodictyol exerts potent anticancer activity against A549 human lung cancer cell line by inducing mitochondrial-mediated apoptosis, G2/M cell cycle arrest and inhibition of m-TOR/PI3K/Akt signalling pathway.* Archives of medical science : AMS, 2019. **16**(2): p. 446-452.

1. Objectives

The objectives of the thesis are divided into three chapters as follows:

Chapter I
Screening and identification of anti-inflammatory polyphenols as potent anti-cancer agents- Identification of Eriodictyol as a selective cytotoxic agent.

Chapter II
Defining the anti-cancer role of Eriodictyol, and delineating the mechanism of its selective cytotoxicity.

Chapter III
Assessment of the role of Eriodictyol in prevention of cancer progression and metastasis in *in vivo* syngeneic mice tumour model.

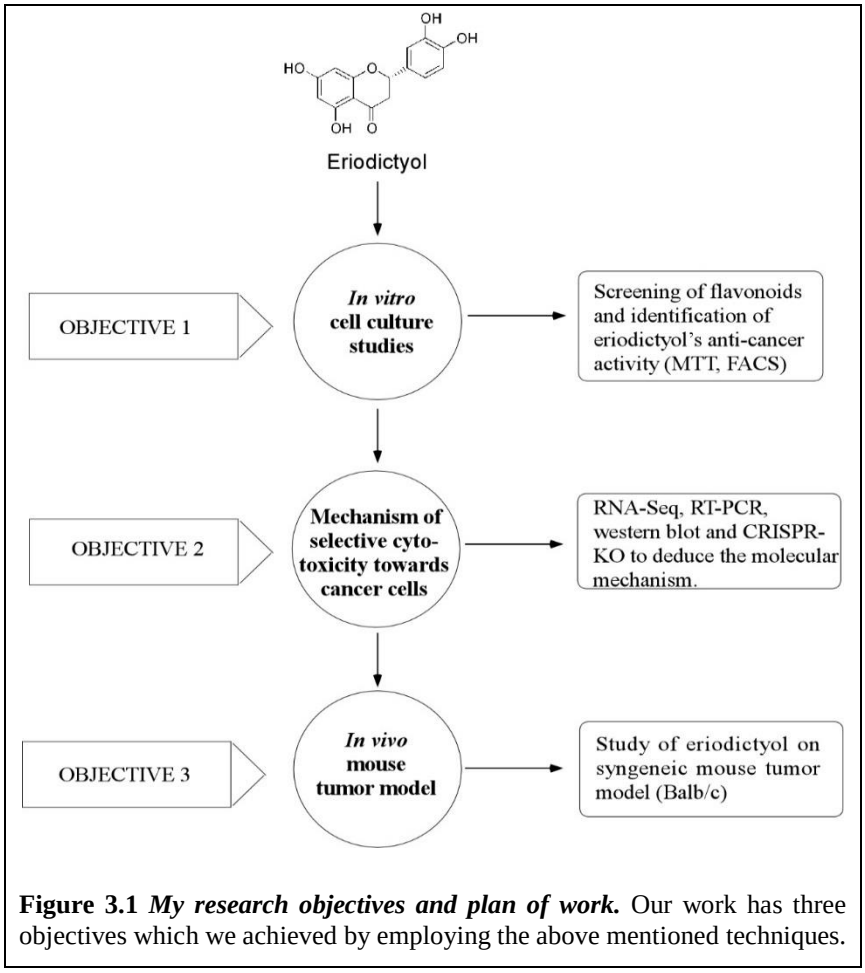

Figure 3.1 ***My research objectives and plan of work.*** Our work has three objectives which we achieved by employing the above mentioned techniques.

2. Chapter I

Screening and identification of anti-inflammatory polyphenols as potent anti-cancer agents - Identification of Eriodictyol as a selective cytotoxic agent

4.1 Abstract

With enough evidences to suggest cancer as a chronic inflammatory disease, we hypothesized whether flavonoids by virtue of being anti-inflammatory might possess anti-cancer activity? Hence, we have screened an array of flavonoid and non-flavonoid polyphenols to assess their anti-inflammatory property *in vitro*. To investigate anti-inflammatory capability, we co-cultured LPS-stimulated human macrophages (THP-1) in the presence or absence of the test compound(s), followed by PCR analysis for the detection of inflammatory mediators such as IL-6, IL-8, MCP-1, and TNF-α. Among the compounds screened, Eriodictyol and Epigallocatechin-3-gallate demonstrated impressive anti-inflammatory properties at a dose as low as 1μM, as evidenced by their potency in inhibiting IL-6 and MCP-1. As there is little information regarding Eriodictyol's anti-cancer role and also its anti-cancer mechanism, we further investigated if the selected compound exhibits selective cytotoxicity towards cancer cells over normal cells. Here we showed that Eriodictyol displays higher selective cytotoxicity in an array of cancer cells (human and mouse) over normal cells, and primarily through induction of apoptosis and G2/M arrest. Eriodictyol significantly blockedclonogenic property of cancer cells. In addition, analysis of the flow cytometry data indicates that Eriodictyol induced substantial apoptosis in HeLa, MCF-7 and HCT-116 as well as in 4T1 and CT-26, relative to the normal cell lines, WI-38 and NKE. Hence, Eriodictyol demonstrates selectively cytotoxicity to cancer cells.

4.2 Introduction

The link between chronic inflammation and the pathogenesis of several disease process is now well established, among which chronic inflammation mediated carcinogenesis are extremely prevalent [180]. Hence, the key to preventing chronic inflammation induced pathogenesis of a disease is to prevent persistent inflammatory conditions to set in at the very first instance.

Although inflammatory symptoms are presently treated with steroidal and non-steroidal anti-inflammatory drugs (NSAIDS), anti-TNF-α blocking antibodies and matrix metalloproteinase (MMPs) inhibitors, most of them present significant negative side effects like increase in the risk of gastrointestinal (GI) bleeding, myocardial infarction, and stroke [181-183]. Anti-inflammatory compounds derived from natural products, particularly from medicinal plants, having fewer risks of side effects offer promising therapeutic strategies against inflammation related conditions [184]. The present study aims towards identifying plant derived flavonoid and non-flavonoid polyphenolic compounds that are able to block inflammation with particular emphasis on carcinogenesis. 11 compounds from plant sources belonging to these two groups of polyphenols were selected. These compounds were studied individually to evaluate their anti-inflammatory potential. *In vitro* cell culture techniques were used by stimulating differentiated monocytic cell line THP-1 with LPS to mimic acute inflammatory conditions in the presence or absence of the test compound, followed by testing of inflammatory mediators like IL-6, MCP-1 and TNF-α. Compounds having potent anti-inflammatory action were further assessed *in vitro* for their possible anti-cancer activity. Out of 11 compounds tested *in vitro* for their anti-inflammatory efficacies, Eriodictyol (isolated from *Eriodictyon californicum*), a flavonoid extracted from citrus fruits [185], is selected based on its potency in blocking LPS induced inflammation as well as for exploration of its anti-cancer efficacy and mechanism.

4.3 Experimental procedures

i. *Culture of monocytic cell lines:* Human monocyte-macrophage cell line THP1 was a kind gift from Dr. Rupak Mukhopadhyay (Tezpur University, Assam) to assess the compounds' anti-inflammatory activities. Cells were grown in complete RPMI-1640 containing 10% Fetal Bovine Serum (FBS), 1 mM of sodium pyruvate, 2 mM of L-glutamine, 1X of non-essential amino acids, 100 units / ml of penicillin, 50µg / ml of streptomycin at 37^0C with 5 % CO2.

ii. *The stimulation of pro-inflammatory cytokines by LPS in differentiated monocytic THP-1 cells:* To assess the induction of pro-inflammatory gene expression, $5 \times 10^5 – 6 \times 10^5$ cells were seeded in 6 well formats with 5 ng PMA (phorbol myristate acetate)/ml for 48 hrs in 2 ml of complete RPMI-1640 medium for inducing differentiation of the monocytes into macrophages. After 48 hrs, cells were washed with 2ml 1X PBS and

fresh 2ml serum free media, was added to each well for 3hrs. Finally, different concentration of LPS (50ng/ml-1µg/ml) was introduced to each well for 2hrs.

iii. *Screening of flavonoid and non-flavonoid polyphenols for their anti-inflammatory activity:* To assess the anti-inflammatory potential of different anti-inflammatory compounds, $5 \times 10^5 - 6 \times 10^5$ cells were seeded in 6 well plate formats with 5 ng PMA (phorbol myristate acetate)/ml for 48 hrs in 2 ml of complete RPMI-1640 medium without Gentamycin/Amphotericin for inducing differentiation of the monocytes into macrophages. After 48 hrs, cells were washed twice with 2ml 1X PBS and replaced with 2 ml of serum-free RPMI mixed with the test compound to each well for 6 hrs. After pre-treatment with the test compound,LPS (500 ng/ml) was added to each well for 2hrs. Finally, RNA was collected from the wells by Trizol reagent.

iv. *Semi-quantitative RT-PCR*: Total RNA was extracted from cells by Trizol reagent. 500 ng of cDNA was prepared from the samples using Verso cDNA synthesis kit (Thermo Fisher Scientific, USA) followed by PCR analysis with gene specific primers for several pro-inflammatory cytokines. Primers used were IL-6: 5'-TACCCCCAGGAGAAGATTCC-3' (For); 5'- TTTTCTGCCAGTGCCTCTTT-3' (Rev), MCP-1: 5'- CTCCGAAGACTTGAACACTCAC-3' (For); 5'-GTAGAACTGTGGTTCAAGAGGAAA-3' (Rev), TNFα: 5'-TGTAGCAAACCCTCAAGC-3' (forward), 5'- TGGGAGTAGATGAGGTACAG-3' (reverse).

v. *Cell culture and maintenance of mammalian cancer cells*. ATCC, USA, was used to obtain HeLa (human cervical cancer cells), WI-38 (human lung fibroblast cells), and HCT116 p53wt (human colon carcinoma cells). THP-1 (human monocyte cancer cells) and MCF-7 (human breast cancer cells), were obtained from the National Center for Cell Science (NCCS) central cell repository in Pune, India, and cultured according to the supplier's instructions. Dr. James H. Finke (Cleveland Clinic Foundation, USA) and Dr. Gerd Ritter (Ludwig Institute of Cancer Research, USA) generously provided NKE and the human renal carcinoma cell line (SK-RC-45), as well as 4T1 (murine mammary carcinoma), CT-26 (murine colon carcinoma), and Renca (murine renal adenocarcinoma) cell lines. Cell lines were cultured either in RPMI 1640 or DMEM with 10% FBS, 1 mM sodium pyruvate, 2mM L-glutamine and non-essential amino

acids, 100 U/ml Penicillin, 100 µg/ml Streptomycin and 50µg/ml Gentamycin at 37^0C in presence of 5% CO_2.

vi. *MTT cell proliferation assay*. In short, cells were grown at 72h in the presence of Eriodictyol (0-200µM) in 48 well-plate formats. Phenol-Red free RPMI withMTT (0.5 mg / mL; 200µL per well) was provided to every well and incubated at 37 ° C for 3 h in a 5% CO2 humidified incubator. The developed purple-colored formazan crystals were dissolved in DMSO, and a microplate reader measured the absorbance at 570 nm [9].

vii. *Clonogenic assay.* Clonogenic assay, also referred to as the colony formation assay, is an *in vitro* cell survival experiment, used to assess the ability of a single cell to develop into a colony. Usually cancer cells develop an inherent ability to rapidly form colonies even from very few cells. Cells were seeded at comparatively low density (200 cells per well in a 6 well format) for clonogenicity testing, grown for 8/10 days, fixed, and labelled with 3.7 percent formaldehyde and 0.05 percent crystal violet. The Gel Doc XR+ was used to capture photographs of wells loaded with cells at 10X magnification (Bio-Rad).

viii. *Effect of Eriodictyol on cell cycle using propidium iodide staining:* In this experiment, HeLa and HCT-116 cells were exposed to Eriodictyol at varying concentrations (0-200 µM) for 24 hours. Post treatment, single cell suspension were fixed in 75 % ethanol overnight at -20°C. Cells were pelleted by centrifugation and resuspended in 1X PBS for 2 hours before being treated with RNaseA (20 µM) at 37°C for 2 hours. Cells were then treated with Propidium Iodide (PI) for 15 mins at room temperature. FACS-Verse was used to analyze the flow cytometry data right away.

ix. *Annexin-V-FITC/PI staining.* Flow cytometric detection and analysis of apoptosis induction following treatment of cells with Eriodictyol was done by labelling with Annexin-V-FITC / PI utilizing the BD Bioscience Flow cytometric staining technique. Post treatment, $2x10^5$ cells were washed with ice-cold 1X PBS and re-suspended in 100 µL of 1X Binding buffer. Cells were incubated at room temperature for 15 mins in dim light with 5 µL of Annexin-V-FITC followed by 5 µL of PI, according to the manufacturer's instructions. Event acquisition was carried out by a BD FACS-Verse

system, and analyzed using BD Flow cytometry analysis software (FACSuite™, 2014) [10].

4.4 Results

i. LPS induces expression of pro-inflammatory cytokines in acute inflammation model.

To optimize the dose of LPS, monocytic cell line (THP-1) were treated with different concentration of LPS (50ng/ml-1 µg/ml) for 2 hrs (Fig. 4.1 A,C-E). LPS proficiently shows induction of signature pro-inflammatory cytokines at both low (50 ng/ml) and high (1 µg/ml) dose of LPS. From this data, we selected 500 ng/ml doses for subsequent screening of natural compounds for their potential anti-inflammatory activity (Fig 4.2).

ii. *Screening of anti-inflammatory efficacies of flavonoid and non-flavonoid polyphenols from natural sources.*

Selected compounds were tested for their ability to block LPS-inducedexpression of pro-inflammatory gene expression by PCR. Dose of LPS-induced pro-inflammatory cytokine gene expression was measured by real time PCR (RT-PCR) as shown in Fig. 4.1 C-E, which clearly follows dose-dependent induction of the pro-inflammatory cytokine genes, TNF-α, IL-6 and MCP-1. Four compounds namely Chrysin, EGCG, Eriodictyol and Quercetin showed strong anti-inflammatory activities at concentrations ranging from 1-100 µM, as shown in Fig. 4.2 A-C which displayed dose-dependent reduction in the expression of the pro-inflammatory cytokine mRNA levels. Interestingly, although Eriodictyol effective inhibits IL-6 and MCP-1 gene expression, it shows negligible effect on LPS-induced TNF-α, as opposed to the other compounds, indicating it may have a different mechanism behind its observed anti-inflammatory activity. Fig. 4.1 B depicts a representative semi-quantitative PCR profile showing the ability of Eriodictyol to specifically inhibit IL-6 and MCP-1 gene expression.

Extensive data regarding the anti-inflammatory efficacy of the 4 compounds were prevalent [175, 186-188] .Although, anti-cancer activities and the mechanism of action of Chrysin, Quercetin and EGCG were extensively researched and documented [189-191], however, neither the anti-cancer efficacy of Eriodictyol or its mechanism of anti-cancer activity was well studied. Only a handful of studies documented the effect of Eriodictyol on certain cancer cell lines, with an even fewer studies on its mechanism. This prompted us to take a deeper look into the range of anti-cancer potential of Eriodictyol, its anti-cancer specificity and an in-depth understanding of its anti-cancer mechanism.

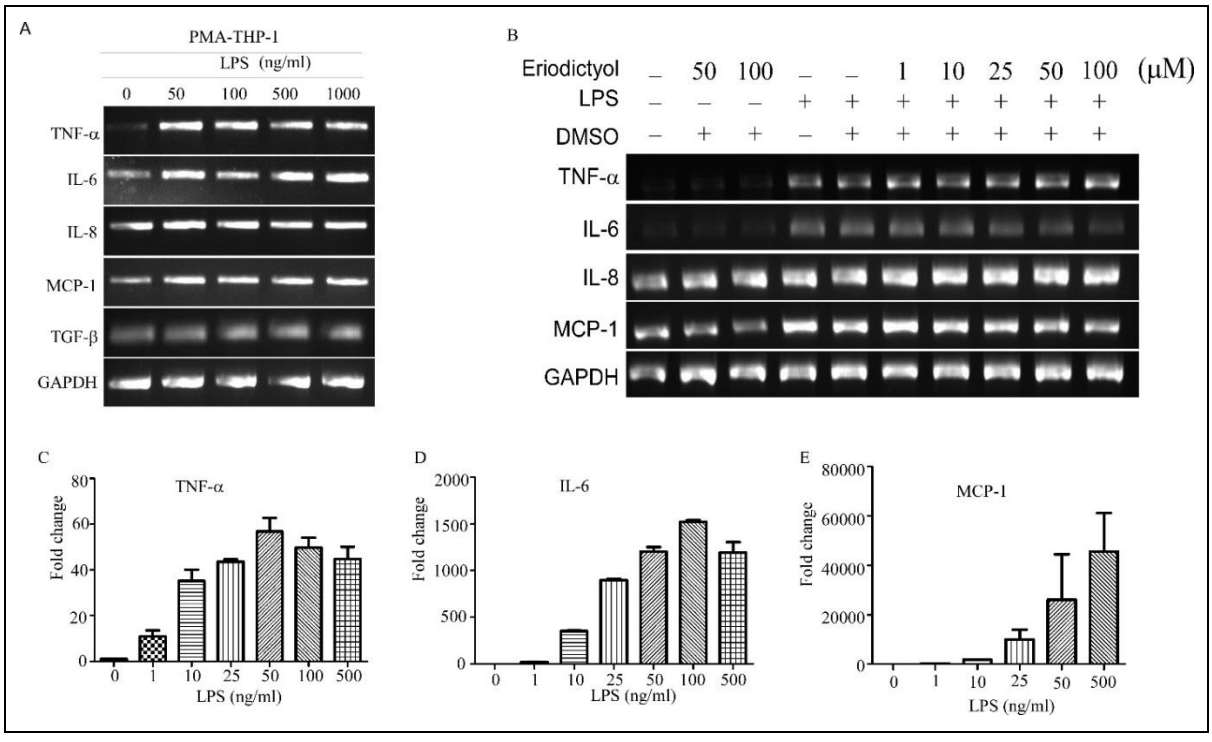

Figure 4.1: ***Optimization of LPS dose for investigating anti-inflammatory flavonoids.*** **A.** Optimization of the dose of LPS required in inducing pro-inflammatory gene expression in human monocyte-macrophage cell line THP-1. **B.** Semi-quantitative PCR showing the efficiency of Eriodictyol in blocking LPS induction of TNF-α, IL-6, MCP-1. **C,D,E.** Real Time PCR data depicting dose curve of LPS induction.

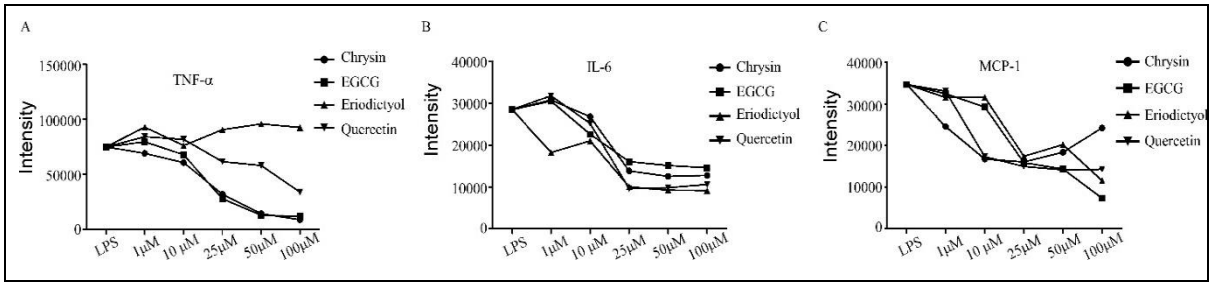

Figure 4.2: ***Screening of anti-inflammatory flavonoids.*** **A-C.** Data shows strong anti-inflammatory efficacy of EGCG, Chrysin, Quercetin and Eriodictyol in blocking LPS-induced expression of genes TNF-α **(A)**, IL-6**(B)**, MCP-1**(C)**.

iii. Eriodictyol induces selective cytotoxicity to cancer cells.

To assess the specificity of Eriodictyol against cancer cells, MTT assay was utilized to monitor its impact on cell proliferation in different human and murine cell lines. Data strongly indicate substantial high cytotoxicity of Eriodictyol in both human (Fig. 4.3 A, B) as well as murine cancer cells (Fig. 4.3 C, D) compared to normal cell lines (Fig. 4.3 E, F) which displayed low or insignificant cytotoxicity in response to Eriodictyol treatment. This was also reflected from the effective concentration of Eriodictyol to cause at least 50% inhibition of cellular

proliferation in the different cell lines, as evidenced from the respective computed IC_{50} values, HeLa (IC_{50} = 107.5 μM), SK-RC-45 (IC_{50}=53.75 μM), HCT-116 (IC_{50} =105 μM), MCF-7 (IC_{50} =75 μM) and mouse cancer cells, 4T1 (IC_{50} =75 μM), CT-26 (IC_{50} =47.5 μM) and Renca (IC_{50} =145 μM). Interestingly, as is evident from the IC_{50}>200 μM (Fig.4.2 E, F), Eriodictyol seems negligibly toxic towards normal human lines NKE and WI-38. The selectivity index (SI) is a measure of cytotoxicity of a compound against cancer cells compared to non-tumor cells. Higher SI value of a compound indicates more selectivity of the lead towards cancer cells [192, 193]. The SI of Eriodictyol was computed by dividing the IC_{50} of normal cell lines (NKE and WI-38) with the IC_{50} of cancer cell lines (SK-RC-45 SI>3.72, HeLa SI>1.86, HCT116 SI>1.9, MCF-7 SI>2.66). In our case study, Eriodictyol displayed a SI value >1.5 in all the human cancer cell lines (Fig. 4.3 B). As a result, this data not only demonstrates Eriodictyol's selective cytotoxicity towards cancer cell lines relative to normal cells, but it also aids in the selection of a mouse tumour cell line for *in* vivo investigation.

iv. Eriodictyol blocks clonogenecity of cancer cells.

A defining characteristic of cancer cells is its colony forming ability or clonogenecity. A colony is considered as having at least 50 cells. The clonogenic assay is the method of choice for determining cell reproductive mortality following treatment with cytotoxic agents. Only a small percentage of implanted cells retain the ability to form colonies. The influence of Eriodictyol on the colony forming ability (clonogenicity) of cancer cells (SK-RC-45 and HeLa) was evaluated for 12 days in response to varying Eriodictyol concentrations (0-50μM) with Eriodictyol replacement at an interval of every 72 hours. Data shows inhibition of colony forming ability of Eriodictyol in SK-RC-45 cells at concentrations as small as 10μM with an almost total elimination of colony forming capacity of the cells at 25μM Eriodictyol dose (Fig. 4.3 G, H). In addition, it

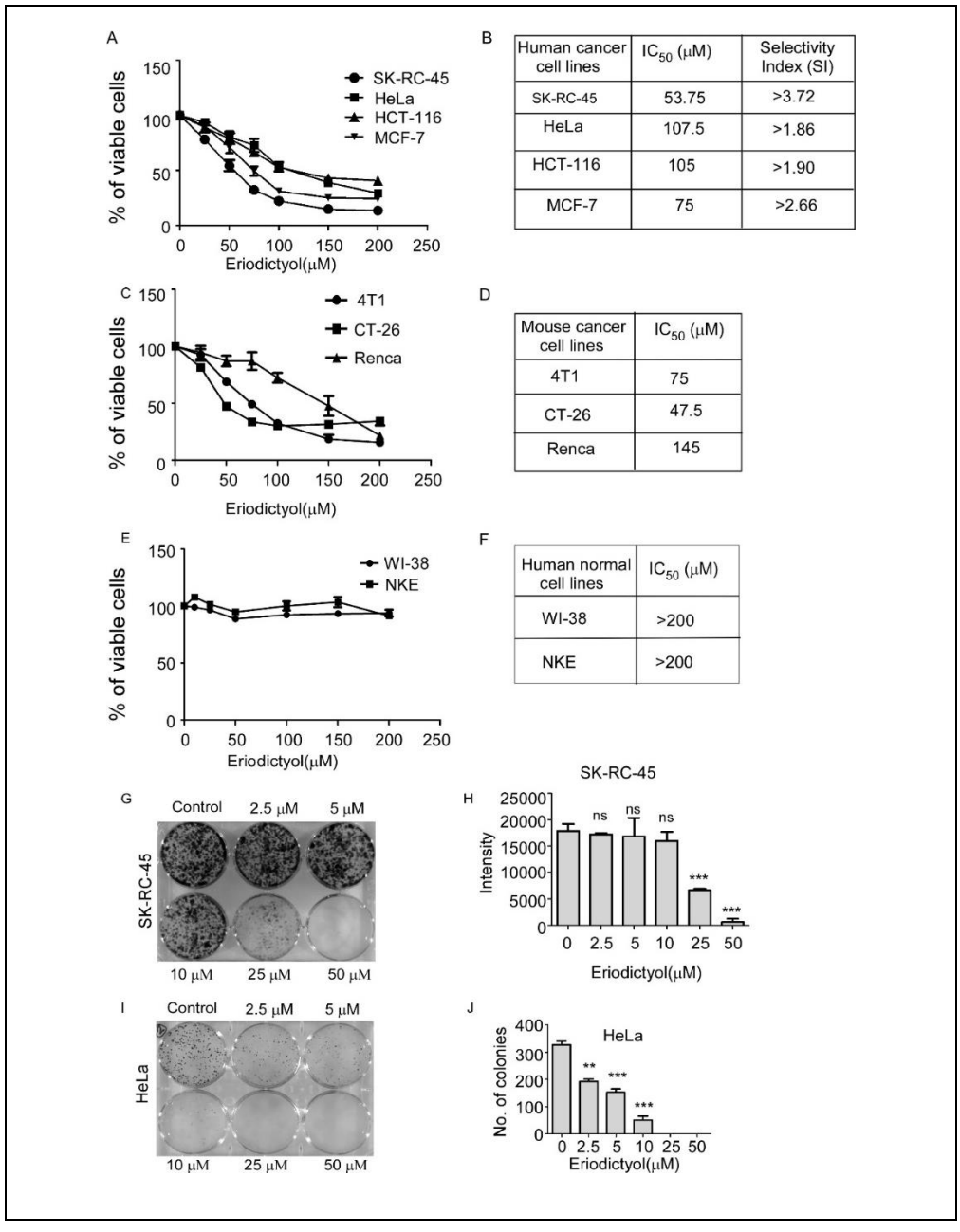

Human cancer cell lines	IC_{50} (μM)	Selectivity Index (SI)
SK-RC-45	53.75	>3.72
HeLa	107.5	>1.86
HCT-116	105	>1.90
MCF-7	75	>2.66

Mouse cancer cell lines	IC_{50} (μM)
4T1	75
CT-26	47.5
Renca	145

Human normal cell lines	IC_{50} (μM)
WI-38	>200
NKE	>200

Figure 4.3 ***Eriodictyol elicits selective cytotoxicity against several cancer cell lines. A, C, E.*** Line graphs showing *in vitro* cytotoxicity in presence of Eriodictyol (0-200 μM) at 72 h in human cancer (SK-RC-45, HeLa, HCT-116, MCF-7), mouse cancer (4T1, CT-26, Renca) and normal human untransformed (WI-38 and NKE) cell lines, as measured by MTT assay. The results are summarized from three independent experiments. ***B, D, F.*** Table depicting IC_{50} values of human cancer, mouse cancer as well as in normal cells. The IC_{50} values were determined using Microsoft Excel software. ***G, I.*** Pictorial representation of plates and ***H, J***. column graph showing dose-dependent inhibition of clonogenicity in SK-RC-45 and HeLa cell lines respectively, in response to Eriodictyol treatment. The results are shown as mean ± SEM.

showed higher effectiveness in HeLa cells with inhibition of clonogenicity starting at 2.5 μM, with almost complete colony formation regression at 10 μM (Fig. 4.3 I, J). While Eriodictyol significantly inhibits colony growth at concentrations as low as 2.5μM in HeLa cells and 25μM in SK-RC-45 cells (Fig. 4.3 G-J), the concentration of Eriodictyol that causes 40-50 percent of cells to undergo apoptosis in HeLa and MCF-7 cells is 125μM (Fig. 4.4 A, B), which is clearly several folds higher than the concentration required to inhibit significant clonogenicity. Therefore, we conclude that Eriodictyol effectively inhibits the reproductive potential of cancer cells to form colonies.

v. Eriodictyol induces apoptosis in human and murine cancer cells.

The translocation of phosphatidyl serine (PS) from the cytosol to the cell membrane characterizes apoptosis, which is detected by the binding of Annexin V-FITC to the PS. For this purpose, both human (HeLa, HCT-116, MCF-7) and murine (CT-26 and 4T1) cancer cells were treated with Eriodictyol (0-150μM) for 48 h and subjected to AnnexinV-FITC / PI staining. Dot plot shown in Fig. 4.4 A-C indicate dose-dependent induction of apoptosis in HeLa, MCF-7 and HCT-116 cells by Eriodictyol upon 48 h of treatment as evident from the increase in percentage of Annexin-V+ve/ PI +ve cell populations reflected in the representative density plot and also from their respective bar graphs. Similar, induction of apoptosis in response to Eriodictyol was also obtained in mouse tumor cells (Fig. 4.4 D,E), as indicated by a dose-dependent increase in the percentage of cells staining positive for AnnexinV-FITC/PI. Moreover, a comparative study of the apoptosis induction between HeLa vs WI-38/NKE (Fig. 4.5) infers that Eriodictyol is highly sensitive to cancerous HeLa cells but not in normal cell lines. Therefore, this data conclusively proves the fact that Eriodictyol's ability to induce apoptosis confers a significant degree of selective towards cancer cells compared to normal cell lines.

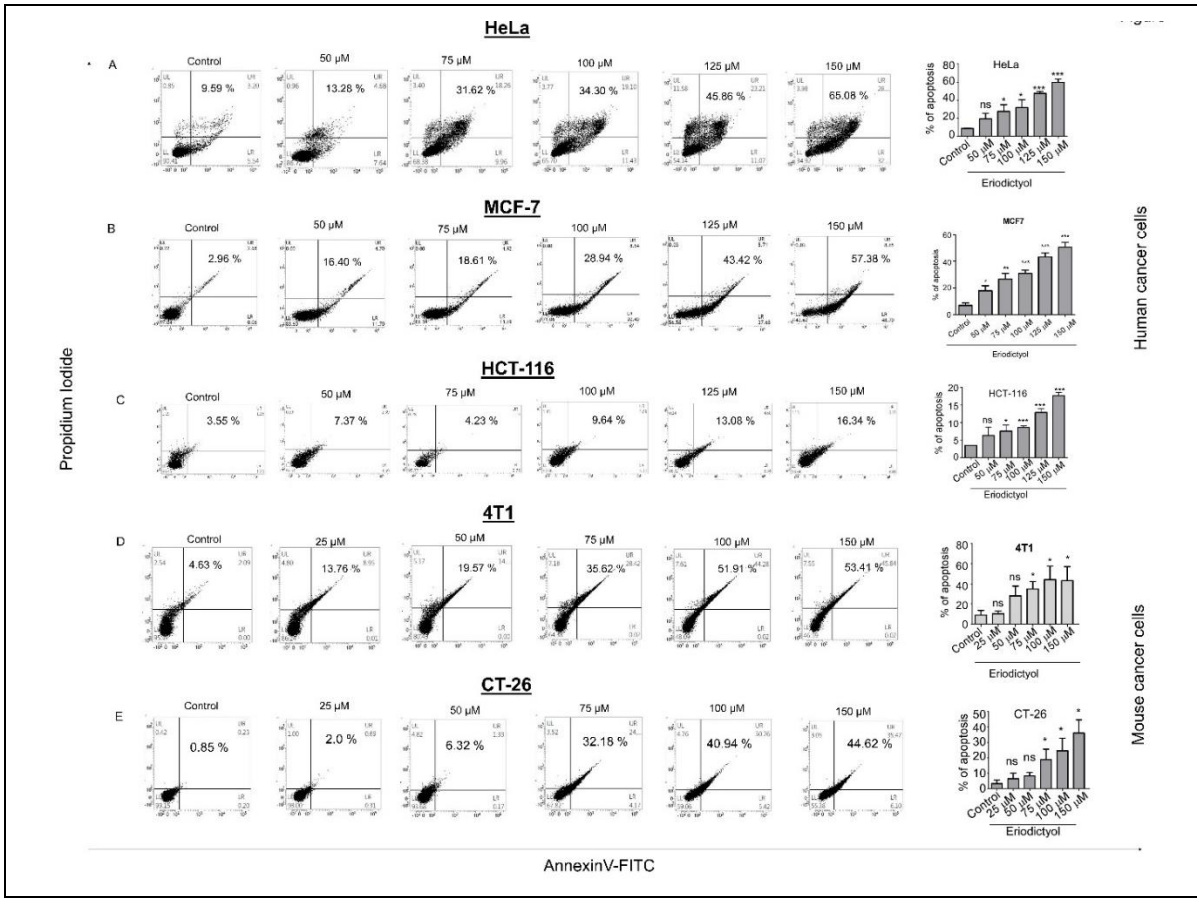

Figure 4.4 ***Eriodictyol treatment induces apoptosis in human and mouse cancer cell lines.*** Flow cytometric density graphs demonstrating a dose-dependent increase in the Annexin V-FITC/PI-positive population of (A) HeLa, (B) MCF-7, (C) HCT-116, (D) 4T1, and (E) CT-26 cells in response to Eriodictyol treatment. Post-treatment with Eriodictyol (0-150 µM) for 48 h, cells were stained with annexin V-FITC/PI and measured in BD FACS Verse instrument and analyzed in BD FACSuite™. Data represent at least three independent experiments. Column graphs representing concentration-dependent induction of apoptosis in the above mentioned cell types, and experimental conditions. The data are represented as Mean ± SEM of three independent experiments and analyzed by Student's t-test (two-tailed); *$p < 0.05$, **$p < 0.01$, ***$p < 0.001$, ns not significant. The total apoptosis population was calculated by combining the quadrants UL+UR+LR.

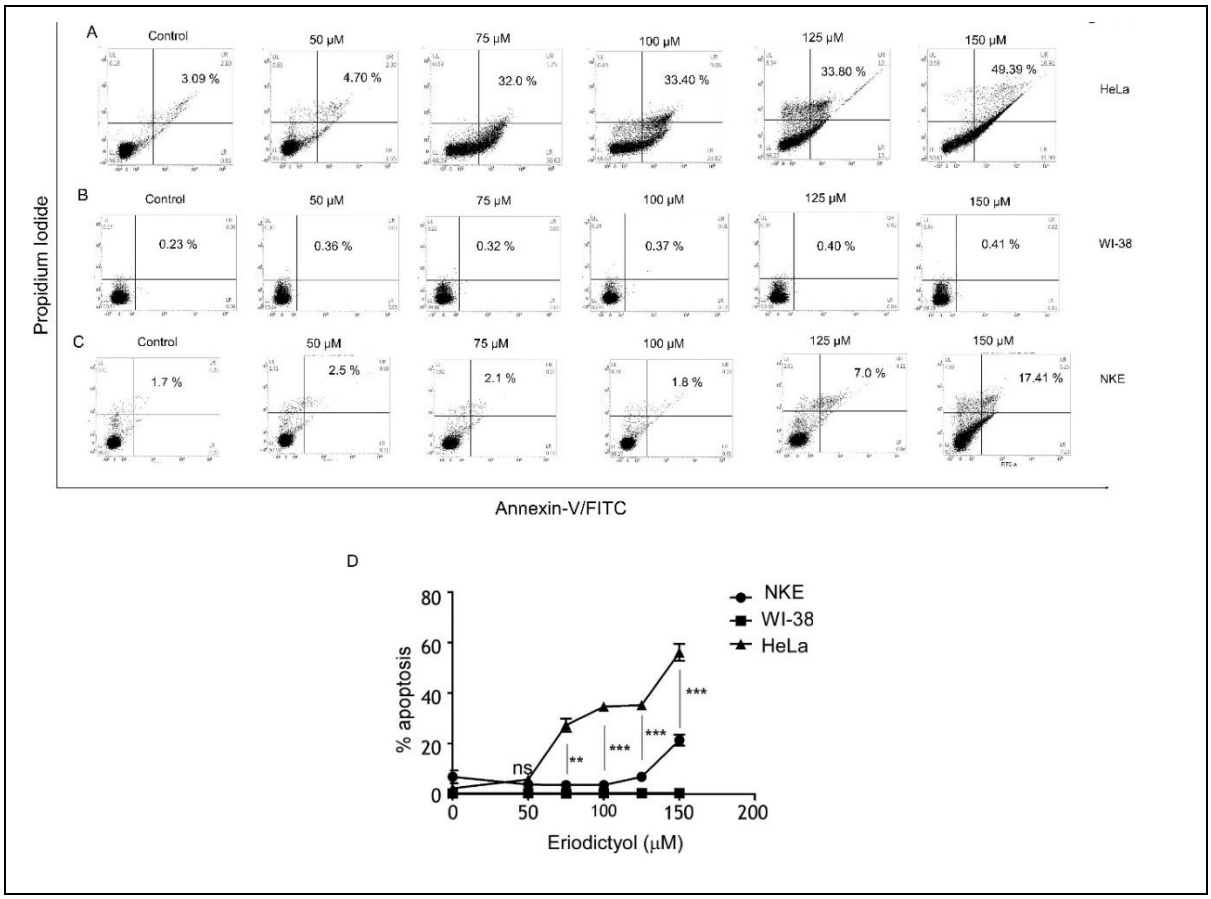

Figure 4.5 ***Eriodictyol induced apoptosis is selective towards cancer cells.*** Density plots showing comparative concentration-dependent induction of apoptosis in **(A)** HeLa versus normal **(B)** WI-38 and **(C)** NKE cell lines upon Eriodictyol treatment. ***D.*** Line graph representing the difference in the percentage of apoptosis in cancer cells compared to normal cell lines. The data are represented as Mean ± SEM of three independent experiments and analyzed by Student's t-test (two-tailed); *p < 0.05, **p < 0.01, ***p < 0.001, ns not significant.

vi. Eriodictyol arrests cell cycle progression at the G2/M phase.

Since, induction of apoptosis and inhibition of cellular proliferation is almost invariably associated with a bias in cell cycle arrest in a particular phase, flow cytometry was conducted to examine the influence of Eriodictyol on various stages of the cell cycle using propidium iodide. Data shown in Fig. 4.6 A-D shows dose-dependent accumulation of HeLa and HCT-116 cells in the G2/M phase of the cell cycle as seen from the histogram and bar graph from three independent experiments (Fig. 4.6). The column graphs (Fig. 4.6B & D) reflecting a concentration-dependent decrease in percentage of cells residing in the G1-phase with almost a parallel increase in cells residing at the G2/M-phase, clearly indicates the ability of Eriodictyol in inducing cell cycle arrest

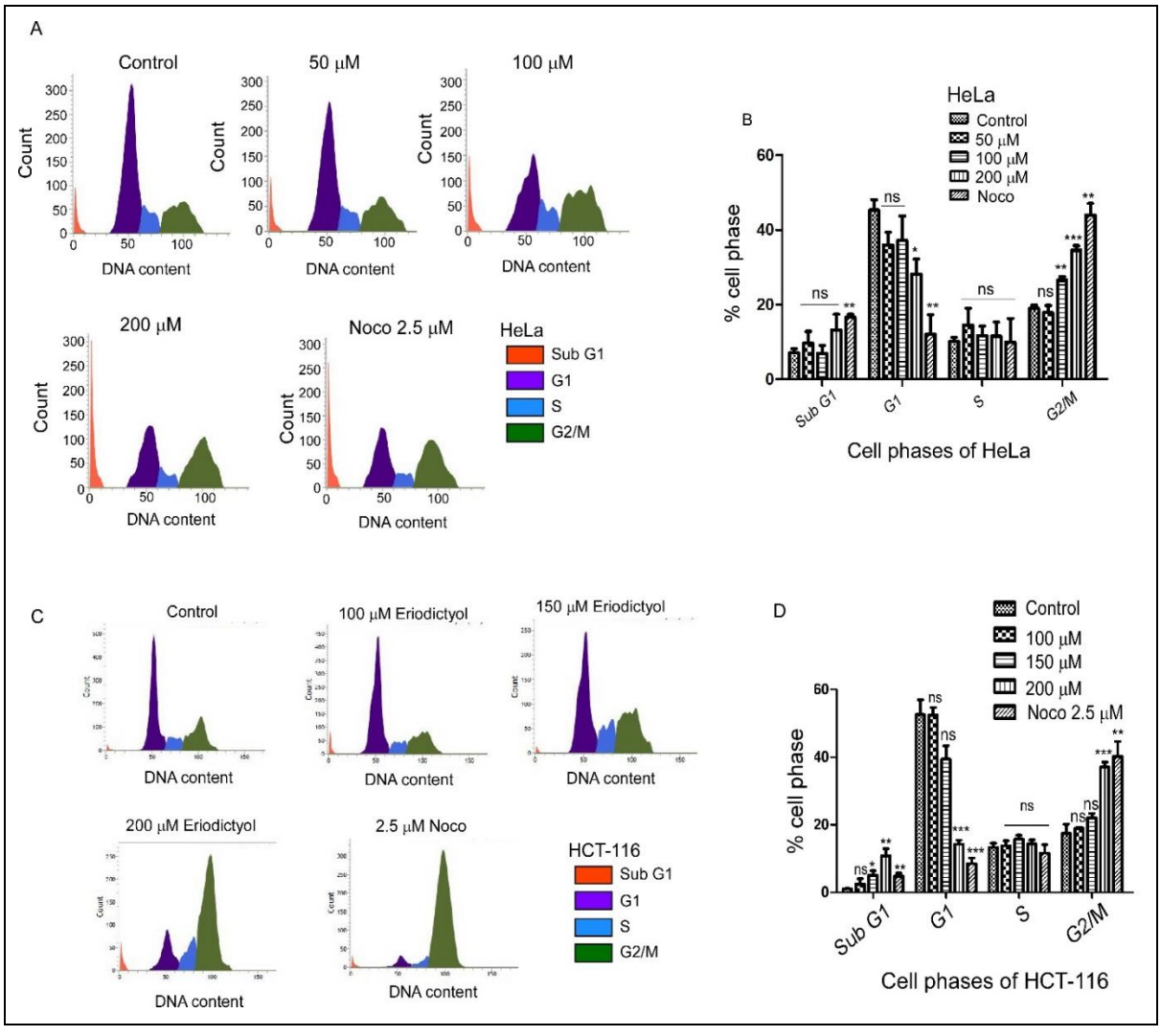

Figure 4.6 ***Eriodictyol arrests cell cycle at G2/M phase. A***. Histogram showing dose-dependent increase in G2/M phase population in HeLa at 24 h post treatment of Eriodictyol. ***B.*** Column graph depicting % of HeLa cells residing in various phases of the cell cycle with corresponding concentrations (0-200 μM) of Eriodictyol. ***C.*** Histogram showing G2/M arrest in HCT-116 in response to Eriodictyol. ***D.*** Column graph representing G2/M arrest in HCT-116 ***E.*** Western Immunoblots showing G2/M phase Cyclins and CDKs protein expression at various time points (0-72h) in response to Eriodictyol treatment. HSP90 was used as loading control.

at the G2/M-phase of the cell cycle. This was further reflected in the de-regulation of the molecular machineries involved in cell cycle regulation (Fig. 4.7). Activation of cdc2 (CDK1) by de-phosphorylation of cdc2 at Thr14 and Tyr15 by a group of phosphatases e.g., cdc 25 is viewed as a crucial regulatory step in cell progression to mitosis [25]. Thus, we examined the expression of cdc2, p-cdc2 and cdc 25 protein levels (Fig. 4.7). We observed that Eriodictyol elicits a time-dependent increase in cdc2 phosphorylation in Tyr15, as well as a decrease in cdc2 and cdc25a expression, indicating cdc2 deactivation and thereby delaying mitosis by arresting and retaining cells at the G2/M-phase. Surprisingly, Cyclin B1 expression

continuously increases possibly indicating its accumulation as cells are unable to undergo mitosis.

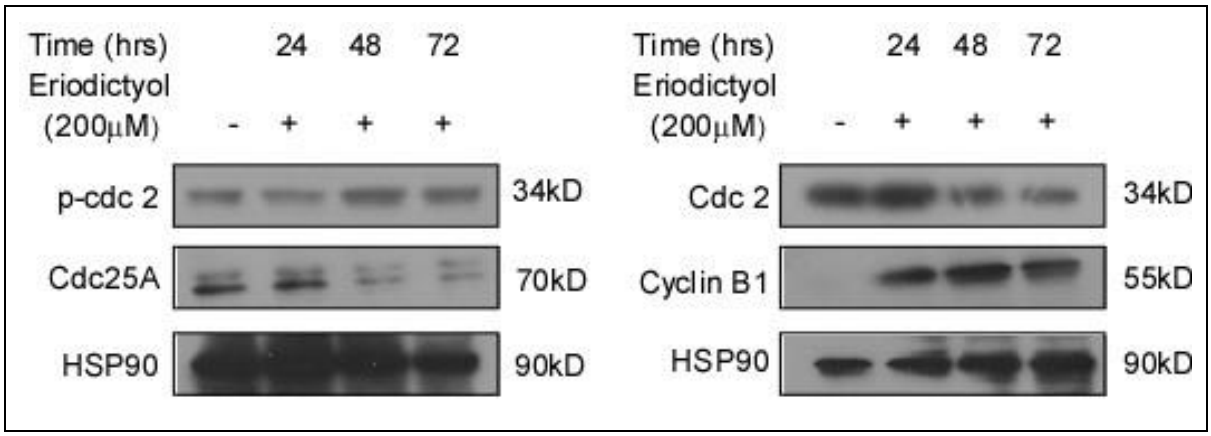

Figure 4.7 ***Mechanism of G2/M phase arrest in response to Eriodictyol treatment.*** Western Immunoblots showing G2/M phase Cyclins and CDKs protein expression at various time points (0-72h) in response to Eriodictyol treatment. HSP90 was used as loading control.

4.5 Discussion

Inflammatory cells promote tumor growth and survival by releasing growth and survival factors, promoting angiogenesis and lymphangiogenesis, stimulates DNA damage, remodels the ECM to facilitate invasion, and also coats tumor cells to make receptors for disseminating cells via lymphatics and capillaries [53]. Cancer patients frequently exhibit a lack of inflammatory responses [194]. Tumor growth is inextricably linked to cancer cell interactions with their microenvironment, which ultimately determines whether the main tumor gets eliminated, metastasizes, or establishes latent micro-metastases [195]. The cytokines and chemokines generated by tumor-associated macrophages (TAMs) and leukocytes cause cancer cells to metastasize and become angiogenic [51]. These cytokines and chemokines promote cell motility and tumor-associated vascular development. Leukocytes also stimulate angiogenesis by causing artery dilatation and tumor cell extravasation. Moreover, immune suppression-induced tolerance protects malignant cells from potentially helpful antitumor immunity, or in neonates with impaired immunocompetence due to the presence of immune-suppressive CD71+ erythroid cells [196].

Nuclear factor-kappa B (NFkB) transcription factor is with a master regulator of inflammatory responses [92]. NFkB activation opens up pathways that allow inflammatory mediators such as leukocyte adhesion molecules, cytokines, and chemokines to be activated. As a result,

mitigating persistent inflammatory conditions that must be generated in the first instance is critical to lowering the etiology of a disease caused by chronic inflammation.

Long-term usage of NSAIDs, for eg. Aspirin that target COX enzymes have been proven to reduce the incidence of colorectal, breast, lung, and bladder cancer in clinical trials [197, 198]. However, considering the GI toxicity and non-specific action of NSAIDs [199], as well as the cardiotoxicity of selective COX-2 inhibitor [200], the use of such compounds remains contentious. As a result, there is a need to identify a potentially non-toxic, anti-inflammatory lead with minimum side effects with potential as an anti-cancer compound, ideally derived from plants. Several attempts were made globally over the last two decades to identify prospective plants with anti-inflammatory properties,that might possess anti-cancer potential [201, 202]. Flavonoids and polyphenolic chemicals were the most researched and described class of anti-inflammatory chemicals derived from plants. Flavonoids are bioactive polyphenolic chemicals found in abundance in a variety of fruits, vegetables, drinks (tea, coffee), nuts, and cereal goods that have a high antioxidant capacity [203]. Many of these flavonoids, possess NFkB inhibitory activity, thereby affecting the expression of pro-inflammatory genes and hence might be exploited for modulating the inflammatory responses underlying different cancer pathologies [204, 205].

Several studies have demonstrated that Eriodictyol, an active element found in the plant Yerba Santa, suppresses inflammation [175]. The focus of this chapter is to investigate the anti-inflammatory efficacies of flavonoid as well as non-flavonoid polyphenols, and thereby identify leads that by virtue of being anti-inflammatory might display potential anti-cancer activities as well. From the initial studies, we identified Eriodictyol as a promising anti-cancer lead, primarily owing to its potent anti-inflammatory activity, and also owing to the lack of existing knowledge on its anti-cancer role or its mechanism thereof. MTT and colony formation experiments in a panel of human and murine cancer cell lines revealed that Eriodictyol greatly inhibits cell proliferation and colony growth. Further, Eriodictyol demonstrated remarkable selectivity in its ability to induce cytotoxicity towards cancer cells over normal cells. Inhibition of cellular proliferation is often a reflection of a cell undergoing programmed cell death or apoptosis, which might again be an inherent cellular mechanism to get rid of cells undergoing faulty cell cycle phases. Eriodictyol caused a dose-dependent induction in apoptosis in cancer cells, both mouse as well as human, which is significantly higher than those in normal cells. The proteins that are in control of the cell's passage through the many phases are predominantly kinases and phosphatases that interact with one another, causing their own activation or

deactivation. Cyclin-dependent kinases (Cdks) are kinases that play a critical role in the activation of other key proteins in the process through phosphorylation. They are influenced by a subset of proteins known as cyclins [206]. This intricacy enables the examination of several therapeutic targets and considerably enhances the possibility of identifying chemical compounds that allow the process to be regulated at numerous stages. They may attach directly to proteins, allowing them to be activated or inhibited, as well as downregulating or upregulating their expression.

Pharmacological intervention with any of these proteins may result in cell cycle stoppage and subsequent cell division control, which would be another viable treatment method. Eriodictyol dramatically reduced cell division cycle rates in both HeLa and HCT-116 cells via regulating phosphatase Cdc25A, cyclin-dependent kinase 1 (CDK1), and cyclin B, resulting in G2 / M cell cycle arrest. These findings suggest that Eriodictyol can cause cell cycle arrest and apoptosis in the G2/M pathway, hence inhibiting cancer cell proliferation. Surprisingly, Eriodictyol's cytotoxic activity is limited to malignant cancer cells. These results prompted us to look into the mechanism behind its selective cytotoxicity.

References

1. Qian, S., O. Golubnitschaja, and X. Zhan, *Chronic inflammation: key player and biomarker-set to predict and prevent cancer development and progression based on individualized patient profiles.* EPMA Journal, 2019. **10**(4): p. 365-381.
2. Diaz-Borjon, A., C.M. Weyand, and J.J. Goronzy, *Treatment of chronic inflammatory diseases with biologic agents: opportunities and risks for the elderly.* Experimental gerontology, 2006. **41**(12): p. 1250-1255.
3. Klein, A. and R. Eliakim, *Non Steroidal Anti-Inflammatory Drugs and Inflammatory Bowel Disease.* Pharmaceuticals (Basel, Switzerland), 2010. **3**(4): p. 1084-1092.
4. Yuan, G., et al., *Natural products and anti-inflammatory activity.* Asia Pac J Clin Nutr, 2006. **15**(2): p. 143-52.
5. Miyake, Y., K. Yamamoto, and T. Osawa, *Isolation of Eriocitrin (Eriodictyol 7-rutinoside) from Lemon Fruit (<I>Citrus limon</I> BURM. f.) and Its Antioxidative Activity.* Food Science and Technology International, Tokyo, 1997. **3**(1): p. 84-89.
6. Kumagai, K., et al., *Pretreatment of plastic petri dishes with fetal calf serum. A simple method for macrophage isolation.* Journal of Immunological Methods, 1979. **29**(1): p. 17-25.
7. Coussens, L.M. and Z. Werb, *Inflammation and cancer.* Nature, 2002. **420**(6917): p. 860-867.
8. Whiteside, T.L., *The tumor microenvironment and its role in promoting tumor growth.* Oncogene, 2008. **27**(45): p. 5904-5912.
9. Lin, Y., J. Xu, and H. Lan, *Tumor-associated macrophages in tumor metastasis: biological roles and clinical therapeutic applications.* Journal of Hematology & Oncology, 2019. **12**(1): p. 76.

10. Liu, T., et al., *NF-κB signaling in inflammation.* Signal transduction and targeted therapy, 2017. **2**: p. 17023.
11. Bosetti, C., S. Gallus, and C. La Vecchia, *Aspirin and cancer risk: an updated quantitative review to 2005.* Cancer Causes & Control, 2006. **17**(7): p. 871-888.
12. Cuzick, J., et al., *Aspirin and non-steroidal anti-inflammatory drugs for cancer prevention: an international consensus statement.* The Lancet Oncology, 2009. **10**(5): p. 501-507.
13. Halter, F., *Mechanism of gastrointestinal toxicity of NSAIDs.* Scand J Rheumatol Suppl, 1988. **73**: p. 16-21.
14. Davies, N.M. and F. Jamali, *COX-2 selective inhibitors cardiac toxicity: getting to the heart of the matter.* J Pharm Pharm Sci, 2004. **7**(3): p. 332-6.
15. Panche, A.N., A.D. Diwan, and S.R. Chandra, *Flavonoids: an overview.* Journal of nutritional science, 2016. **5**: p. e47-e47.
16. Lee, J.K., *Anti-inflammatory effects of eriodictyol in lipopolysaccharide-stimulated raw 264.7 murine macrophages.* Arch Pharm Res, 2011. **34**(4): p. 671-9.
17. Otto, T. and P. Sicinski, *Cell cycle proteins as promising targets in cancer therapy.* Nature Reviews Cancer, 2017. **17**(2): p. 93-115.
18. Shapiro, G.I. and J.W. Harper, *Anticancer drug targets: cell cycle and checkpoint control.* The Journal of clinical investigation, 1999. **104**(12): p. 1645-1653.
19. Lee, J.H. and J.M. Berger, *Cell Cycle-Dependent Control and Roles of DNA Topoisomerase II.* Genes, 2019. **10**(11): p. 859.

3. Chapter II

Defining the anti-cancer role of Eriodictyol, and delineating the mechanism of its selective cytotoxicity

5.1 Abstract

In order to address the precise molecular mechanism underlying Eriodicty'l's anti-cancer effect observed and its selective cytotoxicity towards cancer cells, we took a global transcriptome sequencing approach through NGS, followed by validation using classical biochemical and cell biological studies. Transcriptomic data identified signaling processes involved in TNFR1 signaling in Eriodictyol mediated modulation of gene expression and associated biological processes. We observed marked modulation of genes involved in apoptosis, cell cycle and metastasis. Moreover, mapping of the entire signaling cascade of cell death, revealed that Eriodictyol induced cell death by increasing TNFR1 and DISC complex related proteins, causing a disruption of the homeostasis between pro- and anti-apoptotic proteins, thereby leading to the induction of cancer cell apoptosis. It's worth noting that the baseline level of TNFR1 in normal cells (HEK, NKE and WI-38) is minimal and remains constant even after Eriodictyol administration. However, in cancer cell lines (HeLa and SK-RC-45), a large quantity of basal TNFR1 is present, and it substantially increases following treatment with the compound. Finally, Eriodictyol-mediated induction of apoptosis was significantly blocked in $TNFR1^{KO}$ cells (CRISPR/Cas9) compared to the $TNFR1^{WT}$ Hela cells, confirming that Eriodictyol-mediated cancer cell apoptosis is TNFR1-dependent, and also the underlying reason for its displayed selective cytotoxicity. Here, we not only identified the signaling mechanism behind Eriodictyol's role in inducing apoptosis to cancer cells, but also uncovered the potential mechanism underlying its observed selective cytotoxicity.

5.2 Introduction

Apoptosis induction in tumor cells in response to several anti-cancer drugs have been previously demonstrated [207]. Since this apoptosis program in the tumor cells is critical in removing tumor cells in response to chemotherapy, it is hypothesized that a de-regulation in

the apoptotic signaling pathway may result in a novel type of multidrug resistance (MDR) in tumor cells [208]. The

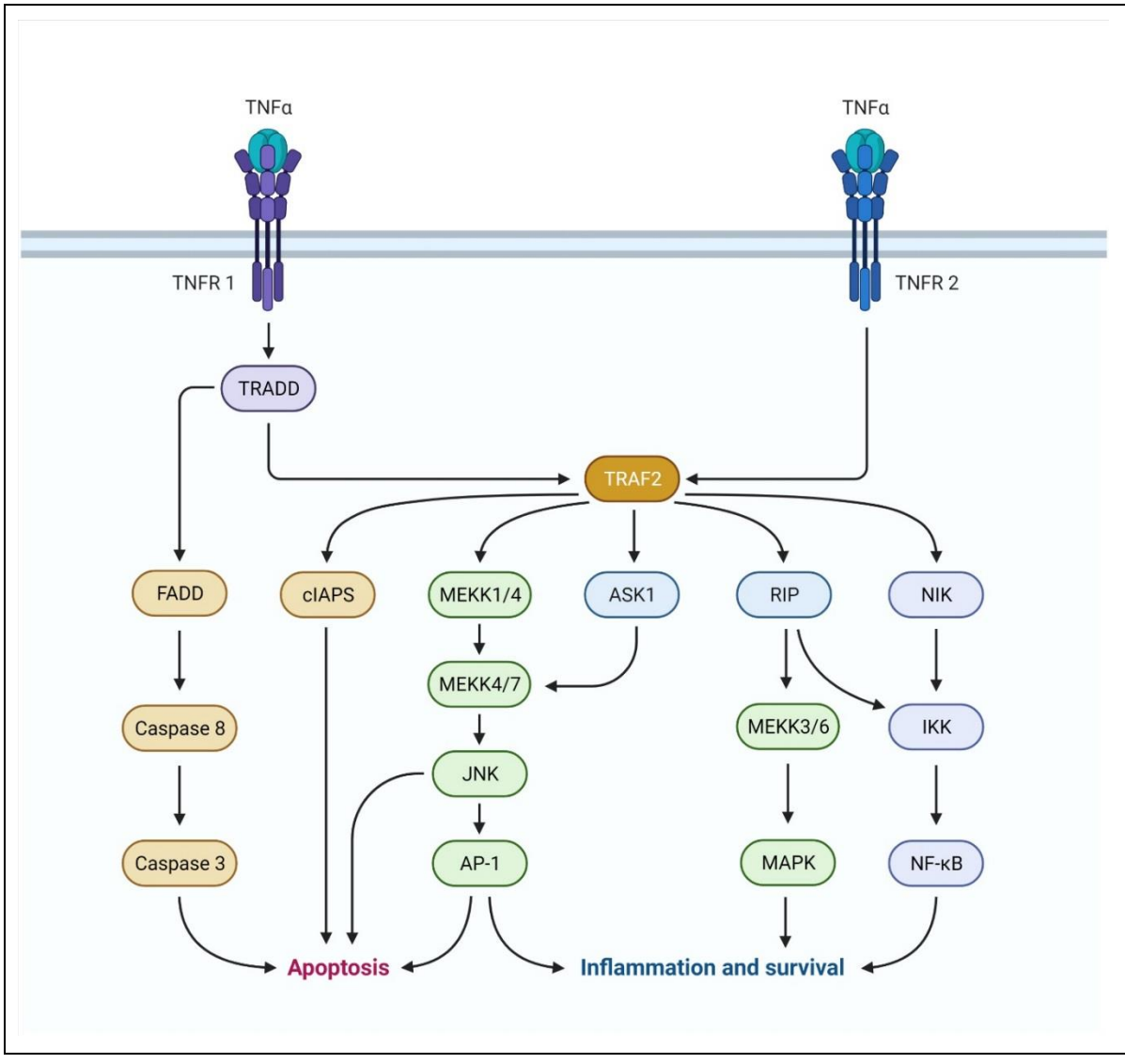

Figure 5.1 ***TNFR1-mediated survival and cell death pathways.*** The binding of TNFα to TNFR1 triggers multiple signaling pathways, including NF-κB, apoptosis and necroptosis. Upon stimulation, TNFα induces the formation of a membrane-associated complex I, which consists of RIPK1, TRADD, TRAF2/5, LUBAC and cIAP1/2. Within complex I, cIAP1/2 and LUBAC induce Lys63-linked polyubiquitination of RIPK1. The polyubiquitin chain of RIPK1 serves as a scaffold for further recruitment of IKK (IKKα, IKKβ) and TAK1(TAK1, TAB1 and TAB2) complexes, eventually leading to activation of NF-κB pathway and cell survival. Deubiquitination of RIPK1 by CYLD or A20 induces the dissociation of TRADD and RIPK1 from TNFR1, which leads to the formation of either of complex IIa or complex IIb. FADD and pro-caspase-8 are recruited to TRADD and RIPK1 to form complex IIa, resulting in the activation of caspase-8 by oligomerization and cleavage. In the absence of cIAP1/2, TAK1 or IKK complex, complex IIb, which contains RIPK1, FADD and pro-caspase-8 except TRADD, is formed and then activate caspase-8. Then, caspase-8 induces apoptosis. RIPK3-dependent necroptosis is induced when caspase-8 activity is blocked, for example by cFLIP or the pan-caspase inhibitor zVAD-fmk.

chemotherapeutic drugs, as the apoptosis signaling pathway malfunction actually save the

tumor cells from apoptosis, resulting in a significant increase in their lifespan. When this occurs in clinical settings, deficiencies in apoptotic signaling may add to treatment challenges since malignancies frequently demonstrate broader patterns of chemotherapy and radiation resistance than those characterized by the typical MDR phenotype. Many additional compounds were identified as apoptosis inducers or tumor-suppressors. Overexpression of apoptotic inhibitors such as Bcl-2 / Bcl-XL has been demonstrated to produce both *in vitro* and *in vivo* treatment resistance [209]. Furthermore, a lack of apoptotic positive mediators such as p53 leads to resistance to many anticancer drugs [210]. Recently, it has been discovered that several oncogenes not only prevent apoptosis but also enhance growth signals. Such data clearly suggest that apoptotic modulators may be one of the key drivers of chemotherapy resistance in tumor cells, and that factors or medicines targeting these molecules may be candidates as novel chemosensitizer [211].

TNF-α causes the extrinsic apoptotic pathway to be activated by interacting to cell surface receptors such as TNFR1 [212]. The tumor necrosis factor receptor 1 (TNFR1) is involved in a variety of cell responses. When its ligand (TNF) activates TNFR1, it can create two complexes with opposing effects on cell fate: a pro-survival complex and a pro-apoptotic complex. The pro-survival activator NF-kB outnumbers the pro-apoptotic Caspase-8 activation in the presence of TRAF2-phosphorylated TNF. TRAF2 phosphorylation on Ser 11 promotes the ubiquitination of the receptor-interacting protein 1 (RIP1), which induces the recruitment and activation of the kinase complex (IKK) downstream. This coincides with NF-kB activation while also inhibiting RIP1 from interacting with the protein and pro-Fas-associated caspase-8's death domain (FADD). Under pro-apoptotic conditions, RIP1 splits from TRAF2 and joins the FADD / Caspase-8 group. Caspase-8 promotes extrinsic apoptosis by cleaving and deactivates RIP1 [213].

Human TNF was used in clinical trials to assess the anticancer activity of TNF family members, mainly in advanced solid tumors [214]. Several clinical trials have looked at humanized monoclonal TNF (rhTNF) as a systemic treatment, both as a single drug and in conjunction with chemotherapeutics [215]. While rhTNF was found to be an efficient anticancer drug in preclinical investigations, clinical action was seldom attained; rhTNF was unable to trigger apoptosis via TNFR1 unless the original NF-kB pathway was repressed. rhTNF, on the other hand, was highly cytotoxic to hepatocytes, resulting in considerable side effects with little or no therapeutic effectiveness [216]. As a conclusion, it is crucial for the establishment of rational

death receptor-targeted treatment to identify medicines that stimulate death receptors without activating the NF-kB cascade.

5.3 Experimental procedures

i. *Reagents.* Eriodictyol (#89061) was purchased from Merck, India. Primers were procured from IDT (USA)-. Antibodies for TRADD (#3994), FADD (#2782), TNFRI (#3736), Bax (#3994), survivin (#2808), H2A.X (#80312), p21 (#2947), caspase7 (#9494), caspase 8 (#9746), HSP90 (#4874), cdc25a (#3652), and PARP1 (#9532) were purchased from Cell Signaling Technology (USA). Biobharati Life Sciences Pvt. Ltd. provided the antibodies for the housekeeping genes β-actin (BB-AB0024) and GAPDH (BB-AB0060). Bcl2 (sc-7382) was purchased from Santa Cruz Biotechnologies (USA). Abcam provided primary antibodies for Cdc2 (ab 18), phospho-Cdc2 (Tyr15) (ab47594), Cyclin B1 (ab32053), and a colorimetric test kit for caspase 3 (ab39401). The Z-VAD-FMK was procured from Santa Cruz Biotechnologies (sc3067). FBS (#16000044), L-glutamine, gentamicin, sodium pyruvate, and MEM non-essential amino acids were all obtained from GIBCO.

ii. *RNA sequencing data analysis.* RNA was isolated using Trizol reagent (Invitrogen) and treated with RNase free DNase (Thermo) to get rid of any contaminating DNA. The quality of the RNA samples were checked on Agilent Tape Station and quantified by Qubit Fluorometer. After obtaining the Qubit concentration for the libraries and the average peak sizes from the Agilent Tape Station profile, the PE Illumina libraries were loaded onto Novaseq6000 for cluster creation and sequencing. Quality check of fastq reads of raw long RNA seq data were performed with FastQC v.0.11.7. This was followed by Adapter trimming with Cutadapt v1.16. The trimmed reads were aligned with Human GENCODE hg38 reference genome with Hisat2 2.1.0. Following the sorting of Bam files with Samtools v1.19, transcripts assembly and differential gene analysis were performed with Cufflinks v2.2.2.1 and Cuffdiff v2.2.1 respectively and differentially expressed genes with fold change greater than equal to 2 and p and q value cut off of less than 0.05 were filtered out. Finally, gene enrichment and pathway analysis were performed with IPA (Ingenuity Pathway Analysis) software (June, 2020).

iii. *Western immunoblotting*. In short, RIPA buffer was employed to generate cell lysates from HeLa cells after Eriodictyol treatment (150 µM). 30–50 µg proteins were resolved on 10–

15% SDS-PAGE, transferred to a PVDF/nitrocellulose membrane (Millipore, USA), blocked with 5% BSA diluted in 1X TBST, and then probed with the appropriate primary and secondary antibodies. Finally, blots were developed on X-Ray films using the ECL (Bio-Rad) process or visualized in the Chemidoc MP system (Bio-Rad).

iv. *Caspase-3/7 activation assay.* Post Eriodictyol treatment, cell lysates from HeLa cells were prepared using RIPA buffer. 150 µg aliquot of protein was loaded in each condition. According to the manufacturer's instructions, DTT and DEVD-p-NA substrate were also added. The samples were mixed thoroughly at 37°C for 90 minutes before measuring the OD at 405 nm in a Multiskan GO microplate reader (Thermo-Fisher Scientific).

v. *Design, construction and validation of TNFR1 CRISPR.* Guide oligos (20 mers) were designed from TNFR1 exon 2 site using ***http://crispr.mit.edu***, to completely disrupt the protein and the sgRNA (guide oligo) was chosen on the basis of high "on-target score" and low "off-target score" in the whole exome. Guide oligo was then cloned into the Cas9 expression vector having a puromycin selection cassette. Guide oligo cloned vector was sequence verified and TNFR1-CRISPR plasmid was then transfected into HeLa cells using lipofectamine LTX reagent (Invitrogen) to check the functionality of the CRISPR plasmids within the cells. Following initial selection with puromycin (1mg/ml) over the week, genomic DNA was isolated from transfected cells and mismatch heteroduplex sensing T7E1 assay was performed [217]. Next, clonal expansion from single cells was performed followed by immunoblotting of clonally expanded cells to screen for stable TNFR1-CRISPR knockout cells.

vi. *RNA isolation and real-time PCR.* Total RNA was extracted with Trizol reagent (Invitrogen). 1 µg of RNA was isolated from HeLa cells treated with either Eriodictyol or DMSO. To convert RNA to cDNA, a Verso cDNA synthesis kit (ThermoFisher Scientific) was utilized. Real-time PCR was carried out in triplicate using a diluted stock of cDNA (1:6) on an Applied Biosystems 7500 Fast or QuantStudio 3 thermal cycler using the SYBR green PCR equipment. Each mRNA quantification data set was normalized to GAPDH and represented as fold changes in target gene expression compared to non-treated samples. Primers used in this study are the following: TNFα: 5'-TGTAGCAAACCCTCAAGC-3' (forward), 5'- TGGGAGTAGATGAGGTACAG-3'

(reverse); TNFR1: 5'- TTCGTCCC TGAGCCTTT-3' (forward), 5'-CAGGAGTGCCAAGTTTCTAT-3' (reverse); GAPDH: 5'-ACAACTTTGGTATCGTGGAAGG-3' (forward), 5'-GCCATCACGCCACAGTTTC-3' (reverse).

5.4 Results

i. *Eriodictyol treatment induces differential expression of various gene sets implicated in proliferation, cell-cycle, and apoptosis-related pathways.*

To have a better understanding of the global modulation in gene expression, we performed transcriptomic analysis of Eriodictyol in HeLa cells treated with 150 µM dose at early (6h) and late (24h) time points, along with DMSO-treated control. Log_2Fold Change (log_2FC) values ≥0.5 were considered upregulated whereas less than 0.5 were downregulated. Differentially Regulated Gene sets (DRGs) sets were analyzed by hierarchical clustering (Heat Map) which indicated distinct differential gene expression signatures among Eriodictyol treated and non-treated samples. The heat map (Fig.5.2A) shows markedly different clustering of gene sets in Eriodictyol treated versus non-treated cells, as evidenced by the primary analysis of the data on the Differentially Regulated Gene sets (DRGs). For our research, we chose transcripts with a fold change (FC) of 2 and a p-value of 0.05. The number of upregulated (apoptosis inducers and tumor suppressors) and downregulated (metastasis inducers and cell cycle regulators) genes have increased dramatically as shown in the volcano plot (Fig. 5.2B). With IPA (Ingenuity Pathway Analysis), gene enrichment and pathway analysis were performed, and the results were divided into three clusters (metastasis, apoptosis, and cell cycle) and shown as Venn diagrams (Fig. 5.2C). Furthermore, we constructed a heat map (Fig. 5.2D) depicting common tumor-related genes that are mostly affected by Eriodictyol, which shows a substantial difference in gene expression profiling in Eriodictyol-treated versus non-treated cells. In response to Eriodictyol, the data clearly reveals unique overexpression of apoptosis inducers and tumor suppressors, as well as a considerable decrease in oncogenes and cell cycle regulators. Finally, considerable modulation of important biological processes in response to Eriodictyol administration is depicted as a bar diagram, many of which are connected to or engaged in apoptosis, metastasis, and cell cycle regulation (Fig. 5.3A). According to the results of the canonical pathway analysis, it appears that

Eriodictyol might be implicated in cell cycle control, particularly at the G2/M phase.. Eriodictyol may be implicated in cell cycle control, particularly at the G2/M phase, according to the results of canonical pathway analysis. Pathway analysis also reveals multiple pathways involved in the modulation of the cell cycle, DNA damage, and apoptotic responses, some of which are depicted

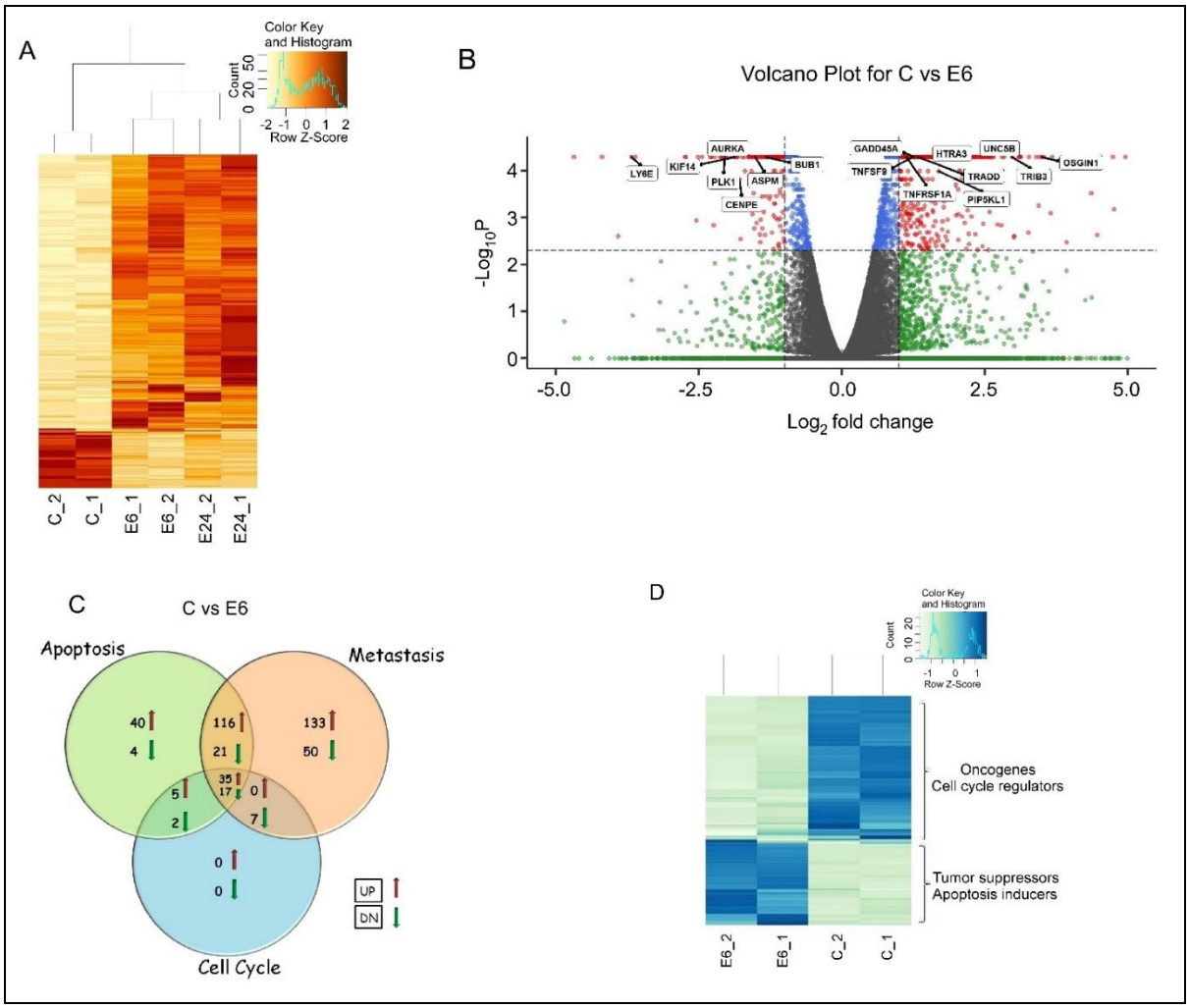

Figure 5.2 ***Eriodictyol treatment causes differential expression of different gene sets involved in apoptosis, metastasis, cell-cycle regulatory genes, and associated pathways in HeLa cells. A***. A heat map showing differential regulation of global genes in response to Eriodictyol treatment in both 6 h (E6_1, E6_2) and 24 h (E24_1, E24_2) in comparison to untreated control (C_1, C_2). ***B.*** Volcano plot depicting the differentially regulated global genes at 6 h post treatment. ***C.*** Venn diagram analysis exhibiting total no. of apoptosis, metastasis and cell cycle regulatory genes at 6h treatment. ***D.*** Heatmap displaying a screened set of genes highly affected by Eriodictyol at 6 h through IPA analysis. C_1- Untreated sample 1, C_2- Untreated sample 2, E6_1 - Treated sample 6h sample 1, E6_2 - Treated sample 6 h sample 2, E24_1 - Treated sample 24h sample 1, E24_2 - Treated sample 24h sample 2.

in Fig. 5.3 B. TNFR1 is an interesting example of a gene that is not only considerably elevated but also frequently engaged in numerous of these pathways. To conclude, Eriodictyol produces differential gene expression, many of which are involved in the induction of apoptosis, cell

cycle arrest, and cytotoxicity in tumor cells, and hence indicative of a potential role of Eriodictyol in modulating these pathways in controlling tumorigenesis.

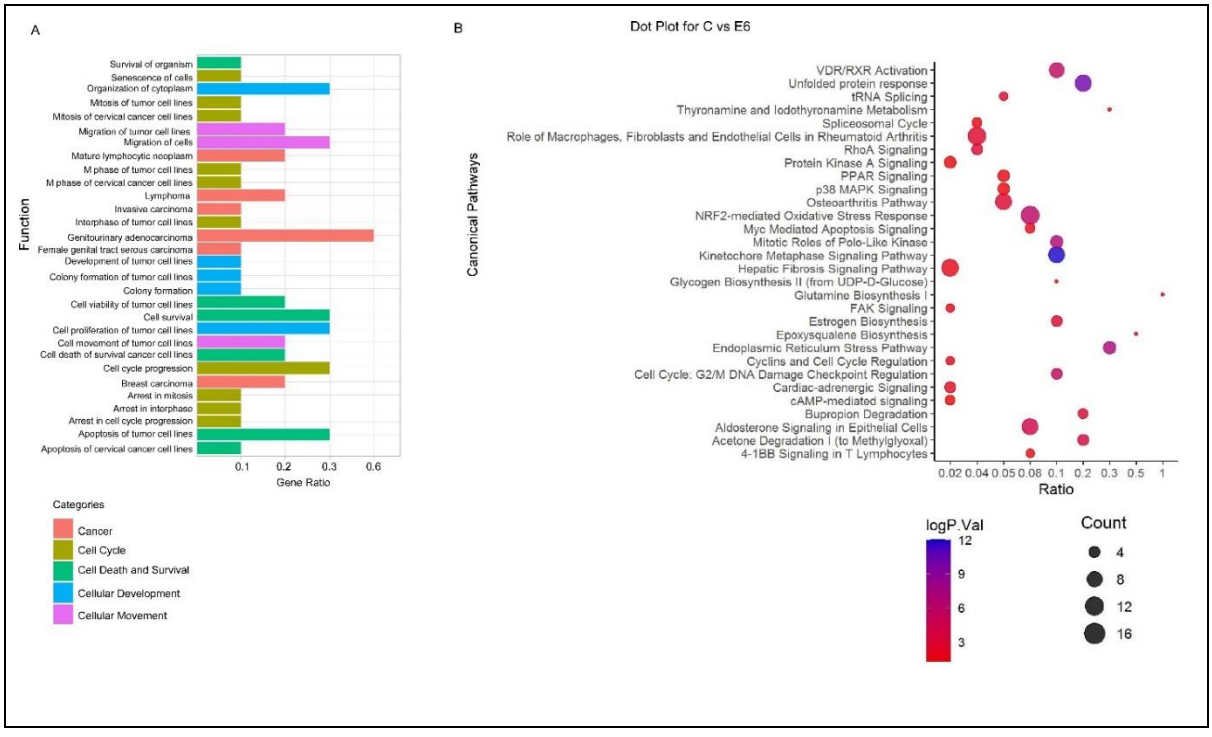

Figure 5.3: ***Eriodictyol treatment causes differential expression of different gene sets involved in apoptosis, metastasis, cell-cycle regulatory genes, and associated pathways in HeLa cells. A.*** Functional analysis represented as bar plot C vs E6. ***B.*** Ingenuity Pathway Analysis. The degree of enrichment of this analysis is shown by the colour intensity of the nodes. The enrich-factor is defined as the ratio of differentiating genes over the entire genome. The number of genes in a pathway is shown by the size of the dots.C_1- Untreated sample 1, C_2- Untreated sample 2, E6_1 - Treated sample 6h sample 1, E6_2 - Treated sample 6 h sample 2, E24_1 - Treated sample 24h sample 1, E24_2 - Treated sample 24h sample 2.

ii. Eriodictyol perturbs the balance between pro-apoptotic/anti-apoptotic signaling in cancer cells.

In order to further confirm and validate the transcriptomic data, we mapped the entire signaling cascade leading to Eriodictyol mediated cell death. Investigation into the molecular events underlying Eriodictyol-induced apoptosis in HeLa cells indicate significant time-dependent up-regulation in the expression of the pro-apoptotic DISC components, i.e. TNFR1, FADD and TRADD in HeLa cells (Fig. 5.4A), suggesting the involvement of the DISC complex in response to Eriodictyol treatment. Eriodictyol also caused a significant time-dependent increase in pro-apoptotic Bax, as well as a substantial time-dependent decrease in anti-apoptotic Bcl2 and Survivin (Fig. 5.4B), tipping the scales in favor of pro-apoptotic outcomes.

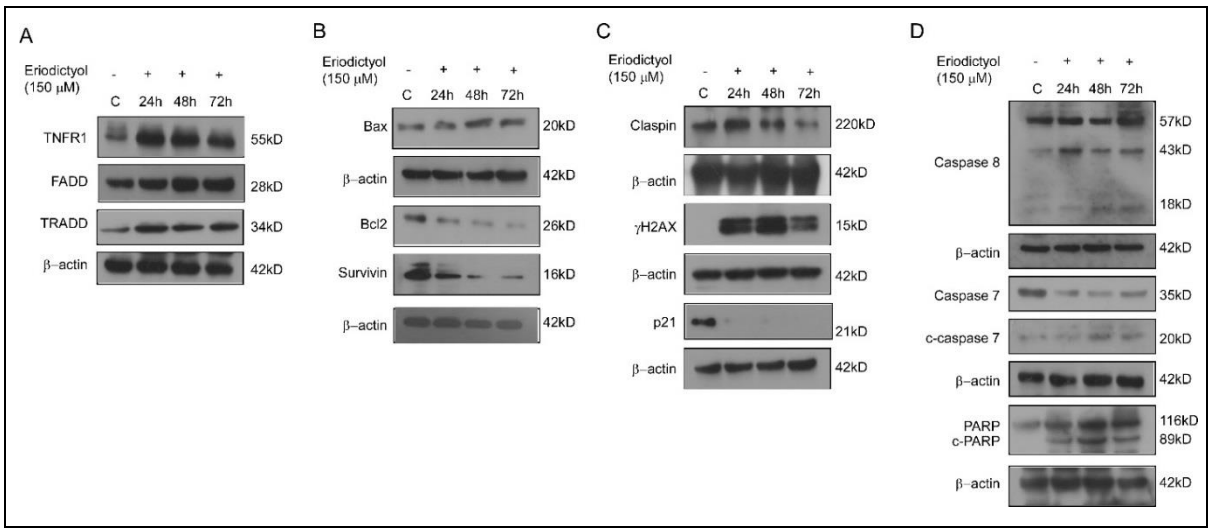

Figure 5.4: ***Cancer cell apoptosis induced by Eriodictyol involves the extrinsic pathway. A.*** Western immunoblots depicting increase in the expression levels of TNFR1, FADD and TRADD expression in HeLa cells upon Eriodictyol treatment. ***B.*** Alteration in Bax, Bcl2 and Survivin expression. ***C.*** Western immunoblots showing activation of DNA damage responsive protein expression in HeLa upon Eriodictyol treatment. ***D.*** Caspase cascade activation and PARP1 cleavage in HeLa cells upon Eriodictyol treatment.

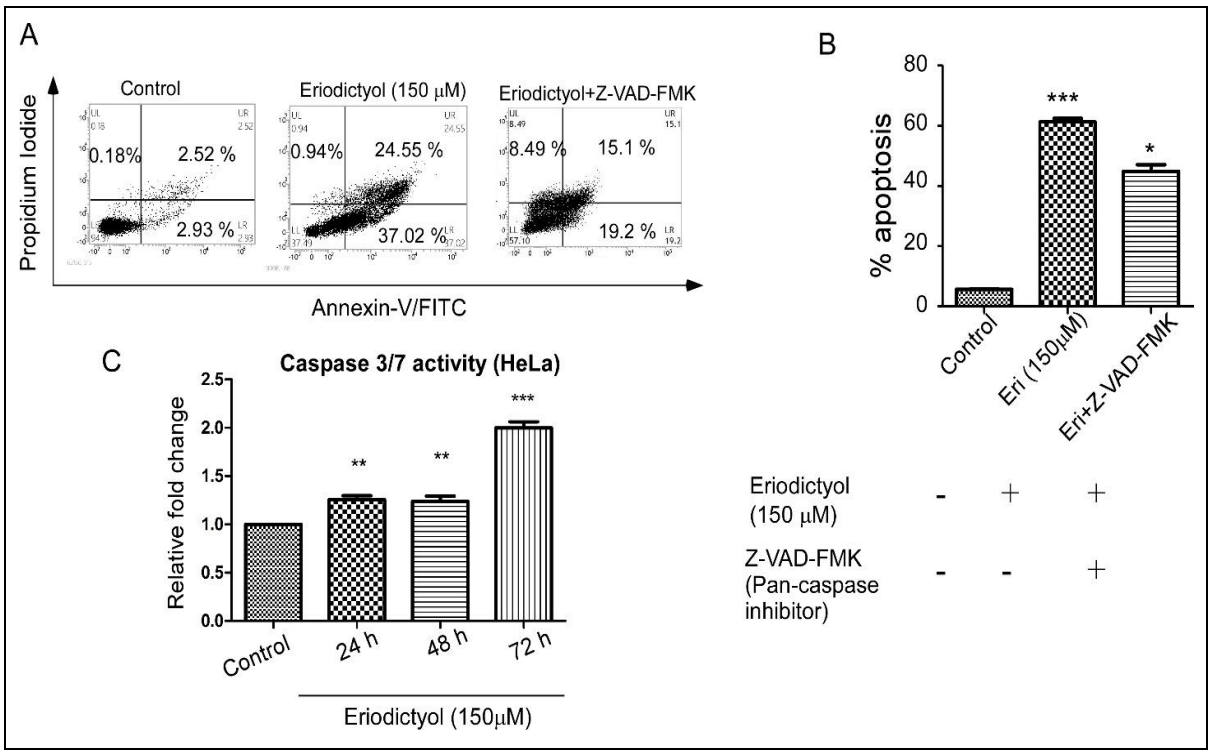

Figure 5.5 ***Eriodictyol mediated apoptosis is caspase-dependent. A, B.*** Density plot and column graph from flow cytometry analysis (BD FACSuite™) showing Eriodictyol mediated apoptosis in presence of pan-caspase inhibitor (Z-VAD-FMK) at 20 μM concentration, indicating that Eriodictyol mediated apoptosis is caspase dependent. ***C.*** Caspase 3/7 activity in response to Eriodictyol treatment at 24, 48, and 72h is depicted in a column graph. Data represent Mean ± SEM, analyzed by Student's t-test (two-tailed); *p < 0.05, **p < 0.01, ***p < 0.001, ns not significant.

In HeLa cells, Eriodictyol caused a time dependent cleavage of the full-length 116 kDa PARP1 to the cleaved 89 kDa form (c-PARP1) (Fig. 5.4D). Pretreatment of HeLa cells with a 20 μM inhibitor of PAN-caspase (Z-VAD-FMK) provided a substantial (31% inhibition) and considerable protection against Eriodictyol-mediated apoptosis (Fig. 5.5 A, B), demonstrating that Eriodictyol-mediated tumor cell apoptosis is at least to some extent caspase-dependent. Fig. 5.5C ultimately confirms activation of caspase 3/7 activity in HeLa cells (24, 48 and 72 h). As a result, we conclude that Eriodictyol upregulates pro-apoptotic proteomes and produces a considerable reduction in survival proteins in cancer cells, thereby disturbing the apoptome homeostasis, resulting in a pro-apoptotic outcome.

iii. TNFR1 is the potential target of Eriodictyol, and the primary player underlying its selective cytotoxicity.

To analyze the molecular mechanism and signaling axes involved in the inhibition of cancer cell proliferation mediated by Eriodictyol, we performed an RNA-sequencing analysis to look for possible Eriodictyol targets (Fig. 5.2). Earlier from the volcano plot data we have seen high up-regulation of TNFR1 (Fig. 5.2 B). Hence, the RNA-seq data was re-analyzed for identifying the genes that might be involved in the TNFR1 signaling pathway (Fig 5.6A). This RNA-seq data is further validated by Real-Time PCR data which shows increased TNF-α and TNFR1 mRNA levels time-dependently (Fig. 5.6 B, C). It is well known that TNFR1 is the active upstream receptor in the extrinsic apoptosis pathway [27]. Moreover, Eriodictyol treatment upregulates the protein expression level of TNFR1 (Fig. 5.6 D). Western blot results clearly demonstrated that the level of TNFR1 protein expression in cancer cells is significantly higher than that in normal cells, thereby implying that lack of TNFR1 receptor expression in normal cells may be the underlying reason for the observed selective activity against the cancer cells (Fig 5.6 E). It was also observed that Eriodictyol treatment at 24 h and 48 h, in contrast to normal cells, led to a substantial time-dependent expression of TNFR1 in only cancer cells (SK-RC-45 and HeLa) (Fig. 5.6 F), thus establishing the basis for the selective cytotoxic efficacy of Eriodictyol in cancer cells. Furthermore, remarkable dose-dependent up-regulation in the induction of TNFR1 expression in HeLa cells initiated at 100 μM concentration of Eriodictyol compared to negligible or no TNFR1 expression in WI-38 and NKE cells, respectively, (Fig. 5.6 G), which correlated with the respective dose-dependent apoptotic window in HeLa cells (Fig 4.5).

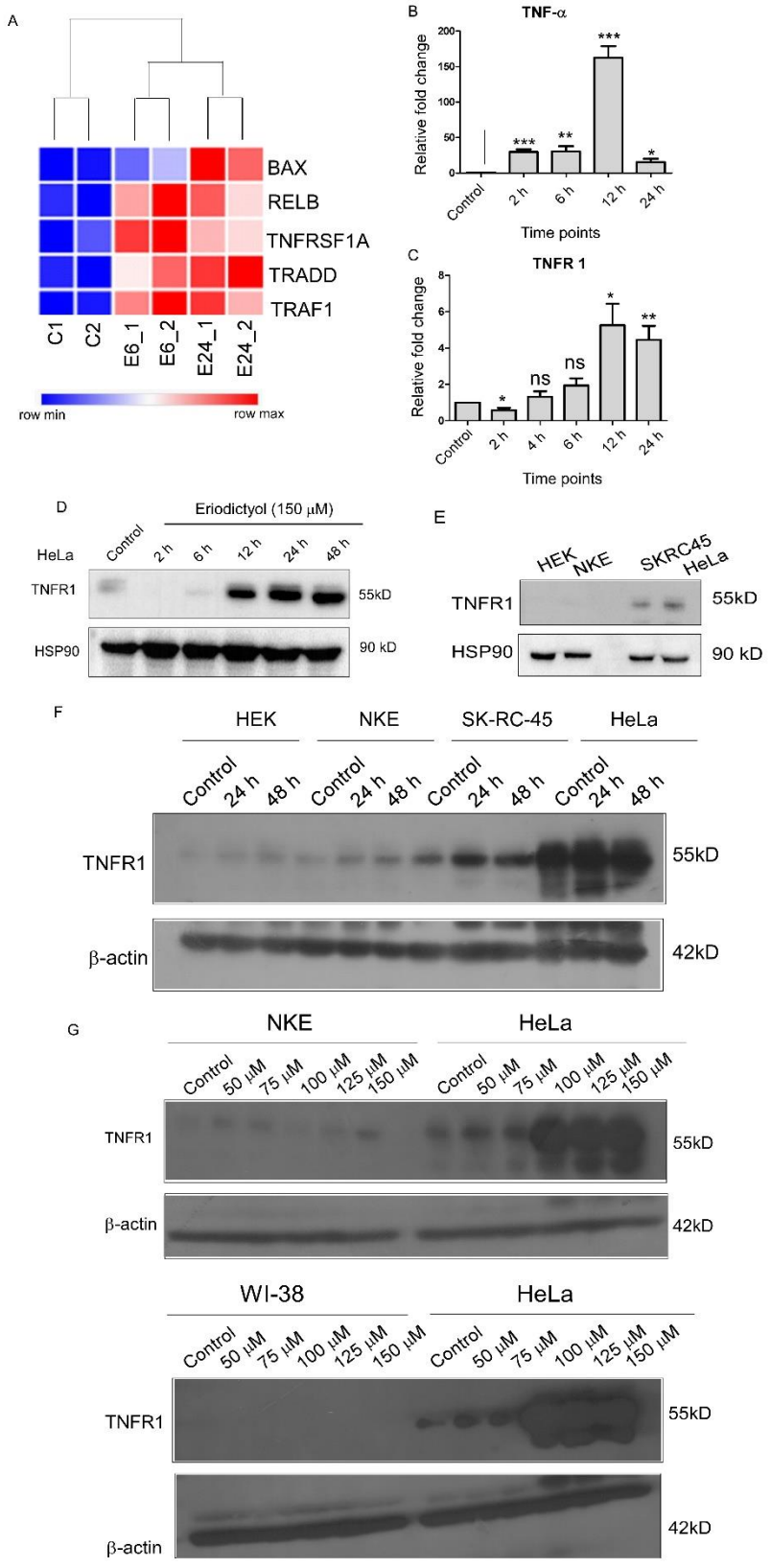

Figure 5.6 ***Eriodictyol selectively activates TNFR1 in cancer cells but not in normal cells.*** **A.** Heat map depicting RNA expression level of TNFR1 target genes. ***B, C.*** Real time PCR reflecting time-dependent relative fold change in mRNA expression of TNF-α and TNFR1 respectively in response to Eriodictyol (150 μM). Relative expression values of target genes were normalized to their corresponding GAPDH Ct value and represented as fold change with respect to untreated control. Data represent mean ± SEM (Student's t-test (two-tailed); *p < 0.05, **p < 0.01, ***p < 0.001, ns-not significant). ***D.*** Western immunoblot data showing time-dependent induction in TNFR1 expression in HeLa cells upon Eriodictyol (150 μM) treatment. ***E.*** Western immunoblot confirming the basal expression level of TNFR1 in cancer lines (SK-RC-45 and HeLa) compared to normal cells (HEK and NKE). ***F***. Western immunoblot showing that Eriodictyol (150 μM) treatment elicits time-dependent (0h, 24h, 48h) induction in TNFR1 expression in the cancer cell line, HeLa but not in normal cell lines (NKE and HEK). ***G.*** Comparison of TNFR1 expression in NKE vs HeLa (Top panel) and WI-38 vs HeLa (Bottom panel) respectively in response to various doses of Eriodictyol.

iv. Eriodictyol-mediated cancer cell apoptosis is TNFR1-dependent.

Finally, we exploited CRISPR-Cas9 genome editing technology to produce TNFR1-knockout cells (Fig. 5.7), to validate that TNFR1 plays a direct role in Eriodictyol-mediated apoptosis regulation (Fig. 5.8 D,E). Four of the ten clones tested for TNFR1 expression patterns (Fig. 5.8 A) appear to have entirely depleted TNFR1 expression. For the following studies, TNFR1 KO clone#6 (Fig. 5.8 B) is used which is completely devoid of TNFR1 expression and also characterization of this clone shows an insertion of 4 bp sequence which causes frameshift mutation (Fig. 5.8 C). While Eriodictyol induces significant apoptosis in wild type HeLa cells (>40 percent annexin V/PI + cells) at 150 µM, the density plot and bar graph (Fig. 5.8 D, E) show a marked decrease in apoptosis in TNFR1 KO clone KO-6 (7% annexin V/PI + cells), confirming that Eriodictyol-mediated tumor cell apoptosis is exclusively TNFR1 dependent.

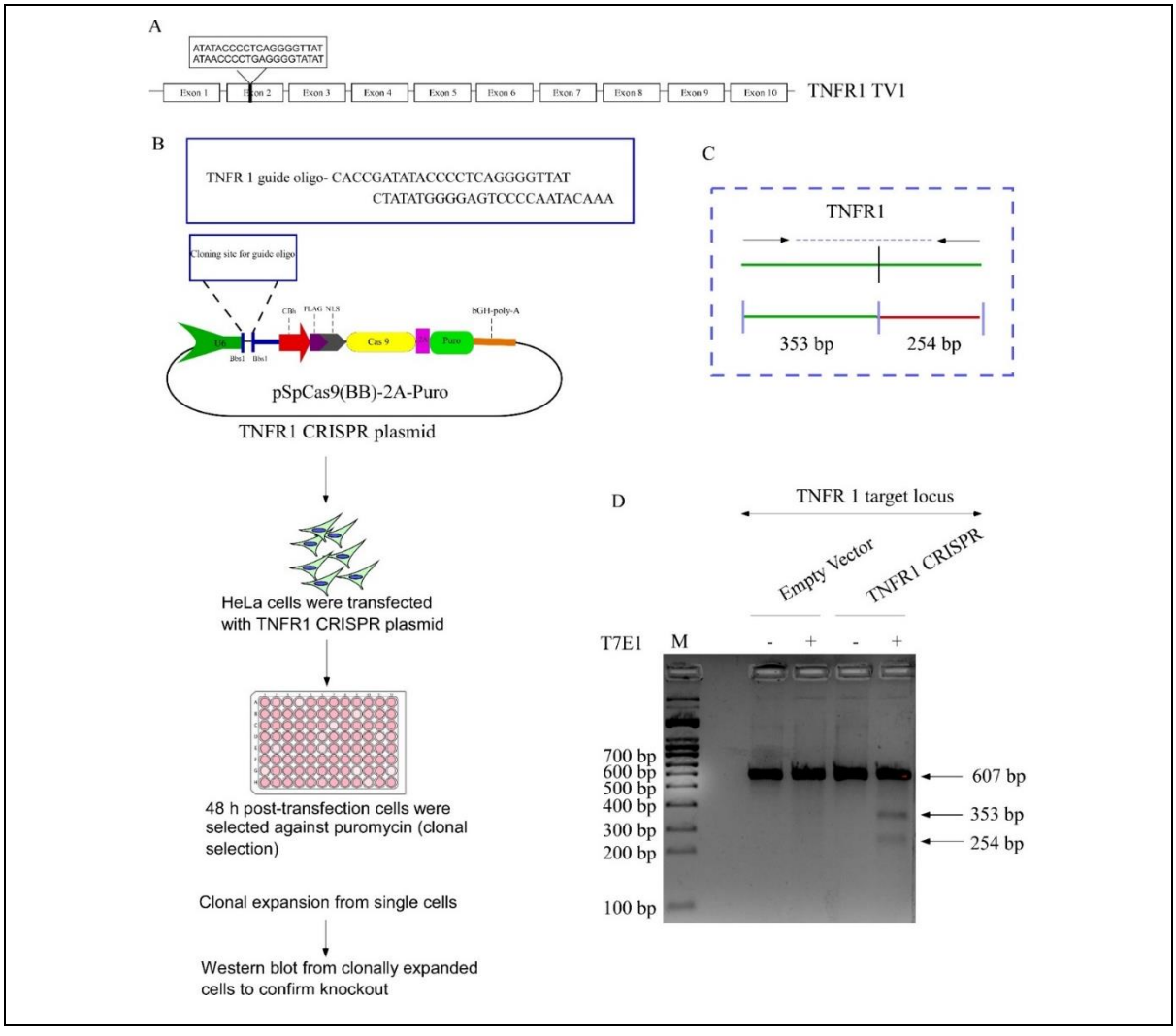

Figure 5.7 ***A.*** Pictorial representation of TNFR1 gene Transcript variant 1 (TV 1). ***B.*** Guide oligo cloned vector inserted into TNFR1-CRISPR plasmid (pSpCas9(BB)-2A-Puro) was transfected into HeLa cells using lipofectamine LTX reagent to check the functionality of the CRISPR plasmids within the cells, followed by selection with puromycin over the week. Clonal expansion from single cells were verified by western immunoblot. ***C.*** The genomic region covering the Cas9 target region was PCR amplified for T7E1 assay. ***D.*** Mismatched heteroduplex genomic DNA isolated from transfected cells were digested with T7E1 endonuclease. It showed that our constructed TNFR1-CRISPR was functional only when guide oligo cloned vectors were transfected into HeLa cells as indicated by two cleaved bands.

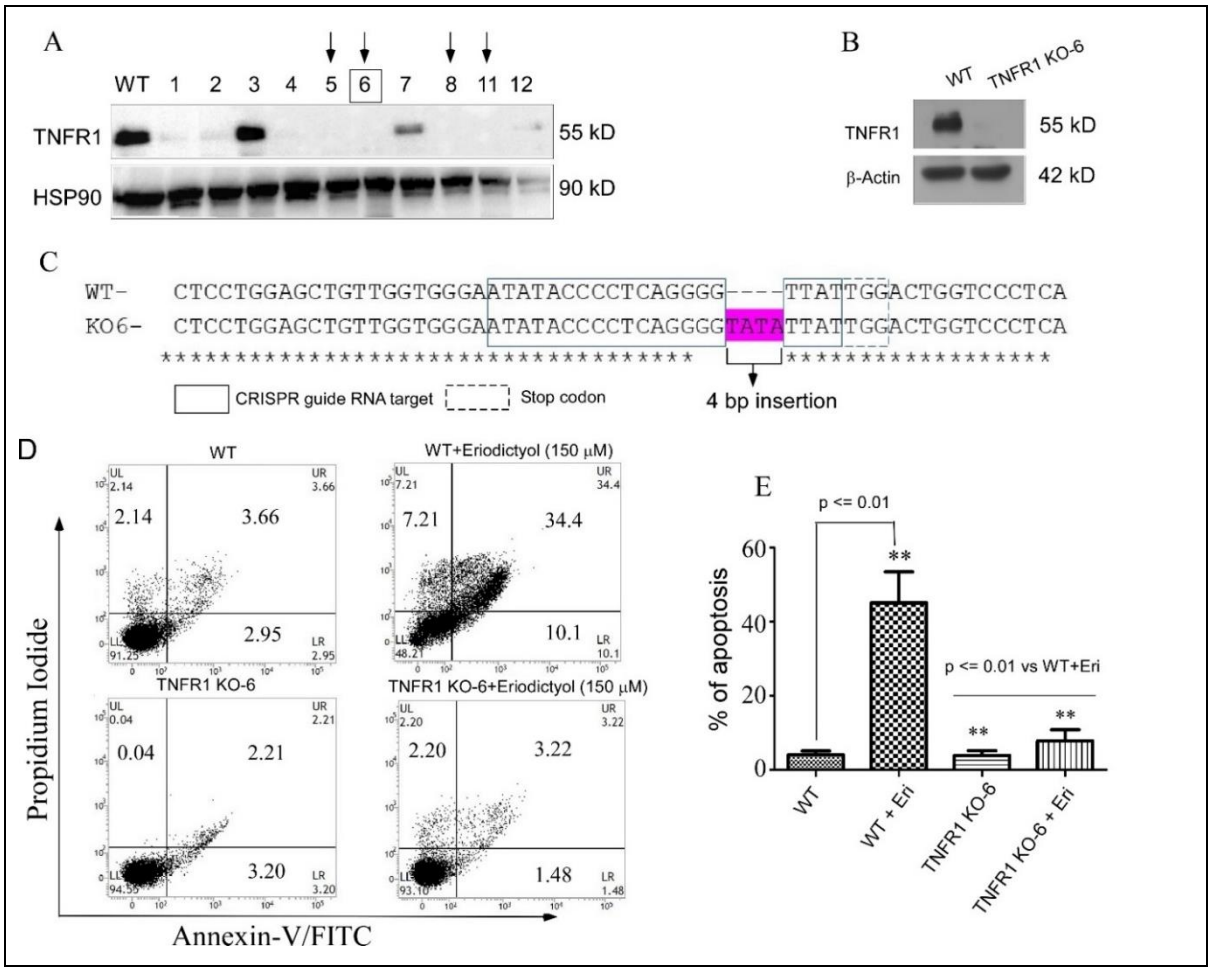

Figure 5.8 ***CRISPR/Cas9 mediated knockout of TNFR1 in HeLa cell resulted in abrogation of eriodictyol mediated apoptosis. A.*** Western immunoblot-based screening and selection of TNFR1 negative clones from an array of clones selected by puromycin treatment (1mg/ml). ***B.*** Western immunoblot showing TNFR1 expression in HeLa (wild-type) versus TNFR1 KO-6 clone. ***C.*** TNFR1 KO-6 clone shows 4bp insertion (TATA) that results in non-functional protein production. Inserted bases highlighted. The boxed portion represents the targeted DNA sequence. ***D, E.*** Density plot and bar graph from FACs analysis showing significant abrogation of apoptosis in TNFR1 KO-6 clone compared to HeLa (wild-type) upon Eriodictyol treatment at 150 μM dose for 48 h. Data has been collected from three independent experiments and analyzed by Student's t-test (two-tailed).

v. Plausible transcription factors (TFs) involved in TNFR1 gene expression regulation in response to Eriodictyol treatment.

A detailed analysis (bioinformatics) of the TNFR1 gene promoter region shows expression of the transcription factors (CEBPB, IRF1 and XBP1) with the following log2 fold change of 1.05, 1.14 and 1.10 respectively from our RNA-Seq data (Control vs 24hrs) represented in Table 5.1. Precise binding sites of these TFs is represented in Fig. 5.9 A. Moreover, we have validated the modulation of these TFs in response to Eriodictyol by Real-Time PCR where it shows time-dependent increase of the mentioned TFs (Fig. 5.9 B).

TF ID	Score	Pos(in chr12)	Str.	Signal Sequence
CEBPB	0.842249	6326812	(+)	GAGATGGGAAAAGC
XBP1	0.741239	6326833	(-)	TAGGGCCAGGTAGCCCA
CEBPB	0.877599	6326906	(+)	CTGTTGCCCAAGCT
CEBPB	0.911029	6326906	(-)	CTGTTGCCCAAGCT
CEBPB	0.816741	6327009	(-)	AATTTTTAAAATTT
CEBPB	0.836057	6327022	(+)	TTTTTTTGTAAAGA
CEBPB	0.835067	6327038	(-)	GGGTTTCCCTATAT
CEBPB	0.838534	6327048	(-)	ATATTGCCCAGGCT
IRF1	0.760223	6327145	(-)	GCAGTCATTTTTA
XBP1	0.742308	6327174	(+)	GGGCTCAGGTGCACCTA
CEBPB	0.862308	6327257	(+)	CCTTTGGGAAATGT
CEBPB	0.847202	6327489	(-)	CTCTTTCTATACTA
CEBPB	0.839525	6327716	(-)	GCATGTCCTCAGCC
CEBPB	0.869242	6327746	(+)	ATGTGTGGCCAGCT
CEBPB	0.826895	6328070	(+)	AGGTGAGGCGAGGG
CEBPB	0.811293	6328182	(-)	ATCTGGCACAAGGG
CEBPB	0.834324	6328215	(-)	TTCTGTCACCACCA
IRF1	0.785874	6328366	(-)	GGTATCATCTTTC
CEBPB	0.821942	6328527	(-)	AACTTACCTGATAT
CEBPB	0.811045	6328561	(-)	TCTTTTCTCCTTAA
CEBPB	0.868995	6328674	(-)	AGCTTGCTCCTCTC
CEBPB	0.871808	6328674	(+)	AGCTTGCTCCTCTC

Table 5.1 ***Analysis of Transcription factors (TFs) having a binding site on the promoter region (>chr12:6326757-6328757(-) TNFRSF1A) of the TNFR1 gene.*** **TF ID** represents Transcription factor label (from TRANSFAC R.3.4). **Score** signifies similarity (0.0-1.0) between a registered sequence for the transcription factor binding sites and the input sequence (at the position shown in Pos(in chr12). **Pos(in chr12)** denotes position of the input sequence. **Strandness (Str)**. + and - means forward and reverse strands that the transcription factor binds, respectively. Signal sequence identifies the input sequence at the position - corresponding to the consensus sequence. CEBPB, IRF1 and XBP1 have several binding sites in the selected region (2000 bp) of TNFR1 gene promoter. All these binding sites with location in chromosome 12 have been identified and represented in the table.

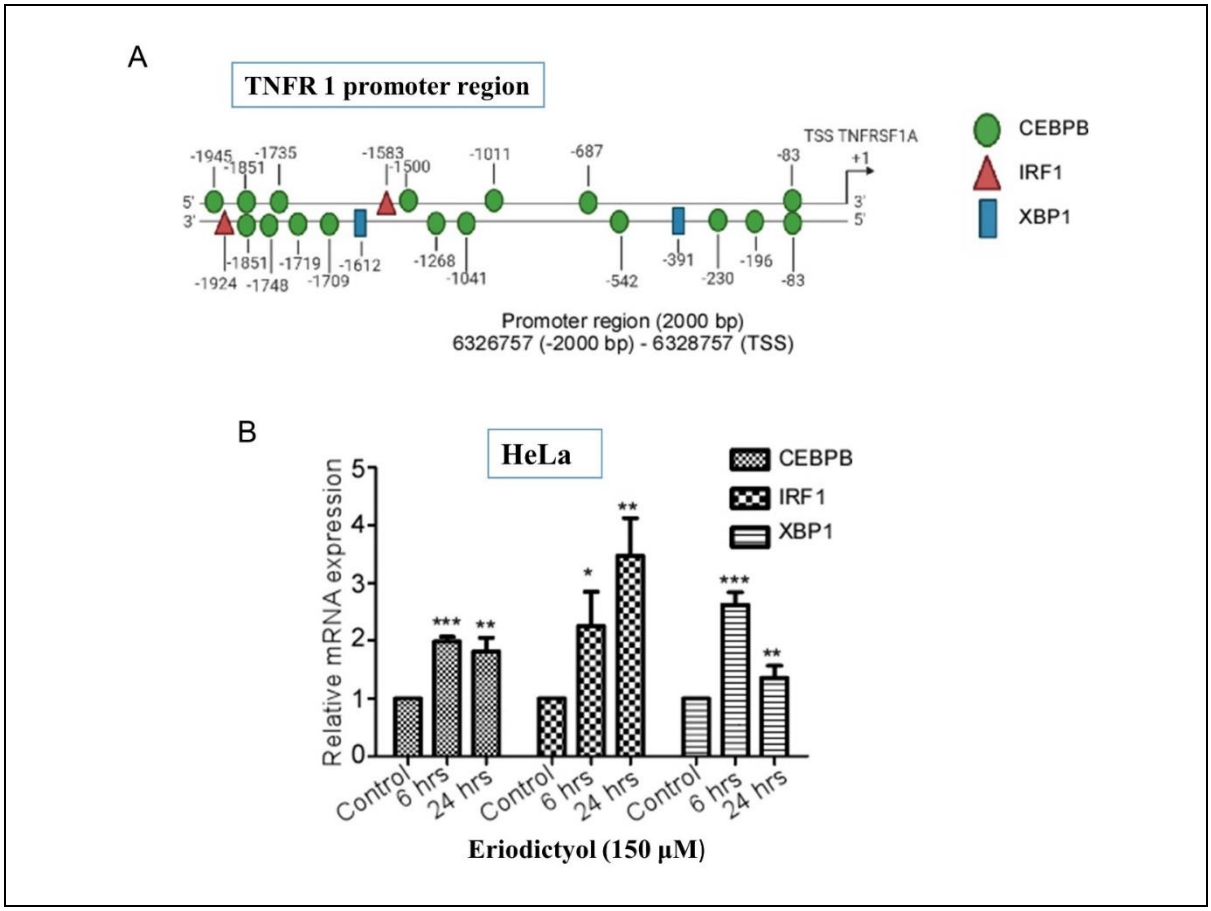

Figure 5.9 ***Transcription factors involved in regulating TNFR1 gene expression in response to Eriodictyol.*** ***A.*** Pictorial depiction showing the binding sites of the Transcription Factors (TFs) CEBPB, IRF1, XBP1 in the TNFR1 promoter region (2000 bp) analysed from transcriptomic data. ***B.*** Validation of the TFs involved in regulating TNFR1 gene by quantitative-PCR. Data has been collected from three independent experiments and analyzed by Student's t-test (two-tailed); *p < 0.05, **p < 0.01, ***p < 0.001, ns-not significant.

5.5 Discussion

To become cancerous, the cell must deactivate the apoptotic pathway. As a result of this inactivation, the cancer cell's proclivity for apoptosis is severely hampered, and alternative

types of death become more critical to DNA-damaging agents for cell killing and tumor response. Assays that exclusively detect apoptosis or other types of death in cells treated with an anticancer drug are likely to produce inaccurate results. A colony formation test, on the other hand, may incorporate all kinds of death and, in most cases, offers a realistic picture of total cell killing connected with *in vivo* tumor response [218]. Finally, the fact that genes that govern apoptosis may not be as significant in determining tumor sensitivity to anticancer therapy as previously thought does not imply that the genetic composition of the cell has no effect on treatment sensitivity. Aside from the many genes that control different forms of DNA repair and are definitely implicated in tumor treatment sensitivity, numerous issues remain concerning the genetic drivers of cell death by pathways other than apoptosis.

Caspases are unique proteases that, when triggered, generate one of the most common forms of apoptosis [119]. When caspase is active, it causes the cleavage of multiple critical proteins required for cellular proliferation and survival. Cleavage of PARP1 is suggested to be a marker of apoptosis. Both caspases can modify PARP1, but caspases 3 and 7 break PARP1 in such a manner that two different fragments result: 116 kDa catalytic fragment and a 89 kDa binding domain of DNA. The 89 kDa fragment has a far lower affinity for DNA and is released from the nucleus into the cytoplasm [219, 220]. While the primary purpose of PARP1 is to detect and repair DNA damage, severe DNA damage may lead to excess NAD+ and ATP consumption as a result of PARP1 over-activation, reducing the cell's ATP reserve. As a consequence, if the injury is "too extreme to handle," caspase action may cause the cell to transition from necrosis to apoptosis via enhanced PARP1 cleavage.

Further investigation of the molecular specifics revealed that Eriodictyol promoted extrinsic and intrinsic apoptosis in cancer cells, as indicated by expression of proteins associated with apoptosis hallmarks. The TNFR1-DISC-Casp-PARP1 axis is the major axis in the extrinsic apoptosis pathway, and we are the first to reveal Eriodictyol's utilization of it in mediating its selective cytotoxicity. In brief, we demonstrated that Eriodictyol administration in cancer cells resulted in the upregulation of TNFR1 receptor as well as components of the DISC complex namely, the adapter proteins (FADD, TRADD). This in turn leads to formation of cleaved caspase 8 triggered by pro-caspase 8 cleavage. Furthermore, Eriodictyol-induced apoptosis was followed by cell cycle arrest at the G2 / M stage, which begin by an increase in γ-H2A.X (an indication of DNA damage), which regulated Cyclin-B1, Cdc25, and Cdc2.

TNF family members are multipurpose cytokines that participate in cell proliferation, cell death, carcinogenesis, growth, inflammatory and immunological responses [221]. In cancer,

the TNF pathway has come to prominence, with the binding of TNF ligands to TNF receptors on cancer cells being shown to activate either the extrinsic or death receptor apoptotic pathway. TNF-'s ability to induce apoptosis in cancer cells has prompted the start of clinical trials to investigate the anti-cancer effectiveness of recombinant human TNF (rhTNF) on advanced solid tumors. Unfortunately, in comparison to the preclinical investigations, the clinical trial results were discouraging, as evidenced by a decrease in rhTNF's apoptosis triggering potential, which was linked to the simultaneous activation of the downstream NF-κB survival pathway [222]. Based on these findings, it was hypothesized that blocking the NF-κB cascade would facilitate TNF-mediated killing of malignant cells via the cell death-receptor pathway. It is reported that Eriodictyol inhibits NF-kB [223, 224], However, further experiments need to be conducted to validate the possibility that Eriodictyol-mediated upregulation of the TNFR1 expression is NF-κB-dependent. Hence, whether Eriodictyol could still induce apoptosis or not in NF-κB over-expressed HeLa cells will ultimately confirm this hypothesis.

Since our transcriptomic data from the RNA-Sequencing study, as well as western blot validation, clearly demonstrated that Eriodictyol augmented the genes involved in the cell cycle (Cyclin B1, p21, etc.) and the pathways relevant to apoptosis (TNFR1, TRADD, Bax, Survivin, etc.), we examined Eriodictyol's potential to target abnormalities that contribute to tumor cell's proliferative advantage while protecting normal cells, that could eventually lead to improved tolerance in clinical studies. Surprisingly, our findings showed that TNFR1 overexpression and endogenous TNF-α production from cancer cells (HeLa) jointly influenced the functional status of the TNF-α pathway, shifting it from NF-kB dependent cell survival to death-inducing complex formation. Furthermore, the significant abrogation of cancer cell apoptosis following TNFR1 deletion validated the function of TNFR1 in Eriodictyol-induced apoptosis. Furthermore, the observation of almost an exclusive expression of TNFR1 on certain cancer cells compared to normal cells, coupled with the inability of Eriodictyol to induce TNFR1 expression even after prolonged exposure in the normal cells as opposed to the cancer cell lines, uncovered the mechanism underlying the specificity of Eriodictyol's selectivity towards cancer cell cytotoxicity over normal cells. In fact, deep analysis of the transcriptomic data, further revealed plausible transcription factors (TFs) like CEBPB, IRF1 and XBP1 that are differentially regulated in response to Eriodictyol treatment, and might play a role in the induction of Eriodictyol-mediated TNFR1. How any of these TFs might regulated TNFR1 in response to Eriodictyol and might also dictate its selectivity towards cancer cells over normal cells is still being investigated and is a focus of a separate study altogether.

References

1. Zhang, J.Y., *Apoptosis-based anticancer drugs.* Nature Reviews Drug Discovery, 2002. **1**(2): p. 101-102.
2. Groth-Pedersen, L. and M. Jäättelä, *Combating apoptosis and multidrug resistant cancers by targeting lysosomes.* Cancer Lett, 2013. **332**(2): p. 265-74.
3. Seimiya, H., et al., *c-Jun NH2-terminal Kinase-mediated Activation of Interleukin-1β Converting Enzyme/CED-3-like Protease during Anticancer Drug-induced Apoptosis*.* Journal of Biological Chemistry, 1997. **272**(7): p. 4631-4636.
4. Srivastava, R.K., et al., *Bcl-2-mediated drug resistance: inhibition of apoptosis by blocking nuclear factor of activated T lymphocytes (NFAT)-induced Fas ligand transcription.* The Journal of experimental medicine, 1999. **190**(2): p. 253-265.
5. Hientz, K., et al., *The role of p53 in cancer drug resistance and targeted chemotherapy.* Oncotarget, 2017. **8**(5): p. 8921-8946.
6. Pommier, Y., et al., *Apoptosis defects and chemotherapy resistance: molecular interaction maps and networks.* Oncogene, 2004. **23**(16): p. 2934-2949.
7. Abbaspour Babaei M, Z.H.H., Kamalidehghan B, Yeap SK, Ahmadipour F. Apoptotic induction and inhibition of NF-κB signaling pathway in human prostatic cancer PC3 cells by natural compound 2,2'-oxybis (4-allyl-1-methoxybenzene), biseugenol B, from Litsea costalis: an in vitro study. Onco Targets Ther. 2017;10:277-294 and https://doi.org/10.2147/OTT.S102894.
8. Kumar, R., P.E. Herbert, and A.N. Warrens, *An introduction to death receptors in apoptosis.* International Journal of Surgery, 2005. **3**(4): p. 268-277.
9. Szlosarek, P.W. and F.R. Balkwill, *Tumour necrosis factor α: a potential target for the therapy of solid tumours.* The Lancet Oncology, 2003. **4**(9): p. 565-573.
10. Zhao, E.F., *[Cytotoxicity of recombinant human tumor necrosis factor (rHTNF) alone and in combination with chemotherapeutic agents on human ovarian cancer cells]*. Zhonghua Fu Chan Ke Za Zhi, 1993. **28**(3): p. 153-6, 188.
11. Krosnick, J.A., et al., *Studies of the mechanisms of toxicity of the administration of recombinant tumor necrosis factor α in normal and tumor-bearing mice.* Cancer Immunology, Immunotherapy, 1989. **30**(3): p. 133-138.
12. Chazotte, B., *Labeling mitochondria with JC-1.* Cold Spring Harb Protoc, 2011. **2011**(9).
13. Sentmanat, M.F., et al., *A Survey of Validation Strategies for CRISPR-Cas9 Editing.* Scientific reports, 2018. **8**(1): p. 888-888.
14. Brix, N., et al., *The clonogenic assay: robustness of plating efficiency-based analysis is strongly compromised by cellular cooperation.* Radiation Oncology, 2020. **15**(1): p. 248.
15. Li, J. and J. Yuan, *Caspases in apoptosis and beyond.* Oncogene, 2008. **27**(48): p. 6194-6206.
16. Chaitanya, G.V., A.J. Steven, and P.P. Babu, *PARP-1 cleavage fragments: signatures of cell-death proteases in neurodegeneration.* Cell communication and signaling : CCS, 2010. **8**: p. 31-31.
17. Boulares, A.H., et al., *Role of Poly(ADP-ribose) Polymerase (PARP) Cleavage in Apoptosis: CASPASE 3-RESISTANT PARP MUTANT INCREASES RATES OF APOPTOSIS IN TRANSFECTED CELLS *.* Journal of Biological Chemistry, 1999. **274**(33): p. 22932-22940.
18. *Tumor necrosis factor alfa,* in *Meyler's Side Effects of Drugs (Sixteenth Edition)*, J.K. Aronson, Editor. 2016, Elsevier: Oxford. p. 230-232.
19. Roberts, N.J., et al., *Systemic use of tumor necrosis factor alpha as an anticancer agent.* Oncotarget, 2011. **2**(10): p. 739-751.

4. Chapter III

Assessment of the role of Eriodictyol in prevention of cancer progression and metastasis in an *in vivo* syngeneic mice tumour model

6.1 Abstract

In our previous chapter we dissected the mechanism of Eriodictyol's selective cytotoxicity. To resolve the question of whether Eriodictyol's anti-cancer activity could be effectively translated into pre-clinical *in vivo* models, we established two syngeneic (Balb/c) mouse cancer models to simulate human pathophysiological conditions. In the localized tumor model, immunocompetent Balb/c mice were injected with 4T1 mice breast cancer cells subcutaneously into the mammary fat pad. The time-dependent decrease in tumor volume demonstrated a considerable suppression of tumor growth. Moreover, in the metastatic tumor model, 4T1 cells were injected via the lateral tail vein for induction of experimental lung metastasis. The remarkable decrease in the number of lung nodules in Eriodictyol treated mice compared to control group clearly demonstrated the anti-metastatic role of Eriodictyol in vivo. Taken together, our *in vivo* studies established the fact that Eriodictyol not only reduced tumor growth and progression, but also suppressed pulmonary lung metastasis of 4T1 cells in immune-competent Balb/c mice.

6.2 Introduction

The ability to replicate tumor growth in mammalian species while recapitulating aspects and characteristics of human illness and demonstrating measurable advantages of an anticancer treatment is crucial to the development of an anti-tumor model as well as in the exploration and design of anticancer medicines [225]. A drug, in the simplest meaning, is a substance that is employed in the diagnosis, treatment, abatement, therapy, or prevention of a disease. Cancer drugs include cytotoxic agents such as cisplatin as well as the humanized monoclonal anti-PD1 antibody Keytruda (pembrolizumab) that has been used in several malignancies [226, 227]. Mice, in particular, have been frequently employed to increase our knowledge of the underlying

etiology and pathogenesis of human malignancies, including phenotypic traits or signatures, as well as to simplify the pharmacological assessment of known and possible new therapies [228].

Several cancer mouse models were proposed as pre-clinical models to better understand critical mechanisms in tumor growth and to evaluate the adequacy of anti-cancer medicines. These models represent critical stages in the development of a normal cell tumor and its progression to an aggressive tumor. These models have been particularly beneficial in identifying factors that contribute to tumor spread, recurrence, and therapy resistance. Pre-clinical mice studies have aided in the assessment of the pharmacokinetics, lethality, and anti-tumor activity of numerous chemotherapeutic drugs in vivo [229]. Clinical development researchers employ mouse cancer models to confirm the biological relevance of drug targets, test diagnostic theories, and uncover novel biomarkers [230]. Mutations in genes assumed to be involved for human cancers are modified, deleted, or overexpressed in genetically engineered mice (GEM) models, and tumor growth is tracked [231]. The existence of a normal immune system could be examined in connection with cancer and chemotherapy responses in this model [232]. Preclinical models are critical for moving a medication concept from drug research and development to FDA approval and eventual commercialization as a licensed pharmaceutical (Figure 6.1).

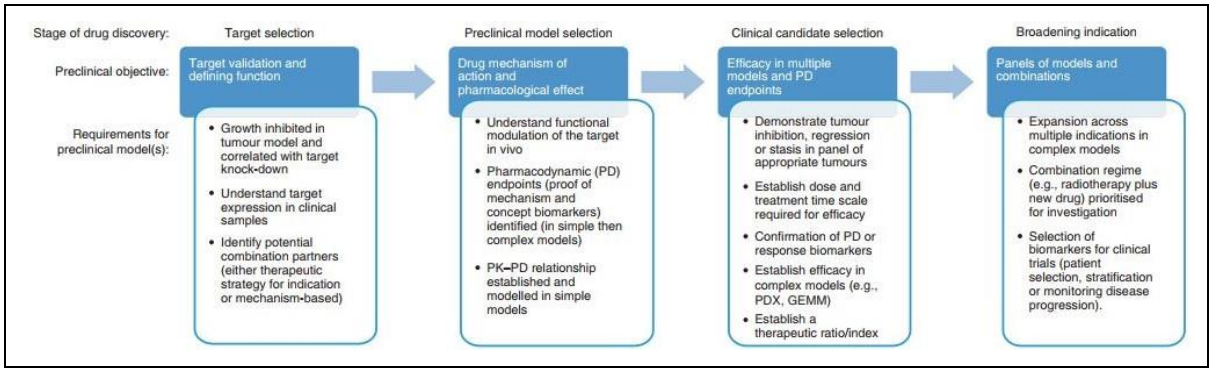

Figure 6.1 ***A graphical diagram depicts preclinical aims and objectives for preclinical models to help in preclinical research at critical phases of drug development.*** The stage of drug discovery starts with 1.Target selection. 2. Preclinical model selection. 3. Clinical candidate selection. 4. Broadening indication.

Nonetheless, since mouse tumor cells can not accurately reflect the tumorigenic process in humans, human tumor xenografts in immunocompromised mice are a common model [233]. In these models, human tumors are grown in various tissues utilizing tumor samples, cell cultures, or cancer stem cells (CD44+/CD24 –). Cancer xenograft studies, on the other hand, were unable to address the significance of tumor microenvironments, tumor-stroma

interactions, and normal tumor immune surveillance [234]. Several new strains of humanized mouse models have also been introduced as a result.

Mouse model	Principal components	Benefits	Caveats
Xenograft models	Human tumor cell lines that have been established and transferred into immune-compromised hosts	• Represent from diverse human tumor subtypes • Tumor microenvironmental features, such as vascular and stromal cells embedded into the tumor • Tumors can be measured precisely and conveniently	• Immune-deficient • Subcutaneous placement may not promote significant tissue-specific stromal infiltrate • In terms of species compatibility, the stromal components are of mouse origin, but the tumor cells are of human origin. • Within the tumor, there is far less genetic variability.
Patient-derived xenograft models	Immune-compromised hosts	• Tumor tissue - specific characteristics, such as the presence of vascular and stromal cells within the tumor • Tumors can be measured precisely and conveniently.	• Immune-deficient • In terms of species compatibility, the stromal components are of mouse origin, but the tumor cells are of human origin. • With passage, there is genetic and phenotypic drift.
Syngeneic models	Established mouse tumor cell lines were implanted into immune-compromised hosts.	• Intact immune system is present • Characteristics of the tumor microenvironment, such as the presence of vascular and stromal cells within the tumor • mouse origin cell types • Tumors can be measured precisely and conveniently.	• Limited number of known cell lines, insufficiently annotated • Some cell lines strong immunogenicity causes spontaneous regression • Many cell lines rapid growth rate limits their application in long-term studies
Genetically engineered mouse models	A genetic change that allows for the growth of tumors, either spontaneous or induced.	• Tissue of origin is the site of tumor development. • Intact immune system is present • Tumor cell types are of mouse origin • Tumor microenvironmental characteristics, such as the existence of vascular and stromal cells well within tumor	• Heterogeneity of tumors are very limited. • Very hard to monitor when tumor originates in internal organs. • High investment is accompanied by low throughput

Table 6.1 ***Oncology drug research depends on preclinical in vivo efficacy models.***

Cancer immunotherapies coordinate with a patient's own immune system to boost responses to anti-tumor antibodies [235]. Traditional patient-derived xenograft (PDX) models are inadequate in the production of these drugs due to the animals' immunocompromised status [236]. Nonetheless, syngeneic mouse models incorporate tumor tissues that have the same genetic history as the mouse strain that is immunocompetent.

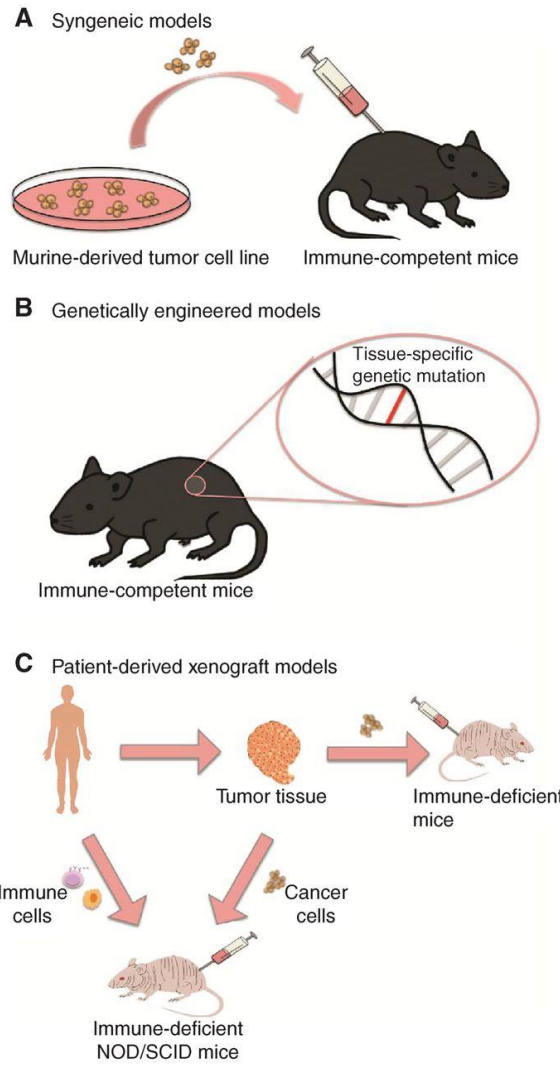

Figure 6.2 ***Preclinical mouse models for immuno-oncology drug screening***
A. In syngeneic tumor models, murine tumor cell lines are grown into immunocompetent hosts (subcutaneously or orthotopically).
B. Expression of tissue-specific oncogenes of tumor suppressors promote the growth of autochthonous tumor cells which are obtained by initiating tumors in a normal cell *de novo* and within the intact organism, in genetically engineered animal models.
C. Patient-derived xenografts are created by taking tumor tissue from patients, putting it into immunocompromised mouse, and then growing it in vivo. Tumor cells can be injected with autologous immune cells to restore immune function
Source: "**Mouse Models for Cancer Immunotherapy Research**" Brian et.al (Cancer Discovery 2018)

The most popular form of model used to research tumor growth and metastasis pathways is a syngeneic murine model, which is characterized by transplanted cells or tissue of same species or type as the host animal [237]. Therefore, utilizing an intact immune system and host stroma and extracellular matrix, these models provide a foundation for analyzing tumor-environment interaction, immune response to anticancer, and primary metastatic tumor relevance [238]. Due to their high invasiveness, 4T1 or 4T1-luc models are helpful tools in mammalian tumor models for studying antitumor and anti-metastatic role of different medications, making it a well-accepted model for a wide range of investigations. Metastatic models with strong metastasis efficiency and a reduced duration are required for cost-effective in vivo drug testing [239]. Presently, transplant models will almost certainly capture some of the heterogeneity present in breast cancer. However, the entire efficacy of both standard and selective treatment techniques is dependent on activating anti-tumor immune responses. The benefits of mouse allograft

models include full immunocompetence, no species mismatch in paracrine interactions between tumor and stroma, fast disease progression, and metastatic burden as a significant endpoint in therapeutic intervention studies [240].

Advantages	Limitations
Small in size, easy to control and care for, and with a short tumor formation time.	Mice are extremely different from humans in terms of size, life duration, organ architecture, and physiology, and hence drug PK and PD.
Cheaper than other cancer animal models, allowing for huge amounts of statistical measurements.	The activity of the telomerase enzyme, which is largely dormant in adult human cells, is one key variation between mice and humans. (Because mouse cells are more easily transformed, malignant transformation necessitates fewer genetic alterations).
Tumor occurrence is high, and tumor progression is relatively fast.	In comparison to human cancers, mice models had fewer metastases or metastases with unique tissue selectivity.
Multiple mice can be administered at the same period to observe dose responses.	In mouse models, differences in metabolic rate and pathways may result in a varied pharmacological response (e.g. the cytochrome P450 pathway for drug metabolism).
The most genetically characterized of all mammals used in cancer research.	Because of the small proportion of initiating genetic mutations, mouse tumors are often more uniform, which can make recreating the heterogeneity of human cancers difficult.

Table 6.2 ***Advantages and limitations of mouse models.***

6.3 Experimental procedure

i. *Culture, maintenance and harvesting of murine tumor cells for injection in mouse syngeneic tumor models*. 4T1 cells were obtained from NCCS (National Centre for Cell Science), Pune. Aforementioned cell line was cultured in RPMI 1640 with 10% FBS, 1 mM sodium pyruvate, 2mM L-glutamine and non-essential amino acids (MEM), 100 U/ml Penicillin, 100 µg/ml Streptomycin and 50µg/ml Gentamycin at 37^0C in presence of 5% CO_2. At passage no. 3 when 4T1 cells were healthy and rate of proliferation was highest, cells were washed with 1X PBS and trypsinized with 0.5X Trypsin and serum added RPMI was added to stop the trypsinization process. Cells were centrifuged at 600 rpm for 3-4 mins and resuspended in serum-free RPMI. Required number of cells were counted in haemocytometer after vigorous pipetting to make single-cell suspension. Finally, for every 100 µl injection required number of cells were diluted with serum-free RPMI according to requirement and collected in 1.5 ml Eppendorf tubes for mice injection.

ii. *4T1 breast tumor model.* 4T1 cells ($1x10^6$ cells/animal) were subcutaneously injected into the mammary fat pad of Balb/c mice to form a solid tumor for an in vivo tumor study. Mice with palpable solid tumors were randomly divided into two classes of at least five animals each. One group received a vehicle control (5 percent DMSO), while the other

received intraperitoneal administration of Eriodictyol (60 mg/kg body weight) beginning about 10 days after the initial injection and lasting up to 22 days (5 doses, 72 h interval). On every third day, the volume of the tumor was measured with vernier calipers to monitor its progression and measured using formula $V = 0.5*a*b^2$ where "a" and "b" represent the major and minor axes.

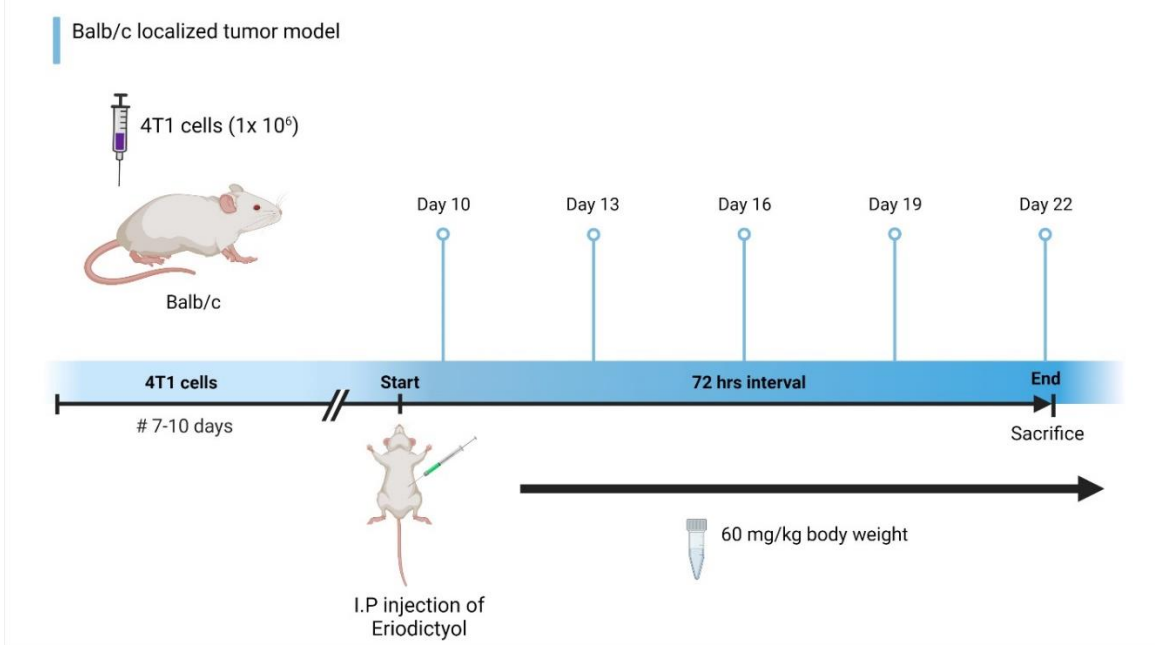

Figure 6.3 ***Schematic of localized tumor model.*** Balb/c mice were injected with $1x10^6$ 4T1 cells. After palpable tumor formation mice were randomly divided into control and treated group. Eriodictyol at a concentration of 60 mg/kg bodyweight of mice were intraperitoneally injected every three days interval. This procedure was followed for a period of 22 days until sacrifice of the mice.

iii. 4T1 tumor metastasis in secondary organs. 4T1 wild type tumor cells (at $1x10^5$) were injected intravenously through the tail vein into syngeneic Balb/c mice. Mice were randomly categorized into three groups after injection and treated three times a week with regular saline and two separate doses of Eriodictyol. Three to four weeks after tumor cell injection, animals were sacrificed and examined for the presence of micro-metastatic nodules in the lungs, showing metastasis. The lung samples from all three groups are cross-sectioned and stained with haematoxylin-eosin (H&E). The procedure was approved by the Bose Institute's Institutional Animal Ethics Committee (Approval No. IAEC/BI/118/2018, dated 20/12/2018), and mice were treated in accordance with CPCSEA recommendations and animal welfare committee guidelines.

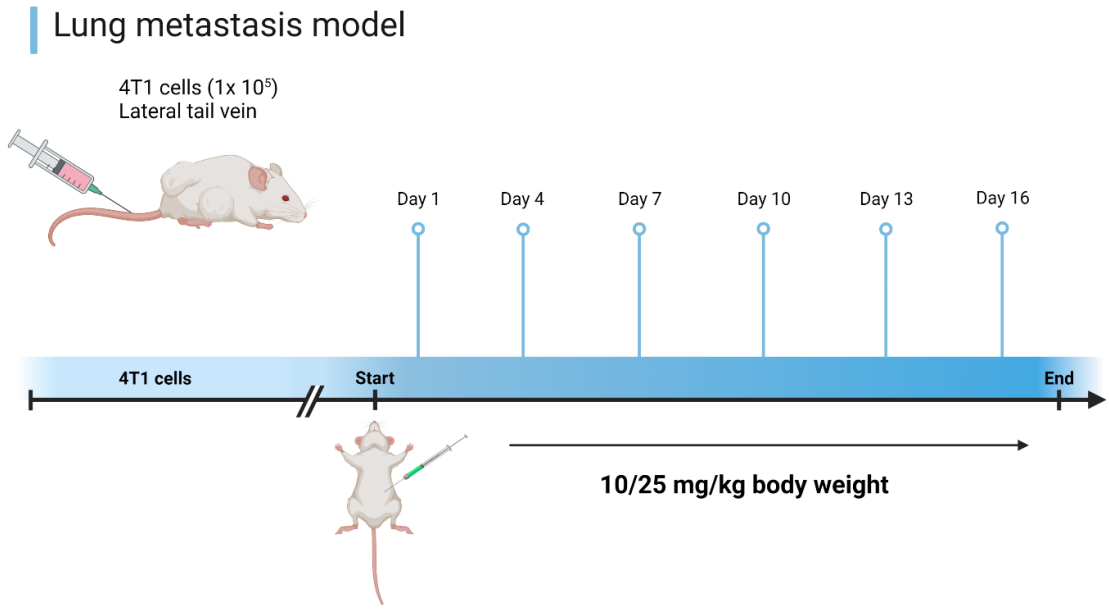

Figure 6.4 ***Schematic of metastasis model.*** $1x10^5$ 4T1 cells were injected through tail vein of Balb/c mice and were randomly divided into groups of control, 10 mg/kg and 25 mg/kg bodyweight of mice. Eriodictyol was injected intraperitoneally starting from the date of injection of cells. At around 19 days mice were sacrificed and lungs were collected for counting of nodules.

6.4 Results

i. *Subcutaneous administration of Eriodictyol leads to significant reduction in tumor volume in BALB/c mice :* To translate the *in vitro* anti-cancer activity of Eriodictyol *in vivo*, syngeneic mouse (Balb-c) tumor model was used. For this, syngeneic mice 4T1 breast tumor model was used to determine its impact on tumor growth and progression. Solid tumors were induced by injecting $1x10^6$ 4T1 cells per specimen subcutaneously in the mammary fat pad. Starting on the 10th day of 4T1 cell injection and visible recognition of tumors (palpable), four doses of Eriodictyol were administered intraperitoneally every three days for a total of 22 days. The reduction in tumor volume indicates that mice treated with 60 mg/kg body weight of Eriodictyol have substantially reduced tumor size than non-treated control mice (Fig. 6.5 A-C). This is also evident in the weight of tumors resected from mice treated with the active compound, which shows a substantial reduction in tumor weight as compared to non-treated mice (Fig.6.5 D). However, as shown in Fig.6.5 E, there seems to be no substantial toxicity in Eriodictyol-treated mice compared to non-treated control as evident from the mice body weight.

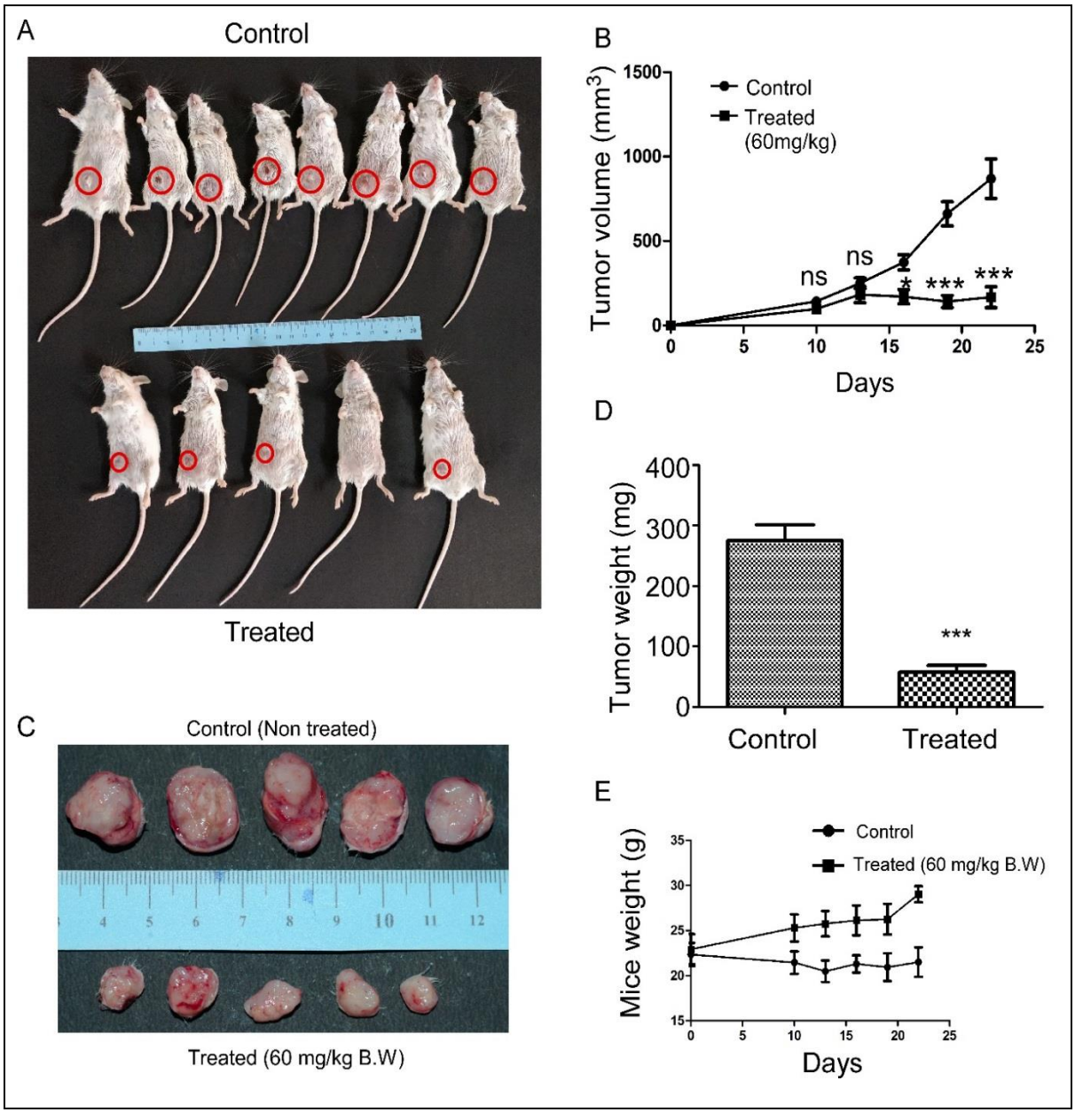

Figure 6.5 ***Eriodictyol impedes the progression of mammary tumors. A.*** Image of mice bearing tumors (indicated by red circles) before sacrifice, injected in the mammary fat pads subcutaneously with 4T1 cells, either treated with Eriodictyol (bottom row) or non-treated (top row). ***B.*** Line graph showing regression of tumor volume (time-dependent) in response to intraperitoneal injection of Eriodictyol, in Balb/c mice injected subcutaneously with 4T1 cells at the mammary fat pads, in comparison with those non-treated. ***C.*** Represents image of resected tumors from mice injected in the mammary fat pads subcutaneously with 4T1 cells, either treated with Eriodictyol (bottom row) or non-treated (top row). ***D.*** Bar graph showing significant reduction in tumor weight of the resected tumors, post-Eriodictyol treatment at 60 mg/kg body weight. ***E.*** Comparison of mice body weight in eriodictyol-treated vs non-treated. The data represents two independent experiments and bar graph represents mean ± SEM (Student's t-test (two-tailed),*$p < 0.05$, **$p < 0.01$, ***$p < 0.001$, ns not significant).

ii. Eriodictyol impedes tumor progression and metastasis in immuno-competent mice: Intraperitoneal Eriodictyol administration results in a dose-dependent decrease in the

number of metastatic lung nodules (0, 10, 25 mg / kg body weight) induced by tail vein injection of 4T1 mouse breast tumor cells in Balb/c mice, as seen visually from the resected lung images (Fig. 6.6 A) as well as from the graph,which represents cumulative mean from at least 2 independent experiments (Fig.6.6 B). Furthermore, histopathological analysis shows that untreated mice has substantially more lung sections with nodules than treated mice (Fig. 6.7 A). Finally, the weight of the lungs is significantly lower in the Eriodictyol-treated groups than those in the control group (Fig.6.7 B). Thus, Eriodictyol inhibits tumor development in the lungs of Balb/c mice in a dose-dependent manner.

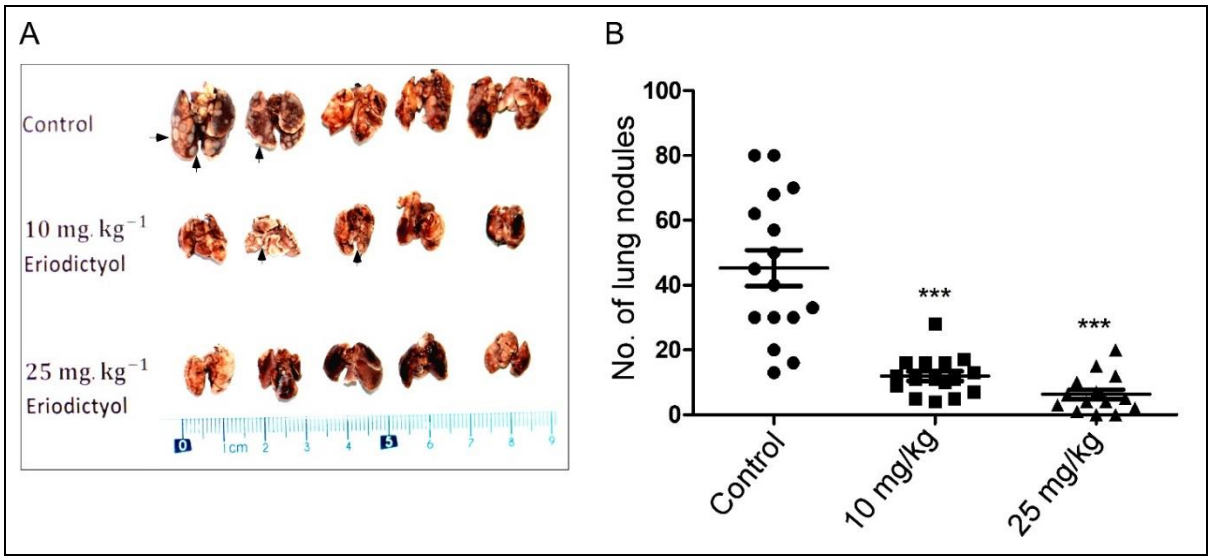

Figure 6.6 ***Eriodictyol impedes lung nodules formation in syngeneic mouse model. A.*** Photomicrographs depicting formalin-fixed whole lungs from male Balb/c mice injected with 4T1 cells (tail vein injection) with or without Eriodictyol treatment at different concentrations (0, 10, 25 mg/kg body weight). ***B.*** Graphical representation of the total number of lung nodules counted at different doses (0, 10, 25 mg/kg body weight) of Eriodictyol. The data represents two independent experiments and bar graph represents mean ± SEM (Student's t-test (two-tailed),*$p < 0.05$, **$p < 0.01$, ***$p < 0.001$, ns not significant).

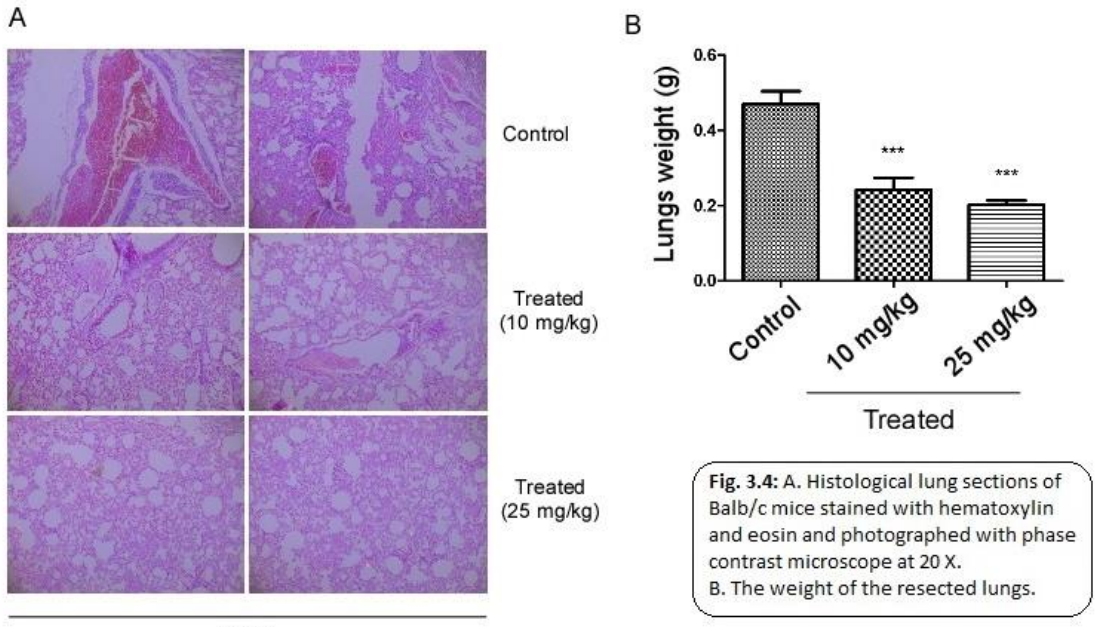

Figure 6.7 ***Histological lung sections of Balb/c mice shows Eriodictyol supresses nodule formation.*** **A**. Lung sections of Balb/c mice stained with hematoxylin and eosin and photographed with phase contrast microscope at 20X. **B.** The weight of the resected lungs.

6.5 Discussion

Tumors are composed of cancer stem cells, stroma, immune cells, and growth factors, all of which combine to form an immune-suppressive and oncogenic system. Tumor cells are genetically, phenotypically, and clinically diverse, with variances in complex signaling cascades occurring frequently within a single patient [232]. A strong statement of efficacy is needed for target validation in a tumor model which also improves the clinical chances of obtaining a strong efficacy response. This goal can be achieved by first demonstrating a therapeutic efficacy in simple subcutaneous models, then building credibility in study designs in complex models, and finally detecting results in selected individuals or disease groups [241]. Syngeneic mouse models are amongst the most commonly used models in pharmacology and preclinical immuno-oncology study. Allografts of immortalized cell lines of mouse cancer are transplanted in immunocompetent mice of the same inbred category, either from resected tumors that form naturally in older animals or after carcinogen induction. Immunocompetence is a critical component of syngeneic mouse models with complete murine defense and stroma. Another reason contributing to their growing popularity is their adaptability in contrast to other immunocompetent models; syngeneic models have ~100 percent penetration and subcutaneous

doses may be precisely timed to synchronize tumor development and mimic architecture of a xenograft experiment. Additionally, there is a huge archive of existing literature utilizing particular immunotherapy research models. It can be used to compare new agent outcomes, essentially making them the "industry standard." Combination investigations, particularly with checkpoint inhibitors, are key uses of syngeneic models in immunotherapeutic evaluation.

Syngeneic model can be thoroughly characterized (e.g., sequenced RNA cell lines and tumors, immunohistochemistry, biomarker recognition), and this data can be correlated with the findings of common checkpoint inhibitors (anti-PD-1, PD-L1, CTLA-4) to enhance in vivo efficacy [242]. Large-scale screening may also use syngeneic model panels to rapidly monitor immunotherapies and combination regimens.

Metastasis refers to the expansion of cancer cells from a primary tumor to distant locations inside the body to produce new tumors. Tumor cell intravasation from the initial tumor site, circulation to distant organs, extravasation, and effective remote site colonization are all involved. As a result, new clinical trials for metastasis in autochthonous models should be carried out in an ideal setting.

The majority of cancer-related deaths are caused by metastatic disease, indicating the lack of successful therapies once cancer has spread outside the primary organ. It is essential to do research concerning the molecular and cellular processes that underpin the metastatic cascade in order to streamline therapeutic options for disseminated illness. To that purpose, much effort has been invested in establishing innovative and therapeutically relevant preclinical *in vivo* models that resemble patient metastasis [243].

Mouse models have shown to be a valuable tool for identifying and understanding the intricate relationship involved in the metastatic cascade. Choosing an appropriate *in vivo* metastasis model is critical for identifying prognostic/predictive markers, validating candidate genes that can modulate metastasis, and assessing the therapeutic efficacy of anti-metastatic agents [244].

Due to the sheer ubiquity and variability of tumours, it has historically been difficult to analyse therapy responses within the tumour microenvironment [245]. Current models can give essential mechanistic and pharmacological insights to progress a lead candidate to the clinical stage and improve critical unmet clinical criteria.

Therefore in our investigation, we employed a syngenic mouse (Balb-c) tumour model to translate Eriodictyol's in vitro anti-cancer potential in vivo. In our current study, demonstration of Eriodictyol's therapeutic efficacy in significant regression of tumor volume as well as tumor weight in the syngenic mouse tumor model without any significant adverse effect on animals,

correlated with its ability to inhibit cell proliferation, cell cycle arrest and induction of apoptosis, selectively in cancer cells over the normal cells.

Several studies on various cancer types have found that YAP/TAZ is closely associated with tumor metastasis, such as promoting tumor cell migration, invasion, anchor-independent growth, epithelial-mesenchymal transition (EMT), and stemness, and that its activation can enhance almost every step of the metastatic cascade [246-248]. As a result, YAP/TAZ are critical cancer-promoting metastatic proteins. In our study, we found that Eriodictyol can increase YAP/TAZ phosphorylation (and hence block YAP/TAZ activation) through increasing LATs phosphorylation (data not shown). Likewise, the dose-dependent reduction in the formation of lung metastatic nodules in Eriodictyol treated mice over non-treated mice, correlated with the ability of Eriodictyol in inhibition of YAP/TAZ-activation, clearly suggesting a potential role of Eriodictyol in blocking metastasis through inhibition of the YAP/TAZ-axis. Whether, the anti-tumor mechanism of Eriodictyol is connected with the anti-metatstatic ability, or they are distinct is still not clearly understood and needs further investigation. In summary, our *in vivo* study indicated that Eriodictyol reduced tumor growth and progression, as well as suppressed pulmonary lung metastasis of 4T1 cells in immune-competent Balb/c mice.

Therefore, according to *in vitro* and *in vivo* studies, Eriodictyol could be perceived as a promising therapeutic agent against cancer. Our research is a preliminary study on the anti-cancer effect of Eriodictyol. In the future, we will further investigate the mechanisms underlying modulation of TNFR1 gene expression, presented in our study, and we will try to modify the structure of Eriodictyol to improve its anti-cancer activity.

References

1. Gao, S., et al., *Efficient Biosynthesis of (2S)-Eriodictyol from (2S)-Naringenin in Saccharomyces cerevisiae through a Combination of Promoter Adjustment and Directed Evolution.* ACS Synthetic Biology, 2020. **9**(12): p. 3288-3297.
2. Kardinal, C.G. and J.W. Yarbro, *A conceptual history of cancer.* Semin Oncol, 1979. **6**(4): p. 396-408.
3. Hajdu, S.I., *A note from history: landmarks in history of cancer, part 1.* Cancer, 2011. **117**(5): p. 1097-102.
4. Ashkenazi, A., *Targeting death and decoy receptors of the tumour-necrosis factor superfamily.* Nat Rev Cancer, 2002. **2**(6): p. 420-30.
5. El-Deiry, W.S., *Insights into cancer therapeutic design based on p53 and TRAIL receptor signaling.* Cell Death Differ, 2001. **8**(11): p. 1066-75.

6. U. S. National Institutes of Health, N.C.I.; Available from: https://training.seer.cancer.gov/.
7. Cowherd, S., *Tumor Staging and Grading: A Primer.* Methods in molecular biology (Clifton, N.J.), 2012. **823**: p. 1-18.
8. America, C.T.C.o.; Available from: https://www.cancercenter.com/carcinoma.
9. Auerbach, C., J.M. Robson, and J.G. Carr, *The Chemical Production of Mutations.* 1947. **105**(2723): p. 243-247.
10. Asthana, S., R.S. Patil, and S. Labani, *Tobacco-related cancers in India: A review of incidence reported from population-based cancer registries.* Indian journal of medical and paediatric oncology : official journal of Indian Society of Medical & Paediatric Oncology, 2016. **37**(3): p. 152-157.
11. Ames, B.N., *Identifying environmental chemicals causing mutations and cancer.* Science, 1979. **204**(4393): p. 587-93.
12. Adams, J.D., S.J. Lee, and D. Hoffmann, *Carcinogenic agents in cigarette smoke and the influence of nitrate on their formation.* Carcinogenesis, 1984. **5**(2): p. 221-3.
13. Adams, J.D., K.J. O'Mara-Adams, and D. Hoffmann, *Toxic and carcinogenic agents in undiluted mainstream smoke and sidestream smoke of different types of cigarettes.* Carcinogenesis, 1987. **8**(5): p. 729-31.
14. Dich, J., et al., *Pesticides and cancer.* Cancer Causes Control, 1997. **8**(3): p. 420-43.
15. National Research Council (US) Committee on Diet, N., and Cancer. Diet, Nutrition, and Cancer. Washington (DC): National Academies Press (US); 1982. THE CARCINOGENICITY OF FOOD ADDITIVES AND CONTAMINANTS. Available from: https://www.ncbi.nlm.nih.gov/books/NBK216646/.
16. *Radiation.* IARC Monogr Eval Carcinog Risks Hum, 2012. **100**(Pt D): p. 7-303.
17. Hatch, M., et al., *The Chernobyl disaster: cancer following the accident at the Chernobyl nuclear power plant.* Epidemiol Rev, 2005. **27**: p. 56-66.
18. Warowicka, A., et al., *[Oncogenic viruses and cancer].* Postepy Biochem, 2020. **66**(4): p. 336-355.
19. Butt, A.Q. and S.M. Miggin, *Cancer and viruses: a double-edged sword.* Proteomics, 2012. **12**(13): p. 2127-38.
20. Willecke, K. and R. Schäfer, *Human oncogenes.* Hum Genet, 1984. **66**(2-3): p. 132-42.
21. Kang, Z.-J., et al., *The Philadelphia chromosome in leukemogenesis.* Chinese journal of cancer, 2016. **35**: p. 48-48.
22. Thomas, D.A., et al., *Burkitt lymphoma and atypical Burkitt or Burkitt-like lymphoma: should these be treated as different diseases?* Current hematologic malignancy reports, 2011. **6**(1): p. 58-66.
23. Witkiewicz, A.K. and E.S. Knudsen, *Retinoblastoma tumor suppressor pathway in breast cancer: prognosis, precision medicine, and therapeutic interventions.* Breast cancer research : BCR, 2014. **16**(3): p. 207-207.
24. Benson, J.R. and M. Baum, *Breast cancer, desmoid tumours, and familial adenomatous polyposis--a unifying hypothesis.* Lancet, 1993. **342**(8875): p. 848-50.
25. Jeong, Y.J., H.K. Oh, and J.G. Bong, *Multiple endocrine neoplasia type 1 associated with breast cancer: A case report and review of the literature.* Oncology letters, 2014. **8**(1): p. 230-234.
26. Gimple, R.C. and X. Wang, *RAS: Striking at the Core of the Oncogenic Circuitry.* 2019. **9**.
27. Aubrey, B.J., A. Strasser, and G.L. Kelly, *Tumor-Suppressor Functions of the TP53 Pathway.* Cold Spring Harbor perspectives in medicine, 2016. **6**(5): p. a026062.
28. Ozaki, T. and A. Nakagawara, *Role of p53 in Cell Death and Human Cancers.* Cancers, 2011. **3**(1): p. 994-1013.

29. Hanahan, D. and Robert A. Weinberg, *Hallmarks of Cancer: The Next Generation.* Cell, 2011. **144**(5): p. 646-674.
30. Ascierto, P.A., et al., *The role of BRAF V600 mutation in melanoma.* Journal of translational medicine, 2012. **10**: p. 85-85.
31. Lukashev, M.E. and Z. Werb, *ECM signalling: orchestrating cell behaviour and misbehaviour.* Trends Cell Biol, 1998. **8**(11): p. 437-41.
32. Amin, A.R.M.R., et al., *Evasion of anti-growth signaling: A key step in tumorigenesis and potential target for treatment and prophylaxis by natural compounds.* Seminars in cancer biology, 2015. **35 Suppl**: p. S55-S77.
33. Amin, A.R.M.R., et al., *Evasion of anti-growth signaling: A key step in tumorigenesis and potential target for treatment and prophylaxis by natural compounds.* Seminars in Cancer Biology, 2015. **35**: p. S55-S77.
34. Aubrey, B.J., et al., *How does p53 induce apoptosis and how does this relate to p53-mediated tumour suppression?* Cell Death & Differentiation, 2018. **25**(1): p. 104-113.
35. Fulda, S. and K.M. Debatin, *Extrinsic versus intrinsic apoptosis pathways in anticancer chemotherapy.* Oncogene, 2006. **25**(34): p. 4798-4811.
36. Fajkus, J., M. Dvorácková, and E. Sýkorová, *Analysis of telomeres and telomerase.* Methods Mol Biol, 2008. **463**: p. 267-96.
37. Trybek, T., et al., *Telomeres and telomerase in oncogenesis (Review).* Oncol Lett, 2020. **20**(2): p. 1015-1027.
38. Jafri, M.A., et al., *Roles of telomeres and telomerase in cancer, and advances in telomerase-targeted therapies.* Genome Med, 2016. **8**(1): p. 69.
39. Dratwa, M., et al., *TERT—Regulation and Roles in Cancer Formation.* 2020. **11**.
40. Kaur, S., et al., *Thrombospondin-1 inhibits VEGF receptor-2 signaling by disrupting its association with CD47.* J Biol Chem, 2010. **285**(50): p. 38923-32.
41. Nishida, N., et al., *Angiogenesis in cancer.* Vascular health and risk management, 2006. **2**(3): p. 213-219.
42. Liberti, M.V. and J.W. Locasale, *The Warburg Effect: How Does it Benefit Cancer Cells?* Trends in biochemical sciences, 2016. **41**(3): p. 211-218.
43. Al Tameemi, W., et al., *Hypoxia-Modified Cancer Cell Metabolism.* 2019. **7**(4).
44. Martin TA, Y.L., Sanders AJ, et al. Cancer Invasion and Metastasis: Molecular and Cellular Perspective. In: Madame Curie Bioscience Database [Internet]. Austin (TX): Landes Bioscience; 2000-2013. Available from: https://www.ncbi.nlm.nih.gov/books/NBK164700/.
45. Mrozik, K.M., et al., *N-cadherin in cancer metastasis, its emerging role in haematological malignancies and potential as a therapeutic target in cancer.* BMC Cancer, 2018. **18**(1): p. 939.
46. Araki, K., et al., *E/N-cadherin switch mediates cancer progression via TGF-β-induced epithelial-to-mesenchymal transition in extrahepatic cholangiocarcinoma.* Br J Cancer, 2011. **105**(12): p. 1885-93.
47. Gheldof, A. and G. Berx, *Cadherins and epithelial-to-mesenchymal transition.* Prog Mol Biol Transl Sci, 2013. **116**: p. 317-36.
48. Birchmeier, W. and J. Behrens, *Cadherin expression in carcinomas: role in the formation of cell junctions and the prevention of invasiveness.* Biochim Biophys Acta, 1994. **1198**(1): p. 11-26.
49. Gottardi, C.J., E. Wong, and B.M. Gumbiner, *E-cadherin suppresses cellular transformation by inhibiting beta-catenin signaling in an adhesion-independent manner.* J Cell Biol, 2001. **153**(5): p. 1049-60.

50. Glinsky, G.V., et al., *Apoptosis and metastasis: increased apoptosis resistance of metastatic cancer cells is associated with the profound deficiency of apoptosis execution mechanisms.* Cancer Letters, 1997. **115**(2): p. 185-193.
51. Lin, Y., J. Xu, and H. Lan, *Tumor-associated macrophages in tumor metastasis: biological roles and clinical therapeutic applications.* Journal of Hematology & Oncology, 2019. **12**(1): p. 76.
52. Pearson, G.W., *Control of Invasion by Epithelial-to-Mesenchymal Transition Programs during Metastasis.* Journal of clinical medicine, 2019. **8**(5): p. 646.
53. Coussens, L.M. and Z. Werb, *Inflammation and cancer.* Nature, 2002. **420**(6917): p. 860-867.
54. Grivennikov, S.I., F.R. Greten, and M. Karin, *Immunity, inflammation, and cancer.* Cell, 2010. **140**(6): p. 883-899.
55. Mantovani, A., et al., *Cancer-related inflammation.* Nature, 2008. **454**(7203): p. 436-444.
56. Meylan, E., et al., *Requirement for NF-κB signalling in a mouse model of lung adenocarcinoma.* Nature, 2009. **462**(7269): p. 104-107.
57. Mori, T., et al., *IL-1β and TNFα-initiated IL-6–STAT3 pathway is critical in mediating inflammatory cytokines and RANKL expression in inflammatory arthritis.* International Immunology, 2011. **23**(11): p. 701-712.
58. Greten, F.R. and S.I. Grivennikov, *Inflammation and Cancer: Triggers, Mechanisms, and Consequences.* Immunity, 2019. **51**(1): p. 27-41.
59. Colotta, F., et al., *Cancer-related inflammation, the seventh hallmark of cancer: links to genetic instability.* Carcinogenesis, 2009. **30**(7): p. 1073-81.
60. Lakatos, P.-L. and L. Lakatos, *Risk for colorectal cancer in ulcerative colitis: changes, causes and management strategies.* World journal of gastroenterology, 2008. **14**(25): p. 3937-3947.
61. Freeman, H.-J., *Colorectal cancer risk in Crohn's disease.* World journal of gastroenterology, 2008. **14**(12): p. 1810-1811.
62. Wroblewski, L.E., R.M. Peek, Jr., and K.T. Wilson, *Helicobacter pylori and gastric cancer: factors that modulate disease risk.* Clinical microbiology reviews, 2010. **23**(4): p. 713-739.
63. El-Serag, H.B., *Epidemiology of viral hepatitis and hepatocellular carcinoma.* Gastroenterology, 2012. **142**(6): p. 1264-1273.e1.
64. Singh, N., et al., *Inflammation and cancer.* Annals of African medicine, 2019. **18**(3): p. 121-126.
65. Pekarek, B., S. Buck, and L. Osher, *A Comprehensive Review on Marjolin's Ulcers: Diagnosis and Treatment.* The journal of the American College of Certified Wound Specialists, 2011. **3**(3): p. 60-64.
66. Noonan, C.W., *Environmental asbestos exposure and risk of mesothelioma.* Annals of translational medicine, 2017. **5**(11): p. 234-234.
67. Thomson, N.C., R. Chaudhuri, and E. Livingston, *Asthma and cigarette smoking.* 2004. **24**(5): p. 822-833.
68. Kim, J.J., et al., *Lung Cancer Associated with Sarcoidosis - A case report.* The Korean journal of thoracic and cardiovascular surgery, 2011. **44**(4): p. 301-303.
69. Mayron, R., et al., *Verrucous carcinoma arising in ulcerative lichen planus of the soles.* J Dermatol Surg Oncol, 1988. **14**(5): p. 547-51.
70. Itatani, Y., et al., *The Role of Chemokines in Promoting Colorectal Cancer Invasion/Metastasis.* International journal of molecular sciences, 2016. **17**(5): p. 643.

71. Luo, J.-L., et al., *Inhibition of NF-κB in cancer cells converts inflammation- induced tumor growth mediated by TNFα to TRAIL-mediated tumor regression.* Cancer Cell, 2004. **6**(3): p. 297-305.
72. Wang, K. and M. Karin, *Tumor-Elicited Inflammation and Colorectal Cancer.* Adv Cancer Res, 2015. **128**: p. 173-96.
73. Taylor, C.T. and S.P. Colgan, *Regulation of immunity and inflammation by hypoxia in immunological niches.* Nature Reviews Immunology, 2017. **17**(12): p. 774-785.
74. Wang, X. and Y. Lin, *Tumor necrosis factor and cancer, buddies or foes?* Acta pharmacologica Sinica, 2008. **29**(11): p. 1275-1288.
75. Al Obeed, O.A., et al., *Increased expression of tumor necrosis factor-α is associated with advanced colorectal cancer stages.* World journal of gastroenterology, 2014. **20**(48): p. 18390-18396.
76. Nakayama, S., et al., *TNF-α receptor 1 expression predicts poor prognosis of diffuse large B-cell lymphoma, not otherwise specified.* Am J Surg Pathol, 2014. **38**(8): p. 1138-46.
77. Tanaka, T., M. Narazaki, and T. Kishimoto, *IL-6 in inflammation, immunity, and disease.* Cold Spring Harbor perspectives in biology, 2014. **6**(10): p. a016295-a016295.
78. Kumari, N., et al., *Role of interleukin-6 in cancer progression and therapeutic resistance.* Tumor Biology, 2016. **37**(9): p. 11553-11572.
79. Wei, L.-H., et al., *The anti-apoptotic role of interleukin-6 in human cervical cancer is mediated by up-regulation of Mcl-1 through a PI 3-K/Akt pathway.* Oncogene, 2001. **20**(41): p. 5799-5809.
80. Gopinathan, G., et al., *Interleukin-6 Stimulates Defective Angiogenesis.* Cancer research, 2015. **75**(15): p. 3098-3107.
81. Sha, Y. and S. Markovic-Plese, *Activated IL-1RI Signaling Pathway Induces Th17 Cell Differentiation via Interferon Regulatory Factor 4 Signaling in Patients with Relapsing-Remitting Multiple Sclerosis.* 2016. **7**(543).
82. Yan, J., M.J. Smyth, and M.W.L. Teng, *Interleukin (IL)-12 and IL-23 and Their Conflicting Roles in Cancer.* Cold Spring Harbor perspectives in biology, 2018. **10**(7): p. a028530.
83. Lust, J.A. and K.A. Donovan, *The role of interleukin-1 beta in the pathogenesis of multiple myeloma.* Hematol Oncol Clin North Am, 1999. **13**(6): p. 1117-25.
84. Pan, Y., et al., *Tumor-Associated Macrophages in Tumor Immunity.* Front Immunol, 2020. **11**: p. 583084.
85. Ley, K., *M1 Means Kill; M2 Means Heal.* The Journal of Immunology, 2017. **199**(7): p. 2191.
86. Martinez, F.O. and S. Gordon, *The M1 and M2 paradigm of macrophage activation: time for reassessment.* F1000Prime Rep, 2014. **6**: p. 13.
87. Sica, A. and A. Mantovani, *Macrophage plasticity and polarization: in vivo veritas.* J Clin Invest, 2012. **122**(3): p. 787-95.
88. Shapouri-Moghaddam, A., et al., *Macrophage plasticity, polarization, and function in health and disease.* Journal of Cellular Physiology, 2018. **233**(9): p. 6425-6440.
89. Loberg, R.D., et al., *CCL2 is a potent regulator of prostate cancer cell migration and proliferation.* Neoplasia (New York, N.Y.), 2006. **8**(7): p. 578-586.
90. Loberg, R.D., et al., *CCL2 is a potent regulator of prostate cancer cell migration and proliferation.* Neoplasia, 2006. **8**(7): p. 578-86.
91. Pujari, R., et al., *A20-mediated negative regulation of canonical NF-κB signaling pathway.* Immunologic Research, 2013. **57**(1): p. 166-171.
92. Liu, T., et al., *NF-κB signaling in inflammation.* Signal transduction and targeted therapy, 2017. **2**: p. 17023.

93. Mussbacher, M., et al., *Cell Type-Specific Roles of NF-κB Linking Inflammation and Thrombosis.* Frontiers in immunology, 2019. **10**: p. 85-85.
94. Szondy, Z., et al., *Anti-inflammatory Mechanisms Triggered by Apoptotic Cells during Their Clearance.* Frontiers in immunology, 2017. **8**: p. 909-909.
95. Nakazawa, H., et al., *iNOS as a Driver of Inflammation and Apoptosis in Mouse Skeletal Muscle after Burn Injury: Possible Involvement of Sirt1 S-Nitrosylation-Mediated Acetylation of p65 NF-κB and p53.* PloS one, 2017. **12**(1): p. e0170391-e0170391.
96. Chen, T., et al., *Chemopreventive effects of a selective nitric oxide synthase inhibitor on carcinogen-induced rat esophageal tumorigenesis.* Cancer Res, 2004. **64**(10): p. 3714-7.
97. Fonseca, S.G., et al., *TNF-alpha mediates the induction of nitric oxide synthase in macrophages but not in neutrophils in experimental cutaneous leishmaniasis.* Eur J Immunol, 2003. **33**(8): p. 2297-306.
98. Tripathi, P., et al., *The role of nitric oxide in inflammatory reactions.* FEMS Immunology & Medical Microbiology, 2007. **51**(3): p. 443-452.
99. Gallo, O., et al., *Role of nitric oxide in angiogenesis and tumor progression in head and neck cancer.* J Natl Cancer Inst, 1998. **90**(8): p. 587-96.
100. Font-Nieves, M., et al., *Induction of COX-2 enzyme and down-regulation of COX-1 expression by lipopolysaccharide (LPS) control prostaglandin E2 production in astrocytes.* J Biol Chem, 2012. **287**(9): p. 6454-68.
101. Muraoka, N., et al., *Role of cyclooxygenase-2-mediated prostaglandin E2-prostaglandin E receptor 4 signaling in cardiac reprogramming.* Nature Communications, 2019. **10**(1): p. 674.
102. FitzGerald, G.A., *COX-2 and beyond: approaches to prostaglandin inhibition in human disease.* Nature Reviews Drug Discovery, 2003. **2**(11): p. 879-890.
103. Pang, L.Y., E.A. Hurst, and D.J. Argyle, *Cyclooxygenase-2: A Role in Cancer Stem Cell Survival and Repopulation of Cancer Cells during Therapy.* Stem Cells Int, 2016. **2016**: p. 2048731.
104. Liu, B., L. Qu, and S. Yan, *Cyclooxygenase-2 promotes tumor growth and suppresses tumor immunity.* Cancer Cell International, 2015. **15**(1): p. 106.
105. Ghosh, N., et al., *COX-2 as a target for cancer chemotherapy.* Pharmacological Reports, 2010. **62**(2): p. 233-244.
106. Huang, R.Y. and G.G. Chen, *Cigarette smoking, cyclooxygenase-2 pathway and cancer.* Biochim Biophys Acta, 2011. **1815**(2): p. 158-69.
107. Eltzschig, H.K. and P. Carmeliet, *Hypoxia and inflammation.* The New England journal of medicine, 2011. **364**(7): p. 656-665.
108. Masoud, G.N. and W. Li, *HIF-1α pathway: role, regulation and intervention for cancer therapy.* Acta Pharm Sin B, 2015. **5**(5): p. 378-89.
109. Balamurugan, K., *HIF-1 at the crossroads of hypoxia, inflammation, and cancer.* International Journal of Cancer, 2016. **138**(5): p. 1058-1066.
110. Imtiyaz, H.Z. and M.C. Simon, *Hypoxia-inducible factors as essential regulators of inflammation.* Curr Top Microbiol Immunol, 2010. **345**: p. 105-20.
111. Jun, J.C., et al., *Hypoxia-Inducible Factors and Cancer.* Current sleep medicine reports, 2017. **3**(1): p. 1-10.
112. Maxwell, S.A. and G.E. Davis, *Differential gene expression in p53-mediated apoptosis-resistant vs. apoptosis-sensitive tumor cell lines.* 2000. **97**(24): p. 13009-13014.
113. Lipponen, P., et al., *Apoptosis suppressing protein bcl-2 is expressed in well-differentiated breast carcinomas with favourable prognosis.* J Pathol, 1995. **177**(1): p. 49-55.

114. Wang, R.A., et al., *Apoptosis drives cancer cells proliferate and metastasize.* J Cell Mol Med, 2013. **17**(1): p. 205-11.
115. Lipponen, P., et al., *Apoptosis in breast cancer as related to histopathological characteristics and prognosis.* Eur J Cancer, 1994. **30a**(14): p. 2068-73.
116. Vaquero, J., et al., *Relationship between apoptosis and proliferation in secondary tumors of the brain.* Neuropathology, 2004. **24**(4): p. 302-5.
117. Pillai, K., et al., *Does the expression of BCL2 have prognostic significance in malignant peritoneal mesothelioma?* American journal of cancer research, 2013. **3**(3): p. 312-322.
118. Wang, R.-A., et al., *Apoptosis drives cancer cells proliferate and metastasize.* Journal of cellular and molecular medicine, 2013. **17**(1): p. 205-211.
119. Li, J. and J. Yuan, *Caspases in apoptosis and beyond.* Oncogene, 2008. **27**(48): p. 6194-6206.
120. Elmore, S., *Apoptosis: a review of programmed cell death.* Toxicologic pathology, 2007. **35**(4): p. 495-516.
121. Schimmer, A.D., *Inhibitor of apoptosis proteins: translating basic knowledge into clinical practice.* Cancer Res, 2004. **64**(20): p. 7183-90.
122. Galluzzi, L., O. Kepp, and G. Kroemer, *5 - Pathophysiology of Cancer Cell Death*, in *Abeloff's Clinical Oncology (Fifth Edition)*, J.E. Niederhuber, et al., Editors. 2014, Churchill Livingstone: Philadelphia. p. 69-77.e3.
123. Carneiro, B.A. and W.S. El-Deiry, *Targeting apoptosis in cancer therapy.* Nature Reviews Clinical Oncology, 2020. **17**(7): p. 395-417.
124. Khan, K.H., M. Blanco-Codesido, and L.R. Molife, *Cancer therapeutics: Targeting the apoptotic pathway.* Critical Reviews in Oncology/Hematology, 2014. **90**(3): p. 200-219.
125. Pfeffer, C.M. and A.T.K. Singh, *Apoptosis: A Target for Anticancer Therapy.* International journal of molecular sciences, 2018. **19**(2): p. 448.
126. Samec, M., et al., *Flavonoids Targeting HIF-1: Implications on Cancer Metabolism.* Cancers, 2021. **13**(1).
127. Liskova, A., et al., *Flavonoids in Cancer Metastasis.* 2020. **12**(6): p. 1498.
128. Abotaleb, M., et al., *Flavonoids in Cancer and Apoptosis.* 2019. **11**(1): p. 28.
129. Vuong, T., et al., *Role of a polyphenol-enriched preparation on chemoprevention of mammary carcinoma through cancer stem cells and inflammatory pathways modulation.* Journal of Translational Medicine, 2016. **14**(1): p. 13.
130. Jiang, M., et al., *Hydroxysafflor yellow A inhibited lipopolysaccharide-induced non-small cell lung cancer cell proliferation, migration, and invasion by suppressing the PI3K/AKT/mTOR and ERK/MAPK signaling pathways.* Thoracic Cancer, 2019. **10**(6): p. 1319-1333.
131. Zhang, X., et al., *Systems pharmacology unravels the synergic target space and therapeutic potential of Rhodiola rosea L. for non-small cell lung cancer.* Phytomedicine, 2020. **79**: p. 153326.
132. Liang, Y.-C., et al., *Suppression of inducible cyclooxygenase and inducible nitric oxide synthase by apigenin and related flavonoids in mouse macrophages.* Carcinogenesis, 1999. **20**(10): p. 1945-1952.
133. Lim, R.Z.L., et al., *STAT-3 regulation of CXCR4 is necessary for the prenylflavonoid Icaritin to enhance mesenchymal stem cell proliferation, migration and osteogenic differentiation.* Biochim Biophys Acta Gen Subj, 2018. **1862**(7): p. 1680-1692.
134. Kim, B. and B. Park, *Baohuoside I Suppresses Invasion of Cervical and Breast Cancer Cells through the Downregulation of CXCR4 Chemokine Receptor Expression.* Biochemistry, 2014. **53**(48): p. 7562-7569.

135. Cao, D., et al., *Luteolin suppresses epithelial-mesenchymal transition and migration of triple-negative breast cancer cells by inhibiting YAP/TAZ activity.* Biomedicine & Pharmacotherapy, 2020. **129**: p. 110462.
136. Subbaraj, G.K., Y.S. Kumar, and L. Kulanthaivel, *Antiangiogenic role of natural flavonoids and their molecular mechanism: an update.* The Egyptian Journal of Internal Medicine, 2021. **33**(1): p. 29.
137. Shukla, K., et al., *Didymin by suppressing NF-κB activation prevents VEGF-induced angiogenesis in vitro and in vivo.* Vascular Pharmacology, 2019. **115**: p. 18-25.
138. Forghani, P., M.R. Khorramizadeh, and E.K. Waller, *Silibinin inhibits accumulation of myeloid-derived suppressor cells and tumor growth of murine breast cancer.* Cancer Med, 2014. **3**(2): p. 215-24.
139. Yahfoufi, N., et al., *The Immunomodulatory and Anti-Inflammatory Role of Polyphenols.* Nutrients, 2018. **10**(11).
140. Kopustinskiene, D.M., et al., *Flavonoids as Anticancer Agents.* Nutrients, 2020. **12**(2).
141. Katiyar, S.K., R. Agarwal, and H. Mukhtar, *Inhibition of both stage I and stage II skin tumor promotion in SENCAR mice by a polyphenolic fraction isolated from green tea: inhibition depends on the duration of polyphenol treatment.* Carcinogenesis, 1993. **14**(12): p. 2641-2643.
142. Granato, M., et al., *Quercetin induces apoptosis and autophagy in primary effusion lymphoma cells by inhibiting PI3K/AKT/mTOR and STAT3 signaling pathways.* The Journal of Nutritional Biochemistry, 2017. **41**: p. 124-136.
143. Zhu, J.f., et al., *Icaritin Shows Potent Anti-Leukemia Activity on Chronic Myeloid Leukemia In Vitro and In Vivo by Regulating MAPK/ERK/JNK and JAK2/STAT3 /AKT Signalings.* PLOS ONE, 2011. **6**(8): p. e23720.
144. Peng, H.-L., et al., *Fisetin inhibits the generation of inflammatory mediators in interleukin-1β–induced human lung epithelial cells by suppressing the NF-κB and ERK1/2 pathways.* International Immunopharmacology, 2018. **60**: p. 202-210.
145. Zhang, X.-J. and S.-S. Jia, *Fisetin inhibits laryngeal carcinoma through regulation of AKT/NF-κB/mTOR and ERK1/2 signaling pathways.* Biomedicine & Pharmacotherapy, 2016. **83**: p. 1164-1174.
146. Johnson, J.J., *Carnosol: a promising anti-cancer and anti-inflammatory agent.* Cancer Lett, 2011. **305**(1): p. 1-7.
147. Shi, B., et al., *Carnosic acid and fisetin combination therapy enhances inhibition of lung cancer through apoptosis induction.* Int J Oncol, 2017. **50**(6): p. 2123-2135.
148. Song, S., et al., *Luteolin selectively kills STAT3 highly activated gastric cancer cells through enhancing the binding of STAT3 to SHP-1.* Cell Death & Disease, 2017. **8**(2): p. e2612-e2612.
149. Jiang, Z.-B., et al., *Luteolin and its derivative apigenin suppress the inducible PD-L1 expression to improve anti-tumor immunity in KRAS-mutant lung cancer.* Cancer Letters, 2021. **515**: p. 36-48.
150. Yang, J., C. Pi, and G. Wang, *Inhibition of PI3K/Akt/mTOR pathway by apigenin induces apoptosis and autophagy in hepatocellular carcinoma cells.* Biomedicine & Pharmacotherapy, 2018. **103**: p. 699-707.
151. Park, C.-H., et al., *Effects of Apigenin on RBL-2H3, RAW264.7, and HaCaT Cells: Anti-Allergic, Anti-Inflammatory, and Skin-Protective Activities.* 2020. **21**(13): p. 4620.
152. Qiu, J.-G., et al., *Apigenin Inhibits IL-6 Transcription and Suppresses Esophageal Carcinogenesis.* 2019. **10**.
153. Abotaleb, M., et al., *Flavonoids in Cancer and Apoptosis.* Cancers (Basel), 2018. **11**(1).
154. Kanakis, C., et al., *An Overview of DNA and RNA Bindings to Antioxidant Flavonoids.* Cell biochemistry and biophysics, 2007. **49**: p. 29-36.

155. Kanakis, C.D., et al., *An overview of DNA and RNA bindings to antioxidant flavonoids.* Cell biochemistry and biophysics, 2007. **49**(1): p. 29-36.
156. Hegde, A.H., S.N. Prashanth, and J. Seetharamappa, *Interaction of antioxidant flavonoids with calf thymus DNA analyzed by spectroscopic and electrochemical methods.* J Pharm Biomed Anal, 2012. **63**: p. 40-6.
157. Tawani, A. and A. Kumar, *Structural Insight into the interaction of Flavonoids with Human Telomeric Sequence.* Scientific Reports, 2015. **5**(1): p. 17574.
158. Yue, E., et al., *Anthocyanin is involved in the activation of pyroptosis in oral squamous cell carcinoma.* Phytomedicine, 2019. **56**: p. 286-294.
159. Liu, X., et al., *Anti-breast cancer potential of daidzein in rodents.* Life Sci, 2012. **91**(11-12): p. 415-9.
160. Amawi, H., C.R. Ashby, Jr., and A.K. Tiwari, *Cancer chemoprevention through dietary flavonoids: what's limiting?* Chinese journal of cancer, 2017. **36**(1): p. 50-50.
161. Los, M., et al., *Activation and Caspase-mediated Inhibition of PARP: A Molecular Switch between Fibroblast Necrosis and Apoptosis in Death Receptor Signaling.* 2002. **13**(3): p. 978-988.
162. Shukla, R., et al., *Chapter 18 - Role of Flavonoids in Management of Inflammatory Disorders*, in *Bioactive Food as Dietary Interventions for Arthritis and Related Inflammatory Diseases (Second Edition)*, R.R. Watson and V.R. Preedy, Editors. 2019, Academic Press. p. 293-322.
163. Fortes Rossato, M., et al., *Eriodictyol: A flavonoid antagonist of the TRPV1 receptor with antioxidant activity.* Biochemical pharmacology, 2010. **81**: p. 544-51.
164. Johnson, J., P. Maher, and A. Hanneken, *The flavonoid, eriodictyol, induces long-term protection in ARPE-19 cells through its effects on Nrf2 activation and phase 2 gene expression.* Investigative ophthalmology & visual science, 2009. **50**(5): p. 2398-2406.
165. Li, C.Z., et al., *Eriodictyol attenuates cisplatin-induced kidney injury by inhibiting oxidative stress and inflammation.* Eur J Pharmacol, 2016. **772**: p. 124-30.
166. Mokdad-Bzeouich, I., et al., *Investigation of immunomodulatory and anti-inflammatory effects of eriodictyol through its cellular anti-oxidant activity.* Cell stress & chaperones, 2016. **21**(5): p. 773-781.
167. Calderón-Oliver, M. and E. Ponce-Alquicira, *Chapter 7 - Fruits: A Source of Polyphenols and Health Benefits*, in *Natural and Artificial Flavoring Agents and Food Dyes*, A.M. Grumezescu and A.M. Holban, Editors. 2018, Academic Press. p. 189-228.
168. Wang, Y., et al., *Eriodictyol inhibits IL-1β-induced inflammatory response in human osteoarthritis chondrocytes.* Biomedicine & Pharmacotherapy, 2018. **107**: p. 1128-1134.
169. Li, W., et al., *Eriodictyol Inhibits Proliferation, Metastasis and Induces Apoptosis of Glioma Cells via PI3K/Akt/NF-κB Signaling Pathway.* 2020. **11**(114).
170. Liu, K., et al., *Eriodictyol Inhibits RSK2-ATF1 Signaling and Suppresses EGF-induced Neoplastic Cell Transformation **.* Journal of Biological Chemistry, 2011. **286**(3): p. 2057-2066.
171. Kumazoe, M., et al., *Metabolic Profiling-based Data-mining for an Effective Chemical Combination to Induce Apoptosis of Cancer Cells.* Scientific Reports, 2015. **5**(1): p. 9474.
172. Tewari, D., P. Rawat, and P.K. Singh, *Adverse drug reactions of anticancer drugs derived from natural sources.* Food and Chemical Toxicology, 2019. **123**: p. 522-535.
173. Liu, Z.-B., et al., *Natural substances derived from herbs or plants are promising sources of anticancer agents against colorectal cancer via triggering apoptosis.* Journal of Pharmacy and Pharmacology, 2021: p. rgab130.

174. Ma, X. and Z. Wang, *Anticancer drug discovery in the future: an evolutionary perspective.* Drug Discovery Today, 2009. **14**(23): p. 1136-1142.
175. Lee, J.K., *Anti-inflammatory effects of eriodictyol in lipopolysaccharide-stimulated raw 264.7 murine macrophages.* Arch Pharm Res, 2011. **34**(4): p. 671-9.
176. Liu, K., et al., *Eriodictyol inhibits RSK2-ATF1 signaling and suppresses EGF-induced neoplastic cell transformation.* J Biol Chem, 2011. **286**(3): p. 2057-66.
177. Kumazoe, M., et al., *Metabolic profiling-based data-mining for an effective chemical combination to induce apoptosis of cancer cells.* Sci Rep, 2015. **5**: p. 9474.
178. Tang, L., et al., *Eriodictyol inhibits the growth of CNE1 human nasopharyngeal cancer growth by targeting MEK/ERK signalling pathway, inducing cellular autophagy and inhibition of cell migration and invasion.* J buon, 2020. **25**(5): p. 2389-2394.
179. Zhang, Y., R. Zhang, and H. Ni, *Eriodictyol exerts potent anticancer activity against A549 human lung cancer cell line by inducing mitochondrial-mediated apoptosis, G2/M cell cycle arrest and inhibition of m-TOR/PI3K/Akt signalling pathway.* Archives of medical science : AMS, 2019. **16**(2): p. 446-452.
180. Qian, S., O. Golubnitschaja, and X. Zhan, *Chronic inflammation: key player and biomarker-set to predict and prevent cancer development and progression based on individualized patient profiles.* EPMA Journal, 2019. **10**(4): p. 365-381.
181. Diaz-Borjon, A., C.M. Weyand, and J.J. Goronzy, *Treatment of chronic inflammatory diseases with biologic agents: opportunities and risks for the elderly.* Experimental gerontology, 2006. **41**(12): p. 1250-1255.
182. Klein, A. and R. Eliakim, *Non Steroidal Anti-Inflammatory Drugs and Inflammatory Bowel Disease.* Pharmaceuticals (Basel, Switzerland), 2010. **3**(4): p. 1084-1092.
183. Davis, A. and J. Robson, *The dangers of NSAIDs: look both ways.* The British journal of general practice : the journal of the Royal College of General Practitioners, 2016. **66**(645): p. 172-173.
184. Yuan, G., et al., *Natural products and anti-inflammatory activity.* Asia Pac J Clin Nutr, 2006. **15**(2): p. 143-52.
185. Miyake, Y., K. Yamamoto, and T. Osawa, *Isolation of Eriocitrin (Eriodictyol 7-rutinoside) from Lemon Fruit (<I>Citrus limon</I> BURM. f.) and Its Antioxidative Activity.* Food Science and Technology International, Tokyo, 1997. **3**(1): p. 84-89.
186. Zeinali, M., S.A. Rezaee, and H. Hosseinzadeh, *An overview on immunoregulatory and anti-inflammatory properties of chrysin and flavonoids substances.* Biomed Pharmacother, 2017. **92**: p. 998-1009.
187. Li, Y., et al., *Quercetin, Inflammation and Immunity.* Nutrients, 2016. **8**(3): p. 167-167.
188. Peairs, A., et al., *Epigallocatechin-3-gallate (EGCG) attenuates inflammation in MRL/lpr mouse mesangial cells.* Cellular & Molecular Immunology, 2010. **7**(2): p. 123-132.
189. Talebi, M., et al., *Emerging cellular and molecular mechanisms underlying anticancer indications of chrysin.* Cancer Cell International, 2021. **21**(1): p. 214.
190. Srivastava, S., et al., *Quercetin, a Natural Flavonoid Interacts with DNA, Arrests Cell Cycle and Causes Tumor Regression by Activating Mitochondrial Pathway of Apoptosis.* Scientific Reports, 2016. **6**(1): p. 24049.
191. Chen, B.-H., et al., *Anticancer effects of epigallocatechin-3-gallate nanoemulsion on lung cancer cells through the activation of AMP-activated protein kinase signaling pathway.* Scientific Reports, 2020. **10**(1): p. 5163.
192. Raybaudi-Massilia, R., et al., *An Analysis In-vitro of the Cytotoxic, Antioxidant and Antimicrobial Activity of Aqueous and Alcoholic Extracts of Annona muricata L. Seed and Pulp.* British Journal of Applied Science & Technology, 2015. **5**: p. 333-341.

193. Torrenegra, R., et al., *Antiproliferative activity of extracts of Gnaphalium Gracile H.B.K. against cancer cell lines.* Pharmacologyonline, 2018. **2**: p. 113-122.
194. Coussens, L.M. and Z. Werb, *Inflammation and cancer.* Nature, 2002. **420**(6917): p. 860-7.
195. Whiteside, T.L., *The tumor microenvironment and its role in promoting tumor growth.* Oncogene, 2008. **27**(45): p. 5904-5912.
196. Elahi, S., et al., *Immunosuppressive CD71+ erythroid cells compromise neonatal host defence against infection.* Nature, 2013. **504**(7478): p. 158-62.
197. Bosetti, C., S. Gallus, and C. La Vecchia, *Aspirin and cancer risk: an updated quantitative review to 2005.* Cancer Causes & Control, 2006. **17**(7): p. 871-888.
198. Cuzick, J., et al., *Aspirin and non-steroidal anti-inflammatory drugs for cancer prevention: an international consensus statement.* The Lancet Oncology, 2009. **10**(5): p. 501-507.
199. Halter, F., *Mechanism of gastrointestinal toxicity of NSAIDs.* Scand J Rheumatol Suppl, 1988. **73**: p. 16-21.
200. Davies, N.M. and F. Jamali, *COX-2 selective inhibitors cardiac toxicity: getting to the heart of the matter.* J Pharm Pharm Sci, 2004. **7**(3): p. 332-6.
201. Shaikh, R., et al., *Evaluation of Anticancer, Antioxidant, and Possible Anti-inflammatory Properties of Selected Medicinal Plants Used in Indian Traditional Medication.* Journal of Traditional and Complementary Medicine, 2014. **4**(4): p. 253-257.
202. Pandey, B.P., et al., *In-vitro antioxidant, anti-cancer, and anti-inflammatory activities of selected medicinal plants from western Nepal.* Future Journal of Pharmaceutical Sciences, 2020. **6**(1): p. 75.
203. Panche, A.N., A.D. Diwan, and S.R. Chandra, *Flavonoids: an overview.* Journal of nutritional science, 2016. **5**: p. e47-e47.
204. Karunaweera, N., et al., *Plant polyphenols as inhibitors of NF-κB induced cytokine production—a potential anti-inflammatory treatment for Alzheimer's disease?* 2015. **8**.
205. Choy, K.W., et al., *Flavonoids as Natural Anti-Inflammatory Agents Targeting Nuclear Factor-Kappa B (NFκB) Signaling in Cardiovascular Diseases: A Mini Review.* Frontiers in pharmacology, 2019. **10**: p. 1295-1295.
206. Otto, T. and P. Sicinski, *Cell cycle proteins as promising targets in cancer therapy.* Nature Reviews Cancer, 2017. **17**(2): p. 93-115.
207. Zhang, J.Y., *Apoptosis-based anticancer drugs.* Nature Reviews Drug Discovery, 2002. **1**(2): p. 101-102.
208. Groth-Pedersen, L. and M. Jäättelä, *Combating apoptosis and multidrug resistant cancers by targeting lysosomes.* Cancer Lett, 2013. **332**(2): p. 265-74.
209. Srivastava, R.K., et al., *Bcl-2-mediated drug resistance: inhibition of apoptosis by blocking nuclear factor of activated T lymphocytes (NFAT)-induced Fas ligand transcription.* The Journal of experimental medicine, 1999. **190**(2): p. 253-265.
210. Hientz, K., et al., *The role of p53 in cancer drug resistance and targeted chemotherapy.* Oncotarget, 2017. **8**(5): p. 8921-8946.
211. Pommier, Y., et al., *Apoptosis defects and chemotherapy resistance: molecular interaction maps and networks.* Oncogene, 2004. **23**(16): p. 2934-2949.
212. Abbaspour Babaei M, Z.H.H., Kamalidehghan B, Yeap SK, Ahmadipour F. Apoptotic induction and inhibition of NF-κB signaling pathway in human prostatic cancer PC3 cells by natural compound 2,2'-oxybis (4-allyl-1-methoxybenzene), biseugenol B, from Litsea costalis: an in vitro study. Onco Targets Ther. 2017;10:277-294 and https://doi.org/10.2147/OTT.S102894.

213. Kumar, R., P.E. Herbert, and A.N. Warrens, *An introduction to death receptors in apoptosis.* International Journal of Surgery, 2005. **3**(4): p. 268-277.
214. Szlosarek, P.W. and F.R. Balkwill, *Tumour necrosis factor α: a potential target for the therapy of solid tumours.* The Lancet Oncology, 2003. **4**(9): p. 565-573.
215. Zhao, E.F., *[Cytotoxicity of recombinant human tumor necrosis factor (rHTNF) alone and in combination with chemotherapeutic agents on human ovarian cancer cells]*. Zhonghua Fu Chan Ke Za Zhi, 1993. **28**(3): p. 153-6, 188.
216. Krosnick, J.A., et al., *Studies of the mechanisms of toxicity of the administration of recombinant tumor necrosis factor α in normal and tumor-bearing mice.* Cancer Immunology, Immunotherapy, 1989. **30**(3): p. 133-138.
217. Sentmanat, M.F., et al., *A Survey of Validation Strategies for CRISPR-Cas9 Editing.* Scientific reports, 2018. **8**(1): p. 888-888.
218. Brix, N., et al., *The clonogenic assay: robustness of plating efficiency-based analysis is strongly compromised by cellular cooperation.* Radiation Oncology, 2020. **15**(1): p. 248.
219. Chaitanya, G.V., A.J. Steven, and P.P. Babu, *PARP-1 cleavage fragments: signatures of cell-death proteases in neurodegeneration.* Cell communication and signaling : CCS, 2010. **8**: p. 31-31.
220. Boulares, A.H., et al., *Role of Poly(ADP-ribose) Polymerase (PARP) Cleavage in Apoptosis: CASPASE 3-RESISTANT PARP MUTANT INCREASES RATES OF APOPTOSIS IN TRANSFECTED CELLS *.* Journal of Biological Chemistry, 1999. **274**(33): p. 22932-22940.
221. *Tumor necrosis factor alfa*, in *Meyler's Side Effects of Drugs (Sixteenth Edition)*, J.K. Aronson, Editor. 2016, Elsevier: Oxford. p. 230-232.
222. Roberts, N.J., et al., *Systemic use of tumor necrosis factor alpha as an anticancer agent.* Oncotarget, 2011. **2**(10): p. 739-751.
223. Wang, Y., et al., *Eriodictyol inhibits IL-1β-induced inflammatory response in human osteoarthritis chondrocytes.* Biomed Pharmacother, 2018. **107**: p. 1128-1134.
224. Wang, X., et al., *Eriodictyol ameliorates lipopolysaccharide-induced acute lung injury by suppressing the inflammatory COX-2/NLRP3/NF-κB pathway in mice.* J Biochem Mol Toxicol, 2020. **34**(3): p. e22434.
225. Ireson, C.R., et al., *The role of mouse tumour models in the discovery and development of anticancer drugs.* British Journal of Cancer, 2019. **121**(2): p. 101-108.
226. Dasari, S. and P.B. Tchounwou, *Cisplatin in cancer therapy: molecular mechanisms of action.* European journal of pharmacology, 2014. **740**: p. 364-378.
227. Kwok, G., et al., *Pembrolizumab (Keytruda).* Hum Vaccin Immunother, 2016. **12**(11): p. 2777-2789.
228. Zuberi, A. and C. Lutz, *Mouse Models for Drug Discovery. Can New Tools and Technology Improve Translational Power?* ILAR journal, 2016. **57**(2): p. 178-185.
229. Kim, W.Y. and N.E. Sharpless, *Drug efficacy testing in mice.* Current topics in microbiology and immunology, 2012. **355**: p. 19-38.
230. Timm, D., et al., *Searching for novel biomarkers using a mouse model of CLN3-Batten disease.* PloS one, 2018. **13**(8): p. e0201470-e0201470.
231. Kersten, K., et al., *Genetically engineered mouse models in oncology research and cancer medicine.* EMBO Mol Med, 2017. **9**(2): p. 137-153.
232. Wei, R., et al., *Cellular and Extracellular Components in Tumor Microenvironment and Their Application in Early Diagnosis of Cancers.* Analytical Cellular Pathology, 2020. **2020**: p. 6283796.
233. Richmond, A. and Y. Su, *Mouse xenograft models vs GEM models for human cancer therapeutics.* Disease models & mechanisms, 2008. **1**(2-3): p. 78-82.

234. Simons, B.W. and C. Brayton, *Chapter 3 - Challenges and Limitations of Mouse Xenograft Models of Cancer*, in *Patient Derived Tumor Xenograft Models*, R. Uthamanthil and P. Tinkey, Editors. 2017, Academic Press. p. 25-36.
235. Baxevanis, C.N., S.A. Perez, and M. Papamichail, *Cancer immunotherapy.* Crit Rev Clin Lab Sci, 2009. **46**(4): p. 167-89.
236. http://dx.doi.org/10.4103/2394-4722.152769, L.G.P.-d.x.m.f.o.d.d.J.C.M.T.-.
237. Zhang, L., et al., *Generation of a syngeneic mouse model to study the effects of vascular endothelial growth factor in ovarian carcinoma.* Am J Pathol, 2002. **161**(6): p. 2295-309.
238. Yu, J.W., et al., *Tumor-immune profiling of murine syngeneic tumor models as a framework to guide mechanistic studies and predict therapy response in distinct tumor microenvironments.* PloS one, 2018. **13**(11): p. e0206223-e0206223.
239. Li, E., et al., *Mouse Models for Immunotherapy in Hepatocellular Carcinoma.* Cancers, 2019. **11**(11): p. 1800.
240. Yang, Y., et al., *Immunocompetent mouse allograft models for development of therapies to target breast cancer metastasis.* Oncotarget, 2017. **8**(19): p. 30621-30643.
241. Zuberi, A. and C. Lutz, *Mouse Models for Drug Discovery. Can New Tools and Technology Improve Translational Power?* Ilar j, 2016. **57**(2): p. 178-185.
242. Lampreht Tratar, U., S. Horvat, and M. Cemazar, *Transgenic Mouse Models in Cancer Research.* Frontiers in oncology, 2018. **8**: p. 268-268.
243. Gómez-Cuadrado, L., et al., *Mouse models of metastasis: progress and prospects.* Disease models & mechanisms, 2017. **10**(9): p. 1061-1074.
244. Pearson HB, P.N.M.M.I.V.I.M.C.B.D.I.A.T.L.B.-A.f.h.w.
245. Chen, F., et al., *New horizons in tumor microenvironment biology: challenges and opportunities.* BMC Medicine, 2015. **13**(1): p. 45.
246. Koo, J.H. and K.-L. Guan, *Interplay between YAP/TAZ and Metabolism.* Cell Metabolism, 2018. **28**(2): p. 196-206.
247. Karpowicz, P., J. Perez, and N. Perrimon, *The Hippo tumor suppressor pathway regulates intestinal stem cell regeneration.* Development, 2010. **137**(24): p. 4135-4145.
248. Warren, J.S., Y. Xiao, and J.M.J.C. Lamar, *YAP/TAZ activation as a target for treating metastatic cancer.* 2018. **10**(4): p. 115.
249. Micheau, O., et al., *NF-κB Signals Induce the Expression of c-FLIP.* Molecular and Cellular Biology, 2001. **21**(16): p. 5299-5305.
250. Josephs, S.F., et al., *Unleashing endogenous TNF-alpha as a cancer immunotherapeutic.* J Transl Med, 2018. **16**(1): p. 242.
251. Savva, C.G., et al., *Selective activation of TNFR1 and NF-κB inhibition by a novel biyouyanagin analogue promotes apoptosis in acute leukemia cells.* BMC cancer, 2016. **16**: p. 279-279.

5. Summary

- Eriodictyol specifically inhibits IL-6 and MCP-1 gene expression in differentiated THP-1 monocytes when induced with Lipopolysaccharide (LPS).

- Eriodictyol induces selective cytotoxicity to cancer cell lines and have negligible effect on normal (untransformed) cell lines as confirmed by both MTT assay and Annexin-V/FITC staining.

- Surprisingly, Eriodictyol also has an anti-tumorigenic impact by blocking the clonogenic ability of cancer cells at doses at least ten times lower than those required to induce apoptosis.

- Mechanistic study reveals that cytotoxicity of Eriodictyol is associated with G2/M cell cycle arrest as revealed by Propidium Iodide staining. Moreover, changes in cell cycle related proteins also confirms G2/M arrest.

- The global change in gene expression in response to Eriodictyol is checked by RNA-seq analysis which reveals significant and differential changes in genes involved in cell cycle and cell death related processes.

- Cancer cell apoptosis involves extrinsic pathways involving TNFR1, TRADD, FADD, Bax, Bcl-2, Survivin, Claspin, and downstream activation of caspase-8 and caspase-7. Moreover, due to PARP cleavage, inhibition of DNA damage repair occurs. Thereby, confirming Eriodictyol is caspase-dependent.

- Normal cell lines don't show any basal TNFR1 expression and its expression remain unaltered following Eriodictyol treatment. Cancer cells, on the other hand, has a high level of intrinsic TNFR1 expression that elevates dramatically in response to Eriodictyol.

- The CRISPR-Cas9 genome engineering technology is used to knock out the TNFR1 gene in the HeLa cell line. Apoptosis significantly increases in wild type cells compared to knock-out cells, which display insignificant apoptosis in response to Eriodictyol.

- Finally, Eriodictyol shows significant anti-tumorigenic potential in *in vivo* immune-competent syngeneic Balb/c mice bearing breast tumor without any adverse side effects.

Eriodictyol also displays its potency in inhibiting nodules formation in lungs of Balb/c mice when treated with the test compound compared to non-treated mice.

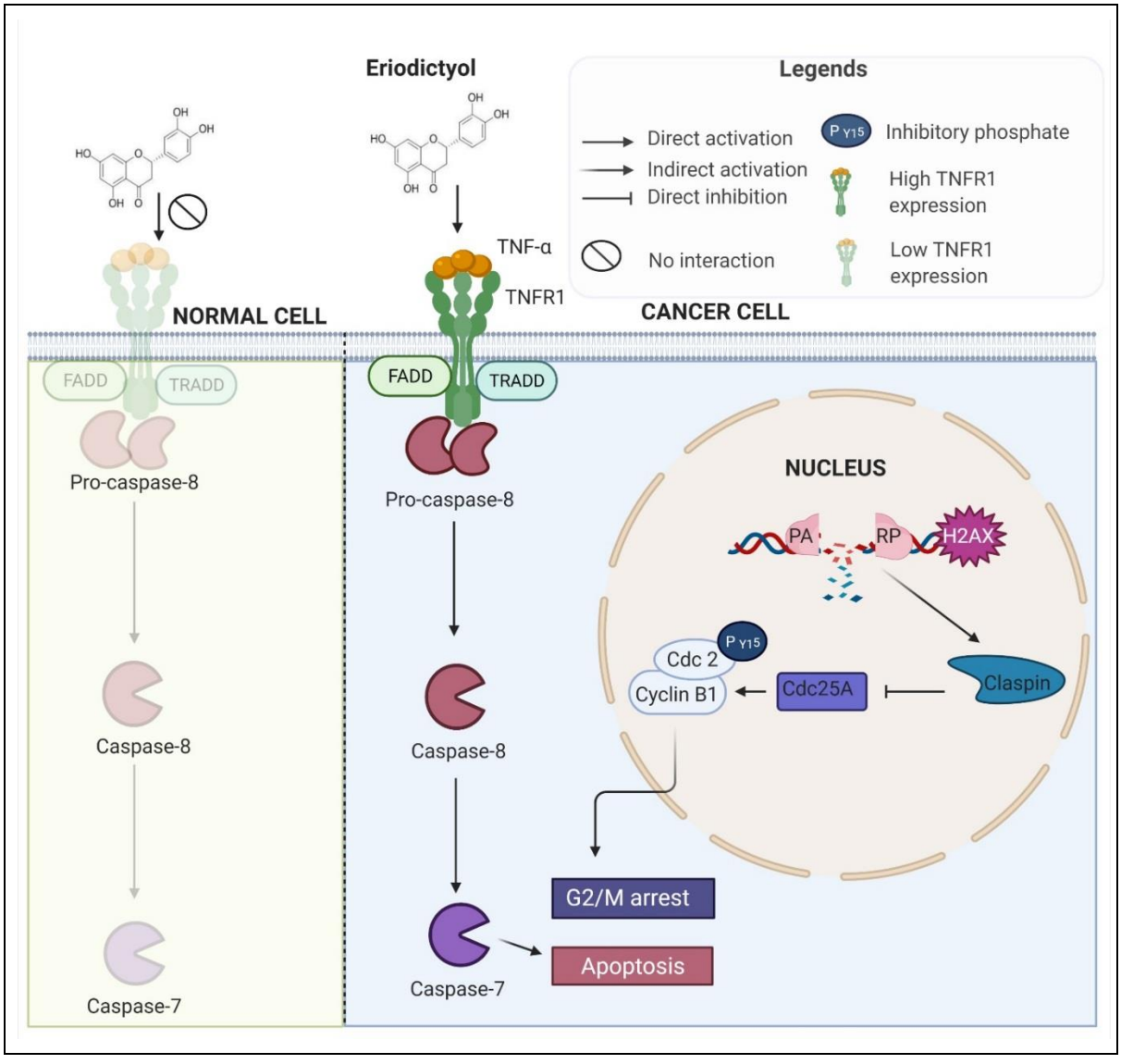

Figure 1 ***An illustration proposing the mechanism how eriodictyol mediated proliferation is selective cytotoxic to cancer cells.*** TNFR1 is expressed in cancer cells. Eriodictyol induces G2/M arrest, apoptosis and DNA damage through extrinsic (TNFR1, TRADD, FADD) and intrinsic (Bax, Bcl-2, Survivin, Claspin, γ-H2A.X) pathways leading to downstream activation of caspase (8 and 7) and PARP cleavage.

9. Conclusion

One of the hallmarks of tumor cells is evasion of apoptosis. Enhancement of the pro-apoptotic ability of the anti-cancer agents through abrogation of the survival signaling has been recognised as an effective strategy towards sensitizing the cancer cells to the chemotherapeutic drugs and preventing chemo-resistance. Recently, several natural compounds including flavonoids have acquired importance as potential anti-cancer agents endowed with the advantage of negligible side – effects and cost-effectiveness. In the present study, we have identified the selectivity of Eriodictyol as an anti-cancer lead, and further addressed the mechanism underlying the selective cytotoxic nature of Eriodictyol.

TNF family members are the multifunctional cytokines involved in a broad spectrum of biological processes which includes cell proliferation, cell death, carcinogenesis, development, inflammatory and immune responses. TNF pathway has come to limelight in cancer wherein binding of TNF ligands to TNF receptors on the cancer cells has been documented to activate the extrinsic or death receptor apoptosis pathway. Hereafter, competence of TNF-α in inducing apoptosis of cancer cells have instigated the initiation of the clinical trials to evaluate the anti-cancer efficacy of recombinant human TNF α (rhTNF-α) on advanced solid cancers. Unfortunately, in contrast to the preclinical studies, outcome of the clinical trials were disappointing as evidenced by decline in apoptosis triggering ability of rhTNF-α, which was attributed to the simultaneous activation of downstream NF-κB survival pathway [249-251]. Based on these findings, it is inferred that the TNF-α mediated killing of malignant cells through cell death-receptor pathway could be augmented upon concomitant blockade of NF-κB cascade. As Eriodictyol inhibits NF-κB, we hypothesized that by inhibiting the same we can activate the endogenous TNF-α mediated apoptosis pathway in cancer cells. In this study, we have attempted to discover an effective TNF-mediated anti-cancer therapeutic with minimal toxicity towards the normal cells. Previously, some reports have suggested the anti-cancer activity of Eriodictyol on different malignant cells. Since our transcriptomic data from RNA-Sequencing analysis, as well western blot validation, clearly elucidated that genes involved in cell cycle (Cyclin B1, p21 etc.) and apoptosis related pathways (TNFR1, TRADD, Bax, Survivin etc.) are modulated by Eriodictyol, we analyzed the mechanism of Eriodictyol-induced cancer cell-specific cytotoxicity. The ability of Eriodictyol to target aberrations that contribute to tumor's proliferative advantage, while sparing normal cells can lead to improve patient tolerance in future clinical trials. Interestingly, our investigation deciphered that TNFR1

upregulation and unleashing of endogenous TNF-α from cancer cells (HeLa), collectively had the fortuitous effect of altering the functional state of TNF-α pathway from NF-kB dependent cell survival to death-inducing complex formation. In addition, the importance of TNFR1 in Eriodictyol-induced apoptosis was further supported by the significant abrogation of cancer cell apoptosis upon TNFR1 knockout. Moreover, we have documented exclusive expression of TNFR1 on cancer cell lines and not the normal cells, wherein Eriodictyol was unable to induce TNFR1 expression even after prolonged exposure, thus, explaining the mystery behind the selectivity of Eriodictyol-mediated cytotoxic phenomena in cancer cells over normal cells. Further investigation of the mechanistic details revealed that Eriodictyol induced both extrinsic and intrinsic apoptosis in cancer cells as evident from the expression profile of hallmark apoptosis-related proteins. TNFR1-DISC-Casp-PARP1 is the major axis in extrinsic apoptosis pathway and we are the first to report its utilization by Eriodictyol to mediate its selective cytotoxicity. In brief, we have demonstrated that Eriodictyol exposure to the cancer cells resulted in binding of endogenous TNF- α to upregulated TNFR1 receptor leading to the formation of the DISC complex comprising of the TNF- α bound death receptor (TNFR1), adapter protein (FADD, TRADD) and initiator pro-caspase 8, which is activated into caspases-8 through cleavage. In addition, Eriodictyol-induced apoptosis is accompanied by cell cycle arrest at G2/M phase, which was initiated by increase of ɣ-H2A.X (an indicator of DNA damage) through regulation of Cyclin-B1, Chk1, Cdc25 and Cdc2. Following that, Eriodictyol inactivated Claspin in cancer cells via caspase-7-mediated cleavage, which played an important role in shifting the tumour cell response from cell cycle arrest to induction of apoptotic cell death in response to prolonged DNA replication arrest or the persistence of DNA damage.

TNFR1 plays a vital role in Eriodictyol mediated selective cytotoxicity as TNFR1 null cells are unable to respond to apoptosis by the compound. This is occurring due to the absence of the extrinsic receptor. Moreover normal cells lack TNFR1 and is expressed only in cancer cells. Finally, testing of the therapeutic efficacy of Eriodictyol in Balb/c (syngeneic) mouse tumor model subcutaneously injected with 4T1 mice breast cancer cells indicated that Eriodictyol treatment resulted in remarkable regression of tumor volume, tumor weight and metastatic potential in *in vivo* mouse model.

Thus, we have identified and established Eriodictyol as a potential anti-tumor compound with a selective cytotoxic effect specific to tumour cells, as well as elucidated its selective anti-cancer mechanism by targeting TNFR1 upregulation, G2/M arrest, and subsequent activation of apoptosis in cancer cells without affecting normal cells. Although natural chemicals, such

as flavonoids, have numerous health benefits, large-scale extraction from natural sources in high-purity form, bioavailability, and tailored distribution to the place of interest are all substantial obstacles for clinical application. In conclusion, Eriodictyol could be a promising lead for development of potential and selective candidate for cancer therapy.

7. Important protocols of chapter I

PMA concentration calculation

PMA molecular weight = 616.8g
Stock concentration= 50 µg/ml = 8.104 * 10^4 nM
Final concentration = 20 nM
For a 6 wells plate 2 ml is to be added in each well which makes the final vol. of RPMI 12 ml
By using the formula $V_1S_1=V_2S_2$
where V_1= Volume to be added from the stock
V_1= (2*1000*6*20)/(8.104*10^4)= 2.96 µl

LPS concentration calculation

Stock concentration= 2 mg/ml=2000µg/ml
Final concentration=2.5µg/ml
In each well 2 ml of RPMI is to be added
We know $V_1S_1=V_2S_2$
or, V_1=(2*2.5)/2000=0.0025ml=2.5µl
Therefore 2.5µl of LPS from stock is to be added in 2 ml

1. Maintenance of THP-1 (human monocyte) cell line

- The full contents (RPMI containing THP-1 cells,) of T-25 or T-125 flask are taken into 15 ml centrifuge tubes.
- The tube is then centrifuged at 1000 rpm for 3-4 minutes.
- Meanwhile the empty flask is rinsed with 1XPBS and fresh RPMI (containing 10% FBS) is added into the flask.
- After centrifugation the supernatant is discarded and 1 ml of fresh RPMI is added and mixed thoroughly with 1 ml pipette.
- About 350 µl of THP-1 is added drop wise into the flask and shaken for uniform mixture.
- The flask is observed under inverted microscope.
- Incubated at 37 degree centigrade and 5 % CO_2.
- On average every 1-2 days interval sub-culturing is required.

N.B. For T-25 flask 10 ml and for T-125 flask 17 ml of RPMI is necessary.
U937 cells are to be subcultured once they reach 70-80 % confluence.

2. PMA induction procedure

- THP-1 cells were seeded in 6-well plates at 5×10^5-6×10^5 cells per condition in presence of 5ng/ml PMA for 48 hrs in complete RPMI.
- The plate is shaken well for uniform distribution of cells in each well.
- Seen under inverted microscope.

N.B. During the first 6 hours of PMA induction it is necessary to check the plate every 2 hours interval as cells tend to accumulate in the middle of each well. So it is necessary to shake the wells in every 2 hour's time interval.

- After 24 hours of PMA induction it is necessary to release the PMA.
- From the six well plates the media is discarded from each well.
- 2 ml of PBS is added to each well and mild rinsing is done.
- The PBS is discarded.
- 3 ml of fresh RPMI containing 10 % FBS is added in each well.
- Observed under inverted microscope.
- Again incubated under 37 degree centigrade and 5 % CO_2 for 24 hours.
- After 24 hours again the media should be changed.
- Now the cells are ready for LPS induction.

LPS treatment

SAMPLE NAME	DURATION OF LPS INDUCTION
CONTROL	NO LPS
6 HOURS LPS	6 HOURS
4 HOURS LPS	4 HOURS
2 HOURS LPS	2 HOURS
1 HOUR LPS	1 HOUR
30 MINS LPS	30 MINUTES

- The media is discarded.
- Washed with 1X PBS.
- Fresh 1 ml RPMI is added.
- 2.5 µl LPS is added in 1 ml of RPMI and added into the well.
- Incubated at 37 degree centigrade and 5 % CO_2.
- After 6 hours the six well plates is taken out from the incubator.
- The medium is discarded from each well.
- Washed with 2 ml of PBS.
- 500 µl of Trizol is added in each well.
- The Trizol in each well is taken in separate 1.5 ml tubes and stored at -80^{0}C.

3. TRIZOL method of RNA isolation

- The Trizol in each 1.5 ml tube is mixed thoroughly.

- Incubated at room temperature for 10 minutes.
- Chloroform is added (1/5 th of the vol. of Trizol).
- The tubes are shaken vigorously by hand for 15-20 secs.
- Incubated at room temperature for 5 minutes.
- Samples are then centrifuged at 12000 g (RCF) for 15 mins. in 4 degree centigrade.
- The aqueous phase is taken into a new 1.5 ml tube (about 50% of the vol. of the aq. phase).
- Isopropanol(1/2 of the vol. of trizol) is added.
- The tube is shaken for 5 secs by hand.
- Incubated at room temperature for 10 mins.
- Centrifuged at 12000 g for 10 minutes.
- The supernatant is discarded carefully.
- Washed with 75 % ethanol in DEPC water (700 µl) twice (centrifuged at 7500 g for 8 minutes).
- The ethanol is removed and dried in hood.
- DEPC water is added according to the amount of pellet and mixed properly.
- The tubes are heated in dry bath at 55-60 degree centigrade for 10 minutes.
- The concentration of RNA is measured and kept in ice for c-DNA preparation.

4. c-DNA synthesis using Verso c-DNA synthesis kit

- Experiments were done using 500ng of RNA for each sample during c-DNA synthesis.
- Volume of RNA and water should be 11 ul and then add 1ul of oligo dT and Random hexamer mixture (1:3 ratio).
- Snap chilling should be done using above 12 ul of sample (RNA +Mol bio Water+ oligo dT/hexamer mix) at 65^0C for 10 minutes, immediately followed by chilling in ice for 1 minute.
- During the 10 minutes of incubation period prepare the RT mix (dNTPs-2ul,RT buffer-4ul, RT enhancer-1ul, RT Enzyme-1ul for each reaction condition).
- Add 8 ul of RT mix to each sample tubeand mix properly followed by pulse spin.
- Condition: - 50^0C=1 hour, 95^0C=2 minutes, 4^0C-∞, lid temperature 105^0C.

5. MTT assay

Day 1

- Count the cells in haemocytometer.
- Seed them in 48 well plate format with 200 µl media and incubate for 24 hrs.

Day 2

- Discard the media.
- Add the test compound in different concentrations (at least triplicate) for 24/48 hrs

Day 3/Day 4

- Discard the media.
- Prepare MTT solution (0.5 mg/ml) in phenol red free media (dark condition).
- Add 300µl in each well and incubate for 3 hrs.
- After 3 hrs add 400 µl DMSO in each well.
- Dissolve the formazon crystals properly and pipette out 200 µl from each well and transfer to 96 well plate.
- Measure in ELISA reader at 584 nm and 620 nm.

Note: Keep a well for only DMSO in 96 well plate as it will be considered as blank and its value will be subtracted from each well.

6. Annexin-V/FITC-PI staining

- Cells are seeded at $2x10^5$ per well at 6 well plate format and incubate 24 hrs.
- Test compound and positive control (Dox/Etoposide) is added.
- Cells are trypsinized (250 µl trypsin) for 2-3 mins.
- 500 µl media is added to halt trypsinization.
- Cells are centrifuged at 3500 rpm for 5 mins.
- Cells are washed with 1X PBS and collected in 1.5 ml Eppendorf tubes.
- Pellet is dissolved in 1X Binding buffer (100 µl).
- 4-5 µl of Annexin-V/FITC is added and incubated for 15 mins.
- 2.5 µl of Propidium Iodide (PI) is added and incubated for 15 mins.
- 500 µl of 1X binding buffer is added and mixed thoroughly with pipette.
- Measure in flow cytometer (FACS Verse).

Note: Controls required for gating are
1.Unstained.
2.Only PI.
3.Only FITC.
4.PI+FITC.
5.Dox/Etoposide

7. Cell cycle profiling assay

- Cells are seeded at $1.5\text{-}2x10^5$ in 6 well plate format for 24 hrs.
- The test compound and nocodazole (positive control) is added and incubated for 24 hrs.
- 250 µl of trypsin is added.
- Cells are washed with 1X PBS and centrifuged at 7000 rpm for 10 mins.
- PBS discarded and the pellet is vortexed.
- 700 µl of chilled 75% ethanol is added and vortexed thoroughly until single cell suspension (Fixation step).
- Stored at -20^0C overnight. (Can be stored for 2-3 months)
- The fixed sample is centrifuged (4000 rpm for 4 mins) and ethanol is discarded.
- The sample is resuspended with 600 µl of ice cold 1X PBS (Rehydration step).
- Incubated at 4^0C for 1.5-2 hrs.

- RNAse is added at 20µg for 1 ml of solution and mixed thoroughly. (For this a stock of 2mg/ml is prepared). Therefore for 600 ul of sample 6 µl of RNAse A (12 µg) is required (For every 100 µl add 2 µg of RNAse A).
- Incubated at 37^0C for 1.5-2 hrs.
- 3 µl of Propidium Iodide is added to each tube and mixed properly.
- Incubated for 15 mins at room temperature (dark condition)
- Measure in BD FACS Verse.

8. Clonogenic assay

- Cell suspension is diluted into the desired seeding concentration (100-200 cells/well).
- After 2 hours the media is replaced carefully with the test compound containing media.
- After every 2 days interval media is replaced with the test compound containing media.
- This is continued for 8/10 days until large colonies are visible.
- Wells are rinsed properly with 1X PBS.
- 0.5 % crystal violet solution in 3.7% formalin (1X PBS) is prepared and 2 ml of this solution is added to each well.
- Incubated at room temperature for 30 mins.
- Crystal violet mixture is removed carefully and rinsed with tap water.
- Note: The sink is filled up with water and plates are immersed carefully.
- The plates with colonies are air dried for 20 mins at room temperature.
- Plates are observed in Gel Doc XR+ (Bio-Rad) under a white background and photos of the plates are captured for counting using ImageJ software.

8. Important protocols of chapter II

1. CRISPR/Cas9 mediated knockout protocol

I. TNFR1 guide RNA design steps

- Go to NCBI website.
- Go to GENE database search TNFR1 (TNFRSF1A) Human
- TNFR1 has only one transcript variant (NM_001065.3 for TNFR1)
- Copy the NM no. and search under NUCLEOTIDE database.
- The Coding sequence (CDS) for TNFR1 lies between nucleotide no. 304 to 1671.
- Exclude Exon 1 (1 to 342).
- Copy the FASTA sequence of Exon 2 (343 to 496) and paste it in CRISPR designing website crispr.mit.edu.
- Select the best scoring sequence (20 nucleotides) and add nucleotide G if the starting nucleotide was not G.
- Reverse complement the sequence.
- Add CACC to the 5' of guide RNA and AAAC to the 5' of new complement sequence.

II. Vector digestion of 48139 [pSpCas9(BB)-2A-Puro (PX459)]

PCR reaction volume = 30 µl

4 µg vector (48139) (9.2 kb size)	3 µl
Bbs1 (Thermo)	3 µl
Fast AP (Thermo)	3 µl
Thermo 10X buffer (fast digest)	3 µl
Mol. Bio. H_20	18 µl

PCR program

Lid temp. =45^0C
Step 1: 37^0C for 30 mins
Step 2: 4^0C infinite hold

Note: Run the digested PCR product in 0.8 % agarose gel and load the undigested vector as control. Gel elute the digested product as per Qiagen gel elution protocol.

III. Annealing and phosphorylation of CRISPR oligos

Dilute 10 µl (100 µM ss oligo) with 10 µl H_20 and prepare 10 µl PCR reaction as follows:

Sense strand (50 µM)	2 µl
Anti-sense (50 µM)	2 µl
T4 ligation buffer (10X)	1 µl
dATP (10mM)	0.5 µl
T4 PNK (NEB)	0.5 µl
H_20	4.0 µl

PCR program

Step 1: 37^0C for 30 mins
Step 2: 95^0C for 5 mins
Step 3: 25^0C for 30 seconds (Ramp down)
Step 4: 4^0C infinite hold

Dilute the annealed oligo (1:40) in H_20 [Recommended 1:50-1:200]

Total volume=80 µl
Mol. Grade H_20= 78 µl
Annealed oligo= 2 µl

IV. Ligation of annealed oligos in Bbs1 digested Cas9 vector

Setup the PCR protocol as follows:

Tube 1

Digested vector	1 µl
Insert	1 µl
2X Q.L. buffer	2.5 µl
Q.L.	0.5 µl

Total volume = 5µl

Tube 2 (Blank)

Vector	1 µl
H_20	1 µl
2X Q.L. buffer	2.5 µl
Q.L.	0.5 µl

Total volume=5µl

PCR program
Lid temp.: 30^0C
Step 1: 25^0C for 15 mins
Step 2: 4^0C infinite hold

V. Transformation of the ligated product in competent cells (XL1 Blue) and streaking in Luria Broth agar plates containing ampicillin.

VI. Mini prep for plasmid extraction from competent cells.

VII. Sanger sequencing for verification of the insert.

VIII. Amplify the plasmid by Midi and proceed to transfection by Liofectamine LTX.

IX. After transfection select the HeLa cells in Puromycin (1µg/µl) for 1 week. Change the dose as per the requirement as it varies from cell to cell.

X. After 1 week of selection seed 200 cells in 100 mm dish for colony selection and collect the remaining cells for T7E1 assay.

XI. T7E1 assay

- Isolate genomic DNA from the cells collected in step X.
- Dilute it to 100-150 ng/µl.
- Setup the PCR reaction for 12 tubes as follows:

Genomic DNA	= 2µl
10X buffer	=2 µl
dNTPS (5mM each)	=0.8µl
Taq polymerase	=0.2µl
Forward primer	= 1µl
Reverse primer	=1µl
H20	= X µl

Total volume= 20 µl

- After the PCR reaction collect all the 12 tubes in a single tube and take 4 µl and run it on 1% agarose gel and if a single band appears proceed to next step
- PCR purification (Qiagen kit)
- Measure 600 ng of DNA and setup a PCR reaction for 4 tubes (15µl each). Two tubes for control untransfected HeLa cells and the other two for transfected HeLa cells.

PCR conditions

Genomic DNA= X (600 ng)
10 X NEB 2 buffer= 1.5 µl
H_20= 15-(X+1.5)

PCR cycle (Slow annealing step)

Step 1: 95^0C for 10 mins
Step 2: Ramp down to 25^0C at 0.1^0C/s

Divide the four tubes as per the following:

1. Control (non-transfected cells) without T7E1 enzyme
2. Control (non-transfected cells) with T7E1 enzyme
3. CRISPR transfected cells without T7E1 enzyme
4. CRISPR transfected cells with T7E1 enzyme

PCR condition for the tubes with T7E1 enzyme

H_20 =4 µl *2
NEB2=0.5 µl *2
T7E1=0.5 µl *2

PCR condition for the tubes without T7E1 enzyme

H_20 = 4.5 µl*2
NEB2=0.5 µl*2

- Incubate all the 4 tubes at 37^0C for 30 mins.

- Stop reaction by adding 3.2 µl of 0.25M EDTA.
- Run on agarose gel based on amplicon size and for long period for better resolution.

2. Caspase3/7 activity assay (# ab39401)

A colorimetric assay following the manufacturer's protocol (Caspase 3 Assay Kit (Colorimetric) (ab39401)) was used to measure the caspase.

- Eriodictyol treated HeLa cells were induced at a concentration of 150 µM for 24 h and 48 h.
- Cell lysates were prepared with RIPA buffer (150µg).
- Each cell lysate was treated for 2 hours at 37 °C with 50µl of 2 X reaction mixture containing (containing 10 mM DTT) and 5 µl of the 4 mM DEVD-p-NA substrate (200 µM).
- The Optical Density was measured at 400 nm in a micro-plate reader.

3. Genomic DNA Isolation

- HeLa cells were seeded in 60 mm dish at $3x10^5$ for 24 hrs and incubated at 37^0C in presence of 5% CO_2.
- Next the cells were trypsinized and the pellet was washed with 1X PBS.
- PBS was discarded.
- RIPA buffer was added (for 100 mm dish 1 ml of RIPA was required)
- Same amount of Phenol, Chloroform and Isoamyl alcohol (25:24:1) was added.
- Vortexed until milky.
- Centrifuged at 13,000 rpm at room temp. for 10 mins.
- Aq. Phase was taken into fresh tube and 2.5 volume of chilled 100% ethanol was added in combination with 1/10 volume NaOAc.
- Vigorous shaking and incubated at -80^0C for 20 mins.
- Centrifuged at 4^0C at 13,000 rpm for 15 mins.
- Supernatant was discarded, pellet was washed with 70% ethanol at 7500 rpm for 5 mins.
- 70 % ethanol wash was repeated.
- Pellet was air dried and dissolved in 30-50 µl Tris-EDTA buffer.
- The concentration of DNA and $A_{260/280}$ (for purity check) was measured.

9. Important protocols of chapter III

1. *In vivo* tail vein injection

- For experimental tail vein metastatic assay, 4T1 cells were used.
- Cells were trypinized using 0.5X trypsin washed thrice with serum free RPMI-1640 and single cell suspension was made.
- Cells were counted in haemocytometer.
- 1×10^5 cells/mice were dissolved in 100µl serum free RPMI-1640 and injected through lateral tail vein of 4-6 weeks old Balb/c female mice via 1 ml insulin syringe.
- 20 days after injection mice were euthanized and lungs were dissected.
- Lungs were kept in 3.7% formaldehyde for 1 week at 4^oC and then photographed using DSLR camera.

2. *In vivo* localized tumor formation assay

- For *in vivo* tumorigenic assay, 4T1 cells were used.
- Cells were trypinized using 0.5X trypsin washed thrice with serum free RPMI-1640 and single cell suspension were made.
- Cells were counted in haemocytometer.
- 1×10^6 cells/mice were dissolved in 100µl serum free RPMI-1640 and injected subcutaneously using 1 ml insulin syringe.
- Perpendicular bi-dimensional measurement was taken in every 3 days using vernier callipers.
- 31 days post injection, mice were euthanized and tumors were dissected out.

10. List of Publications

1. **Eriodictyol mediated selective targeting of the TNFR1/FADD/TRADD axis in cancer cells induce apoptosis and inhibit tumor progression and metastasis.**
   Shibjyoti Debnath, Abhisek Sarkar, Dipanwita Das Mukherjee, Subha Ray, Barun Mahata, Tarun Mahata, Pravat K. Parida, Troyee Das, Rupak Mukhopadhyay, Zhumur Ghosh and Kaushik Biswas. https://doi.org/10.1016/j.tranon.2022.101433.

2. **Ricinus communis L. fruit extract inhibits migration/invasion, induces apoptosis in breast cancer cells and arrests tumor progression in vivo**
   Majumder M, **Debnath S**, Gajbhiye RL, Saikia R, Gogoi B, Samanta SK, Das DK, Biswas K, Jaisankar P, Mukhopadhyay R. Sci Rep. 2019 Oct 10;9(1):14493. doi: 10.1038/s41598-019-50769-x

3. **Structural and Dynamic Insights into a Glycine-Mediated Short Analogue of a Designed Peptide in Lipopolysaccharide Micelles: Correlation Between Compact Structure and Anti-Endotoxin Activity** Datta A, Jaiswal N, Ilyas H, **Debnath S**, Biswas K, Kumar D, Bhunia A.Biochemistry. 2017 Mar 7;56(9):1348-1362. doi: 10.1021/acs.biochem.6b01229. Epub 2017 Feb 21

4. **Ganglioside GM2 mediates migration of tumor cells by interacting with integrin and modulating the downstream signaling pathway**
   Kundu M, Mahata B, Banerjee A, Chakraborty S, **Debnath S**, Ray SS, Ghosh Z, Biswas K. Biochim Biophys Acta. 2016 Jul;1863(7 Pt A):1472-89. doi: 10.1016/j.bbamcr.2016.04.004. Epub 2016 Apr 8

Translational Oncology 21 (2022) 101433

Contents lists available at ScienceDirect

Translational Oncology

journal homepage: www.elsevier.com/locate/tranon

Original Research

Eriodictyol mediated selective targeting of the TNFR1/FADD/TRADD axis in cancer cells induce apoptosis and inhibit tumor progression and metastasis

Shibjyoti Debnath [a], Abhisek Sarkar [a], Dipanwita Das Mukherjee [a], Subha Ray [a], Barun Mahata [a], Tarun Mahata [a], Pravat K. Parida [a], Troyee Das [b], Rupak Mukhopadhyay [c], Zhumur Ghosh [b], Kaushik Biswas [a,*]

[a] Division of Molecular Medicine, Bose Institute, Kolkata, West Bengal, 700054, India
[b] The Bioinformatics Center, Bose Institute, Kolkata, West Bengal, 700054, India
[c] Department of Molecular Biology & Biotechnology, Tezpur University, Assam 784028

ARTICLE INFO

Keywords:
Flavonoids
CRISPR-Cas9
Cell death
Tumorigenesis
Selective cytotoxicity

ABSTRACT

While the anti-inflammatory activities of Eriodictyol, a plant-derived flavonoid is well-known, reports on its anti-cancer efficacy and selective cytotoxicity in cancer cells are still emerging. However, little is known regarding its mechanism of selective anti-cancer activities. Here, we show the mechanism of selective cytotoxicity of Eriodictyol towards cancer cells compared to normal cells. Investigation reveals that Eriodictyol significantly upregulates TNFR1 expression in tumor cells (HeLa and SK-RC-45) while sparing the normal cells (HEK, NKE and WI-38), which display negligible TNFR1 expression, irrespective of the absence or presence of Eriodictyol. Further investigation of the molecular events reveal that Eriodictyol induces apoptosis through expression of the pro-apoptotic DISC components leading to activation of the caspase cascade. In addition, CRISPR-Cas9 mediated knockout of TNFR1 completely blocks apoptosis in HeLa cells in response to Eriodictyol, confirming that Eriodictyol induced cancer cell apoptosis is indeed TNFR1-dependent. Finally, *in vivo* data demonstrates that Eriodictyol not only impedes tumor growth and progression, but also inhibits metastasis in mice implanted with 4T1 breast cancer cells. Thus, our study has identified Eriodictyol as a compound with high selectivity towards cancer cells through TNFR1 and suggests that it can be further explored for its prospect in cancer therapeutics.

Introduction

Chemotherapy alone is seldom a feasible option owing to the development of chemoresistance, thereby, allowing tumor cells to escape drug action and resulting in cancer cell survival and treatment failure [1–3]. Hence, the need is to identify potential anti-cancer compounds, preferably from natural products, with novel modes of action that can selectively target the apoptotic machinery of the tumor cells without affecting the normal cells.

Some natural plant-based medications have limitations, such as adverse drug responses, toxicity, and safety, which restrict their therapeutic potential and necessitate improvement through medicinal chemistry [4–6]. Despite extensive testing of a wide range of natural plant-derived medicines, only a handful (such as Paclitaxel, Vinblastine,

Abbreviations: DISC, Death Inducing Signaling Complex; TNFR1, Tumor Necrosis Factor Receptor 1; FADD, FAS-Associated Death Domain Protein; TRADD, Tumor Necrosis Factor Receptor type 1-Associated DEATH Domain protein; CRISPR-Cas9, Clustered Regularly Interspaced Short Palindromic Repeats/CRISPR associated protein 9; RSK-2, Ribosomal S6 Kinase 2; ATF1, Activating Transcription Factor 1; NFkB, Nuclear Factor Kappa-light-chain-enhancer of activated B cells; TNF-α, Tumor Necrosis Factor-alpha(α); PARP1, Poly [ADP-Ribose] Polymerase 1; DMSO, Dimethylsulfoxide; FACS, Fluorescence Activated Cell Sorting; PE, Paired-End; PI, Propidium Iodide; PBS, Phosphate Buffer Saline; SDS-PAGE, Sodium Dodecyl Sulfate–Polyacrylamide Gel Electrophoresis; TBST, Tris Buffered Saline (Tween 20); PVDF, Polyvinylidene fluoride; ECL, Enhanced Chemiluminescence; OD, Optical Density; DTT, Dithiothreitol; MTT, 3-(4,5-dimethylthiazol-2-yl)-2,5-diphenyl tetrazolium bromide; IC_{50}, Half-maximal Inhibitory Concentration; CDK1, Cyclin-Dependent Kinase 1; IPA, Ingenuity Pathway Analysis; rh TNF, Recombinant human Tumor Necrosis Factor.

* Corresponding author.
E-mail address: kbiswas_1@yahoo.com (K. Biswas).

https://doi.org/10.1016/j.tranon.2022.101433
Received 22 October 2021; Received in revised form 11 April 2022; Accepted 11 April 2022
Available online 21 April 2022

Camptothecin analogues, and others) have been approved for clinical use as potent anti-cancer chemotherapeutics [6]. However, due to the extensive biodiversity of the plants and numerous benefits of the plant-based natural agents (like the ease in availability, prominent efficacy, less toxicity, etc.), worldwide, they are under comprehensive research as promising scaffolds and leads for the development of more effective and selective anti-cancer agents for future therapeutic implication. Eriodictyol, a flavonoid is well-known for its anti-inflammatory and anti-oxidant properties [7]. Literature suggests that Eriodictyol abrogates RSK2-ATF1 signaling thereby inhibiting EGF-triggered neoplastic transformation [8] and inducing tumor cell apoptosis in combination with epigallocatechin-3-gallate [9]. It has also been shown to induce selective cytotoxicity in cancer cells over normal cells, although, the mechanism of its selectivity towards cancer cells is unclear and demands further research [10–12]. This lacuna led us to propose a detailed investigation of its precise molecular mechanism to delineate the cause for its high selectivity towards cancer cells.

The present study explores the contribution of the TNFR1-mediated death pathway in Eriodictyol-induced cytotoxicity in a panel of cancer cell lines, hand-in-hand with normal cells. Data from *in vitro* cell culture-based experiments clearly highlights a significant ability of Eriodictyol to selectively target cancer cell lines, with minimal effect on the normal cells, since it not only inhibits proliferation but also induces cancer cell apoptosis much more effectively than on normal cell lines. Eriodictyol-induced apoptosis is also characterized by an increase in membrane-associated TNFR1, which activates Caspase-8, followed by proteolytic inactivation of PARP1 via caspase-7 activation. Further, HeLa cells display significantly elevated levels of TNFR1 and also, dramatically upregulates the same in response to Eriodictyol, while, normal cells (HEK, NKE and WI-38) neither show any visible TNFR1 expression nor upregulate TNFR1 upon Eriodictyol treatment, thereby, explaining the plausible underlying selectivity of Eriodicytol's anti-cancer activity. An *in vivo* study in syngeneic mice (Balb/c) model implanted with the 4T1 breast cancer cells shows that Eriodictyol impedes tumor growth and metastatic progression with no sign of adverse effects on the animals. Therefore, we have highlighted Eriodictyol as a potent compound specifically targeting cancer cells of the cervical, breast, colon and renal origin and identified the mechanism behind its selective cytotoxicity in cancer cells compared to normal cells. Hence, this study supports the potentiality of Eriodictyol to be investigated as a promising chemotherapeutic agent.

Materials and methods

Reagents

Eriodictyol (#89061) was purchased from Merck, India. Primers were purchased from IDT, USA. Primary antibodies TRADD (#3994), FADD (#2782), TNFRI (#3736), Bax (#3994), Survivin (#2808), Claspin (#2800), γH2A.X (#80312), p21 (#2947), Caspase 7 (#9494), Caspase 8 (#9746), HSP90 (#4874), Cdc25A (#3652) and PARP1 (#9532) were obtained from Cell Signaling Technology (CST), USA. Bcl2 (sc-7382) was bought from Santa Cruz Biotechnologies (USA). Housekeeping genes β-actin (BB-AB0024) and GAPDH (BB-AB0060) were obtained from Biobharati Life Sciences Pvt. Ltd. (India). Cdc2 (ab 18), phospho-Cdc2 (Tyr15) (ab47594), Cyclin B1 (ab32053) primary antibodies and colorimetric assay kit of caspase 3 (ab39401) were obtained from Abcam, Cambridge, UK. Santa Cruz Biotechnologies provided the Z-VAD-FMK (sc3067). Gibco, USA provided FBS (#16000044), L-glutamine, gentamicin, sodium pyruvate and MEM non-essential amino acids.

Cell culture and maintenance

HeLa (Human Cervical cancer), HCT116 (Human Colon cancer) and WI-38 (Normal lung fibroblast) cell lines were originally obtained from ATCC (USA). Additionally, human cell lines, NKE (Normal kidney epithelial) and SK-RC-45 (Renal cancer cells), as well as murine tumor cell lines, 4T1 (Breast cancer), CT-26 (Colon cancer) and Renca (Renal cancer) were a kind gift from Dr. James H. Finke (Cleveland-Clinic, USA) and Dr. Gerd Ritter (Ludwig Institute of Cancer Research, USA) respectively. HEK (Human embryonic kidney) and MCF-7 (Human Breast cancer) cell lines was obtained from NCCS, Pune, India. The cell lines described above were grown in either RPMI 1640 or DMEM with 10% FBS and other supplements at 37 °C in presence of 5% CO_2 [13].

MTT cell proliferation assay

MTT assay was performed to determine the effect of Eriodictyol on cellular proliferation of normal and cancer cell lines. Briefly, cells were grown in 48 well plate formats in presence of Eriodictyol (0–200 μM) for 72 h. Phenol red-free RPMI without serum containing MTT (0.5 mg/mL; 200 μL per well) were added to each well and incubated at 37 °C for 3 h in a humidified incubator containing 5% CO_2. The purple-colored formazan crystals formed by cells were dissolved in DMSO and absorbance was measured at 570 nm in a microplate reader [14]. The selectivity index for human cancer cell lines SK-RC-45, HeLa, HCT-116 and MCF-7 was calculated from the ratio of their respective IC_{50} values and that of normal cell lines (WI-38 and NKE) [15].

Clonogenic survival assay

For clonogenicity assay, cells were plated at very low density (200 cells/well in 6 well plates), grown for either 8/10 days, fixed, and stained with 3.7% formaldehyde and 0.05% crystal violet. The assay provides a measure of the replicative capacity of the cells, which is dependent on the ability of the cells to form clones from a single cell. Images of wells containing cells were captured using Gel Doc XR+ (Bio-Rad). The method of quantification of the clones is mentioned in the respective legend [15].

Cell cycle profiling assay

For this experiment, HCT-116 cells were treated with increasing concentrations (100 μM, 150 μM, 200 μM) of Eriodictyol for 24 h, while HeLa cells were treated with 50 μM, 100 μM, 200 μM of Eriodictyol for 24 h. Post-treatment, cells were harvested into a single cell suspension and fixed by incubating the cells overnight at -20 °C with 75% ethanol. Cells were centrifuged and resuspended in 1 × PBS for 2 h followed by RNase A (20 μM) treatment for 2 h at 37 °C. Finally, cells were incubated with Propidium Iodide (PI) for 15 min at room temperature. Flow cytometric analysis was immediately performed using FACSuite™ software [15].

Annexin-V-FITC/PI staining

Briefly, post-treatment with Eriodictyol, 2×10^5 cells were washed with ice-cold 1X PBS and resuspended in 100 μL of 1X binding buffer. Cells were incubated with 5 μL of annexin-V-FITC followed by 5 μL of PI for 15 min at room temperature in a dark place as per the manufacturer's protocol. Finally, the percentage of stained cells was measured in the FACS-Verse instrument (BD) and analyzed using FACSuite™ software [16].

RNA sequencing data analysis

Total RNA was extracted using TRIzol reagent (Invitrogen) and purified by DNase treatment (ThermoFisher Scientific). The quality of the RNA samples was checked on Agilent TapeStation and quantified by Qubit fluorometer. The PE Illumina libraries were loaded onto NovaSeq6000 for cluster generation and sequencing. The trimmed reads were aligned with Human GENCODE hg38 reference genome using Hisat2

2.1.0. Following the sorting of Bam files with Samtools v1.19, transcripts assembly and differential gene analysis were performed with Cufflinks v2.2.2.1 and Cuffdiff v2.2.1, respectively, and differentially expressed genes with a fold change greater than equal to 2 and p and q value cut off of less than or equal to 0.05 were filtered out. Finally, gene enrichment and pathway analysis were performed with IPA (Ingenuity Pathway Analysis).

Western immunoblotting

Briefly, cell lysates were prepared from HeLa cells post-treatment with Eriodictyol (150 μM) using RIPA buffer. For immunoblotting, 30–50 μg proteins were resolved on 10–15% SDS-PAGE, transferred onto PVDF/nitrocellulose membrane (Millipore, USA), blocked with 5% BSA dissolved in 1X TBST, and subsequently probed with respective primary antibodies and secondary antibodies. Finally, blots were developed onto X-Ray films by the ECL method or by using gel imaging system (ChemiDoc MP, Bio-Rad and iBright Imager, Invitrogen) [13].

Caspase-3/7 activation assay

The assay was based on the ability of the enzyme(s) to detect and cleave the sequence DEVD from the chromophoric substrate DEVD-pNA. Caspase-3/7-dependent sequence specific cleavage of DEVD-pNA to release p-NA (p-nitro-aniline) from the substrate and its colorimetric detection enables quantitative measurement of the activity of Caspase-3/7 in the lysates. For this, cell lysates were prepared from HeLa using RIPA buffer following treatment with Eriodictyol. An aliquot of 150 μg of protein was used for each condition. DTT and DEVD-pNA substrate were added according to the manufacturer's (Abcam #ab30401) instructions. Samples were mixed well and incubated at 37°C for 90 min and finally, OD was measured at 405 nm in Multiskan GO microplate reader (ThermoFisher Scientific) [15].

Design, construction and validation of TNFR1 CRISPR

Guide oligos (20-mers) were designed from TNFR1 exon 2 sites using http://crispr.mit.edu (Supplementary figure S1A), on the basis of high "on-target score" and low "off-target score" in the whole exome. Guide oligo was then cloned into Cas9 expression vector (pSpCas9(BB)-2A-Puro) (Supplementary figure S1 B) having a puromycin selection cassette, sequence verified and TNFR1-CRISPR plasmid was transfected into HeLa cells using lipofectamine LTX reagent (Invitrogen) to check the functionality of the CRISPR plasmids within the cells. Following initial selection with puromycin (1mg/ml) over the week, genomic DNA was isolated from transfected cells and a mismatch heteroduplex sensing T7E1 assay was performed [17]. Next, clonal expansion from single cells was performed followed by immunoblotting of clonally expanded cells to screen for stable TNFR1-CRISPR knockout cells.

Real-time PCR and RNA isolation

Total RNA was extracted using TRIzol reagent (Invitrogen). 1 μg of RNA was extracted from HeLa cells treated with Eriodictyol along with DMSO-treated control. Verso cDNA synthesis kit (ThermoFisher Scientific) was used to convert RNA to cDNA. Real-Time PCR was performed in triplicate with a diluted stock of cDNA (1:6) mixed with SYBR green on Real Time PCR system 7500 Fast (Applied Biosystems) or QuantStudio 3 Real Time PCR system. Every mRNA quantification data were normalized to GAPDH and expressed as the fold differences of target gene expression relative to non-treated samples [18]. Primers used in this study are the following: TNFα: 5'-TGTAGCAAACCCTCAAGC-3' (forward), 5'- TGGGAGTAGATGAGGTACAG-3' (reverse); TNFR1: 5'-TTCGTCCC TGAGCCTTT-3' (forward), 5'- CAGGAGTGCCAAGTTTC-TAT-3' (reverse); GAPDH: 5'-ACAACTTTGGTATCGTGGAAGG-3' (forward), 5'-GCCATCACGCCACAGTTTC-3' (reverse).

4T1 breast tumor model

Female Balb/c mice aged 6–8 weeks were obtained from the Center for Translational Animal Research (CTAR) at the Bose Institute in Kolkata, India. The protocol was approved by the Bose Institute Animal Ethics Committee (Approval No. IAEC/BI/118/2018, dated 20/12/2018) and all animal experiments were performed in accordance with the institutional guidelines and in compliance with the CPCSEA regulations (based on NIH guidelines) based on the recommendations of the institutional animal ethics committee. 4T1 cells (1×10^6 cells/animal) were subcutaneously implanted into the mammary fat pad of Balb/c mice for the *in vivo* tumorigenic experiment. Following the formation of a palpable tumor, animals were randomly divided into two groups: vehicle control (5% DMSO) and Eriodictyol-treated (60 mg/kg), each consisting of at least five animals, and were subjected to intraperitoneal injections beginning around 10 days after tumor formation and lasting until 22 days (5 doses, 72 h interval). On every third day, the volume of the tumor was measured with vernier calipers using the equation Tumor volume $= 0.5 \times a \times b^2$, where "a" and "b" indicate major and minor axis, respectively.

4T1 tumor metastasis in secondary organs

4T1 tumor cells (1×10^5) were injected intravenously through the tail vein in syngeneic Balb/c mice. Post-inoculation, mice were randomly divided into three groups and administered with either 5% DMSO or two different doses of Eriodictyol, thrice a week. 3-4 weeks post-injection of tumor cells, animals were sacrificed and scrutinized for micro-metastatic nodule formation in the lungs, which is indicative of metastasis, and subjected to the counting of the number of micro-metastatic nodules as well as tissue staining of the lung cross-sections with hematoxylin-eosin (H&E).

Statistical analysis

Statistical analysis was performed by Student's t-test using GraphPad Prism 5.0 software. Statistical comparisons between groups were determined by a one-tailed or two-tailed Student's t test. The data are represented as mean ± SEM of at least three independent experiments, unless mentioned otherwise. The p values were used to ascertain if the values were statistically significant ($*p < 0.05$, $**p < 0.01$, $***p < 0.001$, ns = not significant). The statistical analysis of each experiment is detailed in the respective legends.

Results

Eriodictyol induces selective cytotoxicity to cancer cell lines

MTT cell viability assay indicates that Eriodictyol displays high toxicity towards human cancer cells SK-RC-45 (IC_{50}=53.75 μM), HeLa (IC_{50}=107.5 μM), HCT-116 (IC_{50}=105 μM) and MCF-7 (IC_{50}=75 μM) as well as murine cancer cells, 4T1 (IC_{50}=75 μM), CT-26 (IC_{50}=47.5 μM) and Renca (IC_{50}=145 μM) dose-dependently (Figs. 1A-1D). Interestingly, it is negligibly toxic towards normal human lines, NKE and WI-38 as indicated by IC_{50}>200 μM (Figs. 1E, 1F). The selectivity index (SI) measures a compound's cytotoxicity against cancer cells relative to non-tumor cells. The higher a compound's SI value, the more selective it is. The SI of Eriodictyol is calculated as the ratio of IC_{50} on normal cell line (NKE and WI-38) to the IC_{50} on cancer cell line (SK-RC-45 SI>3.72, HeLa SI>1.86, HCT116 SI>1.9, MCF-7 SI>2.66). The SI value of more than 1.5 has been considered as high selectivity. Therefore, this data not only demonstrates the selective cytotoxicity of Eriodictyol against different cancer cell lines over normal cells but also helps us in selecting the mouse tumor cell line for *in vivo* studies.

A

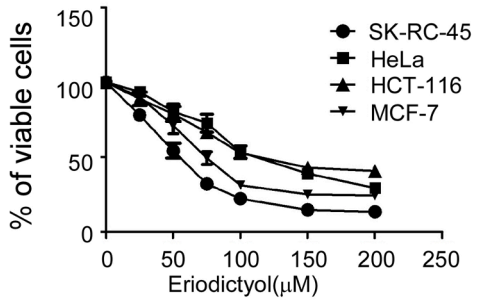

B

Human cancer cell lines	IC_{50} (μM)	Selectivity Index (SI)
SK-RC-45	53.75	>3.72
HeLa	107.5	>1.86
HCT-116	105	>1.90
MCF-7	75	>2.66

C

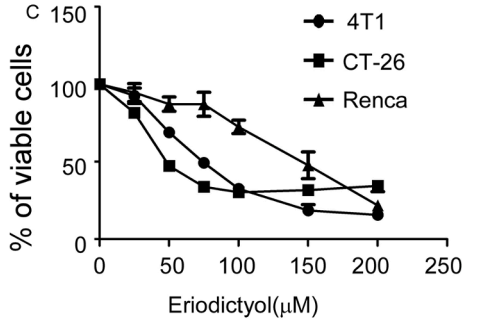

D

Mouse cancer cell lines	IC_{50} (μM)
4T1	75
CT-26	47.5
Renca	145

E

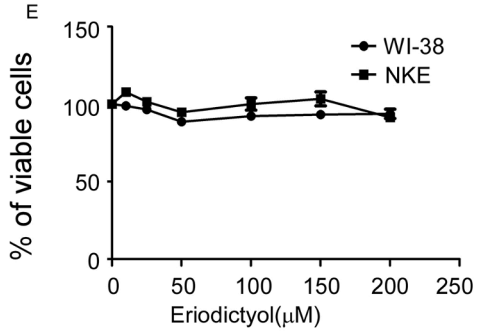

F

Human normal cell lines	IC_{50} (μM)
WI-38	>200
NKE	>200

G

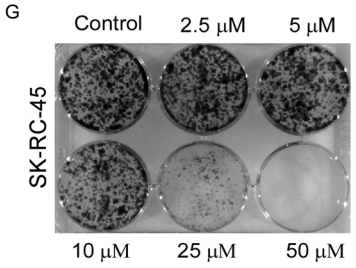

H

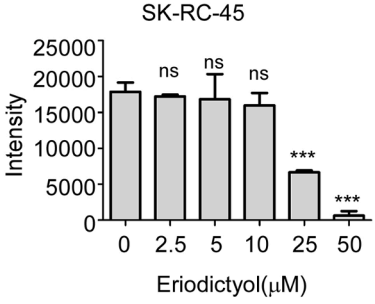

I

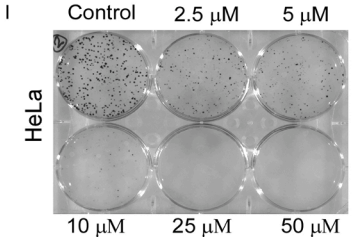

J

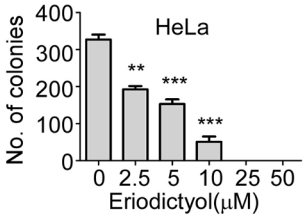

Fig. 1. Eriodictyol elicits selective cytotoxicity against several cancer cell lines. A, C, E. Line graphs showing in vitro cytotoxicity measured through MTT assay in presence of Eriodictyol (0-200 μM) at 72 h in human cancer (SK-RC-45, HeLa, HCT-116, MCF-7), mouse cancer (4T1, CT-26, Renca) and normal human (WI-38 and NKE) cell lines. The results are summarized from at least three independent experiments. **B.** Table depicting IC_{50} values and SI of human cancer cells. Selectivity index = mean IC_{50} ratio (normal cell line/cancer cell line). **D, F.** Displays the IC_{50} values of Eriodictyol in mouse cancer and normal human cell lines respectively. **G, I.** Pictorial representation of plates and **H, J**. Column graph showing dose-dependent inhibition of clonogenicity in SK-RC-45 (quantification of cell viability based on densitometry with image analysis by Bio-Rad ChemiDoc XRS) and HeLa cell lines (quantified by manual cell count) respectively, in response to Eriodictyol treatment. The results are shown as mean ± SEM of three independent experiments. Student's t-test were used for analysis (two-tailed;$^{*}p < 0.05$, $^{**}p < 0.01$, $^{***}p < 0.001$ vs non-treated, ns not significant).

Eriodictyol blocks clonogenicity of cancer cells

The ability of a single cell to form clones, as represented by clonogenicity, is a defining characteristic of cancer cells. Eriodictyol inhibits clonogenicity of SK-RC-45 cells at concentrations as low as 10 μM with a significant reduction in colony formation at 25 μM of Eriodictyol (Figs. 1G, H). Moreover, it shows better efficacy in HeLa cells with inhibition of clonogenicity starting from 2.5 μM with an almost complete regression of colony formation at 10 μM (Figs. 1I, J). It is clearly evident from the data, that while Eriodictyol significantly inhibits colony growth at a concentration as low as 2.5 μM in the case of HeLa cells, and 25μM in SK-RC-45 cells (Figs. 1G-J), the concentration of Eriodictyol that causes ~ 40–50% cells to undergo apoptosis at least in the case of HeLa and MCF-7 cells is 125 μM (Figs. 2A,B), which is evidently several folds higher than that required to inhibit significant clonogenicity. Therefore, we conclude that Eriodictyol effectively inhibits the clonogenicity of cancer cells.

Eriodictyol induces apoptosis in human and murine cancer cells

Apoptosis is characterized by the translocation of the phosphatidylserine (PS) from the cytosol to the cell membrane, which is experimentally detected by binding of annexin V-FITC to PS. Our flow cytometry study reveals that Eriodictyol treatment for 48 hours causes dose-dependent activation of apoptosis in HeLa and MCF-7 cells, as evidenced by a dose-dependent increase in the percentage of annexin-V +ve cell populations (Figs. 2A, B), while it caused only moderate, yet significant induction of apoptosis in HCT-116 cells (Fig. 2C). Similarly, Eriodictyol also induces apoptosis in mouse tumor cells, 4T1 and CT-26 (Figs. 2D, E), as indicated by a dose-dependent increase in the percentage of annexin-V +ve cells. Interestingly, a comparative study of the apoptosis induction between cancer cell lines, HeLa vs normal cell lines, WI-38 and NKE confirms that Eriodictyol induces a significantly higher level of apoptosis in the cancer cell line, HeLa as compared to both the normal cells, WI38 and NKE. However, while Eriodictyol elicits only a negligible level of apoptosis in WI-38 cells, NKE cells display only a moderate level of apoptosis in response to Eriodictyol treatment, and that too from 125 μM (Fig. 3). Collectively, these results confirm that the selective cytotoxicity of Eriodictyol not only resides in its ability to inhibit cancer cell proliferation but also, in inducing differential apoptosis in different cancer cell lines.

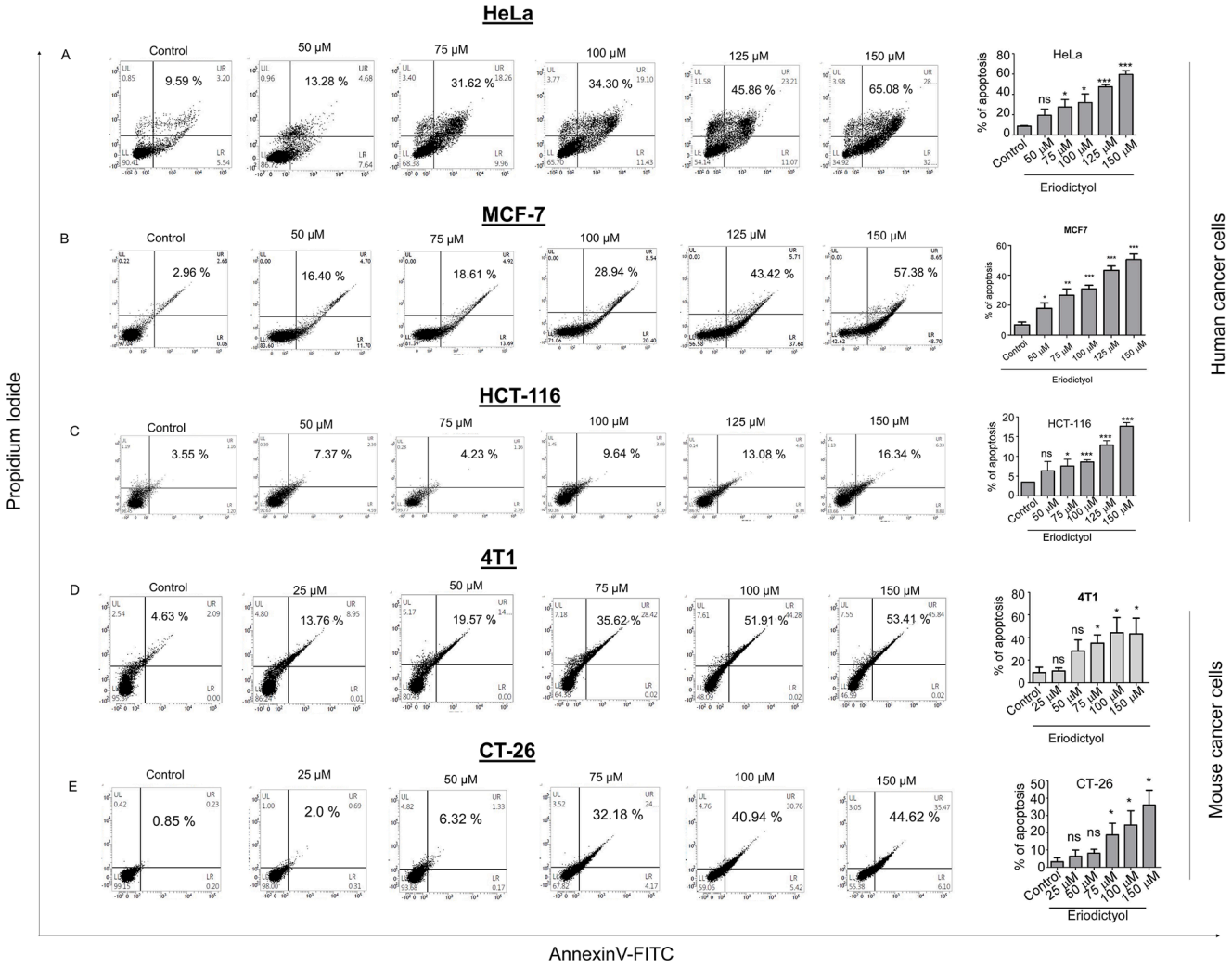

Fig. 2. Eriodictyol treatment induces apoptosis in human and mouse cancer cell lines. Flow cytometric density plots demonstrating a dose-dependent increase in the annexin V-FITC/PI-positive population of (A) HeLa, (B) MCF-7, (C) HCT-116, (D) 4T1, and (E) CT-26 cells in response to Eriodictyol treatment. Post-treatment with Eriodictyol (0–150 μM) for 48 h, cells were stained with annexin V-FITC/PI, apoptosis was measured in BD FACS Verse instrument and analyzed in BD FACSuite™. Data represent at least three independent experiments. Column graphs represent concentration-dependent induction of apoptosis in the above-mentioned cell types and experimental conditions. The data are represented as Mean ± SEM of three independent experiments and analyzed by Student's t-test (two-tailed); $*p < 0.05$, $**p < 0.01$, $***p < 0.001$, ns not significant. The total apoptosis population was calculated by combining the quadrants UL+UR+LR.

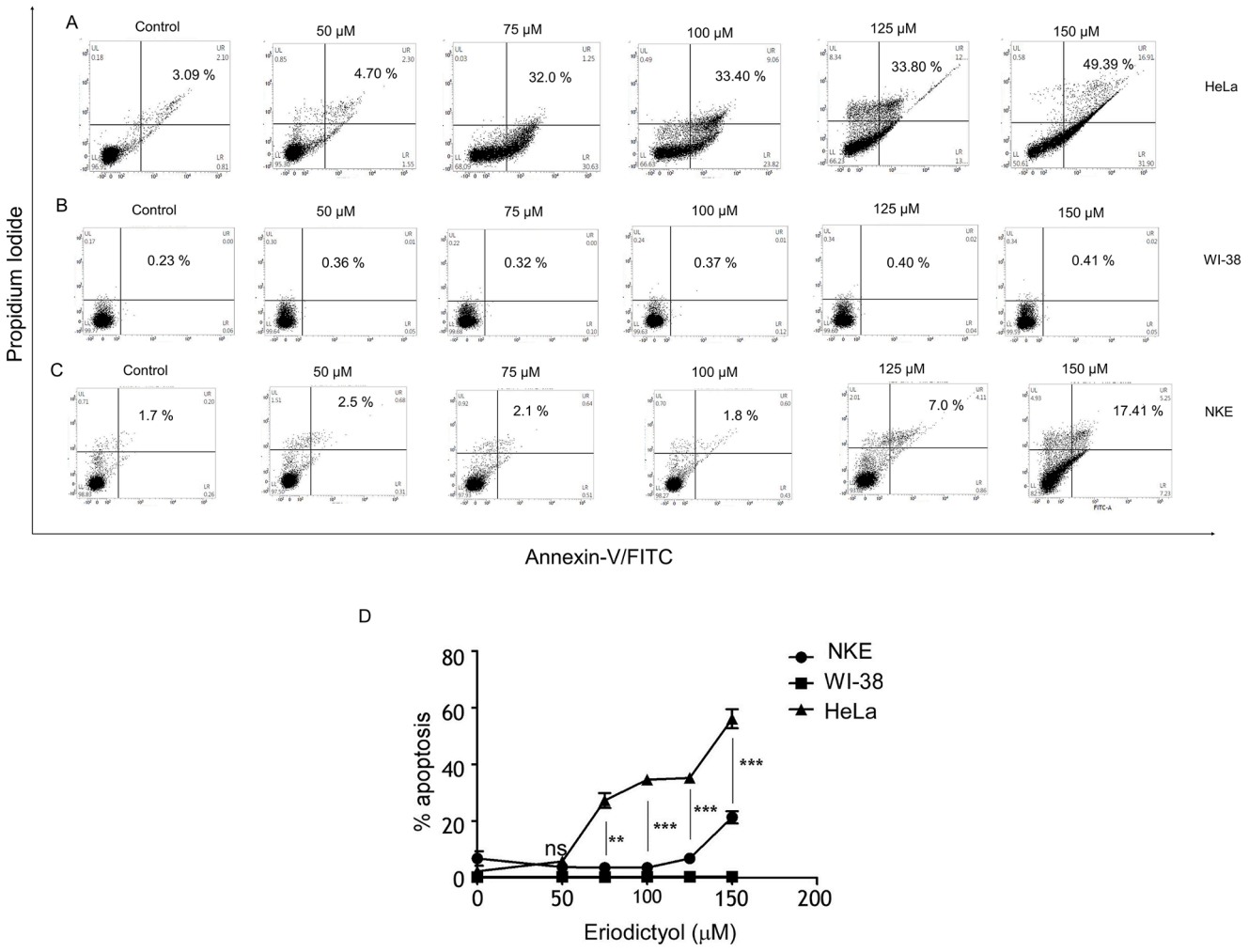

Fig. 3. Eriodictyol induced apoptosis in HeLa cells is significantly higher than that of WI-38 and NKE cells. Density plots showing comparative concentration-dependent induction of apoptosis in **(A)** HeLa versus normal **(B)** WI-38 and **(C)** NKE cell lines upon Eriodictyol treatment. **D.** Line graph representing the difference in the percentage of apoptosis in cancer cells compared to normal cell lines. The data are represented as Mean ± SEM of three independent experiments and analyzed by Student's t-test (two-tailed); $*p < 0.05$, $**p < 0.01$, $***p < 0.001$, ns not significant.

Eriodictyol arrests cell cycle progression at the G2/M phase

Flow cytometric determination of the cell cycle distribution of PI-stained cervical cancer and colon cancer cells indicates dose-dependent accumulation of HeLa (Figs. 4A, B) and HCT-116 (Figs. 4C-E) at the G2/M phase of the cell cycle upon Eriodictyol treatment. The activation of Cdc2 (CDK1) through dephosphorylation of Cdc2 at Thr14 and Tyr15 by a group of phosphatases e.g., Cdc25 has been reported as a critical regulatory step in the progression of cells to mitosis [19]. As evident from the Western blot (Fig. 4E), Eriodictyol causes a time-dependent increase in phosphorylation of Cdc2 at Tyr15, in addition, to a decrease in expression of Cdc2, Cdc25A indicating de-activation of Cdc2 , consequently leading to a delay in cell cycle progression to mitosis and holding the cells at the G2/M checkpoint.

Inhibition of Cdc2 by Eriodictyol results in the accumulation of cells in the G2 phase without mitosis, thus, resulting in the accumulation of Cyclin B1.

Eriodictyol stimulation induces differential expression of distinct gene sets implicated in proliferation, cell-cycle and apoptosis-related pathways in the HeLa cell line

To explore the extent of Eriodictyol mediated modulation of gene expression and associated biological processes, transcriptome sequencing is performed in Eriodictyol-treated versus non-treated cells at both early (6 h) and late (24 h) time points in HeLa cells. The primary analysis of the data on the Differentially Regulated Gene sets (DRGs) show distinctly different clustering of gene sets as evidenced from the heat map (Fig. 5A) in Eriodictyol treated versus non-treated cells. The transcripts with fold change (FC) $\geq$2 with p-value $\leq$0.05 are selected for our analysis. The volcano plot depicts a marked increase in the number of upregulated (apoptosis inducers and tumor suppressors) and down-regulated (metastasis inducers and cell cycle regulators) genes (Fig. 5B). Gene enrichment and pathway analysis have been performed with IPA (Ingenuity Pathway Analysis) and the results are grouped into three clusters (metastasis, apoptosis, and cell cycle) and represented as Venn diagram (Fig. 5C). Moreover, we have established a heat map displaying common tumor-related genes mostly affected by Eriodictyol (Fig. 5D), which displays a distinctly different gene expression profiling in the Eriodictyol treated versus non-treated cells. Data clearly shows distinct upregulation of apoptosis inducers and tumor suppressors and a significant decrease in oncogenes and cell cycle regulators in response to Eriodictyol. Finally, significant modulation of key biological processes in response to Eriodictyol treatment, many of which are closely related to or involved in apoptosis, metastasis and cell cycle regulation are represented as bar diagram (Fig. 5E). The results of canonical pathway analysis indicate that Eriodictyol may be involved in cell cycle regulation, specifically at the G2/M phase. In addition, pathway analysis

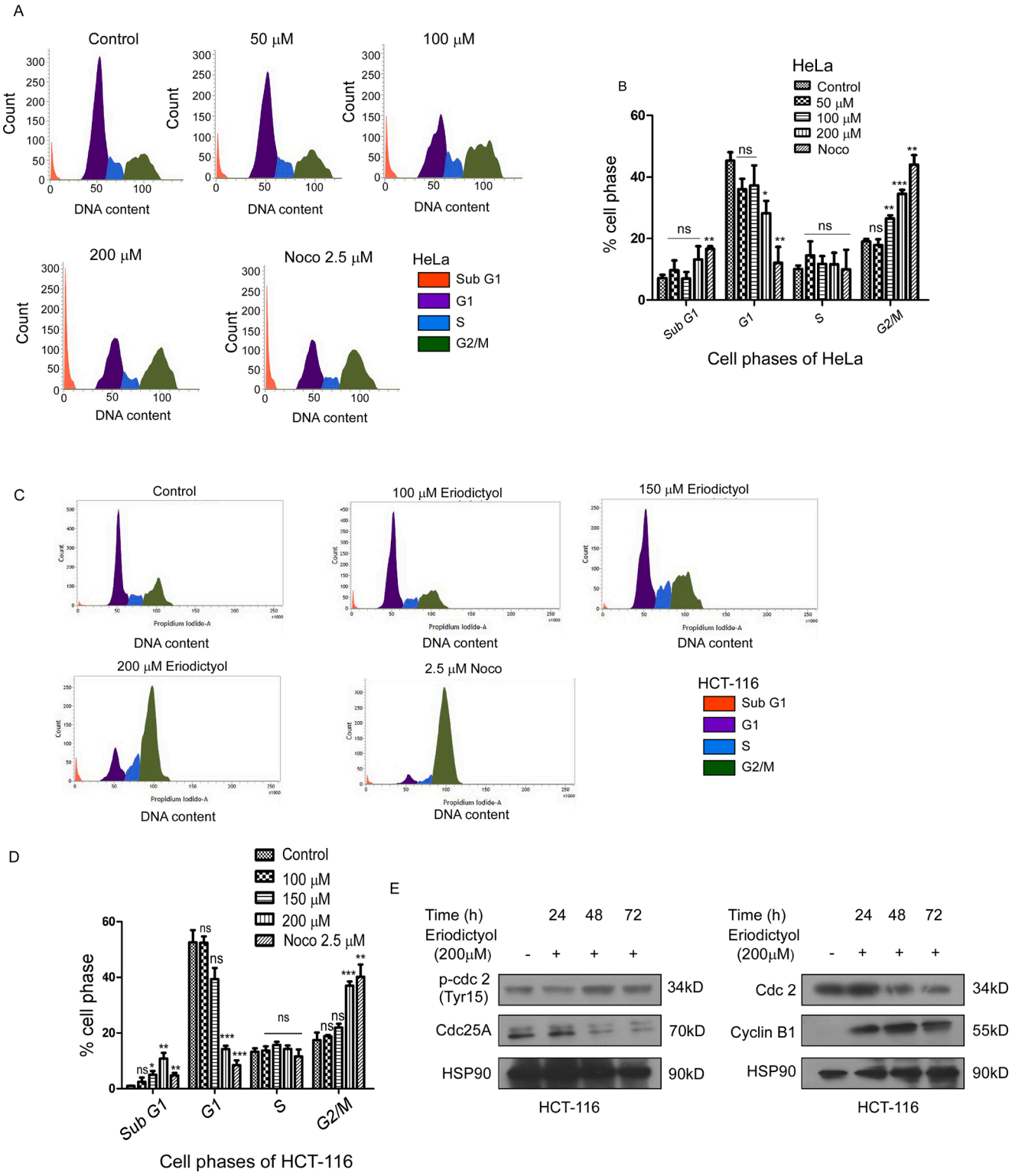

Fig. 4. Eriodictyol disrupts cell cycle progression by causing G2/M arrest. A. Histogram represents a dose-dependent increase in the G2/M phase population of Eriodictyol treated HeLa cells compared to untreated control cells for 24 h. **B.** Bar graph represents the percentage of HeLa cells at various phases of the cell cycle in response to Eriodictyol treatment. **C.** Histogram showing a dose-dependent increase in G2/M population and a corresponding decrease in G1 phase population in HCT-116 at 24 h post-treatment of Eriodictyol. **D.** Column graph depicting % of HCT-116 cells residing in various phases of the cell cycle in response to corresponding concentrations (0–200 μM) of Eriodictyol. Data represents Mean ± SEM of three independent experiments and Student's t-test (two-tailed;*$p < 0.05$, **$p < 0.01$, ***$p < 0.001$, ns not significant) was used for significance analysis. **E.** Western Immunoblots showing G2/M phase Cyclins and CDK protein expression at various time points (0–72 h) in response to Eriodictyol treatment. HSP90 was used as the loading control.

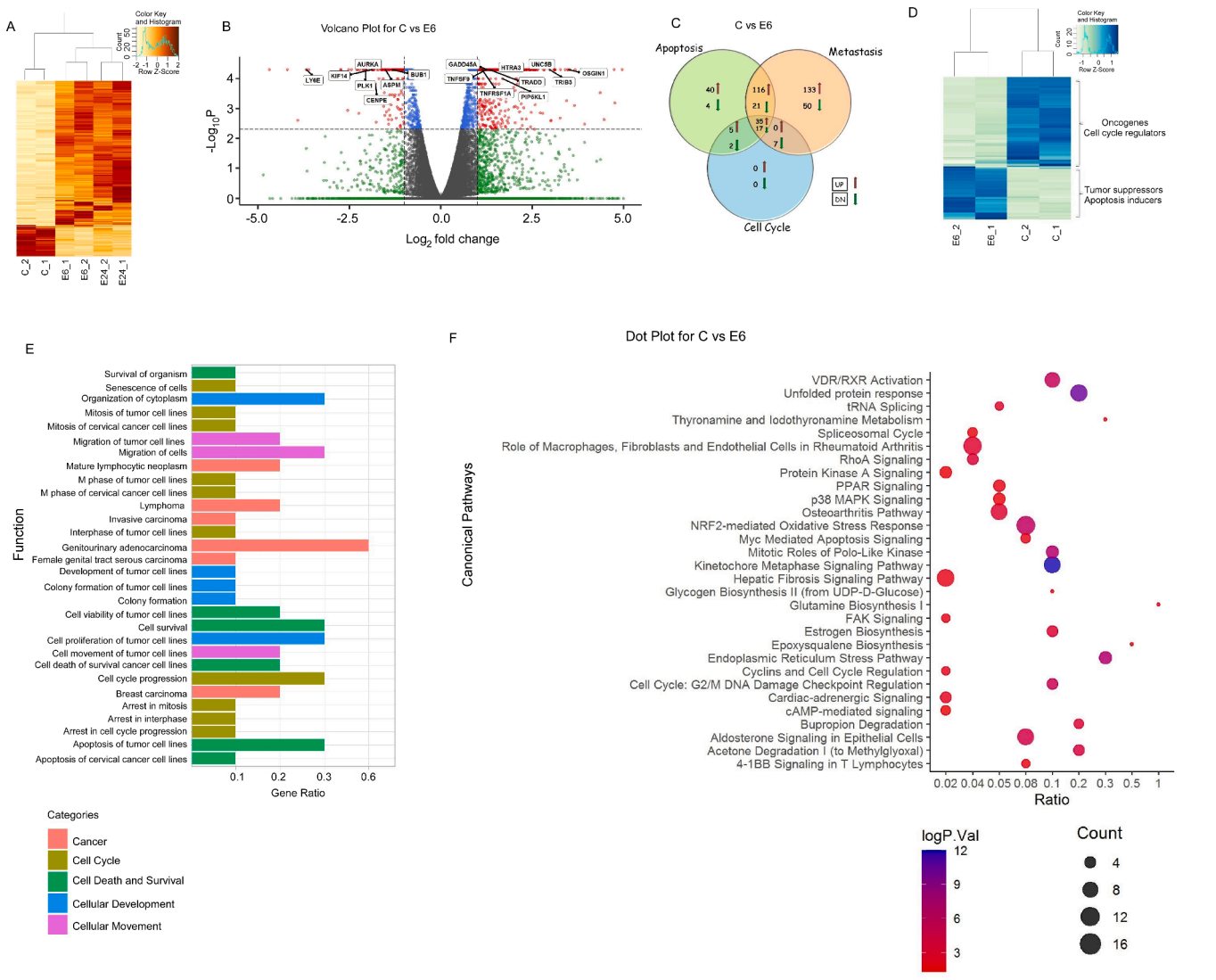

Fig. 5. Eriodictyol treatment induces differential expression of distinct gene sets implicated in apoptosis, metastasis, cell-cycle regulatory genes, and associated pathways in HeLa cells. A. A heat map showing differential regulation of global genes in response to Eriodictyol treatment in both 6 h (E6_1, E6_2) and 24 h (E24_1, E24_2) in comparison to untreated control (C_1, C_2). **B.** Volcano plot depicting the differentially regulated global genes at 6 h post treatment of Eriodictyol. **C.** Venn diagram analysis exhibiting total number of apoptosis, metastasis and cell cycle regulatory genes at 6 h Eriodictyol treatment. **D.** Heat map displaying a screened set of genes highly affected by Eriodictyol at 6 h through IPA analysis. **E.** Functional analysis represented as bar plot C vs E6. **F.** Ingenuity Pathway Analysis. The color intensity of the nodes shows the degree of enrichment of this analysis. The enrich-factor is defined as the ratio of the differential genes in the entire genome. The dot size represents the count of genes in a pathway. C_1- Untreated sample 1, C_2- Untreated sample 2, E6_1 - Treated sample 6 h sample 1, E6_2 - Treated sample 6 h sample 2, E24_1 - Treated sample 24 h sample 1, E24_2 - Treated sample 24 h sample 2.

reflects several pathways that are involved in the regulation of Cell Cycle, DNA-damage as well as Apoptotic responses, some of which are represented in Fig. 5F. Interestingly, TNFR1 is one of the genes that is not only significantly upregulated but also commonly involved in several of these pathways. Taken together, Eriodictyol causes differential regulation of gene expression that translates into the induction of apoptosis, cell cycle arrest and cytotoxicity to the tumor cells.

Eriodictyol disrupts pro-apoptotic/anti-apoptotic signal balance in cancer cells

Investigation of the detailed molecular events indicate the involvement of the DISC complex in Eriodictyol mediated apoptosis of HeLa cells, as evident from significant time-dependent upregulation in expression of the pro-apoptotic DISC components, i.e., TNFR1, FADD and TRADD (Fig. 6A).

In addition, Eriodictyol causes significant time-dependent increase of pro-apoptotic Bax, with a dramatic time-dependent decrease in anti-apoptotic Bcl2 and Survivin (Fig. 6B), thereby tipping the balance towards a pro-apoptotic outcome. Eriodictyol also causes time-dependent downregulation in the expression of the key anti-apoptotic and DNA-damage response protein, p21 in HeLa cells (Fig. 6C).

Furthermore, Eriodictyol treatment results in a time-dependent increase in the expression of the DNA fragmentation marker, γ-H2A.X, indicating that Eriodictyol may have a DNA damaging effect in cancer cells, perhaps leading to the activation of downstream apoptotic processes (Fig. 6C). Eriodictyol-mediated apoptotic cascade involves caspases as evident by a time-dependent reduction in pro-caspase 7 expression and an increase in cleaved caspase 7, activation of caspase 8, as well as a decrease in full-length 116 kDa PARP1 levels and the presence of the cleaved 89 kDa form (c-PARP1) (Fig. 6D). As shown in Fig. 6G, the caspase activity assay also confirms activation of caspase 3/7 in HeLa cells at later time points (24, 48 and 72 h). Pretreatment of HeLa cells with 20 μM inhibitor of PAN-caspase (Z-VAD-FMK) provide a

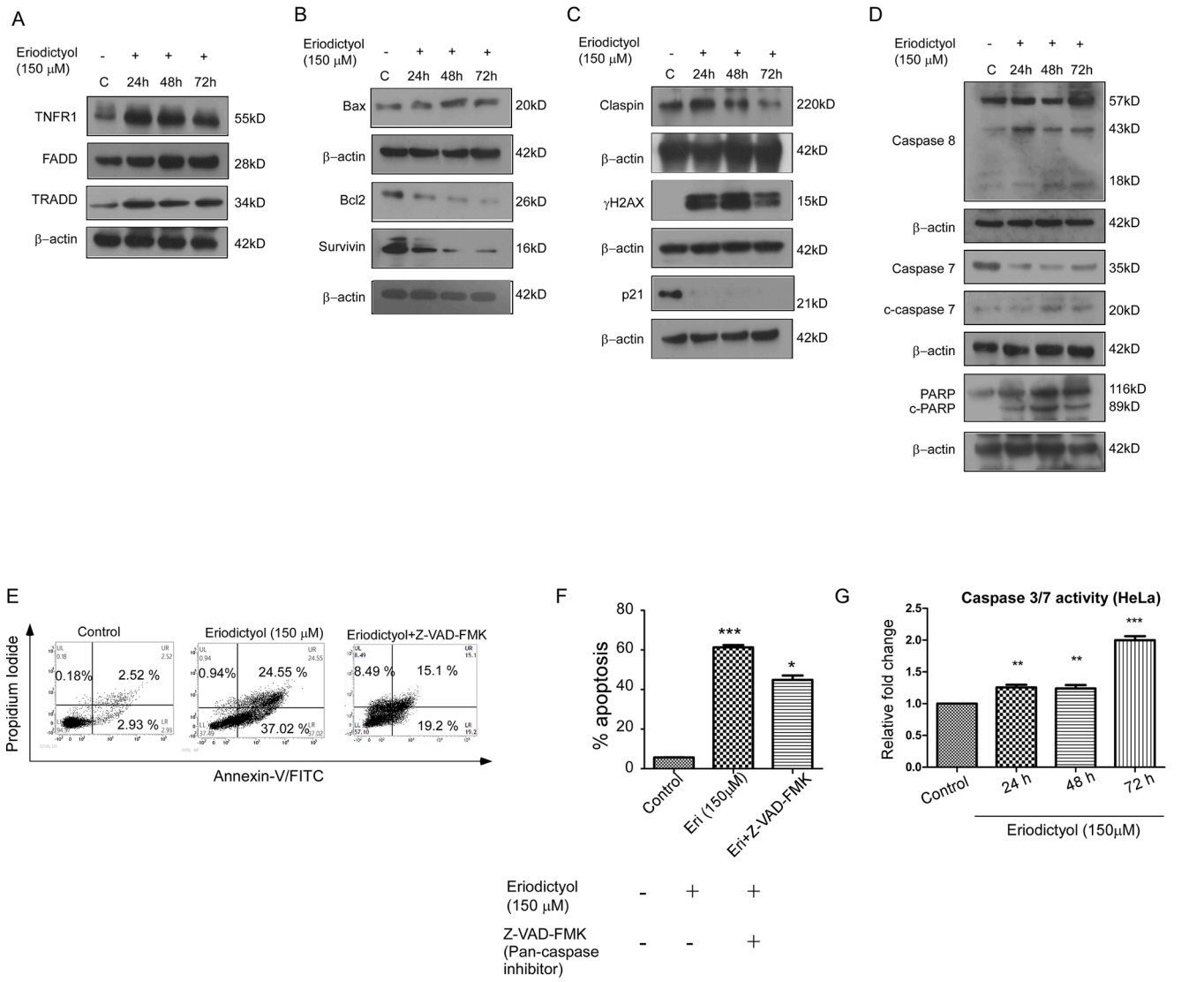

Fig. 6. Cancer cell apoptosis induced by Eriodictyol involves extrinsic pathway. A. Western immunoblots depicting increase in the expression levels of TNFR1, FADD and TRADD in HeLa cells upon Eriodictyol treatment. **B.** Eriodictyol treatment increases the expression of Bax and decreases the expression of Bcl2 and Survivin time dependently. **C.** Western immunoblots showing activation of DNA damage responsive protein expression in HeLa upon Eriodictyol treatment. **D.** Activation of the caspase cascade and PARP1 cleavage in HeLa cells upon Eriodictyol treatment. **E, F.** Density plot and column graph from flow cytometry analysis (BD FACSuite^{TM}) showing Eriodictyol mediated apoptosis in presence of pan-caspase inhibitor (Z-VAD-FMK) at 20 μM concentration, indicating that Eriodictyol mediated apoptosis is partially caspase dependent. **G.** Caspase 3/7 activity in response to Eriodictyol treatment at 24, 48, and 72 h is depicted in a column graph. Data represent Mean ± SEM of three independent experiments, analyzed by Student's t-test (two-tailed); $*p < 0.05$, $**p < 0.01$, $***p < 0.001$, ns not significant.

moderate (~ 31% inhibition), yet significant protection against Eriodictyol-mediated apoptosis (Figs. 6E, F), confirming that Eriodictyol mediated tumor cell apoptosis is at least partially caspases-dependent. Thus, collectively we confirm that Eriodictyol upregulates the pro-apoptotic proteomes and causes a significant reduction in survival proteins, thereby, culminating in a pro-apoptotic outcome in cancer cells.

TNFR1 is the potential target of Eriodictyol and the primary basis behind its selective cytotoxicity

Our preliminary data indicate that Eriodictyol treatment remarkably increases the mRNA levels of both TNF-α and TNFR1 in a time-dependent manner (Figs. 7A, B). Further, both the mRNA and protein levels of TNFR1 are elevated in HeLa cells, post-Eriodictyol treatment at 150 μM (Figs. 7 B, C). Multiple studies have reported that TNFR1 is involved in the extrinsic pathway of apoptosis [20]. To further elucidate the relationship between the selectivity of Eriodictyol towards cancer cells over normal cells, the basal expression level of TNFR1 is checked in non-cancerous cells (HEK, NKE and WI-38) versus cancer (SK-RC-45 and HeLa) cells. Western blot results clearly show that the basal level of TNFR1 protein expression in cancer cells is significantly higher than that in normal cells (Fig. 7D), thereby indicating that lack of expression of TNFR1 receptor in normal cells may be the reason for the observed selective activity of Eriodictyol against the cancer cells.

To further confirm, whether Eriodictyol selectively induces TNFR1 expression, the relative expression of Eriodictyol induced TNFR1 was checked in both cancers as well as normal cells. As shown in Fig. 7E, 24 h and 48 h exposure to Eriodictyol results in a significantly elevated time-dependent induction in TNFR1 expression in cancer (SK-RC-45 and HeLa) cells, while in the normal NKE and HEK cells, induction of TNFR1 expression with time is significantly lower compared to the cancer cells. Hence, this data supports the rationale for Eriodictyol's selective cytotoxicity towards cancer cells. Furthermore, remarkable dose-dependent upregulation in the induction of TNFR1 expression in HeLa cells initiates at 100 μM concentration of Eriodictyol compared to negligible or no TNFR1 expression in NKE (Fig. 7F, top panel) and WI-38 cells (Fig. 7F,

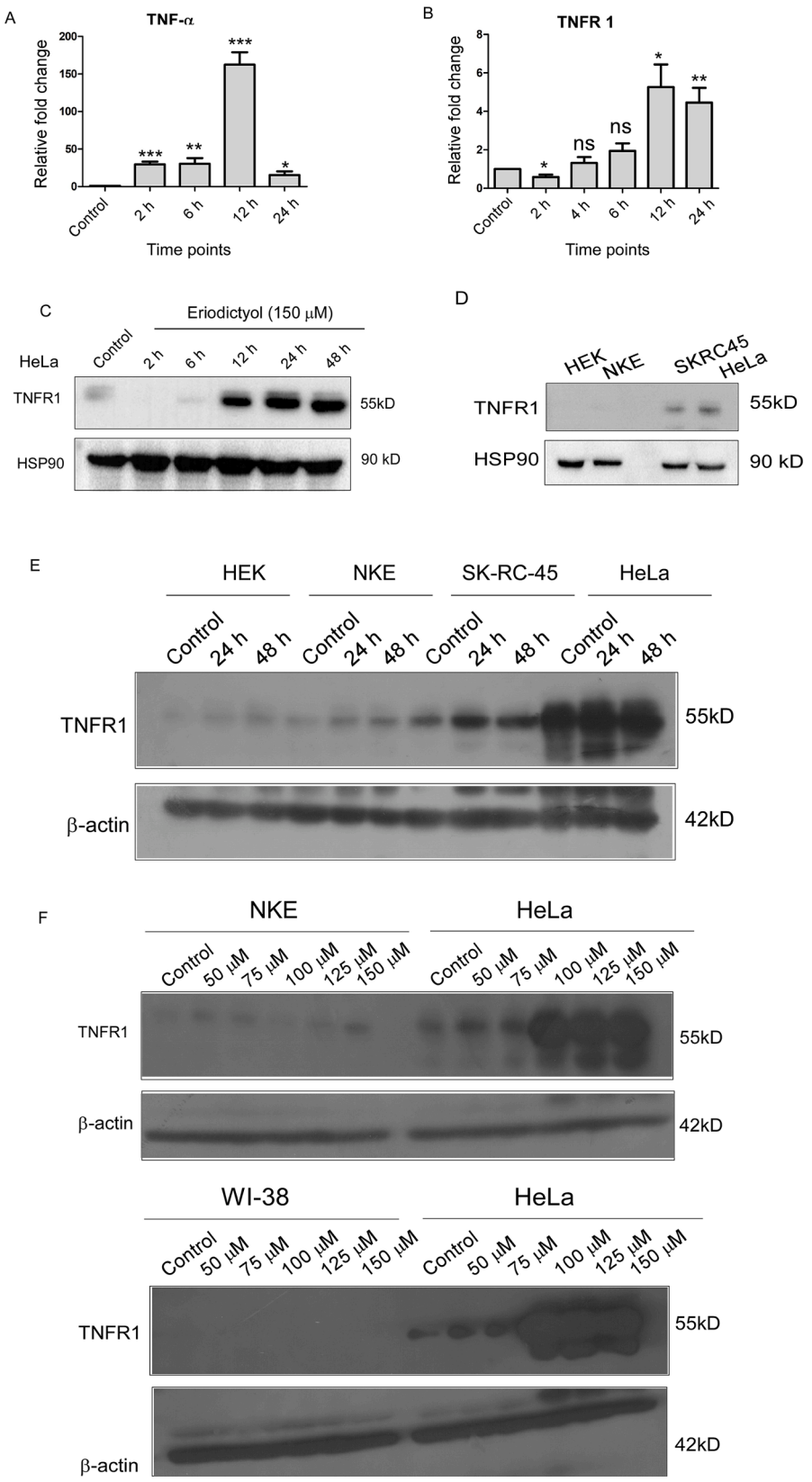

Fig. 7. Eriodictyol selectively activates TNFR1 in cancer cells but not in normal cells. A, B. Real time PCR reflecting time-dependent relative fold change in mRNA expression of TNF-α and TNFR1 respectively in response to Eriodictyol (150 μM). Relative expression values of target genes were normalized to their corresponding GAPDH Ct value and represented as fold change with respect to untreated control. Data represent mean ± SEM of three independent experiments (Student's t-test (two-tailed); $*p < 0.05$, $**p < 0.01$, $***p < 0.001$, ns-not significant). **C.** Western immunoblot data showing time-dependent induction in TNFR1 expression in HeLa cells upon Eriodictyol (150 μM) treatment. **D.** Western immunoblot confirming the basal expression level of TNFR1 in cancer lines (SK-RC-45 and HeLa) compared to normal cells (HEK and NKE). **E.** Western immunoblot showing comparative time-dependent (0h, 24h, 48h) induction of TNFR1 expression between cancer cells (SK-RC-45 and HeLa) and normal cells (HEK and NKE) in response to Eriodictyol (150 μM) treatment. **F.** Comparison of TNFR1 expression in NKE vs HeLa (Top panel) and WI-38 vs HeLa (Bottom panel) in response to various doses of Eriodictyol.

bottom panel), respectively, which correlates with the respective dose-dependent apoptotic window in HeLa cells (Fig. 3C).

Finally, to confirm the direct role of TNFR1 in the regulation of Eriodictyol mediated apoptosis, we have established TNFR1-knockout cells using CRISPR-Cas9 genome editing technology (Figs. 8A-C; Supplementary figure S1). Out of the 10 clones screened for the expression levels of TNFR1, 4 clones (Fig. 8A) appear to have complete depletion of TNFR1 expression. TNFR1 KO clone#6 is used for subsequent studies. While Eriodictyol induces significant apoptosis in wild type HeLa cells (>45% annexin V/PI + cells) at 150 μM, there is a

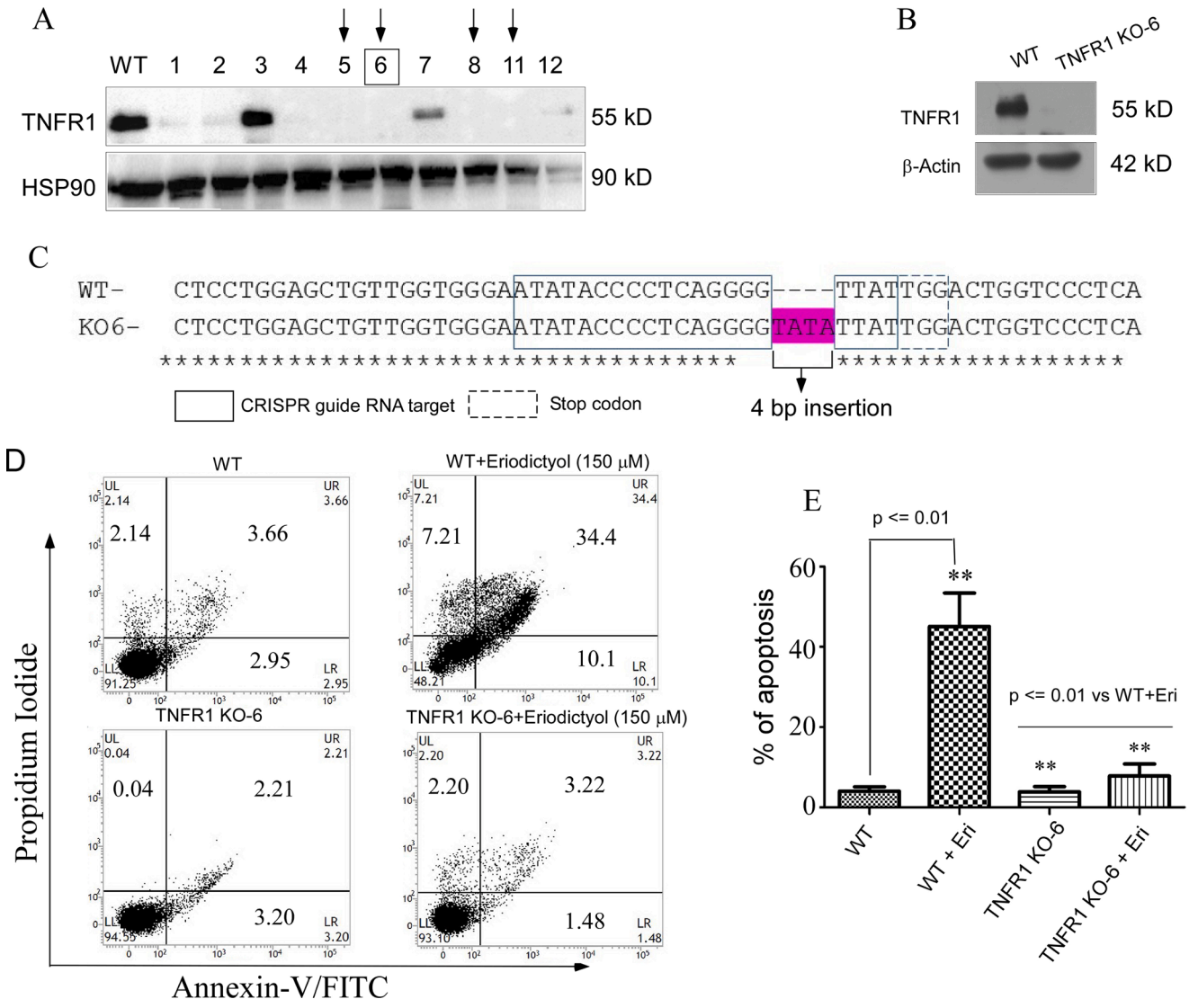

Fig. 8. CRISPR-Cas9 mediated knockout of TNFR1 in HeLa cells resulted in abrogation of Eriodictyol mediated apoptosis. A. Western immunoblot-based screening and selection of TNFR1 negative clones from an array of clones selected by puromycin treatment (1mg/ml). **B.** Western immunoblot showing TNFR1 expression in HeLa (wild-type) versus TNFR1 KO-6 clone. **C.** TNFR1 KO-6 clone shows 4bp insertion (TATA) that results in non-functional protein production. Inserted bases highlighted. The boxed portion represents the targeted DNA sequence. **D, E.** Density plot and bar graph from FACs analysis showing significant abrogation of apoptosis in TNFR1 KO-6 clone compared to HeLa (wild-type) upon Eriodictyol treatment at 150 μM dose for 48 h. Data has been collected from three independent experiments and analyzed by Student's t-test (two-tailed).

marked decrease in apoptosis in TNFR1 knockout clone KO-6 (~7% annexin-V/PI + cells) as evident from the density plot and bar graph (Figs. 8D, E), thereby confirming that Eriodictyol mediated tumor cell apoptosis is TNFR1-dependent. Therefore, we conclude that the TNFR1 signaling axis is important in the Eriodictyol-induced apoptosis of cancer cells.

Eriodictyol inhibits tumor development, progression and metastasis in immuno-competent mice

To translate the *in vitro* anticancer activity of Eriodictyol *in vivo*, a syngeneic mouse (Balb/c) tumor model has been used. *In vivo* findings demonstrate a substantial suppression of tumor development, as evident by a time-dependent decrease in tumor volume (Figs. 9A, B), as well as a decrease in the volume and weight of resected tumors from Eriodictyol-treated mice compared to non-treated animals (Figs. 9C, D). Eriodictyol-treated mice show no signs of toxicity as evident from the measurement of body weight of mice (Fig. 9E).

Moreover, Eriodictyol treatment results in a dose-dependent decrease in the number of lung metastatic nodules, (Figs. 9F, G) and a significant decline in the weight of the lungs in Eriodictyol –treated groups compared to the control group (Supplementary figure S2B). In summary, our *in vivo* study indicates that Eriodictyol reduces tumor growth and progression, as well as suppresses pulmonary lung metastasis of 4T1 cells in immune-competent Balb/c mice.

Discussion

One of the hallmarks of tumor cells is the evasion of apoptosis [21, 22]. Enhancement of the pro-apoptotic ability of the anti-cancer agents through abrogation of the survival signaling has been recognized as an effective strategy towards sensitizing the cancer cells to the chemotherapeutic drugs and preventing chemoresistance [23–25]. Owing to the increasing significance of the TNF pathway in cancer, the primary aim of the present study is to discover an effective TNF-mediated anti-cancer therapeutic with minimal toxicity to the normal cells and

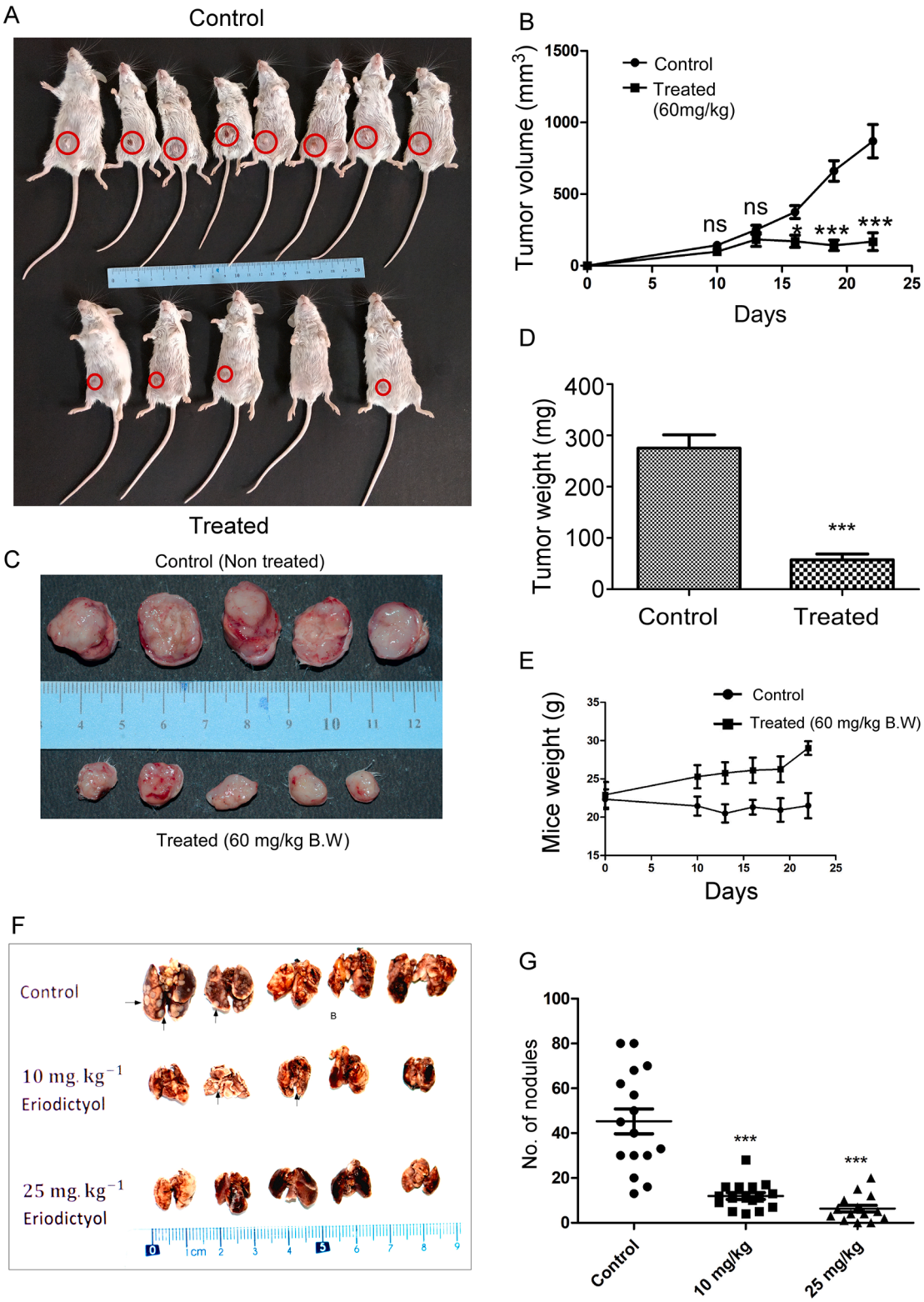

Fig. 9. Eriodictyol impedes the progression of mammary tumors and lung nodules in a syngeneic mouse model. A. Image of mice bearing tumors (indicated by red circles) before sacrifice, injected in the mammary fat pads subcutaneously with 4T1 cells, either treated with Eriodictyol (bottom row) or non-treated (top row). **B.** Line graph showing regression of tumor volume (time-dependent) in response to intraperitoneal injection of Eriodictyol, in Balb/c mice injected subcutaneously with 4T1 cells at the mammary fat pads, in comparison with those non-treated. **C.** Represents image of resected tumors from mice injected in the mammary fat pads subcutaneously with 4T1 cells, either treated with Eriodictyol (bottom row) or non-treated (top row). **D.** Bar graph showing significant reduction in tumor weight of the resected tumors, post-Eriodictyol treatment at 60 mg/kg body weight. **E.** Comparison of mice body weight in eriodictyol-treated vs non-treated. **F.** Photomicrographs depicting formalin-fixed whole lungs from male Balb/c mice injected with 4T1 cells (tail vein injection) with or without Eriodictyol treatment at different concentrations (0, 10, 25 mg/kg body weight). **G.** Graphical representation of the total number of lung nodules counted at different doses (0, 10, 25 mg/kg body weight) of Eriodictyol. The data represents two independent experiments and bar graph represents mean ± SEM (Student's t-test (two-tailed),*$p < 0.05$, **$p < 0.01$, ***$p < 0.001$, ns not significant).

elucidate the comprehensive mechanism of its anti-cancer activity and selectivity towards cancer cells.

TNF family members are the multifunctional cytokines involved in a broad spectrum of biological processes, which includes cell proliferation, cell death, carcinogenesis, immune responses, etc. [26,27]. Binding of TNF ligands to TNF receptors on the cancer cells has been documented to activate the extrinsic apoptosis pathway [28,29], thereby, instigating the initiation of the clinical trials to evaluate the anti-cancer efficacy of rhTNF-α on advanced solid cancers [3,4]. Unfortunately, in contrast to the preclinical studies, the outcome of the clinical trials was disappointing, as evidenced by the decline in apoptosis triggering ability of rhTNF-α, which has been attributed to the simultaneous activation of downstream NF-κB survival pathway [30–32]. Based on these findings, it was inferred that the TNF-α mediated killing of malignant cells through the cell death-receptor pathway could be augmented upon concomitant blockade of NF-κB cascade [33,34]. Since, Eriodictyol activates the downstream signaling that inhibits NF-κB [35,36], we have examined whether inhibition of the same could activate the endogenous TNF-α mediated apoptosis pathway in cancer cells [37]. Previously, some reports have suggested the anti-cancer activity of Eriodictyol on different malignant cells as well as its selectivity towards cancer cells [10,11,38–40]. Nonetheless, the mechanism behind its selective targeting of cancer cells is not yet well-reported, thus, motivating us to understand the underlying mechanism of its selectivity towards cancer cells over normal cells and decipher the precise pathway of Eriodictyol-induced cancer cell death. Here, we have hypothesized that the ability of Eriodictyol to specifically target aberrations contributing to the tumor's proliferative advantage, while sparing normal cells, can lead to a favorable outcome. Our research presents a global as well as differential regulation of gene expression profile in response to Eriodictyol. Among the several biological processes studied, Eriodictyol treatment demonstrated upregulation of a variety of pro-apoptotic and tumor-suppressor genes as well as induction of cell death, confirming its involvement in suppression of tumor cell proliferation. Taken together, our findings offer new possibilities to Eriodictyol's hitherto unrecognized role and unknown mode of action in altering gene transcription as well as unfolding its previously undiscovered anti-cancer characteristics.

Interestingly, our investigation manifests that Eriodictyol-mediated TNFR1 upregulation and releasing of endogenous TNF-α from cancer cells (HeLa), collectively have the fortuitous effect of altering the functional state of the TNF-α pathway from NF-kB dependent cell survival to death-inducing complex formation. In addition, the importance of TNFR1 in Eriodictyol-induced apoptosis is further supported by the exclusive expression of TNFR1 on cancer cells (and not normal cells), wherein Eriodictyol is unable to induce any appreciable TNFR1 expression in normal cells even after prolonged exposure. Additionally, TNFR1 knockout causes significant abrogation of cancer cell apoptosis. Thus, this study uncovers the mechanism behind the selectivity of Eriodictyol-mediated cytotoxic phenomena in cancer cells over normal cells.

Further investigation of the mechanistic details reveals that Eriodictyol induces extrinsic pathways of apoptosis in cancer cells, as evident from the expression profile of hallmark apoptosis-related proteins, which is similar to several previously reported anti-cancer agents [16,41–46]. TNFR1-DISC-Casp-PARP1 is the major axis in the extrinsic apoptosis pathway and we are the first to report the involvement of this pathway in Eriodictyol-mediated selective cytotoxicity in cancer cells. The approach of selectively targeting the extrinsic route to induce apoptosis in tumor cells, such as through ligation of death receptors, is appealing for cancer therapy, since death receptors have a direct link to the cell's death machinery [47]. Furthermore, tumor cell apoptosis has often been shown to occur independently of the p53 tumor suppressor gene, which is lost or inactivated in more than half of human malignancies [48]. PARP-1 cleavage is a crucial event that drives death receptor signaling towards apoptosis or necrosis. TNF-induced oxidative stress and DNA damage activate PARP-1, causing ATP depletion and the subsequent production of necrosis [49]. In brief, we demonstrate that Eriodictyol exposure of the cancer cells causes time-dependent upregulation of endogenous TNF-α and TNFR1 receptor as well as an increase in expression of the DISC complex components (TNFR1, FADD, and TRADD), leading to activation of cleaved caspase 8, activation of effector caspase 7, thus, ultimately resulting in caspases-dependent apoptotic cell death of the cancer cells. Notably, previous studies have already shown TNFR1-induced, however caspase-independent mode of cell death [50,51]. However, the fact that a pan-caspase inhibitor could not completely block Eriodictyol-induced cell death, hints towards a TNFR1-dependent, yet caspase-independent function of Eriodictyol in the induction of cancer cell death. In addition, Eriodictyol-induced apoptosis is accompanied by cell cycle arrest at the G2/M phase, which is initiated by an increase of γ-H2AX (an indicator of DNA damage) through regulation of Cyclin-B1, Cdc25 and Cdc2. Interestingly, Eriodictyol mediated inhibition of Cdc2 leads to accumulation of cells at the G2M phase , thus, resulting in the accumulation of Cyclin B1. Surprisingly, Eriodictyol causes dramatic inhibition of p21. Some reports suggest p21 promotes carcinogenesis and tumor development by promoting transcription of proteins with mitogenic and anti-apoptotic properties [52–54]. Eriodictyol also inactivates Claspin in cancer cells, which plays a vital role in shifting the tumor cell response from cell cycle arrest to induction of apoptotic cell death in response to prolonged DNA replication arrest or the persistence of DNA damage [55,56]. Finally, assessment of the therapeutic efficacy of Eriodictyol in Balb/c (syngeneic) mouse tumor model, subcutaneously injected with 4T1 mice breast cancer cells, indicates that Eriodictyol treatment results in remarkable regression of tumor volume, tumor weight, and metastatic potential in an *in vivo* mouse model without any significant adverse effect on animals as confirmed by body weight difference in untreated vs treated mice.

In the present study, we have elucidated the selective anti-cancer mechanism of Eriodictyol through upregulation of TNFR1 along with G2/M arrest and subsequent, activation of apoptosis in cancer cells without affecting the normal cells. Although the mechanism underlying the Eriodictyol-induced upregulation of TNFR1 in cancer cells is still not clearly understood, the preliminary bioinformatics analysis has shown that several probable TFs as critical targets (data not shown). However, investigation of this phenomenon is beyond the scope of the present study and will be focused on in future research. Although natural plant-based compounds including flavonoids have numerous pharmacological benefits, their large-scale extraction from natural sources in high-purity and consistent form, bioavailability, targeted delivery to the site of interest, toxicity and safety are some of the major challenges in medicinal chemistry. Hence, globally, these compounds are under extensive research as important scaffolds and lead for the development of effective and selective chemotherapeutic agents for clinical application. Henceforth, Eriodictyol might necessitate the development of easy to synthesize (biosynthesis using yeast applying promoter adjustment and directed evolution [57]) and non-toxic chemical derivative, designing strategies to improve its bioavailability by increasing absorption and metabolic stability, as well as its targeted delivery by formulating appropriate microencapsulation, nano-delivery system or micro-emulsion [58–63] for improved anti-cancer strategies. To summarize, Eriodictyol has the capability to be a promising lead for the future development of prospective and efficient candidate for successful cancer therapy.

Fig. 10. Depicts the proposed model of Eriodictyol mediated selective cytotoxicity in cancer cells.

Funding

DBT-Twinning Project (BT/469/NE/TBP/2013), UGC (201314/NETJRF/10501/22 -351787). We acknowledge DST-SERB (Sanction no. EMR/2016/001983) for procurement of the QuantStudio 3 Real Time PCR system, as well as ICMR (Sanction No. 2016-0137/CMB/ADHOC/

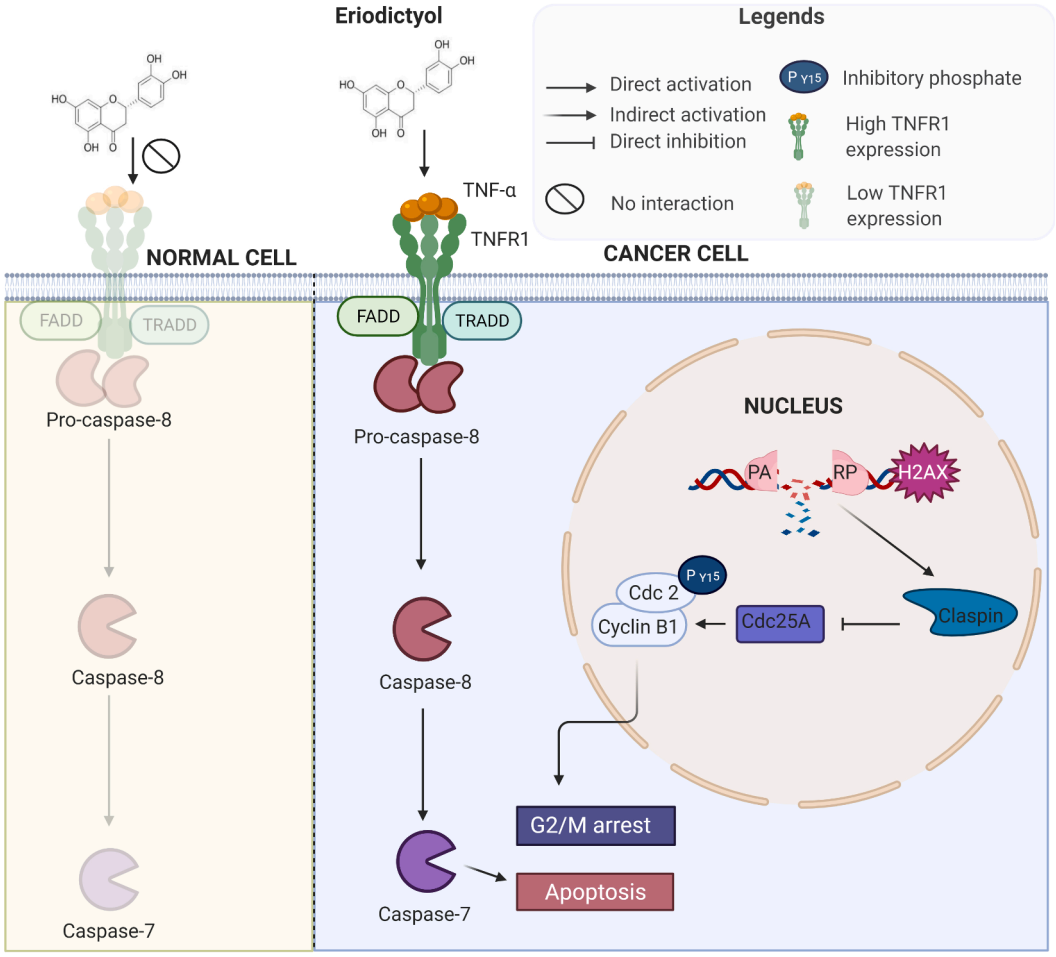

Fig. 10. Proposed model of the role of Eriodictyol mediated selective cytotoxicity of cancer cells. The upregulated expression of TNFR1 on cancer cells lead to Eriodictyol mediated apoptosis.

BMS) for the Gel Imaging System used in this study. Dr. Dipanwita Das Mukherjee is thankful to DBT – Research Associateship (Project ID – P-1453) program in Life Science and Biotechnology, as well as DST-SERB NPDF (Sanction No. PDF/2021/000504) for the post-doctoral fellowships.

Declaration of Competing Interest statement

The authors declare that there is no conflict of interest.

Acknowledgments

We would like to thank BioBharati LifeScience Pvt. Limited for the characterization of TNFR1 KO-6 clones, Dr. Debajyoti Ray for photography of the mice tumors and Mr. Mrinal Das for DNA sequencing. Illustration (Fig. 10) created with https://biorender.com/.

Supplementary materials

Supplementary material associated with this article can be found, in the online version, at doi:10.1016/j.tranon.2022.101433.

References

[1] S. Fulda, Tumor resistance to apoptosis, Int. J. Cancer 124 (3) (2009) 511–515.
[2] R.M. Mohammad, et al., Broad targeting of resistance to apoptosis in cancer, Seminars Cancer Biol. 35 (Suppl(0)) (2015) S78–S103.
[3] T. Mashima, et al., Apoptosis resistance in tumor cells, Cytotechnology 27 (1-3) (1998) 293–308.
[4] D. Tewari, P. Rawat, P.K. Singh, Adverse drug reactions of anticancer drugs derived from natural sources, Food Chem. Toxicol. 123 (2019) 522–535.
[5] Z.-B. Liu, et al., Natural substances derived from herbs or plants are promising sources of anticancer agents against colorectal cancer via triggering apoptosis, J. Pharm. Pharmacol. (2021) rgab130.
[6] X. Ma, Z. Wang, Anticancer drug discovery in the future: an evolutionary perspective, Drug Discovery Today 14 (23) (2009) 1136–1142.
[7] J.K. Lee, Anti-inflammatory effects of eriodictyol in lipopolysaccharide-stimulated raw 264.7 murine macrophages, Arch. Pharm Res. 34 (4) (2011) 671–679.
[8] K. Liu, et al., Eriodictyol inhibits RSK2-ATF1 signaling and suppresses EGF-induced neoplastic cell transformation, J. Biol. Chem. 286 (3) (2011) 2057–2066.
[9] M. Kumazoe, et al., Metabolic profiling-based data-mining for an effective chemical combination to induce apoptosis of cancer cells, Sci Rep 5 (2015) 9474.
[10] L. Tang, et al., Eriodictyol inhibits the growth of CNE1 human nasopharyngeal cancer growth by targeting MEK/ERK signalling pathway, inducing cellular autophagy and inhibition of cell migration and invasion, J. BUON 25 (5) (2020) 2389–2394.
[11] Y. Zhang, R. Zhang, H. Ni, Eriodictyol exerts potent anticancer activity against A549 human lung cancer cell line by inducing mitochondrial-mediated apoptosis, G2/M cell cycle arrest and inhibition of m-TOR/PI3K/Akt signalling pathway, Arch. Med. Sci. 16 (2) (2019) 446–452.
[12] Li, W., et al., *Eriodictyol Inhibits Proliferation, Metastasis and Induces Apoptosis of Glioma Cells via PI3K/Akt/NF-κB Signaling Pathway.*2020. 11(114).
[13] M. Kundu, et al., Ganglioside GM2 mediates migration of tumor cells by interacting with integrin and modulating the downstream signaling pathway, Biochimica et Biophysica Acta (BBA) - Molecular Cell Res. 1863 (7, Part A) (2016) 1472–1489.
[14] J. van Meerloo, G.J. Kaspers, J. Cloos, Cell sensitivity assays: the MTT assay, Methods Mol. Biol. 731 (2011) 237–245.
[15] A. Dutta, et al., C-Glycosylated cinnamoylfuran derivatives as novel anti-cancer agents, RSC Adv. 7 (46) (2017) 28853–28864.
[16] P.K. Parida, et al., Inhibition of cancer progression by a novel trans-stilbene derivative through disruption of microtubule dynamics, driving G2/M arrest, and p53-dependent apoptosis, Cell Death. Dis. 9 (5) (2018) 448.

[17] M.F. Sentmanat, et al., A survey of validation strategies for CRISPR-Cas9 editing, Sci. Rep. 8 (1) (2018), 888-888.
[18] B. Mahata, et al., TALEN mediated targeted editing of GM2/GD2-synthase gene modulates anchorage independent growth by reducing anoikis resistance in mouse tumor cells, Sci. Rep. 5 (1) (2015) 9048.
[19] R. Minorics, et al., A molecular understanding of D-homoestrone-induced G2/M cell cycle arrest in HeLa human cervical carcinoma cells, J. Cell Mol. Med. 19 (10) (2015) 2365–2374.
[20] H. Rauert, et al., TNFR1 and TNFR2 regulate the extrinsic apoptotic pathway in myeloma cells by multiple mechanisms, Cell Death Dis. 2 (8) (2011) e194.
[21] D. Hanahan, R.A. Weinberg, The hallmarks of cancer, Cell 100 (1) (2000) 57–70.
[22] K. Fernald, M. Kurokawa, Evading apoptosis in cancer, Trends Cell Biol. 23 (12) (2013) 620–633.
[23] F. Guestini, K.M. McNamara, H. Sasano, The use of chemosensitizers to enhance the response to conventional therapy in triple-negative breast cancer patients, Breast Cancer Manage. 6 (4) (2017) 127–131.
[24] A.R. Hamed, et al., Targeting multidrug resistance in cancer by natural chemosensitizers, Bull. Natl. Res. Centre 43 (1) (2019) 8.
[25] J.A. Shabbits, Y. Hu, L.D. Mayer, Tumor chemosensitization strategies based on apoptosis manipulations, Mol Cancer Ther 2 (8) (2003) 805–813.
[26] G.D. Kalliolias, L.B. Ivashkiv, TNF biology, pathogenic mechanisms and emerging therapeutic strategies, Nat. Rev. Rheumatol. 12 (1) (2016) 49–62.
[27] H.T. Idriss, J.H. Naismith, TNF alpha and the TNF receptor superfamily: structure-function relationship(s), Microsc. Res. Tech. 50 (3) (2000) 184–195.
[28] O. Micheau, J. Tschopp, Induction of TNF receptor I-mediated apoptosis via two sequential signaling complexes, Cell 114 (2) (2003) 181–190.
[29] E.E. Varfolomeev, A. Ashkenazi, Tumor necrosis factor: an apoptosis JuNKie? Cell 116 (4) (2004) 491–497.
[30] O. Micheau, et al., NF-κB Signals Induce the Expression of c-FLIP, Mol. Cell. Biol. 21 (16) (2001) 5299–5305.
[31] S.F. Josephs, et al., Unleashing endogenous TNF-alpha as a cancer immunotherapeutic, J. Transl. Med. 16 (1) (2018) 242.
[32] C.G. Savva, et al., Selective activation of TNFR1 and NF-κB inhibition by a novel biyouyanagin analogue promotes apoptosis in acute leukemia cells, BMC Cancer 16 (2016), 279-279.
[33] Y. Wang, et al., Eriodictyol inhibits IL-1β-induced inflammatory response in human osteoarthritis chondrocytes, Biomed. Pharmacother. 107 (2018) 1128–1134.
[34] A. Wicovsky, et al., Sustained JNK activation in response to tumor necrosis factor is mediated by caspases in a cell type-specific manner, J. Biol. Chem. 282 (4) (2007) 2174–2183.
[35] Y. Wang, et al., Eriodictyol inhibits IL-1β-induced inflammatory response in human osteoarthritis chondrocytes, Biomed. Pharmacother. 107 (2018) 1128–1134.
[36] X. Wang, et al., Eriodictyol ameliorates lipopolysaccharide-induced acute lung injury by suppressing the inflammatory COX-2/NLRP3/NF-κB pathway in mice, J Biochem. Mol. Toxicol. 34 (3) (2020) e22434.
[37] W. Li, et al., Eriodictyol inhibits proliferation, metastasis and induces apoptosis of glioma Cells via PI3K/Akt/NF-κB signaling pathway, Front. Pharmacol. 11 (2020) 114.
[38] K. Liu, et al., Eriodictyol inhibits RSK2-ATF1 signaling and suppresses EGF-induced neoplastic cell transformation, J. Biol. Chem. 286 (3) (2011) 2057–2066.
[39] M. Kumazoe, et al., Metabolic Profiling-based Data-mining for an Effective Chemical Combination to Induce Apoptosis of Cancer Cells, Sci. Rep. 5 (1) (2015) 9474.
[40] W. Li, et al., Eriodictyol inhibits proliferation, metastasis and induces apoptosis of glioma Cells via PI3K/Akt/NF-κB signaling pathway, Front. Pharmacol. 11 (114) (2020).
[41] B. Mahata, et al., GBM derived gangliosides induce T cell apoptosis through activation of the caspase cascade involving both the extrinsic and the intrinsic pathway, PLoS One 10 (7) (2015), e0134425.
[42] L. Belayachi, et al., Retama monosperma n-hexane extract induces cell cycle arrest and extrinsic pathway-dependent apoptosis in Jurkat cells, BMC Complement. Alternative Med. 14 (2014), 38-38.
[43] S.H. Park, et al., Luteolin induces cell cycle arrest and apoptosis through extrinsic and intrinsic signaling pathways in MCF-7 breast cancer cells, J. Environ. Pathol. Toxicol. Oncol. 33 (3) (2014) 219–231.
[44] B. Wang, X.H. Zhao, Apigenin induces both intrinsic and extrinsic pathways of apoptosis in human colon carcinoma HCT-116 cells, Oncol. Rep. 37 (2) (2017) 1132–1140.
[45] H. Wahl, et al., Curcumin enhances Apo2L/TRAIL-induced apoptosis in chemoresistant ovarian cancer cells, Gynecol. Oncol. 105 (1) (2007) 104–112.
[46] A. Chopra, A. Anderson, C. Giardina, Novel piperazine-based compounds inhibit microtubule dynamics and sensitize colon cancer cells to tumor necrosis factor-induced apoptosis, J. Biol. Chem. 289 (5) (2014) 2978–2991.
[47] A. Ashkenazi, Targeting death and decoy receptors of the tumour-necrosis factor superfamily, Nat. Rev. Cancer 2 (6) (2002) 420–430.
[48] W.S. El-Deiry, Insights into cancer therapeutic design based on p53 and TRAIL receptor signaling, Cell Death Differ. 8 (11) (2001) 1066–1075.
[49] Los, M., et al., *Activation and Caspase-mediated Inhibition of PARP: a molecular switch between fibroblast necrosis and apoptosis in death receptor signaling.*2002. 13(3): p. 978-988.
[50] J. Li, et al., Beta-actin is required for mitochondria clustering and ROS generation in TNF-induced, caspase-independent cell death, J. Cell Sci. 117 (Pt 20) (2004) 4673–4680.
[51] M.J. Morgan, Y.-S. Kim, Z.-g. Liu, TNFα and reactive oxygen species in necrotic cell death, Cell Res. 18 (3) (2008) 343–349.
[52] R.U. Jänicke, et al., The multiple battles fought by anti-apoptotic p21, Cell Cycle 6 (4) (2007) 407–413.
[53] L. Lai, G.Y. Shin, H. Qiu, The role of cell cycle regulators in cell survival-dual functions of cyclin-dependent kinase 20 and p21(Cip1/Waf1), Int. J. Mol Sci. 21 (22) (2020).
[54] I.B. Roninson, Oncogenic functions of tumour suppressor p21(Waf1/Cip1/Sdi1): association with cell senescence and tumour-promoting activities of stromal fibroblasts, Cancer Lett. 179 (1) (2002) 1–14.
[55] J.I. Semple, et al., Cleavage and degradation of Claspin during apoptosis by caspases and the proteasome, Cell Death & Different. 14 (8) (2007) 1433–1442.
[56] C.A. Clarke, L.N. Bennett, P.R. Clarke, Cleavage of claspin by caspase-7 during apoptosis inhibits the Chk1 pathway, J. Biol. Chem. 280 (42) (2005) 35337–35345.
[57] S. Gao, et al., Efficient Biosynthesis of (2S)-Eriodictyol from (2S)-Naringenin in Saccharomyces cerevisiae through a Combination of Promoter Adjustment and Directed Evolution, ACS Synthetic Biol. 9 (12) (2020) 3288–3297.
[58] Q. Shen, et al., Enhanced intestinal absorption of daidzein by borneol/menthol eutectic mixture and microemulsion, AAPS PharmSciTech 12 (4) (2011) 1044–1049.
[59] T. Walle, Methylation of dietary flavones greatly improves their hepatic metabolic stability and intestinal absorption, Mol. Pharmaceutics 4 (6) (2007) 826–832.
[60] H. Cao, et al., Methylation of genistein and kaempferol improves their affinities for proteins, Int. J. Food Sci. Nutr. 64 (4) (2013) 437–443.
[61] I.L. Nielsen, et al., Bioavailability is improved by enzymatic modification of the citrus flavonoid hesperidin in humans: a randomized, double-blind, crossover trial, J. Nutr. 136 (2) (2006) 404–408.
[62] D.J. Bharali, et al., Nanoparticle delivery of natural products in the prevention and treatment of cancers: current status and future prospects, Cancers 3 (4) (2011) 4024–4045.
[63] J.K. Patra, et al., Nano based drug delivery systems: recent developments and future prospects, J. Nanobiotechnol. 16 (1) (2018) 71.

SCIENTIFIC REPORTS
nature research

OPEN

Ricinus communis L. fruit extract inhibits migration/invasion, induces apoptosis in breast cancer cells and arrests tumor progression *in vivo*

Received: 30 October 2017
Accepted: 10 September 2019
Published online: 10 October 2019

Munmi Majumder[1], Shibjyoti Debnath[2], Rahul L. Gajbhiye[3], Rimpi Saikia[1], Bhaskarjyoti Gogoi[4,5], Suman Kumar Samanta[4], Deepjyoti K. Das[1], Kaushik Biswas[2], Parasuraman Jaisankar[3] & Rupak Mukhopadhyay[1]

Medicinal plant-based therapies can be important for treatment of cancer owing to high efficiency, low cost and minimal side effects. Here, we report the anti-cancer efficacy of *Ricinus communis* L. fruit extract (RCFE) using estrogen positive MCF-7 and highly aggressive, triple negative MDA-MB-231 breast cancer cells. RCFE induced cytotoxicity in these cells in dose and time-dependent manner. It also demonstrated robust anti-metastatic activity as it significantly inhibited migration, adhesion, invasion and expression of matrix metalloproteinases (MMPs) 2 and 9 in both cell lines. Further, flow cytometry analysis suggested RCFE-mediated induction of apoptosis in these cells. This was supported by attenuation of anti-apoptotic Bcl-2, induction of pro-apoptotic Bax and caspase-7 expressions as well as PARP cleavage upon RCFE treatment. RCFE (0.5 mg/Kg body weight) treatment led to significant reduction in tumor volume in 4T1 syngeneic mouse model. HPLC and ESI-MS analysis of active ethyl acetate fraction of RCFE detected four compounds, Ricinine, p-Coumaric acid, Epigallocatechin and Ricinoleic acid. Individually these compounds showed cytotoxic and migration-inhibitory activities. Overall, this study for the first time demonstrates the anti-cancer efficacy of the fruit extract of common castor plant which can be proposed as a potent candidate for the treatment of breast cancer.

Breast cancer is the leading cause of cancer death among women worldwide[1]. The main treatment regimens for breast cancer like surgery, radiation therapy, chemotherapy, targeted hormone therapy are either expensive or have various side-effects[2,3]. So, studies towards finding efficient and cost-effective therapeutic strategies with minimal side effects are important for expansion of current treatment options for breast cancer patients. Medicinal plants are rich sources of bioactive molecules and can be exploited for application as anti-cancer agents. Alkaloids vincristine and vinblastine from the plant *Vinca rosea* and taxol, paclitaxel derived from the plant *Taxus brevifolia* are well established anticancer agents owing to their microtubule-targeting efficacy[4–6]. Podophyllotoxin, a lignin derived from *Podophyllum peltatum* L. or *P. emodi* and their derivatives are also used as anti-cancer drugs in market[7]. While podophyllotoxin act by inhibiting microtubule assembly, its derivatives like etoposides and teniposides act by interacting with DNA and inhibition of DNA topoisomerase II[8]. Camptothecin, a quinoline alkaloid from *Camptotheca acuminata* also acts as commercial anti-cancer drug, which inhibits the DNA enzyme topoisomerase I[9]. Furthermore, purified plant polyphenols, baicalin and fisetin were also shown to possess anti-cancer and apoptosis inducing activity in breast cancer cell lines[10,11]. Curcumin inhibited NF-kB pathway and subsequently, the expression of inflammatory cytokines CXCL-1 and -2, up regulated during metastasis[12].

[1]Cellular, Molecular and Environmental Biotechnology Laboratory, Department of Molecular Biology and Biotechnology, Tezpur University, Tezpur, 784028, Assam, India. [2]Division of Molecular Medicine, Bose Institute, P1/12 CIT Road, Scheme VIIM, Kolkata, 700054, India. [3]Laboratory of Catalysis and Chemical Biology, Organic and Medicinal Chemistry Division, CSIR-Indian Institute of Chemical Biology, Jadavpur, Kolkata, 700032, India. [4]Institute of Advanced Study in Science and Technology Vigyan Path, Paschim Boragaon, Guwahati, Assam, 781035, India. [5]Present address: Department of Biotechnology Royal School of Bio-Sciences Royal Global University Guwahati, Assam, 781035, India. Correspondence and requests for materials should be addressed to R.M. (email: mrupak@gmail.com)

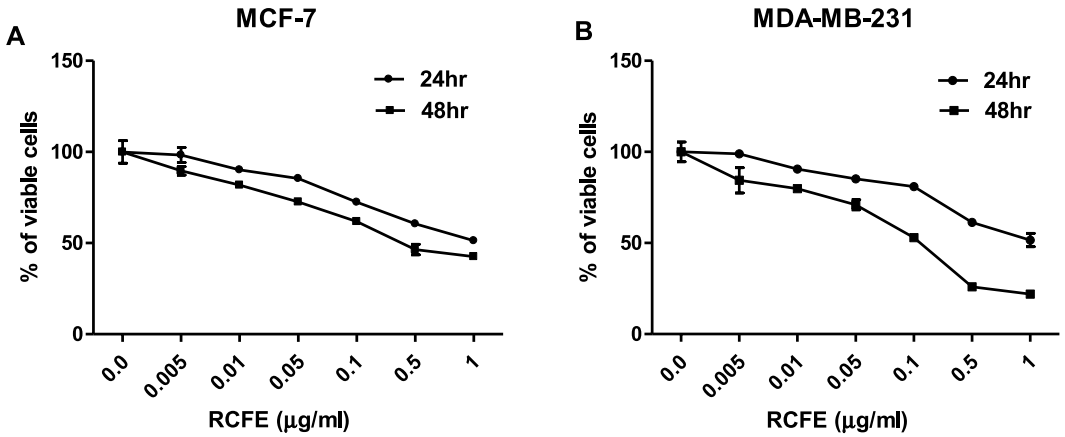

Figure 1. RCFE induced cytotoxicity in breast cancer cells. MCF-7 (**A**) and MDA-MB-231 (**B**) cells were treated with various concentrations of RCFE for 24 and 48 hr. Data represent the mean ± SEM of three independent experiments.

Majority of the breast cancer mortality cases are primarily due to metastasis of the primary cancer to different sites including organs like bones, brain, liver, lymph nodes and lungs[10]. The 5-year survival rate of metastatic breast cancer patients is about 25% suggesting the importance of targeted therapy for metastasis[13,14]. In search of a novel medicinal plant-based therapeutic approach against breast cancer, fruit extract of *Ricinus communis* L. *(Euphorbiaceae)* from North East Indian origin has been studied in detail. North-Eastern part of India is a well-regarded reservoir of traditional medicinal plants as it is one of the prominent biodiversity hotspots of the world[15]. *R. communis* L, commonly known as castor plant, is abundant in North East India and well-known for its traditional and medicinal use globally[16]. In general, various parts of this plant has been used for the treatment of pain, paralysis, constipation, gastritis and warts[17,18]. 50% ethanolic extract of roots of this plants have shown anti-diabetic activity in *in-vivo* rat models[19]. There are other reports which indicate the effectiveness of this plant as anti-fungal agent and also as a pest control measure[19–22]. A volatile extract from the leaves of the plants have shown to induce apoptosis in human melanoma cells (SK-MEL-28)[16]. However, a detailed study on the anti-cancer efficacy of the fruits of *R. communis* L. is not reported.

The current study demonstrates the anti-proliferative activity of *R. communis* L. fruit extract (RCFE) against two breast cancer cell lines MCF-7 and MDA-MB-231. RCFE significantly inhibited migration, adhesion and invasion along with reduction of matrix metalloproteinases 2 and 9 expression. It also induced apoptosis as shown by reduction of anti-apoptotic Bcl-2, induction of pro-apoptotic Bax expression and DNA fragmentation. The induction of apoptosis in both cells was caspase-7 dependent and independent of p53. Interestingly, RCFE inhibited upstream STAT3 activation responsible for induction of MMPs and Bcl-2. RCFE successfully inhibited tumor progression in syngeneic mouse tumor model *in vivo*. HPLC and ESI-MS analysis of the active ethyl acetate fraction of RCFE showed presence of four probable compounds all of which individually showed anti-cancer activities.

Results

RCFE induced cytotoxicity in MCF-7 and MDA-MB-231 cells. To evaluate the cytotoxic effect of RCFE on breast cancer, MCF-7 and MDA-MB-231 cell lines were treated with various concentrations of RCFE for 24 or 48 hr. RCFE treatment significantly increased cytotoxicity in both the cells in dose and time dependent manner (Fig. 1A,B). Treatment with 1 µg/ml RCFE induced cell death by 48.7% and 55.4% in 24 and 48 hr incubation, respectively in MCF-7 cells (Fig. 1A). Treatment with same concentration led to 48.4% and 78.5% cell death in MDA-MB-231 cells at these time points, respectively (Fig. 1B). To understand the cytotoxic specificity of RCFE, additional cell lines of cancer and normal origin were treated with the extract. Amongst these, HER2-postive MDA-MB-453 and triple-positive ZR-75-1 breast cancer cells showed 36.2% and 54.3% cell death when treated with 1 µg/ml RCFE for 48 hr (Supplementary Fig S1). Similar treatment showed significant cytotoxicity in colon cancer cell line HT-29 (64%) and adenocarcinoma cell line A549 (54.2%) after 48 hr (Supplementary Fig S1). In contrast, treatment with similar doses of RCFE showed minimal effect on the HEK293 and mouse embryonic fibroblast (MEF) cells suggesting the extract's cytotoxic specificity against cancer cells (Supplementary Fig S1).

Inhibition of migration, adhesion and invasion of MCF-7 and MDA-MB-231 cells by RCFE. As migration is a primary step in cancer metastasis, we studied the effect of RCFE on migration of MCF-7 and MDA-MB-231 cells using wound healing assay. Near-confluent monolayer of cells was pre-treated with Mitomycin C (1 µg/ml) to confirm the wound healing was due to cell migration and not due to proliferation. RCFE treatment for 24 and 48 hr demonstrated dose-dependent inhibition of migration in both cells (Fig. 2A,B). The inhibition of migration in response to 0.05 µg/ml of RCFE after 24 hr was not significant in MCF-7 cells. However, the same concentration was sufficient to inhibit migration significantly after 48 hr. The effect was highly significant when MCF-7 cells were treated with higher concentration of RCFE (0.1 µg/ml) even at 24 hr. Interestingly, the effect of RCFE on inhibition of migration was robust on highly metastatic MDA-MB-231

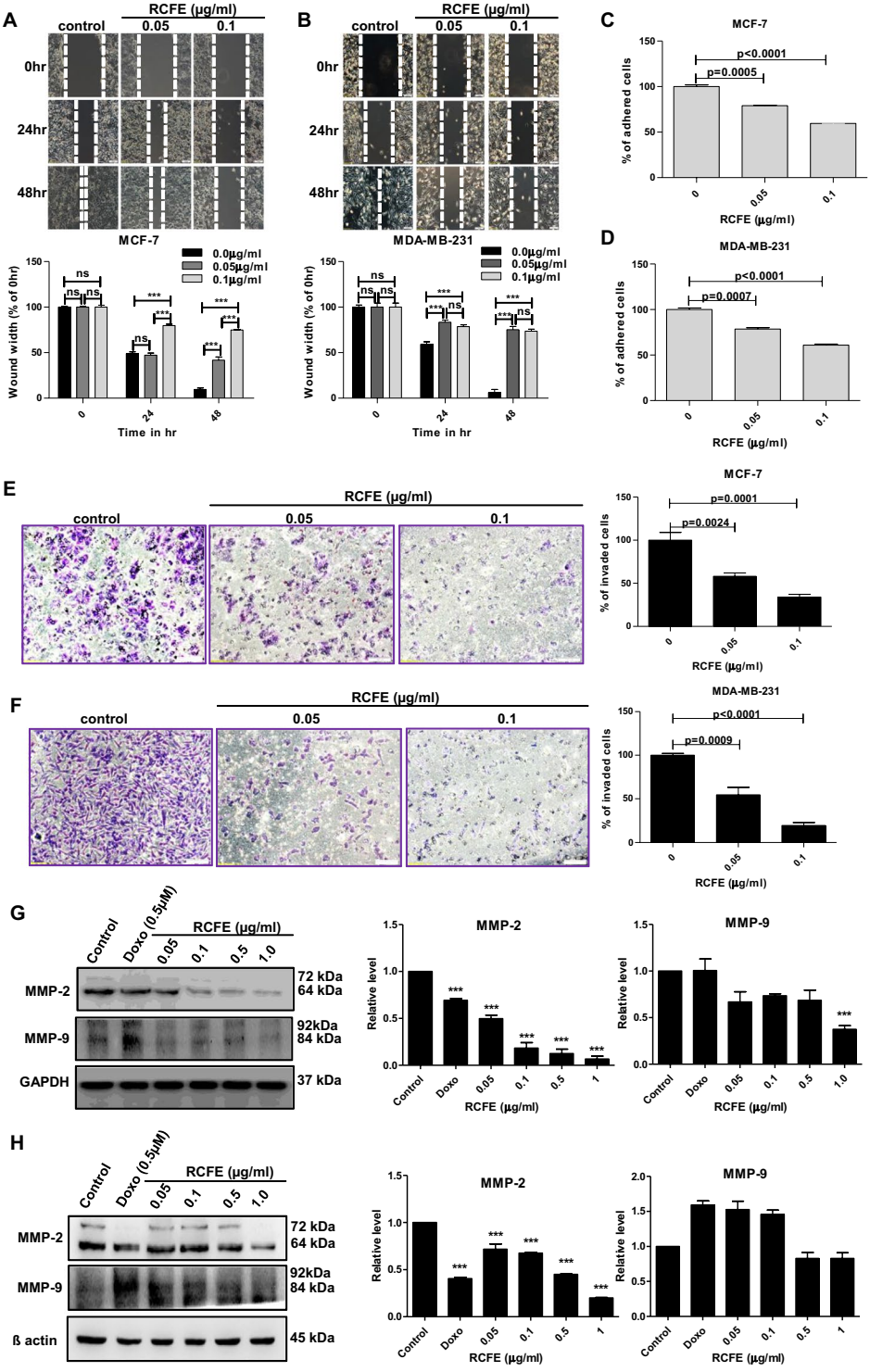

Figure 2. RCFE inhibited metastatic properties of breast cancer cells. Inhibition of migration of MCF-7 (**A**) and MDA-MB-231 (**B**) with treatment of 0.05 and 0.1 µg/ml for 24 and 48 hr. The quantification of wound widths was shown in right panels. Data represent the mean ± SEM of three independent experiments. Statistical differences were analyzed with two-way ANOVA test. p value ns > 0.05, p value *** < 0.0001. Effect of RCFE on adhesion of MCF-7 **(C)** and MDA-MB-231 **(D)**. Data represented as mean ± SEM of three independent experiments. Statistical differences were analyzed with one-way ANOVA test. p value < 0.05 was considered significant. Invasion of MCF-7 **(E)** and MDA-MB-231 **(F)** cells through ECM gel coated transwell inserts in response to RCFE. Data represent the mean ± SEM of five different images of individual set of three independent experiments (shown in right panels). Statistical differences were analyzed with student t-test. p value < 0.05 was considered significant. Western blot analysis of MMP-2 and -9 in MCF-7 **(G)** and MDA-MB-231 **(H)** cells in response to treatment with RCFE. The quantitation of band intensities was represented in bottom panels. Statistical differences were analyzed with one-way ANOVA test. p value < 0.05 was considered significant.

as shown by significant inhibition of migration in these cells after treatment with both the doses for 24 and 48 hr (Fig. 2B). Ability to adhere to extracellular matrices is one of the hallmarks of metastatic cancer cells. Pre-treatment of both MCF-7 and MDA-MB-231 cells with two concentrations of RCFE demonstrated significant reduction in adhesion of the cells to collagen IV coated wells in a dose-dependent fashion (Fig. 2C,D). Treatment with 0.05 µg/ml and 0.1 µg/ml RCFE inhibited adherence by 21% and 41% in MCF-7 cells and 22% and 40% in MDA-MB-231 cells, respectively.

Further, the effect of RCFE on invasion of two breast cancer cells was studied. Cells pre-treated with or without RCFE were allowed to invade through extracellular matrix (ECM) gels in response to 10% FBS-containing medium. In MCF-7 cells, treatment with 0.05 and 0.1 µg/ml of RCFE reduced 42% and 66% invasion compared to control cells (Fig. 2E). Interestingly again, the effect was more prominent in MDA-MB-231 cells as treatment with these two concentrations of RCFE led to 45% and 81% reduction in invasion after 6 hr (Fig. 2F).

As these experiments pointed towards anti-metastatic role of RCFE, the expression of metastasis-associated matrix metalloproteinase 2 and 9 (MMP-2 and 9) were studied next. Western blot analysis suggested treatment of RCFE for 24 hr reduced expression of MMP-2 and MMP-9 in MCF-7 and MDA-MB-231 cells in concentration-dependent manner (Fig. 2G,H). RCFE at a concentration of 1.0 µg/ml reduced the MMP-2 expression by about 10 folds in MCF-7 cells and 4 folds in MDA-MB-231 cells. Treatment with the same concentration of RCFE led to ~ 2 folds reduction in expression of MMP-9 in both the cells.

RCFE induced apoptosis in MCF-7 and MDA-MB-231 cells. Since, apoptosis is a plausible mode of controlling cancer cell proliferation by an anti-cancer agent; we next studied the role of RCFE in inducing apoptosis in two cell lines. Flow cytometric analysis was performed with cells treated with 0.5 and 1.0 µg/ml RCFE for 24 hr (Fig. 3A,B). In MCF-7 cells, both treatments induced more than 3 folds augmentation in apoptosis (early and late). The increase in apoptosis in MDA-MB-231 cells were found to be 2.7 folds (0.5 µg/ml) and 11 folds (1.0 µg/ml), respectively. Genomic DNA isolated from the cells following treatment with 1.0 µg/ml RCFE for 24 and 48 hr showed degradation of DNA (Supplementary Fig S2).

To understand the signaling mechanism leading to RCFE-induced apoptosis in MCF-7 and MDA-MB-231 cells, expression level of apoptosis regulating proteins like Bax, Bcl-2, PARP, and Caspase-7 were assessed by western blot (Fig. 3C,D). Treatment with RCFE augmented expression of apoptotic protein Bax and concomitantly inhibited anti-apoptotic protein Bcl-2 expression in a concentration-dependent manner in both the experimental cells. This led to increase in Bax/Bcl-2 ratio, critical for cells undergoing apoptosis (Right panels; Fig. 3C,D). Bcl-2 inhibition leads to release of cytochrome c from the mitochondrion which induces the caspase pathway. Treatment with RCFE increased expression level of caspase-7 in dose-dependent manner suggesting onset of apoptosis in the cells (Fig. 3C,D). Significant increase in caspase-7 level was found in cells treated with higher concentrations of RCFE (Right panels; Fig. 3C,D). PARP, a DNA repair enzyme, is a substrate of caspases and increase in PARP cleavage indicates apoptosis in the cells. PARP cleavage as a result of RCFE treatment confirmed caspase-mediated apoptosis in both MCF-7 and MDA-MB-231 cells (Fig. 3C,D). Doxorubicin (0.5 µM) was used as positive control in this study. To understand if cell cycle arrest was also involved in anti-cancer activity of RCFE, expression of Cyclin E1 was studied. In both MCF-7 and MDA-MB-231 cells, the expression of Cyclin E1 did not change significantly with increased concentration of RCFE suggesting cells were not arrested in G1/S phase (Supplementary Fig S3). Expression of tumor suppressor gene p53 was also studied as activation of p53 was proposed to play key role in cell cycle arrest and apoptosis[23]. Treatment with RCFE did not show any activation of p53 in the cells suggesting the RCFE-induced apoptosis in these cells was primarily independent of p53 (Supplementary Fig S3).

RCFE inhibited phosphorylation of STAT3. JAK-STAT pathway is involved in activation of proteins related to apoptosis and metastasis including Bcl-2 and MMP2/9. We investigated the status of STAT3 phosphorylation in these cells followed by RCFE treatment. Treatment with increasing concentration of RCFE significantly reduced phosphorylation at Tyr705 of STAT3, without alteration of total STAT3 protein level (Fig. 4A,B). The reduction in STAT3 phosphorylation was more evident in MCF-7 cells as treatment with 1 µg/ml RCFE almost abolished the phosphorylation. All the above observations pointed towards coordinated role of RCFE in induction of apoptosis and reduction of metastasis in breast cancer cells (represented as a model in Fig. 4C).

RCFE inhibited tumor growth in syngeneic mouse model. To understand the effect of RCFE on progression of *in vivo* breast tumor, transplantable mouse mammary carcinoma 4T1 cell induced model was studied. RCFE showed significant cytotoxicity against these cells *in vitro* as shown in Fig. 5A. Tumor was induced in female Balb/c mouse by subcutaneous injection of 4T1 cells in mammary fat pad. After 10 days, intraperitoneal administration of 4 doses of RCFE (at 0.5 mg/kg bodyweight concentration) were given to one set of animals, while the other set of animals received only vehicle (0.9% saline). The tumor continued to increase in the control group while RCFE treated animals showed significant reduction in tumor volume with time (Fig. 5B). The resected tumors from the sacrificed animals at 22 days following 4T1 injection are shown in Fig. 5B (lower panel). RCFE-treated animals showed more than 88% reduction tumor volumes compared to control group animals (Fig. 5C).

Identification of bioactive components in RCFE. To identify bioactive components of RCFE, the dried hydro-ethanolic extract was successively fractionated into ethyl acetate, butanol and aqueous fractions. The cytotoxic activity of these fractions was studied which suggested comparatively higher activity in ethyl acetate fraction (Supplementary Fig S4). Hence, this fraction was subjected to HPLC finger printing analysis. Four characteristic peaks were identified in the RP-HPLC analysis (Fig. 6A,B). Retention time, name, molecular formula, molecular weight and chemical structure of the components are shown in Table 1. The major peaks eluted after HPLC was

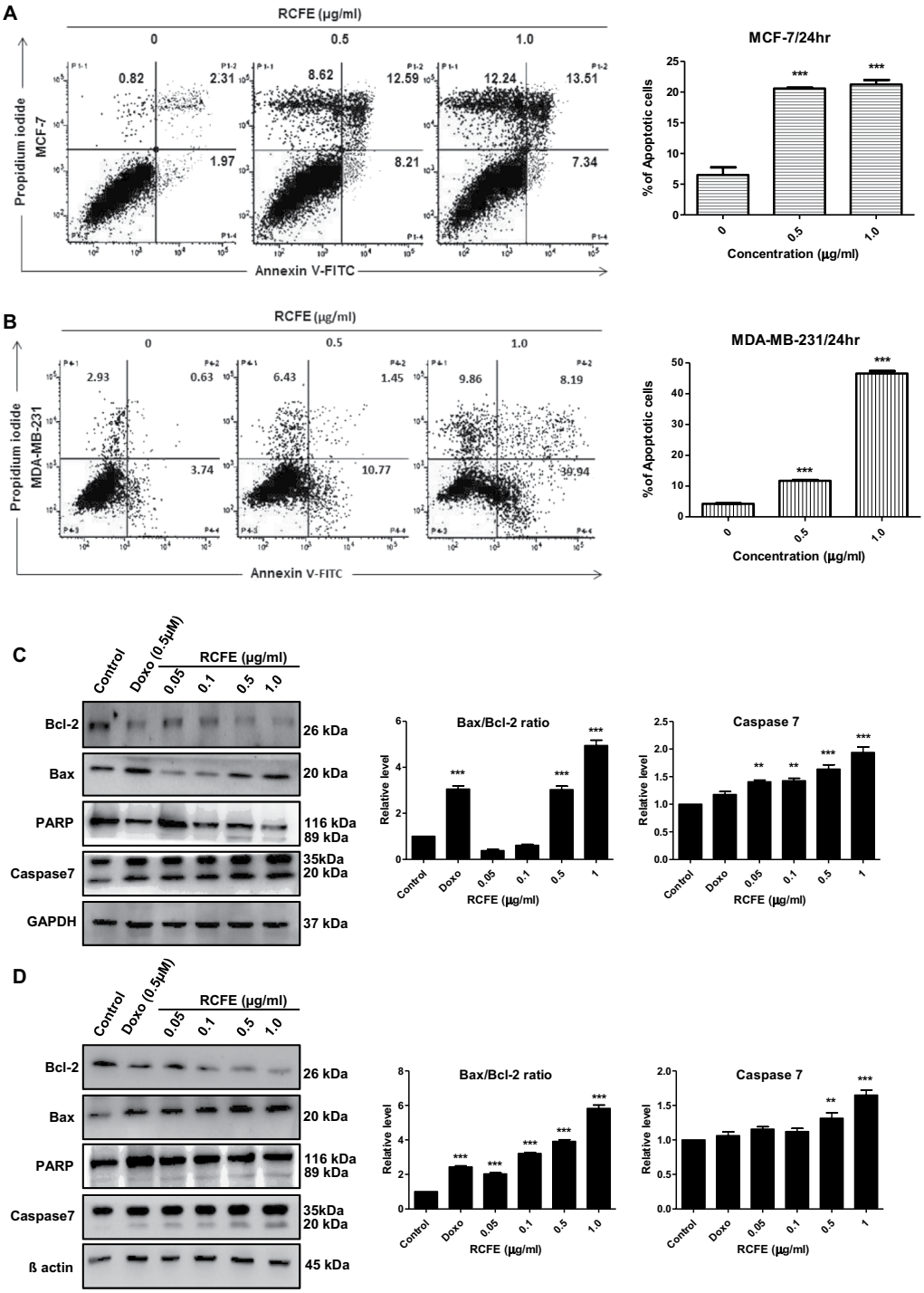

Figure 3. Induction of apoptosis by RCFE. Flow cytometer analysis of MCF-7 (**A**) and MDA-MB-231 (**B**) using Annexin V/PI. The quantitation of three independent analysis was presented in right panels. Western blot analysis of lysates from MCF-7 (**C**) and MDA-MB-231 (**D**) with antibodies against Bcl-2, Bax, PARP and Caspase-7. The ratio of Bax/Bcl-2 and caspase-7 expressions were normalized either to GAPDH or β-actin presented in the right panels. Doxorubicin (Doxo) was used as positive control. Statistical differences were analyzed with one-way ANOVA test. p value < 0.05 was considered significant.

collected, evaporated and their ESI-MS was recorded (Fig. 6C–F). The probable compounds peaks were recognized as Ricinine[24], p-Coumaric acid[25], Epigallocatechin[26] and Ricinoleic acid[25] by comparing ESI-MS spectra with previously reported literature (Table 1).

Cytotoxicity and migration inhibitory activity of pure compounds. To evaluate the cytotoxicity of four compounds identified from RCFE, MCF-7 and MDA-MB-231 cell lines were treated with increasing

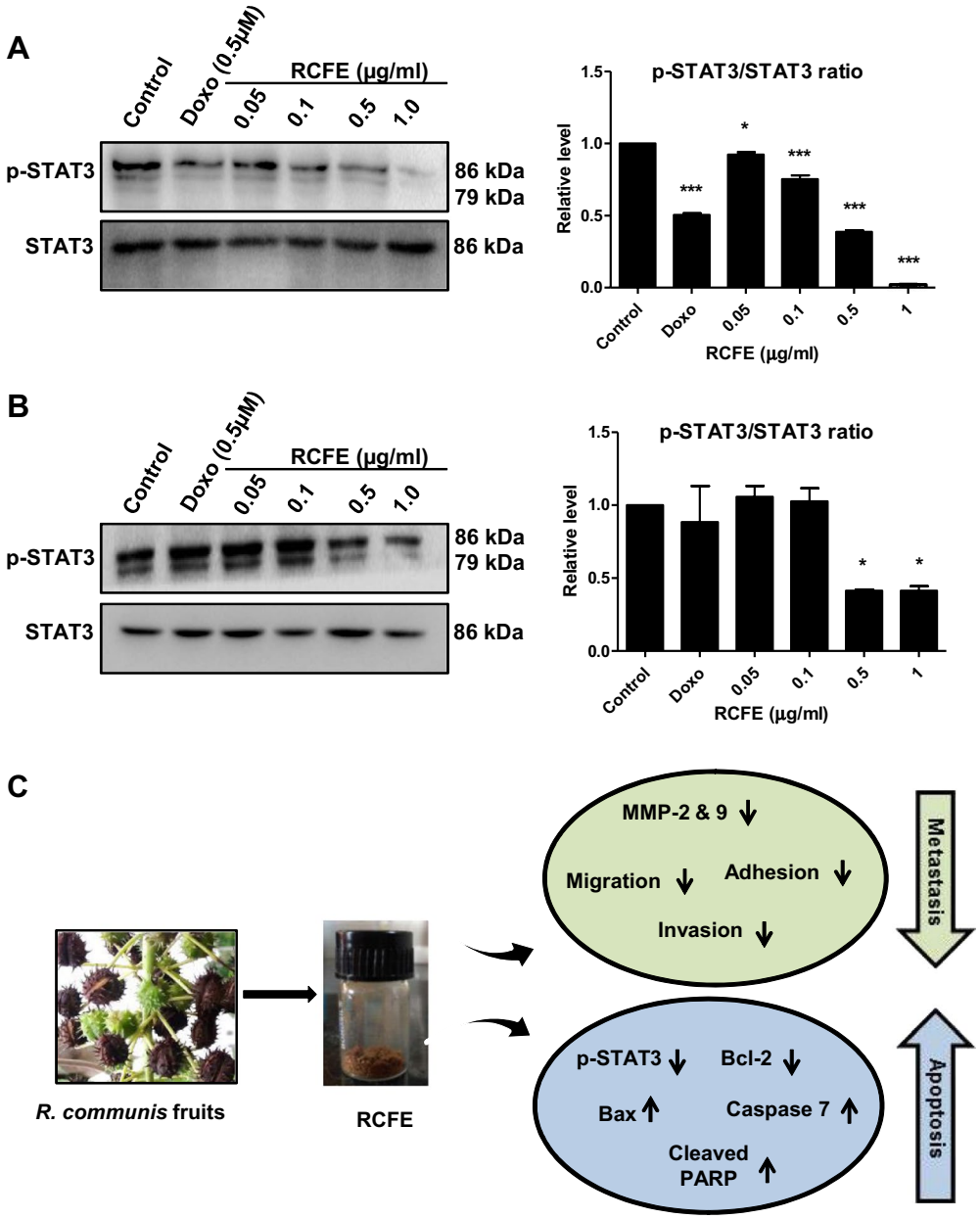

Figure 4. RCFE treatment led to inhibition of STAT3 phosphorylation. Western blot analysis of MCF-7 (**A**) and MDA-MB-231 (**B**) cell lysates with phosphor-STAT3 (Tyr705) and STAT3 antibodies. The quantitation of the expression was presented in right panels. Doxorubicin (Doxo) was used as positive control. Statistical differences of three independent experiments were analyzed with one-way ANOVA test. p value < 0.05 was considered significant. (**C**) Schematic representation of the metastasis inhibition and apoptosis induction by RCFE for its anti-cancer activity.

concentrations of the Ricinine, p-Courmaric acid, Epigallocatechin and Ricinoleic acid for 24 hr. All four compounds showed cytotoxicity against both cells in a dose dependent manner (Fig. 7A). However, our data suggested that, Ricinine, p-Coumaric acid and Ricinoleic acid were more effective against MDA-MB-231 cells, while Epigallocatechin showed better cytotoxic effect against MCF-7.

Next, the effect of these compounds on migration of MCF-7 and MDA-MB-231 cells was studied using wound healing assay (Supplementary Fig S5). The inhibition of MCF-7 cell migration was not significant for the compounds after 24 hr of treatment with two concentrations of 10 and 20 μM (Fig. 7B). However, the effect was more prominent after 48 hr of treatment which showed inhibition of MCF-7 migration by Ricinine, Epigallocatechin and Ricinoleic acid. The scenario was different in MDA-MB-231 cells where Ricinine and p-Coumaric acid showed no effect after 24 hr treatment and moderate effect after 48 hr (Fig. 7C). Interestingly, Epigallocatechin treatment strongly inhibited MDA-MB-231 cell migration in a dose and time-dependent manner (Fig. 7C). The inhibitory effect of Ricinoleic acid on migration of MDA-MB-231 cells was also highly significant after 48 hr of treatment.

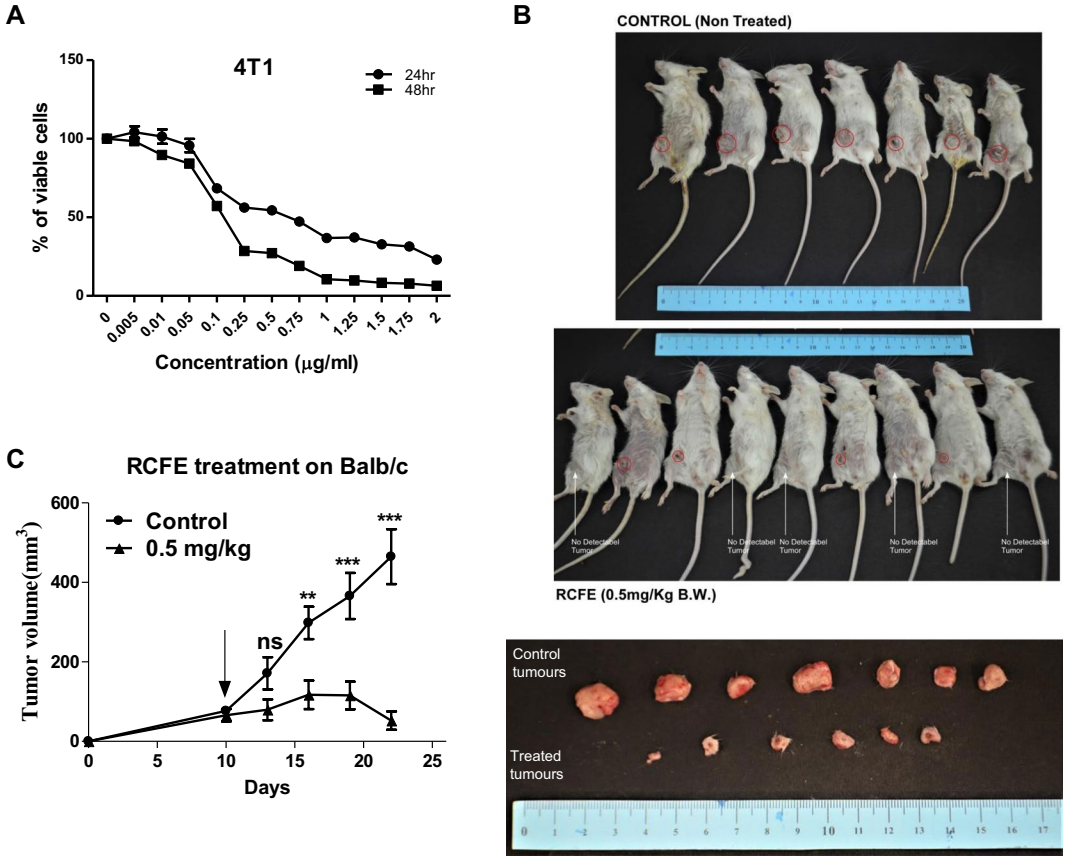

Figure 5. RCFE inhibited tumor progression: (**A**) 4T1 cells were treated with various concentrations of RCFE for 24 and 48 hr. Data represent the mean ± SEM of three independent experiments. (**B**) The animals treated with 0.9% normal saline (upper panel) and RCFE at 0.5 mg/kg bodyweight (middle panel). Animals with visible tumor from outside was pointed with red circles. Animals with no visible tumors from outside was shown by white arrows. The excised tumors from control and RCFE-treated animals (bottom panel). (**C**) Graph represented the measured tumor volumes in two different treatments. Statistical differences were analyzed with two-way ANOVA test. p value ns > 0.05, p value *** < 0.0001.

Discussion

It is now well documented that medicinal plants are a 'treasure trove' of bioactive molecules for the treatment of various human diseases. In the last few decades, numerous traditional knowledge-based drugs have been isolated and commercialized[27–29]. Multiple molecules of medicinal plant origin are currently used as drugs to combat cancer (e.g. vincristine, vinblastine, taxol, paclitaxel, Podophyllotoxin). The current study reports the mechanistic details of anti-cancer activities of the fruit extract of *Ricinus communis* L. (RCFE), commonly known as castor bean plant. Oil and seeds of this plant are widely used in folk medicine as purgative, against worm infestation and arthritis. It has also been reported to have anti-inflammatory effects. However, there are no detailed reports on the mechanism of anti-cancer efficacy of this plant.

Metastasis, the property that empowers certain cancer cells to spread into local or distant tissues is a complex process involving migration, adhesion and invasion. These processes can be targeted by an anti-metastatic agent leading to attenuated aggression of cancer cells. Migration of cancer cells to different tissues is an important initial step in metastasis. Treatment with RCFE inhibited migration of both MCF-7 and MDA-MB-231 in a dose-dependent manner. Initiation of metastasis also depends on adhesion property of the cells that involves interaction with extracellular matrix following detachment from the primary sites. RCFE at very low concentrations significantly inhibited adhesion of cells with collagen IV which is an integral part of the basement membrane[30]. The process of invasion is critical for metastasis because the motile cells needs to cross the extracellular matrix and spread into surrounding tissues[31]. In this study, RCFE substantially inhibited efficacy of the cells to invade ECM gel to reach other side of the insert in response to a media containing 10% FBS. The highest inhibition of invasion (81%) was achieved in MDA-MB-231 cells after treatment with a very low concentration of 0.1 μg/ml of RCFE for 24 hr. Remarkably, RCFE showed greater inhibition of cell migration and invasion in highly aggressive triple negative MDA-MB-231 cells compared to MCF-7 cells suggesting its probable application to manage highly aggressive cancer cells. The process of invasion and metastasis is accompanied with degradation of connective tissues and as a result expression of matrix degrading enzymes e.g. matrix metalloproteinases (MMPs) increases. MMP-2 and 9 have been shown to overexpress and contribute to metastatic efficacy of MDA-MB-231[30]. Here, we showed that expression of MMP-2 and 9 were inhibited by RCFE emphasizing its effect on ECM degradation and invasion of cancer cells.

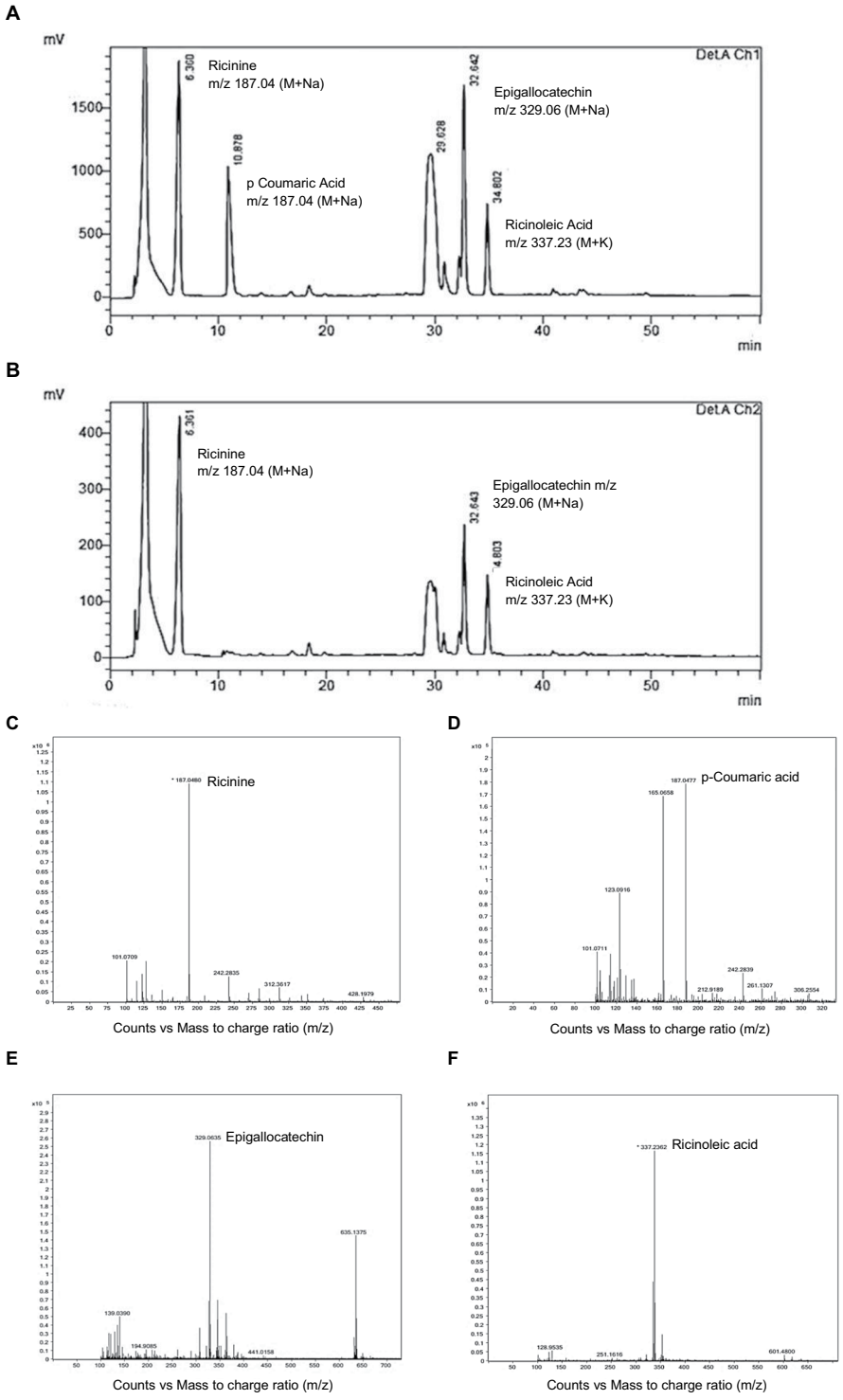

Figure 6. Fingerprint analysis of ethyl-acetate fraction of RCFE. RP-HPLC chromatogram of the ethyl-acetate fraction at a wavelength of (**A**) 210 nm (Det A Ch1) and (**B**) 254 nm (Det B Ch2). ESI-MS spectra of fractions collected after RP-HPLC were identified as Ricinine (**C**), p-Coumaric acid (**D**), Epigallocatechin (**E**) and Ricinoleic acid (**F**).

We studied the mechanism of RCFE-induced cell death in MCF-7 and MDA-MB-231 cells. Cell death in these cells via apoptosis was confirmed by flow cytometry analysis using Annexin V/PI. It is clear from the analysis that, RCFE induced apoptosis in a significant percentage of cells. DNA fragmentation assay, a widely used biochemical marker of apoptosis, was performed to confirm this observation. DNA fragmentation occurs at the inter-nucleosomal linker regions in the cells undergoing apoptosis[32–34]. To elucidate the mechanism of apoptosis expression of several pro and anti-apoptotic proteins were studied. RCFE inhibited the expression of

Peak No.	t_R (min)	Comparative Area%	m/z (M^+)	m/z (M + Na)	m/z (M + K)	Molecular Formula	Compound name & Structure	Reference
1	6.36	26.015	164	187.04	—	$C_8H_8N_2O_2$	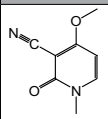 **Ricinine**	Wachira *et al.*[24]
2	10.87	14.387	164	187.04	—	$C_9H_8O_3$	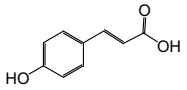 **p Coumaric Acid**	Wafa *et al.*[25]
3	32.64	14.499	306	329.06	—	$C_{15}H_{14}O_7$	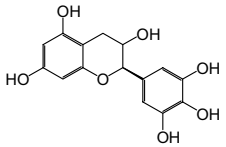 **Epigallocatechin**	Singh *et al.*[26]
4	34.80	7.661	298	—	337.23	$C_{18}H_{34}O_3$	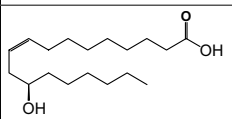 **Ricinoleic Acid**	Wafa *et al.*[25]

Table 1. Probable compounds identified by HPLC and ESI-MS technique.

anti-apoptotic protein Bcl-2 and induced the expression of pro-apoptotic protein Bax. Expression of Bcl-2 and Bax family proteins plays significant role in the decision of inducing apoptosis in a cell by altering the release of cytochrome c from mitochondria by regulating mitochondrial membrane permeability[35]. Inhibition of Bcl-2 by RCFE possibly induces the cytochrome c production that leads to expression of caspases. Caspases are the key players of apoptosis and a variety of caspases are involved in intrinsic, extrinsic and execution of apoptotic pathway[35]. Caspases use PARP as substrate and cleave PARP during apoptosis[35–37]. We found one of the family members, Caspase 7, a major caspase involved in execution pathway was up regulated in both MCF-7 and MDA-MB-231 validating its role in inducing apoptosis in response to RCFE treatment. Further, increased PARP cleavage with treatment of increasing concentration of RCFE confirmed apoptosis inducing activity of the extract. Expression of p53, a key factor known to induce apoptosis, did not increase suggesting the minimal effect of p53 in inducing apoptosis by treatment of RCFE.

Attenuation of metastasis and induction of apoptosis by RCFE might be attributed to its activity to down regulate phosphorylation of STAT3, a master regulator for these two pathways in cancer cells. Aberrant JAK-STAT signaling (specifically STAT3) is common in various cancer due to their constitutive activation in response to stimulators e.g. cytokines, growth factors, receptors (TLRs/GPCRs), polypeptide ligands and miRNAs[38]. STAT3 induces expression of MMPs and promotes invasion and metastasis in cancer cells. In addition, it induces anti-apoptotic Bcl-2 expression leading to survival of the cells. So, targeting STAT3 has been suggested as a viable therapeutic strategy against cancer[38]. RCFE mediated deactivation of Tyr705 phosphorylation of STAT3 inhibited these two critical steps leading to attenuation of metastatic and induction of apoptosis suggesting possible application of this extract against breast cancer therapy.

The anti-cancer efficacy of RCFE was highlighted by the 4T1 syngeneic mouse model. 4T1 cells are highly tumorigenic and thus suitable for generation of mammary tumors in animals with characters close to human mammary tumors[39]. Our data suggested that 4 doses of intraperitoneal administrations of RCFE at a concentration as low as 0.5 mg/kg bodyweight reduced the tumor volume by about 88% emphasizing its role in limiting breast tumors *in vivo*. Several animal models are reported to study efficacy of drugs against breast cancer: xenograft, genetically engineered (transgenic) and syngeneic models being the most common of them. While xenograft models are popular as it mimics human tumors, it eliminates the possibility of immune response against the tumor leading to host-tumor interaction unnatural to human tumor development[40]. Transgenic animal models overcome this problem and can be used to screen drugs against tumorigenesis. However, genetic changes should be tissue specific in these models, as oncogene-bearing or tumor suppressor gene-knock out systemically may not imitate tumors arising out of mutations in normal microenvironment[40]. These models also take several months to generate tumor and are expensive. Syngeneic models, on contrary, are simple and inexpensive model. Murine adenocarcinoma 4T1 cells implanted in immunocompetent Balb/c, as used in this study, is the most widely used syngeneic model to study tumor progression and metastasis[41]. In future we would like to use this model to understand the efficacy of RCFE to reduce tumor volume through host immune modulation, which would be the subject and focus of an entirely independent study. It would also be interesting to know if the extract would regulate 4T1 cells-induced metastasis in these animals and map the metastatic signaling pathways that might be modulated upon RCFE treatment. We plan to study these aspects in detail to confirm *in vivo* anti-metastatic activity of RCFE.

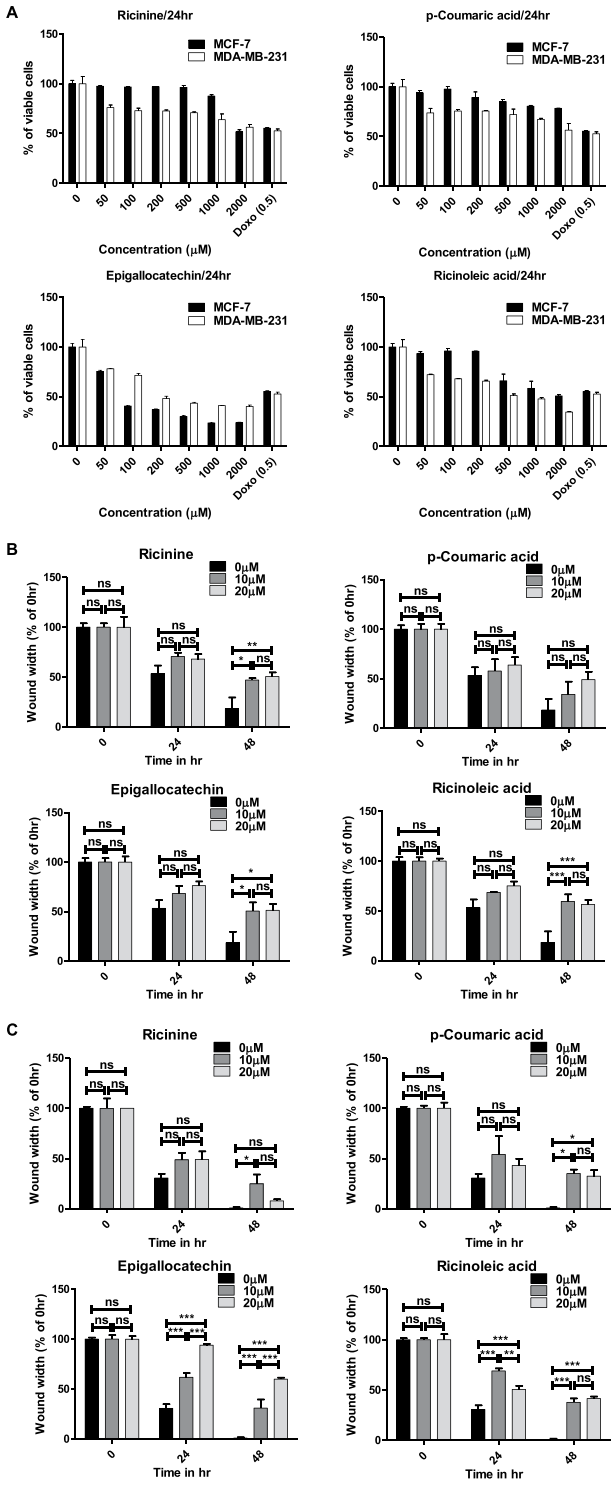

Figure 7. Pure compounds showed significant biological activity. (**A**) The cytotoxic effect of Ricinine, p-Coumaric acid, Epigallocatechin and Ricinoleic acid in MCF-7 and MDA-MB-231 cells after 24 hr treatment. Doxorubicin (Doxo) was used as positive control. Quantitative representation of migration of MCF-7 (**B**) and MDA-MB-231 (**C**) cells by wound healing assay. Data represent the mean ± SEM of three independent experiments. Statistical differences were analyzed with two-way ANOVA test for wound healing assay. p value ns > 0.05, p value *** < 0.0001.

It is important to have knowledge about constituent molecule(s) of a bioactive plant extract for its probable use as therapy. We performed HPLC and ESI-MS analysis of the ethyl acetate fraction of the extract which revealed the presence of four individual compounds namely, Ricinine, p-Coumaric acid, Epigallocatechin and

Ricinoleic Acid. Of them, Ricinine and Ricinoleic Acid have not been reported for any anti-cancer activity albeit their prominent pharmacological importance[42–44]. However, p-Coumaric acid, a hydroxy derivative of cinnamic acid was shown to inhibit proliferation of colon cancer cells in dose-dependent manner[45]. It induced apoptosis accompanied with increasing reactive oxygen species (ROS) levels, a fall in the mitochondrial membrane potential and increased lipid layer breaks. Ethanolic extract of Chinese propolis, where p-Coumaric acid is one of the components, exert antitumor effects mainly through inducing apoptosis of breast cancer cells[46]. Furthermore, Epigallocatechin was also reported for inducing apoptosis and cell cycle arrest[47]. We studied the cytotoxic and migration-inhibitory efficacy of all four compounds to have insight on their individual roles as anti-cancer molecules. Though all four compounds showed cytotoxicity, their efficacy varied with cell types. The inhibition of migration in MCF-7 cells was possibly due to combination of Ricinine, Epigallocatechin and Ricinoleic acid as effect of p-coumaric acid was found to be nominal. Interestingly, in highly metastatic MDA-MB-231 cells, Epigallocatechin contributed most significantly in abrogating migration. However, Ricinoleic acid and Ricinine also contributed moderately to inhibit migration in MDA-MB-231 cells. It may be assumed that the anti-cancer efficacy of RCFE is contributed by synergistic effect of either the identified compounds or their combination with some unidentified compounds.

In summary, our study demonstrated the efficacy of the fruit extract of common castor plant *R. communis* L. against two breast cancer cells of distinctive characteristics. The extract inhibited aggressiveness of the cancer cells by inhibiting characters of metastasis such as cell motility, adhesion, invasion and reduced MMP-2 and 9 expressions. Treatment with the extract induced apoptosis in the cells by augmenting Bax/Bcl-2 ratio that is known to induce caspases and subsequent cleavage of PARP. The phosphorylation of STAT3, a central regulator for activation of metastasis and anti-apoptotic molecules, was inhibited by the extract. The extract significantly reduced tumor volumes in 4T1 syngeneic mouse model. HPLC fingerprinting along with ESI-MS analysis suggested presence of four compounds, all of which showed anti-cancer efficacy individually. The current report contributes significantly to the repertoire of plant-derived therapeutic strategies for the treatment of breast cancer. In future, it would be interesting to study the extract's role in inhibiting metastasis and modulating immune response for tumor reduction in suitable animal model.

Methods

Cell lines and reagents. The cell lines MCF-7, MDA-MB-231, MDA-MB-453, ZR-75-1, HT-29, A549 and HEK293 were purchased from NCCS Pune, India. MEF was a gift from Dr. Sougata Saha, Tezpur University, India. DMEM (Dulbecco's Modified Eagle Medium) and FBS (Fetal Bovine Serum) were purchased from Life Technologies, USA. MTT (3-(4, 5-dimethylthiazolyl-2)-2, 5-diphenyltetrazolium bromide), Collagen IV, ECM gel and Doxorubicin were also purchased from Sigma Aldrich and Mitomycin C was purchased from HiMedia, India. Annexin-V-FLUOS Staining Kit purchased from Roche, USA and Annexin V FITC Assay Kit was purchased from Cayman, USA. Antibodies used in this study were procured from Cell Signalling Technology, USA.

Preparation of extracts. Fresh fruits of the plant *Ricinus communis* L. were collected from the Golaghat district of the state of Assam in North East India and morphological identification of the specimen were done at the Botanical Survey of India, Shillong, Meghalaya. The dried fruits were extracted with 50% denatured ethanol at room temperature for 48 hr each time. The extract was filtered and then concentrated under reduced pressure to remove excess ethanol and finally was lyophilised to obtain ethanolic extract (named RCFE). A part of RCFE (5 gm) was then suspended in sterile de-ionised water and partitioned successively with ethyl acetate and n-Butanol. Each fraction was evaporated under vacuum and lyophilized to yield the EtOAc [RC(E)], n-BuOH [RC(B)] and aqueous [RC(A)] fractions. All the fractions were stored at 4 °C and checked for the biological activity.

Cell culture. MCF-7, MDA-MB-231, MDA-MB-453, HT-29, A549, MEF and HEK293 cell lines were routinely maintained in Dulbecco's modified Eagle's medium (DMEM; Gibco), and ZR-75-1 in RPMI1640 supplemented with 10% fetal bovine serum and 1% antibiotic. Cell lines were kept in a CO_2 incubator at 5% CO_2 and 37° C temperatures.

Cytotoxicity assay. In this assay, cells (5000 each) were plated in a 96 well plate and incubated for 48 hr. Cells were treated with different concentrations of RCFE up to 48 hr. Following incubation, cells were treated with MTT and incubated for 3.5 hr. The media was removed carefully and MTT dissolving solution was added and absorbance was taken at 590 nm wavelength using UV-Vis spectrophotometer (Multiscan Go, ThermoScientific).

Migration assay. Cells were seeded in a 24 well plate till 90% confluency. The media was replaced by FBS-devoid media for at least 6 hr and mitomycin C (1 µg/ml) was added before 1 hr of treatment to stop proliferation. Using a sterile pipette tip, a straight scratch was made simulating a wound in each of the wells. The extract at various concentrations were added and images were taken at 0, 24 and 48 hr following the treatment from at least 3 different fields of each well. The width of the wound was measured and quantified.

Adhesion assay. To evaluate the efficacy of the extracts to inhibit adhesion, 2×10^5 cells/ml were pre-treated with different doses of extracts in serum free media for 24 hr. Cells were then plated in 96-well plates pre-coated with collagen IV and allowed to adhere for 60 min. The media was gently removed, and the wells were washed. The attached cells were quantified using MTT.

Invasion assay. 2.5×10^5 cells/well were plated in a 6 well plate with or without treatment in a serum free media for 24 hr. Then cells were trypsinised and resuspended in 200 µl serum-free media and placed in the upper chamber of ECM gel pre-coated transwell inserts. The lower chamber was filled with 10% FBS containing media

to create a concentration gradient and incubated for 24 hr in case of MCF-7 and 6 hr in case of MDA-MB-231. Then inserts were washed and cells were fixed with formaldehyde and permeabilized with methanol. The cells were then stained with Giemsa stain. Non -invasive cells were removed by scrapping with a cotton swab and bright field images of invasive cells were taken using Olympus IX83 microscope. The cells were counted from photomicrographs of 10 random fields of a single membrane.

DNA fragmentation assay. Both MCF-7 and MDA-MB-231 cells were treated with RCFE (1 μg/ml) for 0, 24 and 48 hr. Cells were trypsinised and genomic DNA was isolated using PureLink™ Genomic DNA Mini Kit (Invitrogen, USA). Concentration was measured, and DNA was run on 2% agarose gel.

Flow cytometer analysis. MCF-7 and MDA-MB-231 cells (1×10^5 cells/well) were seeded in 12 well culture plates and incubated for overnight. Then adhered cells were treated with RCFE 0.5 μg/ml and 1 μg/ml for 24 hr. No treatment was given to the control cells. After incubation, both floating as well as adherent cells from each well were collected in tubes and washed with PBS. The cell pellets were resuspended in 200 μL of binding buffer and required proportions of FITC-Annexin V/PI were added to each sample according to manufacturer's protocol of Annexin V FITC Assay Kit (Cayman, USA). The samples were then allowed to incubate in dark for 15 min and then analyzed with FACSChorus software on a FACS Melody flow cytometer (BD Biosciences).

Western blot analysis. Cells were seeded in 100 mm dish at 1×10^6 cells per dish and incubated overnight before treating with the indicated concentrations for 24 hr. Proteins were extracted from RCFE treated MCF-7 and MDA-MB-231 cells with ice cold RIPA buffer (Thermo Scientific, USA) containing protease and phosphatase inhibitor cocktail (Thermo Scientific, USA). Equal amount of proteins from different experimental samples was run in SDS-PAGE and proteins were transferred to a PVDF membrane using semidry electrophoresis transfer unit (GE Healthcare, UK). After blocking with 3% BSA in TBS-Tween 20 for at least 1 hr at room temperature, the membranes were probed with the corresponding primary antibody (1:1000 dilutions) overnight at 4° C and secondary antibodies for 1 hr at room temperature. The blots were then incubated with chemiluminescence substrate (Bio-Rad, USA) and bands were visualized using Chemidoc XRS+ system (Bio-Rad, USA). Quantification of the bands was done using Gel Quant software.

***In vivo* study of mouse tumor model.** Female Balb/c mice 6–8-week-old were obtained from Center for Translational Animal Research (CTAR), Bose Institute, Kolkata, India and were maintained as per the guidelines of the animal ethical committee in accordance with the Committee for the Purpose of Control and Supervision of Experiments on Animals (CPCSEA) guidelines. For *in vivo* tumorigenic assay, 4T1 cells (1×10^6 cells/animal) were subcutaneously injected into the mammary fat pad of Balb/c mice to develop solid tumor. Animals with solid tumor were randomly distributed into two groups each containing ten animals. One group was treated with vehicle only (0.9% normal saline) whereas, other group was subjected to intraperitoneal injection of RCFE (0.5 mg/kg) starting after 10 days of tumor development and continued until 22 days (4 doses, 72 hr interval). Tumor progression was monitored by measuring the volume of the tumor with vernier calipers on every third day. The tumor volume was calculated by using the formula $V = 0.5 \times a \times b2$, where "a" and "b" indicate length and width diameter, respectively. All animal experiments were conducted in accordance with CPCSEA guidelines and all experimental protocols have been approved by the animal ethics committee of Bose Institute (Ref. No. IAEC/BI/87/2017, dated Dec. 13, 2017) registered with the CPCSEA.

Fingerprint analysis of *R. Communis L.* fruit extracts. HPLC and ESI-MS techniques was used to identify the phytochemicals present in the *R. Communis* L. extracts. HPLC fingerprint analysis was performed at 25 ± 1 °C using ethyl acetate fraction of *R. Communis* L. which was dissolved in acetonitrile solvent and filtered through membrane filters (0.45 μm pore size). The sample (20 μL injected volume) was analysed using a Shimadzu system (Kyoto, Japan) equipped with LC-20AT Prominence liquid chromatograph pump, DGU-$20A_3$ Prominence Degasser, CBM-20A Prominence communications bus module, SPD-20A Prominence UV/VIS detector, LC solution software, and a Rheodyne injector with 100 μL loop.

Separation was achieved using Phenomenex RP C18 column, 250 × 4.6 mm, 5 μm; a gradient mobile phase consisted of water (A) and acetonitrile (B) with a gradient elution program, i.e., 0–40 min, 80–50% B; 40–70 min, 50–0% B; 70–80 min, 0% B; 80–90 min, 0–90% B and 90–100 min 80% B, flow 1 mL/min. The elute was monitored at 210 nm and 254 nm. Mass analysis of the major HPLC peak was recorded on Agilent 6540 Q-TOF LC/MS system.

Statistical analysis. Statistical analysis was performed using Graph Pad Prism and data were expressed as mean ± standard deviation (mean ± SD). Results were analyzed either by two-way analysis of variance (two-way ANOVA) or one-way analysis of variance (one-way ANOVA) or Student's t-test as required by the experimental system and difference were considered to be significant at $p < 0.05$.

References

1. Siegel, R. L. *et al*. Colorectal cancer statistics, 2017. *CA: a cancer journal for clinicians* **67**, 177–193 (2017).
2. Tinoco, G., Warsch, S., Glück, S., Avancha, K. & Montero, A. J. Treating breast cancer in the 21st century: emerging biological therapies. *Journal of Cancer* **4**, 117 (2013).
3. Hassan, M., Ansari, J., Spooner, D. & Hussain, S. Chemotherapy for breast cancer. *Oncology reports* **24**, 1121–1131 (2010).
4. Joyce, C. Taxol: search for a cancer drug. *Bioscience* **43**, 133–136 (1993).
5. Noble, R. L. The discovery of the vinca alkaloids—chemotherapeutic agents against cancer. *Biochemistry and cell biology* **68**, 1344–1351 (1990).
6. Xie, S. & Zhou, J. Harnessing Plant Biodiversity for the Discovery of Novel Anticancer Drugs Targeting Microtubules. *Frontiers in plant science* **8** (2017).

7. Canel, C., Moraes, R. M., Dayan, F. E. & Ferreira, D. Podophyllotoxin. *Phytochemistry* **54**, 115–120 (2000).
8. Gordaliza, M., Castro, M. D., Miguel del Corral, J. & Feliciano, A. S. Antitumor properties of podophyllotoxin and related compounds. *Current pharmaceutical design* **6**, 1811–1839 (2000).
9. Moraes, D. F. C., de Mesquita, L. S. S., do Amaral, F. M. M., de Sousa Ribeiro, M. N. & Malik, S. In *Biotechnology and Production of Anti-Cancer Compounds* 121–142 (Springer, 2017).
10. Wang, L. *et al*. Flavonoid baicalein suppresses adhesion, migration and invasion of MDA-MB-231 human breast cancer cells. *Cancer Letters* **297**, 42–48, https://doi.org/10.1016/j.canlet.2010.04.022 (2010).
11. Yang, P.-M., Tseng, H.-H., Peng, C.-W., Chen, W.-S. & Chiu, S.-J. Dietary flavonoid fisetin targets caspase-3-deficient human breast cancer MCF-7 cells by induction of caspase-7- associated apoptosis and inhibition of autophagy. *Nternational Journal of Oncology* **40**, 469–478, https://doi.org/10.3892/ijo.2011.1203 (2012).
12. Bachmeier, B. E. *et al*. Curcumin downregulates the inflammatory cytokines CXCL1 and-2 in breast cancer cells via NFκB. *Carcinogenesis* **29**, 779–789 (2007).
13. Hortobagyi, G. The curability of breast cancer: present and future. *European Journal of Cancer Supplements* **1**, 24–34 (2003).
14. Bishop, A. J. *et al*. Prognosis for patients with metastatic breast cancer who achieve a no-evidence-of-disease status after systemic or local therapy. *Cancer* **121**, 4324–4332 (2015).
15. Sajem, A. L. & Gosai, K. Traditional use of medicinal plants by the Jaintia tribes in North. *Journal of Ethnobiology and Ethnomedicine* **2**, 1, https://doi.org/10.1186/1746-4269-2-33 (2006).
16. Darmanin, S., Wismayer, P. S., Camilleri Podesta, M. T., Micallef, M. J. & Buhagiar, J. A. An extract from Ricinus communis L. leaves possesses cytotoxic properties and induces apoptosis in SK-MEL-28 human melanoma cells. *Nat Prod Res* **23**, 561–571, https://doi.org/10.1080/14786410802228579 (2009).
17. Prakash, E. & Gupta, D. K. *In Vitro* Study of Extracts of Ricinus communis Linn on Human Cancer Cell lines. *Journal of Medical Sciences and Public Health* **2**, 15–20 (2014).
18. Jena, J. & Gupta, A. K. Ricinus Communis Linn: A Phytopharmacological Review. *International Journal of Pharmacy and Pharmaceutical Sciences* **4**, 25–29 (2012).
19. Shokeen, P., Anand, P., Murali, Y. K. & Tandon, V. Antidiabetic activity of 50% ethanolic extract of Ricinus communis and its purified fractions. *Food and Chemical Toxicology* **46**, 3458–3466, https://doi.org/10.1016/j.fct.2008.08.020 (2008).
20. Gargade, D. G. & Screening, K. of antibacterial activity of Ricinus communisL. leaves extracts against Xanthomonas axonopodis pv. punicae. *International Journal of Advanced Research in Biological Sciences* **2**, 47–51 (2015).
21. Sitton, D. & West, C. A. Casbene: An Anti-Fungal Diterpene Produced In Cell-Free Extract's Of Ricznus Communis Seedlings. *Phytochemistry* **14**, 1921–1925 (1957).
22. Upasani, S. M., Kotkar, H. M., Mendki, P. S. & Maheshwari, V. L. Partial characterization and insecticidalproperties of Ricinus communis Lfoliage flavonoids. *Pest Management Science* **599**, 1349–1354, https://doi.org/10.1002/ps.767 (2003).
23. Attardi, L. D., de Vries, A. & Jacks, T. Activation of the p53-dependent G1 checkpoint response in mouse embryo fibroblasts depends on the specific DNA damage inducer. *Oncogene* **23**, 973–980 (2004).
24. Wachira, S. W. *et al*. Toxicity of six plant extracts and two pyridone alkaloids from Ricinus communis against the malaria vector Anopheles gambiae. *Parasites & vectors* **7**, 312 (2014).
25. Wafa, G., Amadou, D. & Larbi, K. M. Larvicidal activity, phytochemical composition, and antioxidant properties of different parts of five populations of Ricinus communis L. *Industrial Crops and Products* **56**, 43–51 (2014).
26. Singh, P. P. & Chauhan, S. Activity guided isolation of antioxidants from the leaves of Ricinus communis L. *Food chemistry* **114**, 1069–1072 (2009).
27. Chin, Y.-W., Balunas, M. J., Chai, H. B. & Kinghorn, A. D. Drug Discovery From Natural Sources. *The AAPS Journal* **8**, E239–E253 (2006).
28. Gordon, M. *et al*. Natural Products in Drug Discovery and Development. *J. Nat. Prod.* **60**, 52–60 (1997).
29. Rates, S. M. K. Plants as source of drugs. *Toxicon* **39**, 603–613 (2001).
30. Leea, H. S., Seob, E. Y., Kangc, N. E. & Kim, W. K. [6]-Gingerol inhibits metastasis of MDA-MB-231 human breast cancer cells. *Journal of Nutritional Biochemistry* **19**, 313–319, https://doi.org/10.1016/j.jnutbio.2007.05.008 (2008).
31. Krakhmal, N., Zavyalova, M., Denisov, E., Vtorushin, S. & Perelmuter, V. Cancer invasion: patterns and mechanisms. *Acta Naturae (англоязычная версия)* **7** (2015).
32. Choi, Y. H. & Yoo, Y. H. Taxol-induced growth arrest and apoptosis is associated with the upregulation of the Cdk inhibitor, p21WAF1/CIP1, in human breast cancer cells. *Oncology Reports* **28**, 2163–2169, https://doi.org/10.3892/or.2012.2060 (2012).
33. Nagata, S. Apoptotic DNA Fragmentation. *Experimental Cell Research* **256**, 12–18, https://doi.org/10.1006/excr.2000.4834 (2000).
34. Leist, M., Single, B., Castoldi, A. F., Kühnle, S. & Nicotera, P. Intracellular Adenosine Triphosphate (ATP) Concentration: A Switch in the Decision Between Apoptosis and Necrosis. *Journal of Experimental Medicine* **185**, 1481–1486 (1997).
35. Elmore, S. Apoptosis: A Review of Programmed Cell Death. *Toxicologic Pathology* **35**, 495–516, https://doi.org/10.1080/01926230701320337 (2007).
36. Lazebnik, Y. A., KaufmannH, S. H., Desnoyers, S., Poirier, G. G. & Earnshaw, W. C. Cleavage of poly(ADP-ribose) polymerase by a proteinase with properties like ICE. *Nature* **371**, 346–347 (1994).
37. Boulares, A. H. *et al*. Role of Poly(ADP-ribose) Polymerase (PARP) Cleavage in Apoptosis. *The Journal Of Biological Chemistry* **274**, 22932–22940 (1999).
38. Yue, P. & Turkson, J. Targeting STAT3 in cancer: how successful are we? *Expert opinion on investigational drugs* **18**, 45–56 (2009).
39. Pulaski, B. A. & Ostrand-Rosenberg, S. Mouse 4T1 breast tumor model. *Current protocols in immunology* Chapter 20, Unit 20 22, https://doi.org/10.1002/0471142735.im2002s39 (2001).
40. Rashid, O. M. *et al*. An improved syngeneic orthotopic murine model of human breast cancer progression. *Breast cancer research and treatment* **147**, 501–512 (2014).
41. Rashid, O. M. & Takabe, K. Animal models for exploring the pharmacokinetics of breast cancer therapies. *Expert opinion on drug metabolism & toxicology* **11**, 221–230 (2015).
42. Ferraz, A. C. *et al*. Pharmacological evaluation of ricinine, a central nervous system stimulant isolated from Ricinus communis. *Pharmacology Biochemistry and Behavior* **63**, 367–375 (1999).
43. Ohishi, K. *et al*. Ricinine: a pyridone alkaloid from Ricinus communis that activates the Wnt signaling pathway through casein kinase 1α. *Bioorganic & medicinal chemistry* **22**, 4597–4601 (2014).
44. Vieira, C. *et al*. Effect of ricinoleic acid in acute and subchronic experimental models of inflammation. *Mediators of inflammation* **9**, 223–228 (2000).
45. Jaganathan, S. K., Supriyanto, E. & Mandal, M. Events associated with apoptotic effect of p-coumaric acid in HCT-15 colon cancer cells. *World Journal of Gastroenterology: WJG* **19**, 7726 (2013).
46. Xuan, H. *et al*. Antitumor activity of Chinese propolis in human breast cancer MCF-7 and MDA-MB-231 cells. *Evidence-Based Complementary and Alternative Medicine* **2014** (2014).
47. Ahmad, N., Feyes, D. K., Agarwal, R., Mukhtar, H. & Nieminen, A.-L. Green tea constituent epigallocatechin-3-gallate and induction of apoptosis and cell cycle arrest in human carcinoma cells. *Journal of the National Cancer Institute* **89**, 1881–1886 (1997).

Acknowledgements
The study has been performed without funding from any specific agencies. However, RM gratefully acknowledges instrumental facilities provided by Department of Biotechnology, Govt. of India through the projects BT/469/NE/TBP/2013 and BT/410/NE/U-Excel/2013 to his laboratory. MM acknowledges DST-INSPIRE fellowship from Department of Science and Technology for her Ph.D. work.

Author Contributions
M.M., P.J., K.B. and R.M. designed the experiments. M.M., S.D., R.L.G., R.S., B.G., S.K.S. and D.K.D. performed the experiments. M.M., R.L.G., S.K.S., P.J., K.B. and R.M. analyzed the data. M.M., P.J., K.B. and R.M. wrote and edited the manuscript. All authors approve the manuscript.

Additional Information
Supplementary information accompanies this paper at https://doi.org/10.1038/s41598-019-50769-x.

Competing Interests: The authors declare no competing interests.

Publisher's note Springer Nature remains neutral with regard to jurisdictional claims in published maps and institutional affiliations.

Biochemistry

Article

pubs.acs.org/biochemistry

Structural and Dynamic Insights into a Glycine-Mediated Short Analogue of a Designed Peptide in Lipopolysaccharide Micelles: Correlation Between Compact Structure and Anti-Endotoxin Activity

Aritreyee Datta,[†] Nancy Jaiswal,[‡] Humaira Ilyas,[†] Shibjyoti Debnath,[§] Kaushik Biswas,[§] Dinesh Kumar,*[,‡] and Anirban Bhunia*[,†]

[†]Department of Biophysics and [§]Division of Molecular Medicine, Bose Institute, P-1/12 CIT Scheme VII (M), Kolkata 700054, India
[‡]Center of Biomedical Research, SGPGIMS Campus, Lucknow 226014, India

Supporting Information

ABSTRACT: In this study, we report an interaction study of a 13-residue analogue peptide VG13P (VARGWGRKCPLFG), derived from a designed VG16KRKP peptide (VARGWKRKCPLFGKGG), with a Lys6Gly mutation and removal of the last three residues Lys[14]-Gly[15]-Gly[16], in lipopolysaccharide (LPS), a major component of the outer membrane of Gram-negative bacteria and responsible for sepsis or septic shock. VG13P displays an enhanced anti-endotoxin property as evident from significant reduction in LPS-induced TNF-α gene expression levels in a monocytic cell line, while it retains almost unchanged antimicrobial activity as its parent VG16KRKP against Gram-negative bacterial as well as fungal pathogens. In addition, *in vitro* LPS binding properties of VG13P in comparison to its parent VG16KRKP also remained unhindered, suggesting that the flexible C-terminal end of VG16KRKP may not play a major role in its observed antibacterial and LPS binding properties. An NMR-resolved solution structure of VG13P in LPS reveals two consecutive β-turns: one at the N-terminus, followed by another at the central region, closely resembling a rocking chair. The crucial Lys6Gly mutation along with C-terminal truncation from VG16KRKP reorients the hydrophobic hub in VG13P in a unique way so as to fold the N-terminal end back on itself, forming a turn and allowing Val1 and Ala2 to interact with Leu11 and Phe12 to bring the hydrophobic residues closer together to form a more compact hub compared to its parent. The hub is further strengthened via CH-π interaction between Gly4 and Phe12. This accounts for its improved anti-endotoxin activity as well as to its uninterrupted antimicrobial activity.

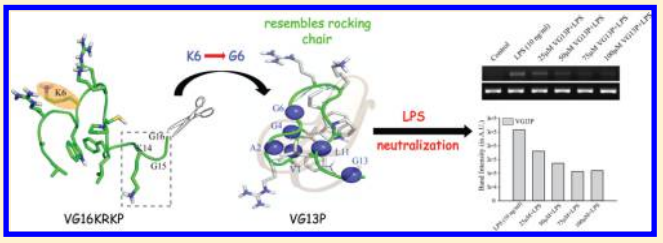

Infectious diseases caused by Gram-negative bacteria continue to remain one of the most severe health threats faced by the global community.[1−4] Lipopolysaccharide (LPS), a key component of the Gram-negative bacterial outer membrane, is chiefly responsible for the lethality associated with septicemia/septic shock, a fatal syndrome.[5−7] Sepsis is one of the major causes of mortality in hospital acquired infections in the intensive care units, causing death of around 2 million infected individuals in the United States alone.[8] It is well-known that LPS upon entering into the bloodstream of infected individuals is intercepted by circulating phagocytes that get activated and ultimately lead to a deregulated expression of pro-inflammatory cytokines, such as TNF-α, Ile-6, and Ile-1β, which in turn cause septic shock, characterized by tissue damage, coagulopathy, and multiple organ failure, often leading to death.[9,10] The activation of macrophages through interaction with LPS and subsequent production of pro-inflammatory cytokines is a complex cascade of signaling events that includes initial recognition of LPS by a serum protein called lipopolysaccharide-binding protein (LBP). The LPS/LBP complex next interacts with the CD14 receptors present on the surface of circulating macrophages. This in turn activates a Toll-like pattern recognition receptor (TLR) that subsequently activates a cascade of signaling events overproducing the aforementioned inflammatory cytokines and reactive oxygen species.[11,12] Independently, LPS also hinders the entry of antimicrobial agents into the bacteria by acting as a permeability barrier, providing them with an advantage to survive.[13] Consequently, a sustained increase in the drug-resistant strains has developed into a grave issue that requires immediate intervention to alleviate the mortality and morbidity rates associated with these Gram-negative infections.[14−16] In this regard, host defense antimicrobial peptides (AMPs) have attracted immense attention as new generation anti-infective agents due to their large spectrum of antimicrobial activity and indiscriminate mode of action that makes it difficult for the bacterial pathogens to acquire resistance.[2,10,17−21] Some of these AMPs are also known to have immune-modulatory functions[17,20,22] that can bind to and neutralize LPS. Thus,

Received: December 6, 2016
Revised: January 23, 2017
Published: February 7, 2017

DOI: 10.1021/acs.biochem.6b01229
Biochemistry 2017, 56, 1348−1362

there is scope for the use of such peptides to alleviate sepsis.[23,24]

AMPs are short peptides (10−50 amino acids) ubiquitously present as part of the innate defense response of living organisms.[17] They are known to be unstructured when solitary, but readily adopt an amphipathic orientation upon interaction with the membrane surface.[25] This endows them with the ability to penetrate the membrane surface, causing extensive membrane damage and eventually resulting in cell death.[26,27] However, they have been restricted only to topical applications owing to their cytotoxicity that also include hemolysis/nephrotoxicity/neurotoxicity in animal models upon systemic use.[17,28,29] In this context, NMR-resolved structures of naturally occurring AMPs have potentially contributed to identification of structural motifs responsible for their biological activities enabling a correlation between their structure and function.[30−32] There has also been a considerable interest among researchers to indulge in rational designing of AMPs based on certain design principles in order to overcome the troubles of toxicity and poor bioavailability.[33−36] Shorter analogues of active peptides with retained or enhanced biological properties have also been considered to reduce the burden on production costs.[37,38] Structural studies of such short peptides in the context of LPS using various biophysical tools as well as NMR spectroscopy would help provide valuable insights for the development of novel antimicrobial and antisepsis agents.

In this study, we have reported the structural and dynamical properties of a nontoxic and non-hemolytic peptide VG13P (VARGWGRKCPLFG) (Figure 1), obtained from the wild type VG16KRKP (VARGWKRKCPLFGKGG) in LPS.[39] It is worth mentioning that the wild type peptide VG16KRKP is a designed peptide, obtained from a dengue viral fusion peptide VG16 (VDRGWGNGCGLFGKGG), upon subsequent modification based on first principle of AMP design.[39] VG13P significantly enhances LPS neutralization when compared to its parent VG16KRKP, as evident from the significantly higher efficacy of VG13P over VG16KRKP in blocking LPS-induced expression of the pro-inflammatory cytokine gene TNF-α. In addition, VG13P has almost identical antimicrobial as well as LPS-binding properties. NMR-based structural characterization at the atomistic level reveals that the structure is primarily stabilized by crucial hydrophobic contacts among Gly4, Trp5, Gly6, Pro10, Leu11, and Phe12, thus forming two consecutive turns closely resembling a rocking chair. The polar residues are directed away from the hydrophobic cluster pertaining to an amphipathic orientation. These structural attributes directly correlate with its enhanced LPS neutralization/anti-endotoxin properties and undisturbed antimicrobial properties, as compared to its parent VG16KRKP. It is worth mentioning that for therapeutic applications of any peptide, it is important to stabilize the peptide in solution and consider its biocompatibility in the human system.[40−42] Long peptides are believed to be less stable in solution compared to small-chain peptides and might often produce immunological reactions, owing to the possibility to be recognized as nonhuman peptides. On the basis of this belief and the observed enhancement in anti-inflammatory properties, we foresee that the small peptide fragment used in this study would be of potential therapeutic relevance in developing future peptide-based antimicrobial and/or antisepsis agents.

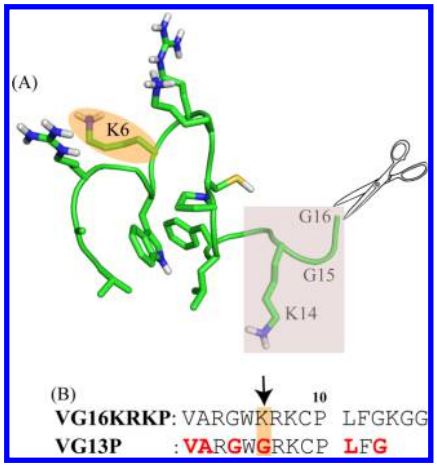

Figure 1. (A) Scheme showing the cartoon structure of VG16KRKP along with the principle of analogue design. (B) Peptide sequences of VG16KRKP and its shorter analogue VG13P with the mutation highlighted in a box and the ^{15}N-labeled amino acid residues highlighted in red.

MATERIALS AND METHODS

Reagents. *Escherichia coli* 0111:B4 LPS, 1-*N*-phenyl naphthylamine (NPN), acrylamide, and Polymyxin B were purchased from Sigma-Aldrich Co. (St. Louis, USA). 4,4-Dimethyl-4-silapentane-1-sulfonic acid (DSS), deuterium oxide (D_2O), and ^{15}N-labeled glycine, valine, alanine, and leucine were purchased from Cambridge Isotope Laboratories, Inc. (Tewksbury, USA). All bacterial and fungal media components were purchased from Himedia Laboratories Pvt. Ltd., Mumbai, India.

Cell Lines and Culture. THP-1 human monocytes and NKE normal kidney epithelial cell lines were obtained from the National Cell Repository of the National Center for Cell Science (NCCS), Pune, India. THP-1 was grown in complete RPMI-1640 (Himedia Laboratories Pvt. Ltd., Mumbai, India) supplemented with 10% heat inactivated fetal bovine serum (FBS; Invitrogen), 1 mM sodium pyruvate, 2 mM L-glutamine, 1× nonessential amino acids, 100 U/mL penicillin, and 50 μg/mL streptomycin. NKE was maintained in DMEM. All cells were maintained at 37 °C in a humidified 5% CO_2 incubator.

Bacterial and Fungal Strains. *Bacillus subtilis* (obtained from ATCC) and a common laboratory strain such as *E. coli* DH5α and *E. coli* BL21(DE3) were used for antimicrobial activity. Plant pathogenic bacterial strain *Xanthomonas campestris pv campestris* was isolated from the fields of Kalyani, West Bengal, India, while *Xanthomonas vesicatoria* and *Xanthomonas oryzae* were kind gifts from Dr. Christian Lindermayer, Helmholtz-Munich, Germany, and Prof. Sampa Das, Bose Institute, India, respectively. Fungal strains of *Candida albicans* (SC5314) and *Cryptococcus neoformans var. grubii* H99 were a gift from Prof. Kaustuv Sanyal, JNCASR, India.

Media Composition. *E. coli*, *B. subtilis*, and *X. vesicatoria* were grown in Nutrient broth. *C. albicans* and *C. neoformans var. grubii* were grown in YPD broth (1% yeast extract, 1% peptone, 2% dextrose); *X. oryzae* was grown in PS broth (1% peptone, 1% sucrose). *E. coli* and *B. subtilis* were grown at 37 °C. All other strains were incubated at 28 °C with 150 rpm for 24−48 h.

Peptide Synthesis. The unlabeled VG13P peptide was obtained from GL Biochem (Shanghai, China) with 95% purity, which was further confirmed using NMR spectroscopy, HPLC,

DOI: 10.1021/acs.biochem.6b01229
Biochemistry 2017, 56, 1348−1362

and mass spectrometry. The ^{15}N-labeled peptide was synthesized on a solid phase peptide synthesizer (Aapptec Endeavor 90) based on solid phase Fmoc chemistry[43] using ^{15}N-labeled Fmoc protected Val/Ala/Gly/Leu. A Rink Amide MBHA resin (substitution 0.69 mmol/g; Novabiochem, San Diego, California) was used, and a solid phase peptide synthesis protocol was followed.[43,44] The synthesized peptide was then purified using reverse phase HPLC (SHIMADZU, Japan) on a Phenomenix C_{18} column (dimension 250 × 10 mm, pore size 100 Å, 5-μm particle size). A linear gradient elution technique was used with water and methanol containing 0.1% TFA (ion pairing agent) as solvents. The purity was further confirmed using mass spectrometry and NMR spectroscopy. The calculated and actual molecular weight of the peptide as obtained from mass spectrometry was 1689.01 and 1688.98 Da, respectively. The peptide was stored at −20 °C. 1 mM peptide stock solution was prepared either in sterile water or 10 mM phosphate buffer (pH 7.4) and used for respective experiments. Stock solution was stored at 4 °C.

***In Vitro* LPS Neutralization Assay.** Since LPS is known to induce the expression of several pro-inflammatory cytokine genes in a human monocytic cell line, THP-1, *in vitro* LPS neutralization was determined by monitoring the decrease in the level of induction of the pro-inflammatory cytokine gene (TNF-α), in THP-1 cells in response to LPS. In brief, THP-1 human monocytes (2.5×10^5 cells/well) were seeded in a six-well tissue culture plate (Nunc, USA) in complete supplemented RPMI-1640, with 5 ng/mL phorbol myristate acetate (PMA, Sigma, USA) for 48 h. A neutralization reaction was done between 10 ng/mL *E. coli* LPS 0111: B4 (Sigma-Aldrich, 500.000 EU/mg) and varying concentrations of VG13P as well as between 1 ng/mL *E. coli* LPS 0111: B4 and varying concentrations of VG16KRKP in phosphate buffer (pH 7.4). Following differentiation by PMA, the cells were kept in serum-free RPMI 1640 for 3 h, before being stimulated with either LPS alone, or LPS neutralized by either VG16KRKP/VG13P for 2 h as described above. 25 μM each of polymyxin B and VG16A peptides was used as positive and negative controls, respectively, for the experiment.

RNA Isolation and PCR. In brief, total RNA was extracted from both treated with peptides and nontreated THP-1 cells using TRIzol reagent (Invitrogen BioServices India Pvt. Ltd.) in accordance with the manufacturer's protocol. The samples having an A_{260}/A_{280} ratio greater or equivalent to 1.8 were used for cDNA synthesis using a cDNA synthesis kit (BioBharati Life Sciences Pvt. Ltd., India). Briefly, 1 μg of RNA and 1 μL of oligo-dT (500 ng) were added and incubated at 65 °C for 10 min, following which reverse transcriptase (RT)-enhancer, dNTP mix (0.5 mM final), and enzyme mix including an RNase inhibitor were added to make a final volume of 20 μL. The cDNA synthesis was carried out at 50 °C for 1 h and then 95 °C for 2 min. TNF-α gene expression in different conditions was assessed by semiquantitative PCR. GAPDH was used as a housekeeping gene. The PCR conditions are given in Figure S1.

Antimicrobial Activity. *E. coli* DH5α, *X. campestris pv campestris, X. oryzae, C. albicans*, and *C. neoformans var. grubii* were grown overnight. They were reinoculated in fresh media to obtain mid log phase cultures that were centrifuged at 6000 rpm for 10 min to obtain a cell pellet. 10 mM phosphate buffer of pH 7.4 was used to wash twice and resuspend the cells to obtain a bacterial suspension of 10^5 CFU/mL and a fungal suspension of 10^4 CFU/mL. An MIC assay was set up in a 96-well plate format, where 50 μL of this suspension was incubated with different concentrations of peptide (ranging from 1 μM to 100 μM) prepared from 100 μM/1 mM peptide stock in 10 mM phosphate buffer of pH 7.4 and incubated at 28 or 37 °C for 3 to 6 h. A positive control containing only cell suspension and a negative control containing 10 μM polymyxin B along with cell suspension was maintained. 190 μL of suitable media was added to each well and incubated overnight with shaking at 28 or 37 °C. Bacterial growth was monitored by reading the absorbance of the culture at 600 nm. Minimum inhibitory concentration (MIC) of the peptide was given by its concentration at which no growth ($MIC_{100\%}$) was observed. All experiments were carried out in triplicates.

NPN Dye Uptake Assay. An overnight stationary phase culture of *E. coli* BL21(DE3) in LB was subcultured to obtain mid log phase cells. 10 mM phosphate buffer of pH 7.4 was used to wash cell pellets thrice and for resuspension to an OD_{600} of 0.5. 10 μM 1-*N*-phenylnaphthylamine (NPN), a hydrophobic dye, from stock solutions made in acetone, and subsequently diluted in the same buffer, was added to the cells and left to stabilize for 30 min. A similar acetone control was maintained to rule out contributions from acetone. Peptide was then added to the cells in increasing concentrations, ranging between 5 μM and 20 μM, to monitor subsequent enhancement in NPN fluorescence on a Hitachi F-7000FL spectrophotometer, owing to a disruption in the outer membrane. 0.1% Triton X100 was used as a positive control. A bandwidth of 5 nm was employed with the sample being excited at 350 nm, and its emission was measured at 410 nm. The percentage increase in NPN fluorescence was calculated using the following equation:

$$\text{percentage increase in fluorescence} = (F - F_0)/(F_T - F_0) \times 100 \quad (1)$$

where F is fluorescence intensity after addition of peptide, F_0 is basal fluorescence intensity, and F_T is maximum fluorescence intensity after addition of 0.1% Triton X100.

Hemolytic Assay. Fresh human blood was centrifuged at 4000*g* for 10 min at 4 °C. The blood cell pellet thus obtained was washed thrice with PBS, pH 7.4, and resuspended to obtain a suspension containing 1×10^9 erythrocytes/mL. This was incubated at 37 °C for 1 h with equal volumes of VG13P in increasing concentrations of up to 100 μM, with shaking. Samples were again centrifuged for 10 min at 3500*g* at 4 °C. 1% Triton X100 was used as a control, considered to cause complete (100%) lysis. The absorbance of the supernatant was read at 540 nm to quantify the percentage of RBC lysis using the equation:

$$\%\text{hemolysis} = (\text{Op} - \text{Ob}/\text{Om} - \text{Ob}) \times 100 \quad (2)$$

where Op is the optical density of sample after addition of a given peptide concentration, Ob is the optical density of the buffer, and Om is the optical density of Triton X100.

Cytotoxicity Assay. Cell cytotoxicity was quantified using the MTT cell proliferation reagent (Himedia Laboratories Pvt. Ltd. (Mumbai, India) according to the manufacturer's instructions. NKE cell line was treated with varying concentrations of the respective peptides, VG16KRKP or VG13P, for 24 h in serum free media, following which cells were processed for MTT assay. Etoposide was used a positive control for all experiments.[45] Briefly, MTT (0.5 mg/mL) was added to 4×10^4 cells seeded per well for 24 h. After 3 h of incubation at 37 °C, cells were washed with 1× PBS, followed

DOI: 10.1021/acs.biochem.6b01229
Biochemistry 2017, 56, 1348−1362

by addition of 1 mL DMSO, and absorbance was measured at 570 nm.

Fluorescence Spectroscopy. Binding interaction of the peptide with LPS was monitored using the intrinsic Trp fluorescence, present in the peptide using Hitachi F-700 FL spectrometer in a quartz cuvette with a path length of 0.1 cm. Trp fluorescence emission of 5 μM of peptide solution upon excitation at 280 nm was measured in the range of 300−400 nm after addition of LPS in increasing concentrations (ranging from 0 to 10 μM) at 25 °C. All stocks and solutions were prepared in 10 mM phosphate buffer of pH 7.2. Both excitation and emission slits were set at 5 nm. A quencher acrylamide was added in increasing concentrations (0−0.5 M) to both free and bound peptide to obtain the Stern−Volmer's quenching constant (K_{sv}), which is a measure of the extent of exposure of the Trp residue to the quencher, using the following equation:

$$F_0/F = 1 + K_{sv}[Q] \quad (3)$$

where F_0 = fluorescence intensity in the absence of quencher, F = fluorescence intensity in the presence of quencher at each titration, and [Q] = concentration of quencher in molarity.

Steady-state anisotropy experiments of the peptide in the presence of LPS were also recorded using a polarization accessory. 5 μM peptide in solution was titrated with increasing concentrations of LPS up to a maximum of 10 μM. An excitation slit of 5 nm was used to excite the sample with a vertically polarized light. Anisotropy (r) values of the intrinsic fluorescence of Trp were obtained using the following equation:

$$r = (I_{VV} - GI_{VH})/(I_{VV} + 2GI_{VH}) \quad (4)$$

where G is the sensitivity factor of the instrument. I_{VV} and I_{VH} are the vertically and horizontally polarized components of probe, respectively.

Solution NMR Experiments. All NMR experiments were carried out either on a Bruker Avance III 500 MHz NMR spectrometer equipped with a 5 mm SMART probe (at Bose Institute, Kolkata, India) or a Bruker Avance III 800 MHz spectrometer equipped with cryoprobe (at CBMR Luckow, India). Topspin v3.1 (Bruker Biospin, Switzerland) software suite was used for data acquisition and processing. 2,2-Dimethyl-2-silapentane 5-sulfonate sodium salt (DSS) served as an internal standard (0.0 ppm) for all experiments. To probe the residue specific changes in peptide structure and dynamics upon its binding to LPS, the selectively ^{15}N-labeled peptide was used.

To elucidate the structure of the free peptide in solution, two-dimensional (2D) homonuclear total correlation spectroscopy (TOCSY) and nuclear Overhauser effect spectroscopy (NOESY) were acquired for an aqueous solution of 1 mM of peptide at pH 4.5, supplemented with 10% D_2O, using a mixing time of 80 and 200 ms for TOCSY and NOESY experiments, respectively. Next, to understand the binding interaction of the peptide with LPS, a one-dimensional (1D) ^{1}H proton NMR spectra of the peptide (1 mM) at pH 4.5 and 298 K was acquired, and line broadening effects in the proton resonances were observed through a series of (1D) ^{1}H proton NMR experiments upon addition of small aliquots of LPS. Two-dimensional transferred NOESY (trNOESY) experiments of VG13P in LPS were performed upon significant line broadening, with three different mixing times: 100, 150, and 200 ms. The spectra were acquired with 2048 (t_2) × 456 (t_1) complex points, States-TPPI[46] for quadrature detection, and excitation sculpting for water suppression.[47]

The sequence specific assignment of ^{15}N-labeled amide cross peaks were established by the composite use of three-dimensional (3D) ^{15}N edited TOCSY HSQC and NOESY HSQC experiments. The spectra were acquired on a Bruker Avance III 800 MHz spectrometer (equipped with a cryoprobe) with TOCSY and NOESY mixing times of 80 and 300 ms, respectively, and 1024 (t3) × 44 (t2) × 156 (t1) complex data points. The spectra were first processed using Topspin v2.1 (Bruker software suite) and then were analyzed using CARA. The ^{15}N relaxation parameters R_1, R_2, and [^{1}H]-^{15}N steady-state heteronuclear NOE were measured on the Bruker Avance III 800 MHz NMR spectrometer using 1.0 mM solution of the selectively ^{15}N-labeled VG13P peptide prepared in 90% H_20 and 10% D_20 solution (pH 4.5). Following this, the relaxation experiments were carried out using the 2D sensitivity-enhanced heteronuclear single quantum correlation (HSQC) based pulse sequences described by Peng and Wagner (1992)[48] and Farrow et al.[49] The complete set of R_1, R_2, and [^{1}H]-^{15}N NOE data sets were recorded at 298 K with 1024 (t_2) and 256 (t_1) complex data points, respectively, along the ^{1}H (SW = 12 ppm, offset = 4.701 ppm) and ^{15}N (SW = 22 ppm, offset =117.5 ppm) dimensions. All these spectra were processed and analyzed using the Topspin software suite. Prior to Fourier transformation and zero-filling, data were apodized with a sine-squared function shifted by 60° along each dimension.

Each R_1 and R_2 data sets were collected using eight scans and a recycle delay of 2.5 s. For R_1 measurements, the following relaxation delays were used: 10, 50, 90, 150, 250, 350, 550, 770, 990, and 1100 ms. For R_2 measurements (with an spin−echo time of $2\tau_{CP}$ = 900 μs), the following relaxation delays were used: 0.00, 16.96, 33.92, 50.88, 67.84, 101.76, 135.68, 169.60, and 237.44 ms. The R_1 and R_2 values with their errors were extracted using the Mathematica notebook "Relaxation Decay" developed in the Spyracopoulos lab.[50] Steady state [^{1}H]-^{15}N heteronuclear NOE (hetNOE) measurements were carried out with a proton saturation time of 3 s and a relaxation delay of 3 s. For the experiment without proton saturation, the relaxation delay was set to 6 s. The NOE intensities for every residue were calculated as I_{sat}/I_{ref}, where I_{sat} and I_{ref} are intensities of the peaks in the HSQC spectra, with and without proton saturation, respectively. The error (σ_{NOE}) was determined using the following equation:

$$\sigma_{NOE} = \frac{I_{sat}}{I_{ref}}\left(\left(\frac{\sigma_{sat}}{I_{sat}}\right)^2 + \left(\frac{\sigma_{ref}}{I_{ref}}\right)^2\right)^{1/2} \quad (5)$$

where σ_{sat} and σ_{ref} represent the RMS variation in the noise in empty spectral regions of the spectra with and without proton saturation.

Relaxation dispersion data were obtained using a modified (relaxation compensated) proton-detected ^{15}N Carr−Purcell−Meiboom−Gill (CPMG) spin echo pulse sequence[51] performed in a constant time (CT) manner with a CT delay of 100 ms.[52,53] Each 2D spectrum was acquired on a 800 MHz Bruker spectrometer with 1024 (t_2) × 180 (t_1) data points, with 32 scans per each t_1 point and a relaxation delay of 3 s to avoid sample heating. Inhomogeneous heating of sample in different experiments was also minimized using a heat compensation pulse train during the recycle delay. Relaxation decay curves

DOI: 10.1021/acs.biochem.6b01229
Biochemistry 2017, 56, 1348−1362

Table 1. Minimum Inhibitory Concentrations ($MIC_{100\%}$) of the Peptides (in μM) against the Tested Bacterial and Fungal Strains

	minimum inhibitory concentration ($MIC_{100\%}$) in μM					
peptide name	*E. coli*	*X. campestris*	*X. oryzae*	*X. vesicatoria*	*C. neoformans*	*C. albicans*
VG16KRKP	8	10	15	5	5	2
VG13P	10	10	20	10	5	5

were measured for 10 values of τ_{cp} (25.0, 12.5, 6.25, 5.0, 3.125, 2.5, 1.5625, 1.25, 1.0, and 0.625 ms), where $2\tau_{cp}$ is the interpulse delay in the CPMG pulse train. The intensities of cross-peaks in the 2D spectra recorded for a given length of CPMG train T (~100 ms) and τ_{cp} delays are converted into the effective relaxation rates[54] as follows:

$$R_2^{\text{eff}}(\nu_{\text{CPMG}}) = -\frac{1}{T}\ln\frac{I(\nu_{\text{CPMG}})}{I_0} \quad (6)$$

where $I(\nu_{\text{CPMG}})$ and I_0 are the signal intensities in the presence and absence of the CPMG element, respectively, and $\nu_{\text{CPMG}} = 1/(2\tau_{cp})$ Hz. A plot of R_2^{eff} as a function of field strength,ν_{CPMG}, gives a relaxation dispersion profile for each residue from which exchange parameters were obtained. Simply, the fast-limit expression for exchange between two-sites (i.e., $k_{ex} \gg \delta\omega$, where $\delta\omega$ is the difference between the ^{15}N chemical shifts of the two sites A and B) was used to fit the relaxation dispersion data:[55]

$$R_2^{\text{eff}} = R_2^0 + R_{ex}\left[1 - \frac{2\tau_{cp}}{k_{ex}}\tanh\left(\frac{k_{ex}}{2\tau_{cp}}\right)\right] \quad (7)$$

Here, k_{ex} is the sum of the forward and reverse exchange rate constants, $R_{ex} = p_A.p_B.\delta\omega^2/k_{ex}$ and R_2^0 is the transverse relaxation rate in the limit of infinitely fast pulsing.

To probe the specific binding of LPS to peptide, a series of $^1H-^{15}N$ HSQC spectra were recorded on the ^{15}N-labeled peptide with LPS concentration varying from 0 to 70 μM, in steps of 14 μM. To further understand the binding interaction of peptide with LPS, the normalized amide cross-peak intensities of ^{15}N-labeled amino acids were plotted as a function of increasing LPS concentration. The resulting intensity profiles followed simple two-state cooperative binding, where the probability of finding an alternative bound conformation is low. The intensity profiles for such a binding interaction can be analyzed according to two-state model (Free ↔ Bound) following a sigmoidal three-parameter equation (eq 8) derived from the well-known logistic sigmoid function curve.[56,57]

$$S(x) = \frac{S_{\text{Free}}}{1 + e^{-(x-x_0)/S_{\text{Bound}}}} \quad (8)$$

where $S(x)$ is the varying amide-cross peak intensity as a function of LPS concentration (x), x_0 is the mean LPS concentration (corresponding to the mid of the slope and referred to here as LPS binding transition point), while S_{Free} and S_{Bound} are the intensities in the absence of LPS and in the completely bound state of peptide.

Calculation of Solution-State NMR Derived Structures. Depending upon the intensities of the NOE cross peaks in the NOESY spectra of the peptide in the presence of LPS, the NOE volume integrals were differentiated quantitatively for NMR structure calculation as described earlier.[32] The upper bound distance constraints were calculated with respect to the NOE intensities between the resolved ring protons of Phe-12 (viz. Phe12-2H and Phe12-3H). The lower bound distance constraint was fixed at 2.0 Å. The upper bound distances that were calculated as mentioned above were next categorized into strong (2.5 Å), medium (2.6−3.5 Å), and weak (3.6−5.0 Å) for structure calculation. To limit the conformational space for all the residues, the backbone dihedral angle (phi) was allowed to vary from −30° to −120°. No hydrogen bond constraints were used in the structure calculation. All structure calculations were performed using the CYANA program v2.1 with iterative refinement of the structure as previously described.[58] PyMol, MOLMOL, and Chimera software were used to analyze the NMR-derived structures. The stereochemistry of the structures was checked using Procheck.[59] The calculated structure has been deposited to the Protein Data Bank (PDB) with accession code 5WRX for VG13P in LPS.

RESULTS AND DISCUSSION

Designing of VG13P. In a recent study, we reported a potent 16-residue peptide VG16KRKP (VARGWKRKCPL-FGKGG) (Figure 1A) against Gram-negative bacterial strains *Escherichia coli*, *Xanthomonas campestris*, *Xanthomonas oryzae*, and *Xanthomonas vesicatoria* with minimum inhibitory concentrations in the μM range[39] (Table 1). The limulus amoebocyte lysate (LAL) based LPS neutralization assay, which is a quantitative chromogenic assay to test LPS neutralization *in vitro*, also showed that the peptide was capable of neutralizing LPS in the μM range.[39] Deeper structural insights into its observed biological activities revealed that its structure was stabilized at the LPS micellar interface mainly via a hydrophobic triad that was formed between Trp5, Leu11, and Phe12. Val1 and Ala2 were also found to share hydrophobic interactions with Trp5, thus participating in the hydrophobic stabilization. The C-terminal end, comprising Gly13, Lys14, Gly15, and Gly16, however, remained flexible and did not participate in any interaction with LPS[39] (Figure 1). On the basis of these observations, we have designed for the present study, a truncated analogue VG13P (Figure 1B), where the last three residues (Lys14, Gly15, and Gly16) were removed based on its 3D structure in LPS, which showed that the C-terminal end remains fairly flexible. It is also reported in the literature that the loop structure can be stabilized by CH/π interactions.[60] Thus, for the purpose of enhancing the hydrophobic stabilization through loop conformation observed in VG16KRKP, Lys6 was replaced with Gly to facilitate the interactions between Trp5, Leu11, and Phe12, as Gly has been observed to mediate hydrophobic and CH/π interactions with aromatic amino acids.[61]

VG13P Has Enhanced Antiendotoxic Effects As Opposed to Its Parent. In an earlier study, VG16KRKP was shown to bind to *E. coli* LPS and promote its disaggregation as observed from ^{31}P NMR, DLS, and TEM studies.[39] Separately, the LAL assay also showed its ability to neutralize an endoxin unit (1 EU = 0.1 ng LPS) by 50% at a concentration of 12 μM.[39] However, its effect on LPS induced

DOI: 10.1021/acs.biochem.6b01229
Biochemistry 2017, 56, 1348−1362

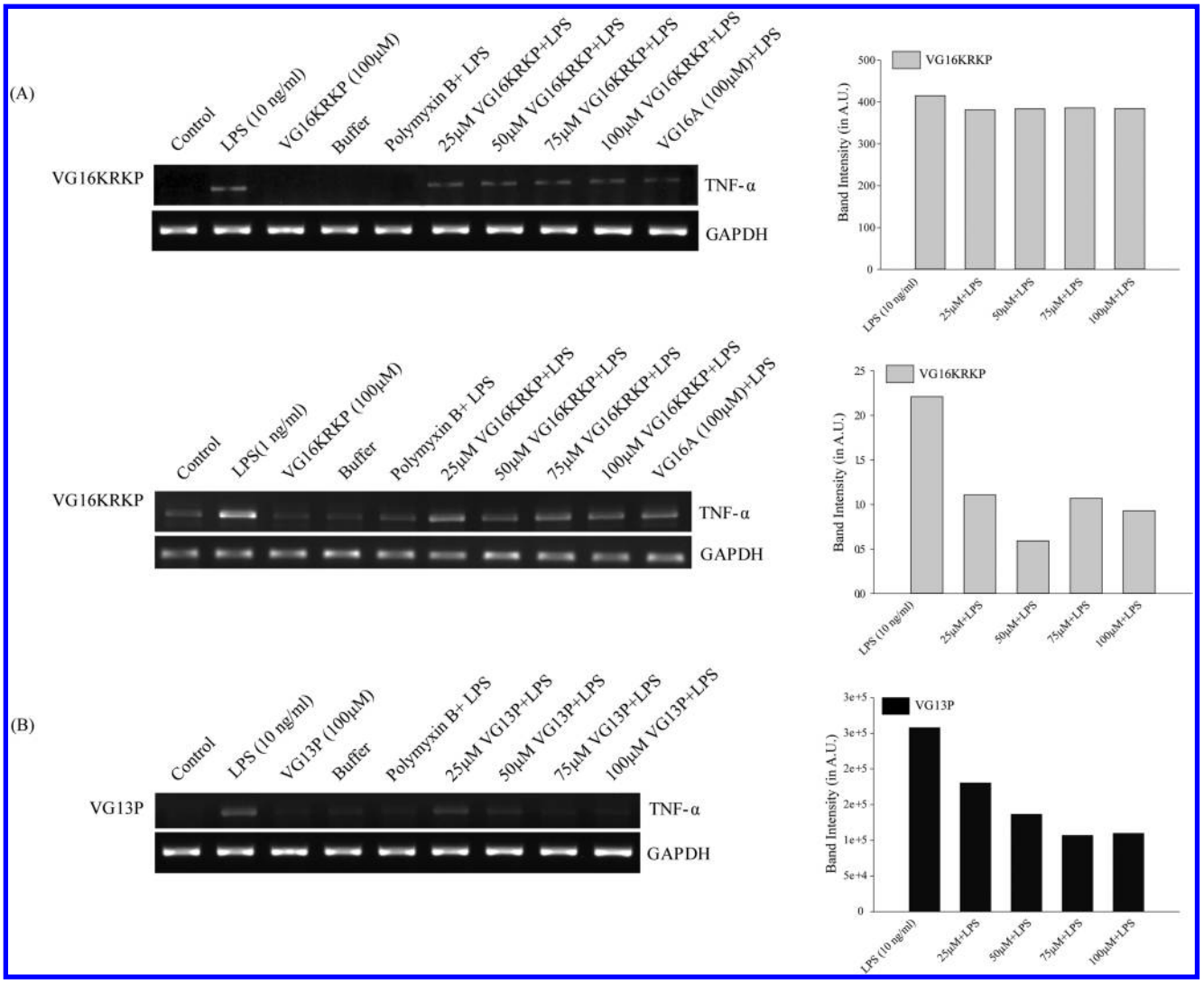

Figure 2. Effect of the marked peptides on LPS induced gene expression in human monocyte-macrophage cell line. THP-1 cells were treated with *E. coli* LPS (1 ng/mL and 10 ng/mL) after a neutralization reaction with the peptides, VG16KRKP (A) and VG13P (B) in a concentration-dependent manner. Following treatment, the level of TNF-α was monitored by PCR analysis. (A) VG16KRKP showed effective neutralization of 1 ng/mL LPS (bottom panel), while there was no effect on 10 ng/mL of LPS (top panel) as also evident from densitometric analysis (top and bottom right panel). (B) The second-generation peptide, VG13P, effectively detoxified 10 ng/mL LPS starting from 25 μM as also reflected in densitometric analysis (right panel), demonstrating improved neutralization property compared to its parent VG16KRKP.

in vitro cytokines production remained unknown. Therefore, both VG16KRKP and its analogue VG13P were tested for their LPS neutralization activity. PCR data show that the LPS alone (either at 10 ng/mL in the case of VG16KRKP/VG13P, or with 1 ng/mL in the case of VG16KRKP) causes a significant induction in the mRNA expression of the pro-inflammatory cytokine TNF-α (Figure 2). Surprisingly, VG16KRKP failed to neutralize *E. coli* LPS at 10 ng/mL even up to 100 μg/mL concentrations (Figure 2A, upper panel). However, densitometry data showed that it caused a significant decrease (50%) in TNF-α gene expression at a concentration of 25 μM, where 10-fold lower concentrations of LPS (1 ng/mL) were used for induction (Figure 2A, lower panel). Nevertheless, a saturation in the decrease of TNF-α gene expression was observed starting from 50 μg/mL, after which the TNF-α mRNA levels remained the same up to 100 μg/mL (Figure 2A lower right panel). In contrast, VG13P (Figure 2B) affected a dose-dependent decrease in LPS-induced TNF-α gene expression, clearly highlighting the LPS neutralizing activity of both peptides. As observed from the densitometry data, VG13P caused a 50% reduction in TNF-α mRNA expression levels at a concentration of 50 μM, while a 70% reduction was observed in the case of 75 μM, when compared to untreated controls, with LPS induction doses as high as 10 ng/mL (Figure 2B right panel). These results signify that while VG16KRKP displayed only a moderate effect on LPS neutralization, which leveled off at 50 μg/mL, VG13P was more potent and efficient in neutralizing LPS, even with 10-fold higher concentrations of LPS in a dose-dependent manner. Recent studies on a frog skin derived antimicrobial peptide Esc (1−21) and its diastereomer Esc (1−21)-1c have also shown potent neutralization of *P. aeruginosa* LPS in CFTR expressing bronchial cell lines, when used in concentrations that mimic lung infection.[62] Another frog skin derived AMP Esc-1a(1−21) and its D-amino acid containing analogue also showed similar immunomodulating effects and LPS detoxification activities.[63]

VG13P Is Nontoxic and Nonhemolytic and Mediates Bacterial Killing through Membrane Perturbation.

DOI: 10.1021/acs.biochem.6b01229
Biochemistry 2017, 56, 1348−1362

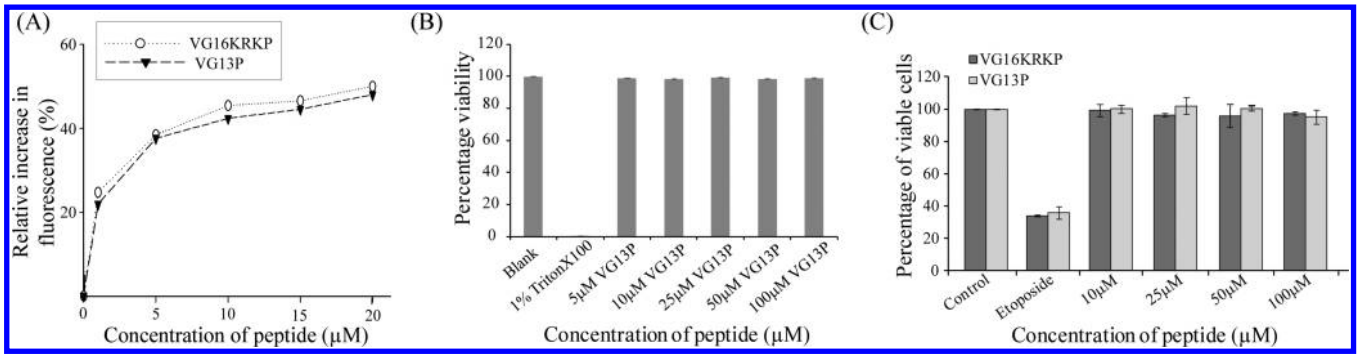

Figure 3. (A) NPN dye uptake by *E. coli* BL21(DE3) upon treatment with VG16KRKP or VG13P, as a measure of membrane permeabilization. Both VG16KRKP and VG13P showed a ~50% increase in NPN fluorescence intensity, indicating similar membrane perturbing abilities for both peptides. (B) Hemolytic activity assay of VG16KRKP and VG13P against human blood showing that both peptides are non-hemolytic up to 100 μM as indicated from an insignificant decrease in the percentage of viable cells as opposed to 1% Triton X100 used as a positive control known to lyse cells completely at the said concentration. (C) Cell cytotoxicity assay of VG16KRKP and VG13P against the NKE cell line showing that the peptides were non-cytotoxic. Etoposide used as a positive control caused growth inhibition in almost 65% of the cells under similar conditions.

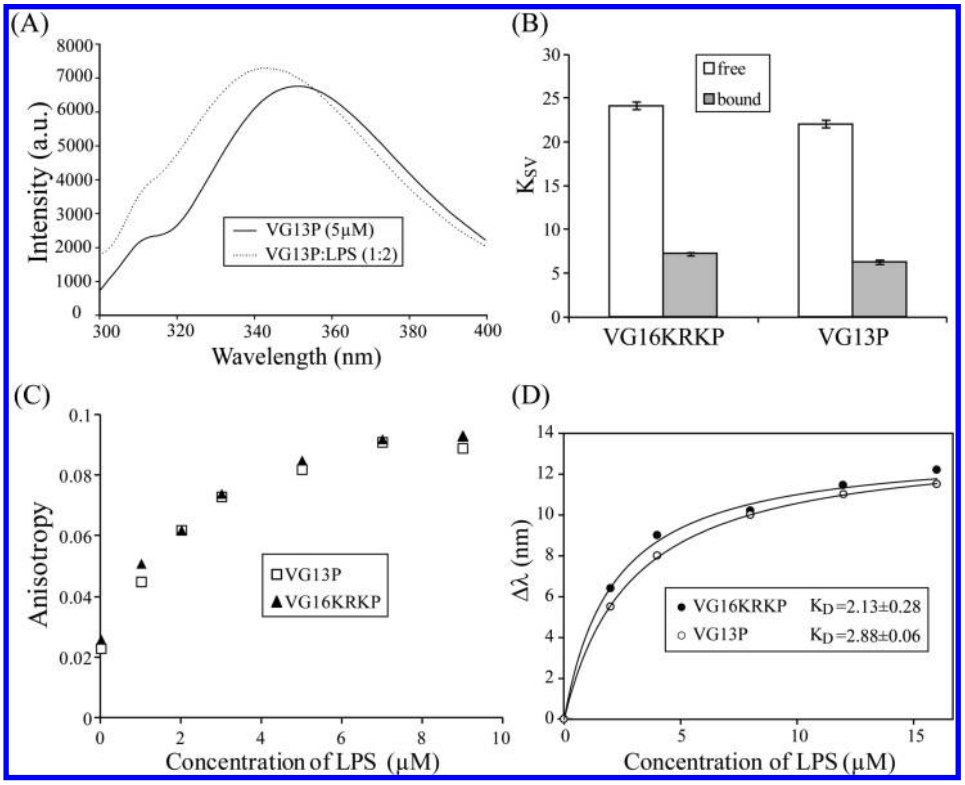

Figure 4. (A) The emission spectra of the intrinsic fluorescence of Trp present in VG13P alone and upon addition of LPS, showing a 12 nm blue shift and indicating binding. (B) A bar plot showing the Stern Volmer quenching constant (K_{Sv}) values of VG16KRKP/VG13P alone and in the presence of LPS, as obtained from fluorescence quenching experiments using acrylamide as a quencher. Both VG16KRKP and VG13P showed similarly low K_{SV} values in the LPS bound form than their free form, indicating a decrease in the accessibility of the Trp residue to the quencher, also supporting binding. (C) A scatter plot showing a consistent concentration-dependent increase in the fluorescence anisotropy of Trp in both VG16KRKP and VG13P upon addition of increasing concentrations of LPS indicative of binding. (D) A plot of the shift in the emission maxima of Trp in both VG16KRKP and VG13P against LPS concentration fitted to a single site binding equation to yield the dissociation constant (K_D) values of peptide interaction with LPS. Both the peptides yielded almost similar K_D values.

Microbroth dilution assays clearly indicated that VG13P was equally potent in killing the tested Gram-negative bacteria when compared to VG16KRKP. It displayed a minimum inhibitory concentration ($MIC_{100\%}$) similar to VG16KRKP (Table 1) when tested against several Gram-negative bacterial pathogens such as *E. coli*, *X.campestris*, *X.oryzae*, and *X.vesicatoria* and opportunistic fungal pathogens *C. albicans* and *C. neoformans var. grubii*. These results suggested that the flexible C-ter end of VG16KRKP probably had no role in its observed antimicrobial activities as reflected from its NMR resolved structure. Further, membrane perturbation was assayed using NPN dye uptake in the presence of living bacterial cells, upon treatment with peptide at various increasing concentrations (Figure 3A). NPN is a hydrophobic dye that is not taken up by healthy living cells. However, upon membrane compromise NPN gets access into the hydrophobic core of the lipid membrane that is reflected directly from an enhancement in its fluorescence emission spectra. Upon

DOI: 10.1021/acs.biochem.6b01229
Biochemistry 2017, 56, 1348−1362

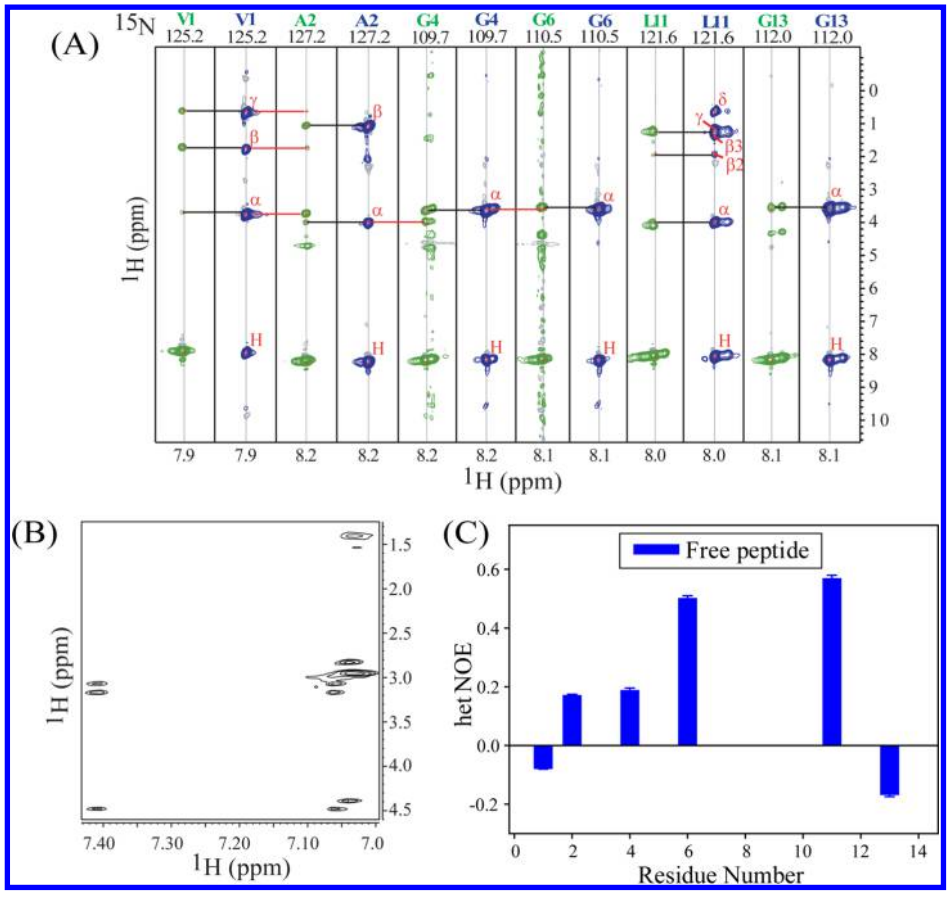

Figure 5. (A) The spin-system identification made for the individually assigned HSQC cross peaks from $F_1(^1H)$ $F_3(^1H)$ planes of the ^{15}N edited TOCSY HSQC spectrum of ^{15}N-labeled VG13P peptide (at 298 K and pH 4.5). The $F_2(^{15}N)$ chemical shift values are shown at the top of each strip. The corresponding NOESY strips (containing green peaks) are shown to the left of each TOCSY strip (containing blue peaks) and are further used to confirm the sequence specific assignment (black and red lines signify self-and sequential NOEs, respectively). Residues Val1, Ala2, and Leu11 were identifed through an amino-acid specific TOCSY peak pattern; Gly4 was confirmed by the sequential NOE from Hα proton of Ala2, whereas Gly13 was differentiated from Gly6 based on its higher intensity owing to its terminal position. (B) The 2D $^1H-^1H$ NOESY spectrum of free peptide VG13P (pH 4.5 and at 298 K) indicating a random coil conformation in solution. (C) $[^1H]$-^{15}N heteronuclear NOE plot of free peptide as determined for the labeled amino acids at 800 MHz field strength is shown.

addition of increasing concentrations of peptide to bacteria, >50% increase in its fluorescence intensity was observed in the case of VG13P at a maximum tested concentration of 20 μM (Figure 3A). This observation was strikingly similar to that obtained for VG16KRKP indicating that truncation and/or single amino acid modification did not compromise its membrane perturbing abilities (Figure 3A). Alternately, the hemolytic activity assay with VG13P against human RBC showed that the peptide was non-hemolytic, similar to its parent VG16KRKP (Figure 3B). A cytotoxicity assay of both VG16KRKP and VG13P was also performed against a normal kidney epithelial (NKE) cell line. Both the peptides were not seen to have any toxic effects on the said cell line even up to concentrations of 100 μM (Figure 3C) as opposed to etoposide, the positive control that was seen to inhibit the growth of ~65% of cells.

VG13P Has Retained LPS Binding Abilities. To characterize the effects of the truncation and a single amino acid modification in VG13P on its LPS binding abilities, different fluorescence experiments were conducted making use of the intrinsic fluorescence of the Trp residue present in its sequence. Upon gradual addition of small aliquots of LPS into the peptide in solution, a concentration-dependent blue shift in the emission spectra of Trp was observed that directly indicates burial of Trp in the hydrophobic interior of the LPS micelles (Figure 4A). A remarkable 12 nm blue shift was observed for VG13P, which was comparable to the blue shift observed for VG16KRKP (Figure 4A).[39] Trp fluorescence quenching experiments using acrylamide, a neutral quencher, revealed ~3 times lower Stern Volmer quenching constants (K_{SV}) for VG13P in its LPS bound form compared to its free form, which is quite similar for VG16KRKP. This also indicated that Trp was buried inside the hydrophobic LPS core upon binding that reduced its accessibility to the quencher, hence giving rise to lower K_{SV} values in its bound form (Figure 4B). Anisotropy experiments on VG13P upon gradual addition of LPS also showed a steady concentration-dependent increase in its anisotropy values, again quite identical to that obtained for VG16KRKP (Figure 4C). A plot of change in the emission maxima of Trp fluorescence versus concentration of LPS yielded a dissociation constant (K_D) value of ~2.8 ± 0.1 μM for VG13P binding to LPS. This value, $K_D \approx 2.1 \pm 0.3$ μM, is almost identical for the binding of VG16KRKP to LPS (Figure 4D). Collectively, VG13P and VG16KRKP have almost identical LPS neutralization activities.

Solution Structure and Dynamics of VG13P in Aqueous Solution. Out of 13 amino acid residues in VG13P, six amino acids (Val1, Ala2, Gly4, Gly6, Leu11, and

DOI: 10.1021/acs.biochem.6b01229
Biochemistry 2017, 56, 1348−1362

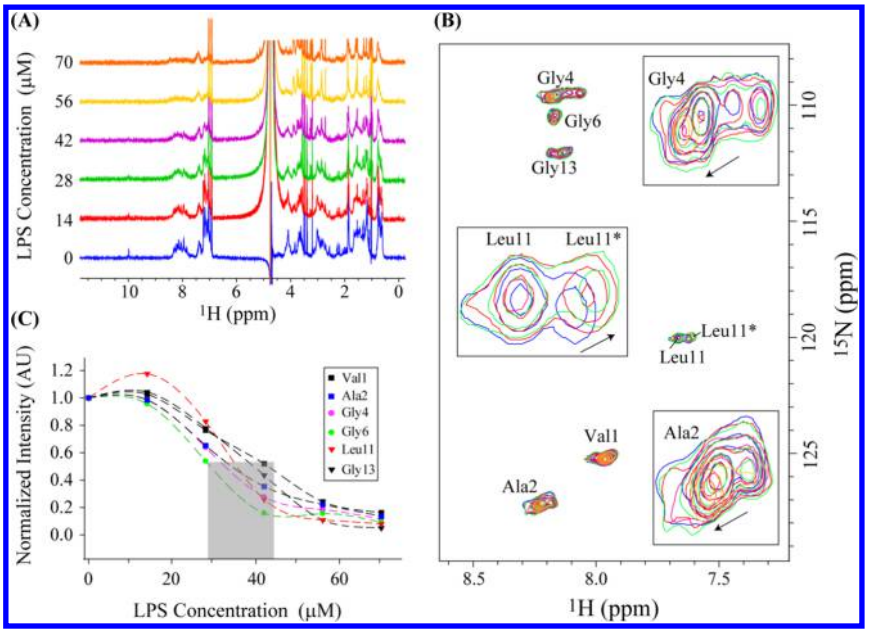

Figure 6. Interaction of peptide with LPS using NMR. (A) Stack plot of 1D ^{1}H NMR spectra of peptide of concentration ~1.0 mM (pH of solution 4.0 and temperature at 298 K) recorded after subsequent addition of LPS (1 mg dissolved in 50 μL). The progressive decrease in intensity on increasing the LPS concentration clearly revealed that the peptide is binding to LPS (B). Overlay of ^{15}N-HSQC spectra of 1.0 mM ^{15}N-labeled VG13P peptide (at 298 K, pH 4.5) recorded upon titration with increasing concentrations of LPS (ranging from 0 to 70 μM). Residue specific assignment for each peak is marked on the spectrum. The amino acid sequence of the peptide is shown at the top of the HSQC spectrum with selectively ^{15}N-labeled residues (Val1, Ala2, Gly4, GLy6, Leu11, and GLy13) highlighted in blue. Except for Leu11 residue, the exchange peaks for all other ^{15}N-labeled residues were broadened and overlapping with the major conformational peak, whereas Leu11 clearly showed two cross peaks signifying largely different conformations exchanging slowly. The HSQC cross-peak of Leu11 corresponding to minor conformational state have been highlighted in the spectrum by an asterisk (*). (C) Normalized intensity profiles of amide cross-peaks of ^{15}N labeled residues plotted as a function of increasing LPS concentration.

Gly13) were selectively labeled with ^{15}N F-moc amino acids. The assignment of VG13P in aqueous solution was performed using two 3D NMR experiments, viz. ^{15}N edited TOCSY HSQC and ^{15}N edited NOESY HSQC (Figure 5A). As the VG13P peptide is very small, it is highly dynamic in aqueous solution, reflected by very few NOEs between backbone-side chain or side chain-side chain or aromatic-side chain resonances in the NOESY spectra (Figure 5B). Apart from the intraresidual as well as sequential NOEs, no other medium or long-range NOEs were observed, indicating that VG13P is highly flexible and do not adopt any folded conformation in aqueous solution. These data were further supported by heteronuclear NOE experiments of VG13P in aqueous solution (Figure 5C). The terminal residues Val1 and Gly13 both showed negative heteronuclear NOE values, indicating higher conformational flexibility. The N-ter adjacent residues Ala2 and Gly4 also exhibited lower heteronuclear NOE values of ~0.20. By contrast, Gly6 and Leu11 displayed higher heteronuclear NOE values, ranging from 0.50−0.58, suggesting their conformational rigidity due to association with neighboring hydrophobic residues such as Pro10 and Phe12. Taken together, VG13P is a highly dynamic peptide in aqueous solution, similar to VG16KRKP.[39]

NMR Studies of VG13P in the LPS Bound State. In order to study the peptide−LPS interaction using NMR, the 1.0 mM solution of ^{15}N selectively labeled peptide (pH 4.5 and temperature 298 K) was titrated with 1.0 mM LPS stock solution (final concentration varying from 0 to 70 μM) (Figure 6A). As evident, the amide signals of the peptide decreased regressively upon increasing the LPS concentration, and at 70 μM concentration the signal intensity decreased by more than 80% (Figure 6A). To reveal whether the peptide binding is LPS specific (i.e., a particular segment binds first, followed by the whole peptide) or nonspecific (i.e., the peptide binds to LPS as a whole), the sequence specific amide shift perturbations in the 2D ^{1}H−^{15}N HSQC spectra were analyzed. Few residues such as Ala2, Gly4, Leu11, and Gly13 exhibited multiple amide cross peaks in the HSQC spectrum, suggesting that there is a slow conformational exchange ($\ll 10^{3}$ s^{-1}) between multiple conformations at the NMR time scale. Close inspection clearly suggests that these residues are adjacent to either positively charged residue such as Arg3 or could be due to the presence of Pro10. The multiple conformations are quite possible with such short-length peptide, owing to transient but complex interplay between hydrophobic interactions (between local side chain atoms), electrostatic interactions between charged amino acids and H-bond interactions.[64] Figure 6B also shows the overlay of HSQC spectra recorded on the peptide before (blue) and after subsequent addition of LPS concentration (other colors). Interestingly, no significant amide chemical shift perturbations were observed, suggesting that the peptide binding to LPS is a fast conformational exchange between free and bound form on the NMR time scale. This phenomenon can be attributed to the strong electrostatic interaction between positively charged (cationic) peptide and negatively charged (anionic) surface of the LPS system. To validate this phenomenon, the ^{1}H−^{15}N cross-peaks from the HSQC spectrum were normalized with respect to the intensity in the free state, and the intensity profile of each ^{15}N-labeled amino acid was then observed as a function of added LPS concentration (Figure 6C). Although an overall decrease in the intensity profiles for all the residues was observed and the decrease in each intensity profile was about

DOI: 10.1021/acs.biochem.6b01229
Biochemistry 2017, 56, 1348−1362

the same level (~10% to 20%), a close investigation suggests that the binding of peptide to LPS is residue specific (Figure 6C, highlighted in a gray box) (Table 2). The calculated

Table 2. Residue Specific Binding Transition Point in LPS Micelle, Estimated Using Logistic Sigmoid Equation (eq 8)

residue	binding transition point (μM)
Val1	40.70 ± 3.33
Ala2	32.84 ± 5.46
Gly4	31.92 ± 4.65
Gly6	28.64 ± 3.86
Leu11	35.27 ± 2.67
Gly13	38.54 ± 1.56

binding transition point, as observed from the line broadening of 2D $^{1}H-^{15}N$ HSQC cross-peaks, was more in the case of Gly6, followed by Gly4, Ala2, and Leu11 (Table 2). Both terminal residues Val1 and Gly13 needed relatively higher LPS concentrations for close association with the LPS molecule. It is supposed that there is a strong electrostatic interaction between the phosphate groups of LPS with Arg7 and Lys8 of VG13P. As LPS is a huge molecule, the Gly6 residue, adjacent to Arg7 and Lys8, comes in close contact with LPS first and adopts increased T_2 relaxation similar to LPS. In a similar fashion, Gly4 and Ala2, juxtaposed to Arg3, are directly involved in complex formation with LPS micelle; thereby a line-broadening effect was observed. Leu11 might not be involved in an immediate association with LPS, in comparison to the Gly6/Gly4/Ala2. In other words, Leu11 comes close to LPS after the peptide adopts a folded conformation in LPS. Collectively, these results represent the systematic folding of VG13P in LPS micelle at an atomic resolution.

Insights into Adopted VG13P Structure in LPS Micelles. To find a correlation between the VG13P structure in LPS and the enhancement in its anti-endotoxic activity as well as its retained antimicrobial activities, we embarked on an effort to determine its 3D structure in LPS micelles using 2D transferred NOESY (trNOESY) NMR experiments. It should be noted here that LPS forms high molecular weight aggregates or micelles in solution at very low concentrations (~14 μg/mL).[65] The 2D $^{1}H-^{1}H$ NOESY spectra of the peptide alone in aqueous solution were characterized by only sequential NOEs between the backbone and side chain protons, thus indicating a random structure (Figure S2). In contrast, the 2D $^{1}H-^{1}H$ spectra acquired in the presence of LPS, at a concentration of 28 μM where significant line broadening was observed in the 1D proton spectra, showed a considerably higher number of medium- and long-range NOE cross peaks. Medium range NOEs (i, i+2/i+3/i+4) were observed between the side chain and amide protons and/or side chain and ring protons of residue-pairs Val1/Trp5, Ala2/Trp5, Cys9/Trp5, and Pro10/Phe12 (Figure 7A–C). A large number of long-range NOEs were also observed between side chain and ring protons of Leu11/Trp5, Pro10/Trp5, and Trp5/Phe12 pairs (Figure 7A, C). A few interesting long-range NOEs were also observed between side chain and ring protons of residue pairs Val1/Phe12 and Ala2/Phe12 and Gly4/Phe12 (Figure 7A, C), and between side chain and amide protons of residue pairs Leu11/Val1 and Leu11/Ala2 (Figure 7C).

Next, the 3D structure was calculated with the help of the NOE driven distance constraints that were obtained from the 2D trNOESY spectra. The transient binding to LPS in solution resulted in increased stability of VG13P as evident from the perfect convergence of the backbone atoms (C^{α}, N, and C') of all the 20 lowest energy structures (Figure 8A) that represent

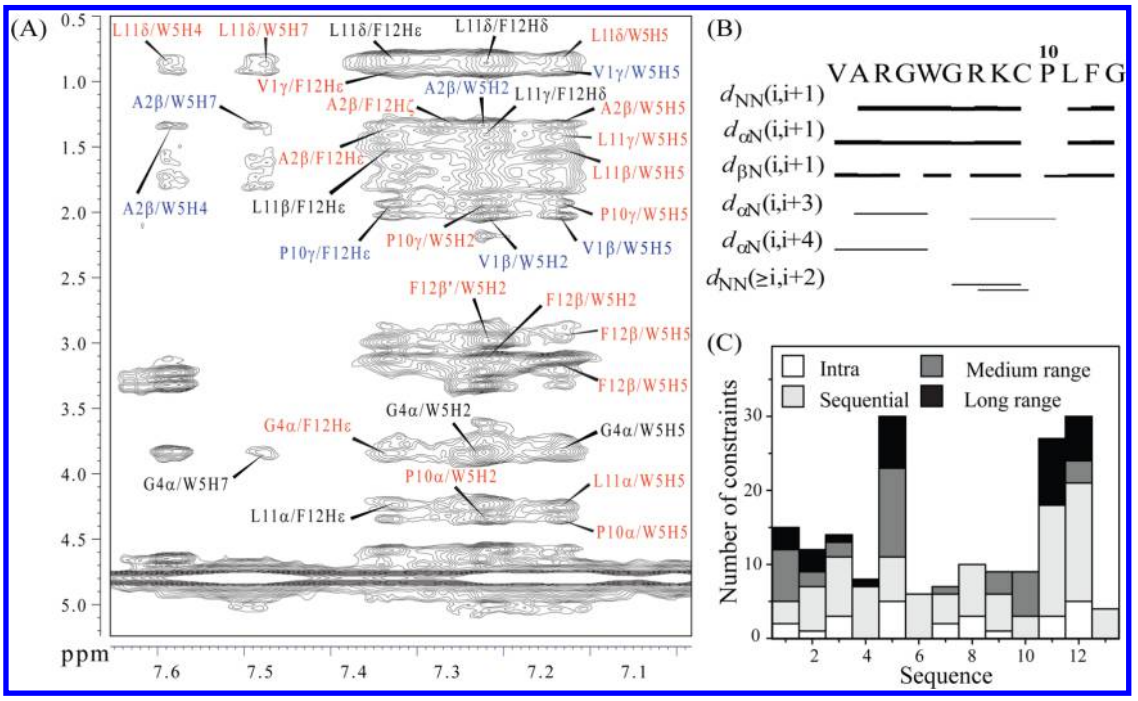

Figure 7. (A) TrNOESY spectra of VG13P upon addition of LPS showing a large number of NOE cross peaks indicating a well-folded conformation. The important medium-range and long-range NOEs are highlighted in blue and red, respectively. (B) A bar diagram showing the short- and medium-range NOE contacts in the trNOESY spectra of VG13P in LPS micelles, between the backbone/backbone and backbone/side-chain resonances. (C) A histogram showing the number of NOEs observed for VG13P in LPS micelles per residue.

DOI: 10.1021/acs.biochem.6b01229
Biochemistry 2017, 56, 1348–1362

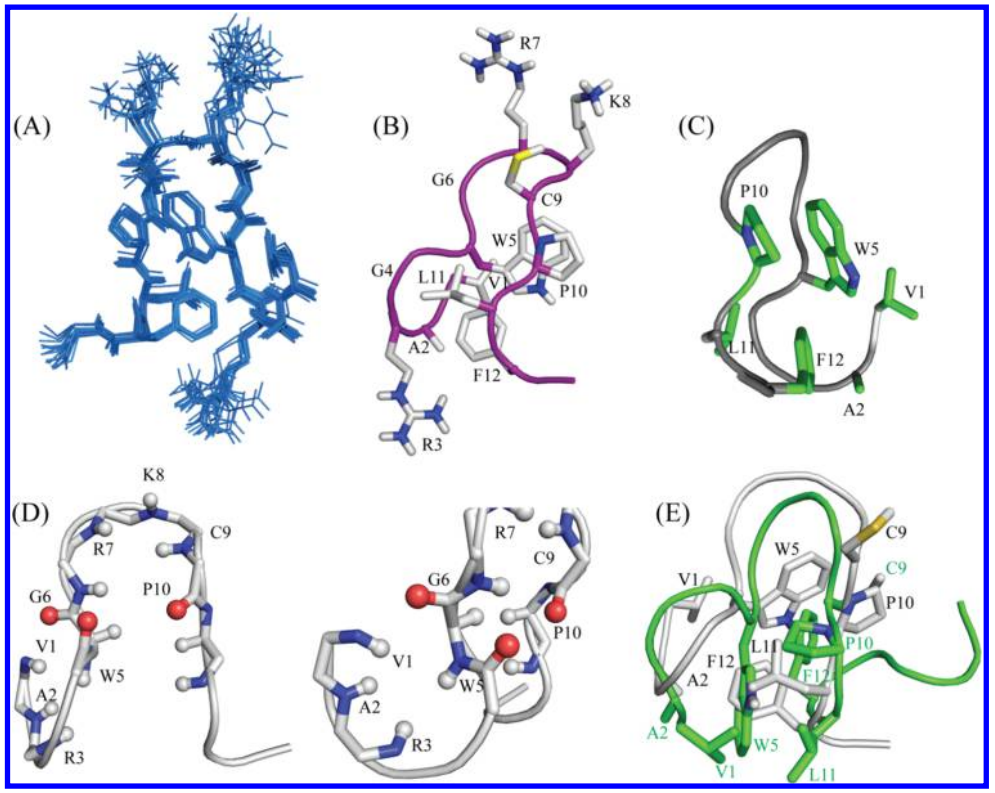

Figure 8. (A) Stick representation of the ensemble of 20 lowest energy structures of VG13P in LPS micelles showing a convergence of the backbone (N, C^{α}, and C′) and side chain atoms. (B) Cartoon and stick representation of a single representative structure of VG13P in LPS micelles characterized by two consecutive turns, closely resembling a rocking chair. (C) Cartoon and stick representation of VG13P with the hydrophobic and aromatic residues that form the hydrophobic core that drives structural stabilization in LPS micelles, highlighted in green. (D) Cartoon, ball and stick representation of VG13P showing the plausible backbone/side chain hydrogen bond and side chain/side chain van der Waals interactions that are thought to play an important role in structural stabilization. (E) An overlay of the single structures of VG16KRKP (green cartoon) and VG13P (gray cartoon) showing the structural differences owing to the orientation of their respective hydrophobic hubs.

the ensemble, having an average backbone and side chain RMSD value of 0.08 and 0.71, respectively (Table 3). The 3D structure closely resembles a rocking chair (Figure 8B), where the major hydrophobic stabilizing force was provided by a hydrophobic cluster formed by Gly4-Trp5-Gly6-Pro10-Leu11-Phe12 (Figure 8C). The structure contains two consecutive turns: one at the N-terminal end formed by Val1-Ala2-Arg3-Gly4, and the other is at the central region containing Gly6-Arg7-Lys8-Cys9-Pro10 (Figure 8D), which were evident from several NH-NH NOEs such as Ala2/Arg3 and Trp5 or Arg7 and Cys9 (Figure S3). Both turns were stabilized by hydrogen bonding between the backbone amide proton of Val1 and the carbonyl group of Trp5/Gly6, and also between the amide proton of Gly6 and the carbonyl group of Pro10 (Figure 8D). Strikingly, Val1 and Ala2 also shared close contacts with Trp5, Leu11 and Phe12 (Figure 8C left panel). However, the positively charged Arg3, Arg7, and Lys8 residues were directed away from the hydrophobic face, assuming an amphipathic orientation (Figure 8B). The side chains of the positively charged residues remained relatively flexible as observed from the ensemble structure and can be thought to mediate the initial electrostatic interaction with the negatively charged phosphate head groups of LPS. Interestingly, the distance between guanidinium and ammonium groups of Arg7 and Lys8, respectively, was ∼12 Å, which is close to the interphosphate distance between the two phosphate head groups of LPS (Figure 8B). An overlay of the cartoon structures of VG16KRKP (marked in gray) and VG13P (marked in green) shows the difference in the oriented hydrophobic hub (Figure 8E) where VG13P is seen to form a more compressed hydrophobic core than that of VG16KRKP. This is not surprising, as the mutation of Lys6 to Gly in VG13P helped the N-terminal end to fold back on the peptide structure forming a

Table 3. Summary of Structural Statistics for the 20 Lowest Energy Ensemble Structures of VG16KRKP in LPS

Distance restraints	
intraresidue ($i - j = 0$)	26
sequential ($\|i - j\| = 1$)	44
medium-range ($2 \leq \|i - j\| \leq 4$)	16
long-range ($\|i - j\| \geq 5$)	17
total	103
Angular restraints	
Φ	11
Ψ	11
Distance restraints from violations (≥0.4 Å)	0
Deviation from mean structure (Å)	
average backbone to mean structure	0.08 ± 0.04
average heavy atom to mean structure	0.71 ± 0.19
Ramachandran plot[a]	
% residues in the most favorable and additionally allowed regions	90.5
% residues in the generously allowed region	9.5
% residues in the disallowed region	0.0

[a]Procheck NMR based analysis.

DOI: 10.1021/acs.biochem.6b01229
Biochemistry 2017, 56, 1348−1362

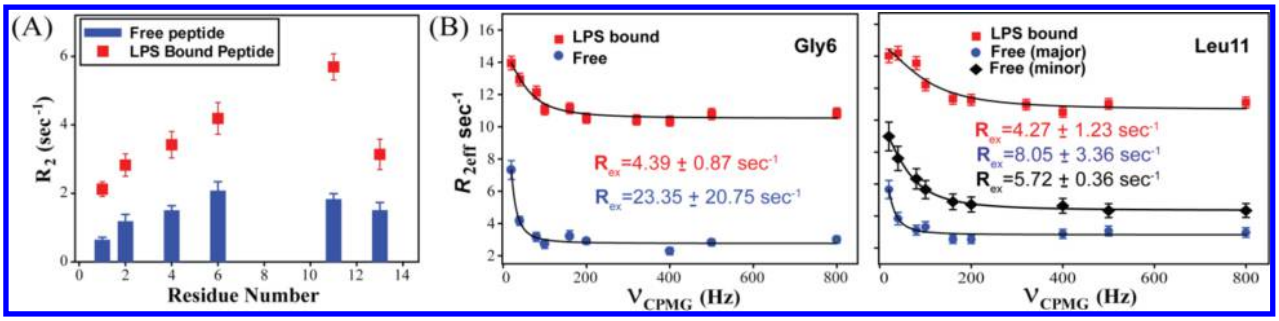

Figure 9. ^{15}N relaxation parameters R_2 (transverse relaxation rate; for the τ_{cp} = 450 μs) as determined for these labeled amino acids at 800 MHz field strength are shown. The comparison of R_2 values of VG13P peptide in the absence and presence of LPS are shown in (A). In (B), the ^{15}N relaxation dispersion profiles and conformational exchange rates of ^{15}N labeled residues Gly6 and Leu11, respectively, in the absence and presence of LPS, as determined at 800 MHz field strength are shown.

tight turn stabilized by interactions between Val1/Ala2 with Trp5/Leu11/Phe12 (Figure 8E). It must be noted here that Gly and Pro have a tendency to influence the formation of short loops of 2−10 amino acid residues and are frequently found in such structures playing a vital role in chain compaction in initial steps of protein folding.[66] Thus, replacement of Lys6 by Gly in VG13P plays a crucial role in compacting the peptide hydrophobic core by CH-π interaction between Gly4 and Phe12 (Figure 8C). This compact structure could be directly correlated with its enhanced endotoxin neutralization properties.

Backbone Dynamics of VG13P Structure in LPS Micelles. To further rationalize the structural stability of peptide in solution containing LPS, the backbone dynamical properties of peptide were studied at an atomic resolution using ^{15}N NMR relaxation parameters (R_2) and CPMG (Figure 9). These relaxation rates are strongly influenced by local motions in the polypeptide chain; therefore, they can provide useful information for depicting the regions of motional restrictions formed due to either hydrophobic or electrostatic interactions.[57] In completely unstructured peptides, the R_2 rates are relatively uniform (Figure 9A), but when hydrophobic residues participate in either local- or long-range contacts (further stabilized by electrostatic/charge interactions), this tends to restrict the motions of the peptide backbone in a manner that leads to exchange broadening of NMR signals due to conformational flexibility.[56] This effect can often be detected as local regions of unusually high R_2 values influenced by chemical exchange on the microsecond-to-millisecond (μs-ms) time scale. In other words, the limited conformational sampling is expected due to reduction of conformational exchange. In our study, we used selectively ^{15}N labeled peptide, therefore, the backbone ^{15}N relaxation parameteres cannot be obtained uniformly along the peptide sequence. Nevertheless, the sparsely obtained relaxation data also provided useful insights into the peptide conformational dynamics: (a) N- and C-terminal residues of peptide are relatively flexible and exhibit fast nanosecond to pico-second time scale motions as inferred by the negative hetNOE values of terminal residues (Figure 5C); (b) the peptide chain is relatively more restricted toward central region of peptide sequence as inferred by the elevated hetNOE and R_2 values of residues Gly6 and Leu11 (Figure 5C). The R_2 values of free peptide have also been compared to those obtained in the presence of 28 μM LPS (Figure 9A). The comparison clearly revealed that there is systemic increase in the R_2 values in the presence of LPS, suggesting that the rotational correlation time of peptide has decreased owing to its interaction with LPS in the solution. This is also well in concordance with conformational exchange parameters derived from ^{15}N relaxation dispersion experiments (Figure 9B). CPMG is an important relaxation method which provides μs-ms dynamics of ^{15}N-labeled peptide in the absence and presence of LPS. Surprisingly, only two of the VG13P residues, namely, Gly6 and Leu11, exhibited relaxation dispersion effects both in the free and bound form of LPS. It is worth mentioning that the Leu11 residue is present next to Pro10 and the residue Gly6 is the first residue of the flexible turn comprised of Gly6-Arg7-Lys8-Cys9 (Figure 9B). It is well-known that the proline residue often exhibits cis−trans conformational exchange and the presence of two well-separated amide cross peaks of Leu11 (Figure 6) might reflect this phenomenon. However, in the presence of LPS, this conformational exchange is limited, as inferred by the decreased chemical exchange parameters for both Gly6 and Leu11 residues (Figure 9B), despite the fact, that their effective R_2 values have increased. The obvious reason is that Gly6 and Leu11 are instrumental for folding the VG13P peptide in LPS, which was evident from Figure 6C and Table 2. Altogether, the structural and dynamics features of VG13P peptide in the presence of LPS suggest that the glycine-mediated compact peptide conformation is crucial for its efficient binding with LPS and it further causes an increased anti-endotoxin activity.

In conclusion, NMR investigations of structural and dynamics features were very essential to rationalize the increased antimicrobial activity of peptide VG13P, derived from VG16KRKP, which led to an enhancement in its LPS neutralization abilities *in vitro* while retaining its antimicrobial properties. The analogue VG13P peptide was found to be equally potent against Gram-negative bacterial plant pathogens of *Xanthomonas* species and the opportunistic fungal pathogens. LPS neutralization effects were seen to be boosted with the peptide being able to neutralize 10-fold higher concentrations of LPS, as opposed to its parent peptide. We have also elucidated the folding of VG13P in LPS micelle in a systematic way, providing its 3D structure and correlated its structural features with the corresponding enhanced LPS neutralization activity. The replacement of Lys6 by Gly, with Gly6 being a flexible amino acid with a short side chain, allowed the N-terminal end to fold back on itself forming a turn, thereby making the hydrophobic hub more compact. Gly4 also contributed in the hydrophobic packing through CH-π interaction with Phe12. Structurally, the two peptides were different in the orientation of their hydrophobic and aromatic residues, with the more condensed hydrophobic hub in VG13P

DOI: 10.1021/acs.biochem.6b01229
Biochemistry 2017, 56, 1348−1362

facilitating increased structure stabilization in the context of LPS micelles that manifested itself in the form of enhanced LPS neutralizing effects. Collectively, we have presented a shorter equally potent antimicrobial analogue peptide VG13P with enhanced antiendotoxin properties that can further help in the development of novel antimicrobial and/or antisepsis agents.

■ ASSOCIATED CONTENT

Supporting Information

The Supporting Information is available free of charge on the ACS Publications website at DOI: 10.1021/acs.biochem.6b01229.

Conditions for semiquantitaive PCR experiments (Figure S1); NOESY and trNOESY spectra of VG13P in the absence and presence of LPS, respectively (Figure S2); Selected amide region of trNOESY spectra (Figure S3); Determination of LPS binding transition point at an atomic resolution using eq 8 (Figure S4) (PDF)

■ AUTHOR INFORMATION

Corresponding Authors

*(D.K.) E-mail: dineshcbmr@gmail.com. Tel: +91-8005409932.

*(A.B.) E-mail: anirbanbhunia@gmail.com, bhunia@jcbose.ac.in. Tel: +91-33-2569 3336.

ORCID

Anirban Bhunia: 0000-0002-8752-2842

Author Contributions

A.B. conceived, designed, and funded the research work; A.D. synthesized the ^{15}N labeled peptide, conducted biophysical experiments, analyzed the results, calculated the three-dimensional structure using NMR spectroscopy, and wrote the manuscript; N.J. and D.K. performed the CPMG experiments, analyzed the data, and wrote the manuscript; H.I. and S.D. conducted and analyzed cell line experiments under the guidance of K.B.; K.B., D.K., and A.B. analyzed the data and wrote the manuscript. All authors reviewed the manuscript.

Funding

This study was supported partly by Bose Institute (Plan Project-II (to AB)), India and partly by Indo-Swedish research collaboration (DST-VR) (to A.B.). A.D., S.D., and H.I. are grateful to CSIR, UGC, and Bose Institute, Government of India, for their Senior, Junior, and Institute research fellowships, respectively. Central Instrument Facility (CIF) of Bose Institute is greatly acknowledged.

Notes

The authors declare no competing financial interest.

■ DEDICATION

The paper is dedicated to Professor Dr. Thomas Peters, University of Lübeck, Germany, for his 60th birthday.

■ ABBREVIATIONS

(AMP), antimicrobial peptide; (LPS), lipopolysaccharide; (TOCSY), total correlation spectroscopy; (trNOESY), transferred nuclear Overshauser effect spectroscopy; (hetNOE), heteronuclear nuclear Overhauser effect; (HSQC), heteronuclear single quantum correlation; (CPMG), Carr−Purcell−Meiboom−Gill; (MIC), minimum inhibitory concentration; (LBP), lipopolysaccharide binding protein; (TLR), toll like receptor; (NPN), 1-*N*-phenyl naphthylamine; (DSS), 4, 4-dimethyl-4-silapentane-1-sulfonic acid; (NKE), normal kidney epithelial cell; (CFU), colony forming unit; (EU), endotoxin unit

■ REFERENCES

(1) Levy, S. B., and Marshall, B. (2004) Antibacterial resistance worldwide: causes, challenges and responses. *Nat. Med.* *10*, S122−129.

(2) Zasloff, M. (2002) Antimicrobial peptides of multicellular organisms. *Nature* *415*, 389−395.

(3) Walsh, F. M., and Amyes, S. G. B. (2004) Microbiology and drug resistance mechanisms of fully resistant pathogens. *Curr. Opin. Microbiol.* *7*, 439−444.

(4) Taubes, G. (2008) The Bacteria Fight Back. *Science* *321*, 356−361.

(5) Bhunia, A., Mohanram, H., Domadia, P. N., Torres, J., and Bhattacharjya, S. (2009) Designed beta-boomerang antiendotoxic and antimicrobial peptides: structures and activities in lipopolysaccharide. *J. Biol. Chem.* *284*, 21991−22004.

(6) Snyder, D. S., and McIntosh, T. J. (2000) The lipopolysaccharide barrier: correlation of antibiotic susceptibility with antibiotic permeability and fluorescent probe binding kinetics. *Biochemistry* *39*, 11777−11787.

(7) Rosenfeld, Y., Barra, D., Simmaco, M., Shai, Y., and Mangoni, M. L. (2006) A synergism between temporins toward gram-negative bacteria overcomes resistance imposed by the lipopolysaccharide protective layer. *J. Biol. Chem.* *281*, 28565−28574.

(8) Martin, G. S., Mannino, D. M., Eaton, S., and Moss, M. (2003) The epidemiology of sepsis in the United States from 1979 through 2000. *N. Engl. J. Med.* *348*, 1546−1554.

(9) Angus, D. C., and van der Poll, T. (2013) Severe sepsis and septic shock. *N. Engl. J. Med.* *369*, 840−851.

(10) Fjell, C. D., Hiss, J. A., Hancock, R. E., and Schneider, G. (2012) Designing antimicrobial peptides: form follows function. *Nat. Rev. Neurosci.* *11*, 37−51.

(11) Hardaway, R. M. (2000) A review of septic shock. *Am. Surg.* *66*, 22−29.

(12) Poltorak, A., He, X., Smirnova, I., Liu, M. Y., Van Huffel, C., Du, X., Birdwell, D., Alejos, E., Silva, M., Galanos, C., Freudenberg, M., Ricciardi-Castagnoli, P., Layton, B., and Beutler, B. (1998) Defective LPS signaling in C3H/HeJ and C57BL/10ScCr mice: mutations in Tlr4 gene. *Science* *282*, 2085−2088.

(13) Nikaido, H. (1994) Prevention of drug access to bacterial targets: permeability barriers and active efflux. *Science* *264*, 382−388.

(14) Peleg, A. Y., and Hooper, D. C. (2010) Hospital-Acquired Infections Due to Gram-Negative Bacteria. *N. Engl. J. Med.* *362*, 1804−1813.

(15) Folgori, L., Livadiotti, S., Carletti, M., Bielicki, J., Pontrelli, G., Ciofi Degli Atti, M. L., Bertaina, C., Lucignano, B., Ranno, S., Carretto, E., Muraca, M., Sharland, M., and Bernaschi, P. (2014) Epidemiology and clinical outcomes of multidrug-resistant, gram-negative bloodstream infections in a European tertiary pediatric hospital during a 12-month period. *Pediatr Infect Dis J.* *33*, 929−932.

(16) Kaye, K. S., and Pogue, J. M. (2015) Infections Caused by Resistant Gram-Negative Bacteria: Epidemiology and Management. *Pharmacotherapy* *35*, 949−962.

(17) Hancock, R. E., and Sahl, H. G. (2006) Antimicrobial and host-defense peptides as new anti-infective therapeutic strategies. *Nat. Biotechnol.* *24*, 1551−1557.

(18) Kondejewski, L. H., Jelokhani-Niaraki, M., Farmer, S. W., Lix, B., Kay, C. M., Sykes, B. D., Hancock, R. E., and Hodges, R. S. (1999) Dissociation of antimicrobial and hemolytic activities in cyclic peptide diastereomers by systematic alterations in amphipathicity. *J. Biol. Chem.* *274*, 13181−13192.

(19) Hancock, R. E., and Lehrer, R. (1998) Cationic peptides: a new source of antibiotics. *Trends Biotechnol.* *16*, 82−88.

(20) Mangoni, M. L., Epand, R. F., Rosenfeld, Y., Peleg, A., Barra, D., Epand, R. M., and Shai, Y. (2008) Lipopolysaccharide, a key molecule involved in the synergism between temporins in inhibiting bacterial

DOI: 10.1021/acs.biochem.6b01229
Biochemistry 2017, 56, 1348−1362

growth and in endotoxin neutralization. *J. Biol. Chem.* *283*, 22907−22917.
(21) Brogden, K. A. (2005) Antimicrobial peptides: pore formers or metabolic inhibitors in bacteria? *Nat. Rev. Microbiol.* *3*, 238−250.
(22) Brown, K. L., and Hancock, R. E. (2006) Cationic host defense (antimicrobial) peptides. *Curr. Opin. Immunol.* *18*, 24−30.
(23) Hancock, R. E., and Diamond, G. (2000) The role of cationic antimicrobial peptides in innate host defences. *Trends Microbiol.* *8*, 402−410.
(24) Scott, M. G., Davidson, D. J., Gold, M. R., Bowdish, D., and Hancock, R. E. (2002) The human antimicrobial peptide LL-37 is a multifunctional modulator of innate immune responses. *J. Immunol.* *169*, 3883−3891.
(25) Haney, E. F., and Vogel, H. J. (2009) NMR of Antimicrobial Peptides. *Annu. Rep. NMR Spectrosc.* *65*, 1−51.
(26) Matsuzaki, K. (1998) Magainins as paradigm for the mode of action of pore forming polypeptides. *Biochim. Biophys. Acta, Rev. Biomembr.* *1376*, 391−400.
(27) Shai, Y. (2002) Mode of action of membrane active antimicrobial peptides. *Biopolymers* *66*, 236−248.
(28) Papo, N., and Shai, Y. (2003) Can we predict biological activity of antimicrobial peptides from their interactions with model phospholipid membranes? *Peptides* *24*, 1693−1703.
(29) Prenner, E. J., Lewis, R. N., Neuman, K. C., Gruner, S. M., Kondejewski, L. H., Hodges, R. S., and McElhaney, R. N. (1997) Nonlamellar phases induced by the interaction of gramicidin S with lipid bilayers. A possible relationship to membrane-disrupting activity. *Biochemistry* *36*, 7906−7916.
(30) Bhunia, A., Mohanram, H., Domadia, P. N., Torres, J., and Bhattacharjya, S. (2009) Designed beta-boomerang antiendotoxic and antimicrobial peptides: structures and activities in lipopolysaccharide. *J. Biol. Chem.* *284*, 21991−22004.
(31) Bhunia, A., Ramamoorthy, A., and Bhattacharjya, S. (2009) Helical hairpin structure of a potent antimicrobial peptide MSI-594 in lipopolysaccharide micelles by NMR spectroscopy. *Chem. - Eur. J.* *15*, 2036−2040.
(32) Datta, A., Bhattacharyya, D., Singh, S., Ghosh, A., Schmidtchen, A., Malmsten, M., and Bhunia, A. (2016) Role of Aromatic Amino Acids in Lipopolysaccharide and Membrane Interactions of Antimicrobial Peptides for Use in Plant Disease Control. *J. Biol. Chem.* *291*, 13301−13317.
(33) Hancock, R. E., and Patrzykat, A. (2002) Clinical development of cationic antimicrobial peptides: from natural to novel antibiotics. *Curr. Drug Targets: Infect. Disord.* *2*, 79−83.
(34) Powell, W. A., Catranis, C. M., and Maynard, C. A. (1995) Synthetic antimicrobial peptide design. *Mol. Plant-Microbe Interact.* *8*, 792−794.
(35) van Abel, R. J., Tang, Y. Q., Rao, V. S., Dobbs, C. H., Tran, D., Barany, G., and Selsted, M. E. (1995) Synthesis and characterization of indolicidin, a tryptophan-rich antimicrobial peptide from bovine neutrophils. *Int. J. Pept. Protein Res.* *45*, 401−409.
(36) Tiozzo, E., Rocco, G., Tossi, A., and Romeo, D. (1998) Wide-spectrum antibiotic activity of synthetic, amphipathic peptides. *Biochem. Biophys. Res. Commun.* *249*, 202−206.
(37) Lyu, Y., Yang, Y., Lyu, X., Dong, N., and Shan, A. (2016) Antimicrobial activity, improved cell selectivity and mode of action of short PMAP-36-derived peptides against bacteria and Candida. *Sci. Rep.* *6*, 27258.
(38) Deslouches, B., Steckbeck, J. D., Craigo, J. K., Doi, Y., Mietzner, T. A., and Montelaro, R. C. (2013) Rational design of engineered cationic antimicrobial peptides consisting exclusively of arginine and tryptophan, and their activity against multidrug-resistant pathogens. *Antimicrob. Agents Chemother.* *57*, 2511−2521.
(39) Datta, A., Ghosh, A., Airoldi, C., Sperandeo, P., Mroue, K. H., Jiménez-Barbero, J., Kundu, P., Ramamoorthy, A., and Bhunia, A. (2015) Antimicrobial Peptides: Insights into Membrane Permeabilization, Lipopolysaccharide Fragmentation and Application in Plant Disease Control. *Sci. Rep.* *5*, 11951.
(40) Giuliani, A., and Rinaldi, A. C. (2011) Beyond natural antimicrobial peptides: multimeric peptides and other peptidomimetic approaches. *Cell. Mol. Life Sci.* *68*, 2255−2266.
(41) Rotem, S., and Mor, A. (2009) Antimicrobial peptide mimics for improved therapeutic properties. *Biochim. Biophys. Acta, Biomembr.* *1788*, 1582−1592.
(42) Marr, A. K., Gooderham, W. J., and Hancock, R. E. (2006) Antibacterial peptides for therapeutic use: obstacles and realistic outlook. *Curr. Opin. Pharmacol.* *6*, 468−472.
(43) Chan, W. C., and White, P. D. (2000) *Fmoc Solid Phase Peptide Synthesis*; Oxford University Press, Oxford, U.K.
(44) Ghosh, A., Datta, A., Jana, J., Kar, R. K., Chatterjee, C., Chatterjee, S., and Bhunia, A. (2014) Sequence context induced antimicrobial activity: insight into lipopolysaccharide permeabilization. *Mol. BioSyst.* *10*, 1596−1612.
(45) Montecucco, A., and Biamonti, G. (2007) Cellular response to etoposide treatment. *Cancer Lett.* *252*, 9−18.
(46) Marion, D., Ikura, M., Tschudin, R., and Bax, A. (1989) Rapid recording of 2D NMR spectra without phase cycling. Application to the study of hydrogen exchange in proteins. *J. Magn. Reson.* *85*, 393−399.
(47) Sklenar, V., Piotto, M., Leppik, R., and Saudek, V. (1993) Gradient-tailored water suppression for 1H-15N HSQC experiments optimized to retain full sensitivity. *J. Magn. Reson., Ser. A* *102*, 241−245.
(48) Peng, J. W., and Wagner, G. (1992) Mapping of the spectral densities of N-H bond motions in eglin c using heteronuclear relaxation experiments. *Biochemistry* *31*, 8571−8586.
(49) Farrow, N. A., Muhandiram, R., Singer, A. U., Pascal, S. M., Kay, C. M., Gish, G., Shoelson, S. E., Pawson, T., Forman-Kay, J. D., and Kay, L. E. (1994) Backbone dynamics of a free and phosphopeptide-complexed Src homology 2 domain studied by 15N NMR relaxation. *Biochemistry* *33*, 5984−6003.
(50) Spyracopoulos, L. (2006) A suite of Mathematica notebooks for the analysis of protein main chain 15N NMR relaxation data. *J. Biomol. NMR* *36*, 215−224.
(51) Loria, J. P., Rance, M., and Palmer, A. G. (1999) A relaxation-compensated Carr-Purcell-Meiboom-Gill sequence for characterizing chemical exchange by NMR spectroscopy. *J. Am. Chem. Soc.* *121*, 2331−2332.
(52) Tollinger, M., Skrynnikov, N. R., Mulder, F. A., Forman-Kay, J. D., and Kay, L. E. (2001) Slow dynamics in folded and unfolded states of an SH3 domain. *J. Am. Chem. Soc.* *123*, 11341−11352.
(53) Ishima, R., and Torchia, D. A. (2003) Extending the range of amide proton relaxation dispersion experiments in proteins using a constant-time relaxation-compensated CPMG approach. *J. Biomol. NMR* *25*, 243−248.
(54) Vallurupalli, P., Hansen, D. F., Lundström, P., and Kay, L. E. (2009) CPMG relaxation dispersion NMR experiments measuring glycine 1H alpha and 13C alpha chemical shifts in the 'invisible' excited states of proteins. *J. Biomol. NMR* *45*, 45−55.
(55) Loria, J. P., Berlow, R. B., and Watt, E. D. (2008) Characterization of enzyme motions by solution NMR relaxation dispersion. *Acc. Chem. Res.* *41*, 214−221.
(56) Dyson, H. J., and Wright, P. E. (2001) Nuclear magnetic resonance methods for elucidation of structure and dynamics in disordered states. *Methods Enzymol.* *339*, 258−270.
(57) Bai, Y., and Nussinov, R. (2006) Protein Folding Protocols, *Methods Mol. Biol.*, Vol. *350*, Humana Press, New York.
(58) Domadia, P. N., Bhunia, A., Ramamoorthy, A., and Bhattacharjya, S. (2010) Structure, interactions, and antibacterial activities of MSI-594 derived mutant peptide MSI-594F5A in lipopolysaccharide micelles: role of the helical hairpin conformation in outer-membrane permeabilization. *J. Am. Chem. Soc.* *132*, 18417−18428.
(59) Laskowski, R. A., Rullmannn, J. A. C., MacArthur, M. W., Kaptein, R., and Thornton, J. M. (1996) AQUA and PROCHECK-NMR: programs for checking the quality of protein structures solved by NMR. *J. Biomol. NMR* *8*, 477−486.

DOI: 10.1021/acs.biochem.6b01229
Biochemistry 2017, 56, 1348−1362

(60) Kumaki, Y., Kawano, K., Hikichi, K., Matsumoto, T., and Matsushima, N. (2008) A circular loop of the 16-residue repeating unit in ice nucleation protein. *Biochem. Biophys. Res. Commun.* *371*, 5−9.
(61) Zondlo, N. J. (2013) Aromatic-proline interactions: electronically tunable CH/π interactions. *Acc. Chem. Res.* *46*, 1039−1049.
(62) Cappiello, F., Di Grazia, A., Segev-Zarko, L. A., Scali, S., Ferrera, L., Galietta, L., Pini, A., Shai, Y., Di, Y. P., and Mangoni, M. L. (2016) Esculentin-1a-Derived Peptides Promote Clearance of Pseudomonas aeruginosa Internalized in Bronchial Cells of Cystic Fibrosis Patients and Lung Cell Migration: Biochemical Properties and a Plausible Mode of Action. *Antimicrob. Agents Chemother.* *60*, 7252−7262.
(63) Di Grazia, A., Cappiello, F., Cohen, H., Casciaro, B., Luca, V., Pini, A., Di, Y. P., Shai, Y., and Mangoni, M. L. (2015) D-Amino acids incorporation in the frog skin-derived peptide esculentin-1a(1−21)NH2 is beneficial for its multiple functions. *Amino Acids* *47*, 2505−2519.
(64) Guan, J. Y., Foerster, J. M., Drijfhout, J. W., Timmer, M., Blok, A., Ullmann, G. M., and Ubbink, M. (2014) An ensemble of rapidly interconverting orientations in electrostatic protein-peptide complexes characterized by NMR spectroscopy. *ChemBioChem* *15*, 556−566.
(65) Yu, L., Tan, M., Ho, B., Ding, J. L., and Wohland, T. (2006) Determination of critical micelle concentrations and aggregation numbers by fluorescence correlation spectroscopy: aggregation of a lipopolysaccharide. *Anal. Chim. Acta* *556*, 216−225.
(66) Krieger, F., Möglich, A., and Kiefhaber, T. (2005) Effect of proline and glycine residues on dynamics and barriers of loop formation in polypeptide chains. *J. Am. Chem. Soc.* *127*, 3346−3352.

DOI: 10.1021/acs.biochem.6b01229
Biochemistry 2017, 56, 1348−1362

Biochimica et Biophysica Acta 1863 (2016) 1472–1489

Contents lists available at ScienceDirect

Biochimica et Biophysica Acta

journal homepage: www.elsevier.com/locate/bbamcr

Ganglioside GM2 mediates migration of tumor cells by interacting with integrin and modulating the downstream signaling pathway

Manjari Kundu [a], Barun Mahata [a], Avisek Banerjee [a], Sohini Chakraborty [b], Shibjyoti Debnath [a], Sougata Sinha Ray [c], Zhumur Ghosh [b], Kaushik Biswas [a,*]

[a] Division of Molecular Medicine, Bose Institute, Kolkata, West Bengal 700054, India
[b] The Bioinformatics Center, Bose Institute, Kolkata, West Bengal 700054, India
[c] Wipro GE Healthcare, Kolkata, India

ARTICLE INFO

Article history:
Received 1 September 2015
Received in revised form 1 April 2016
Accepted 6 April 2016
Available online 8 April 2016

Keywords:
Ganglioside
Tumor cell migration
Tumor cell proliferation, integrin
MAP kinases
Microarray
RNAi

ABSTRACT

The definitive role of ganglioside GM2 in mediating tumor-induced growth and progression is still unknown. Here we report a novel role of ganglioside GM2 in mediating tumor cell migration and uncovered its mechanism. Data shows differential expression levels of GM2-synthase as well as GM2 in different human cancer cells. siRNA mediated knockdown of GM2-synthase in CCF52, A549 and SK-RC-26B cells resulted in significant inhibition of tumor cell migration as well as invasion *in vitro* without affecting cellular proliferation. Over-expression of GM2-synthase in low-GM2 expressing SK-RC-45 cells resulted in a consequent increase in migration thus confirming the potential role GM2 and its downstream partners play in tumor cell migration and motility. Further, treatment of SK-RC-45 cells with exogenous GM2 resulted in a dramatic increase in migratory and invasive capacity with no change in proliferative capacity, thereby confirming the role of GM2 in tumorigenesis specifically by mediating tumor migration and invasion. Gene expression profiling of GM2-synthase silenced cells revealed altered expression of several genes involved in cell migration primarily those controlling the integrin mediated signaling. GM2-synthase knockdown resulted in decreased phosphorylation of FAK, Src as well as Erk, while over-expression and/or exogenous GM2 treatment caused increased FAK and Erk phosphorylation respectively. Again, GM2 mediated invasion and Erk phosphorylation is blocked in integrin knockdown SK-RC-45 cells, thus confirming that GM2 mediated migration and phosphorylation of Erk is integrin dependent. Finally, confocal microscopy suggested co-localization while co-immunoprecipitation and surface plasmon resonance (SPR) confirmed direct interaction of membrane bound ganglioside, GM2 with the integrin receptor.

1. Introduction

Sialylated glycosphingolipids (GSLs) or gangliosides are integral components of eukaryotic cell membranes that are involved in critical cellular functions [1,2]. Tumor gangliosides were shown to be expressed and shed actively into the tumor microenvironment [3–5]. These tumor-shed gangliosides modulate the function of adjacent tumor cells either by promoting or inhibiting their invasion, migration or angiogenic property or by suppressing and interfering with host cellular immune response thus acting as a double edged sword in cancer progression. Enhanced expression of disialylgangliosides like GD3/GD2/GM2 was observed in various cancer cells [6–9]. GM2/GD2-synthase mRNA expression was found to be elevated in gastrointestinal cancers signifying a correlation of GM2 with this disease [10]. Interestingly in spite of this deregulated expression of gangliosides as well as ganglioside synthetic enzymes, tumor cells themselves escape their deleterious effects and continue to grow and progress. This suggests that either tumor cells have specific machinery to deal with these products or some of them actually enhance tumor growth and survival.

Among the various complex gangliosides, GM2 is one of the key members of GSLs involved in various intercellular crosstalks modulating signal transduction, cell cycle events, cell adhesion and cell motility [11,12]. Several studies have demonstrated that tumor-shed gangliosides, including GM2 play a critical role as modulators of the host immune system [13–18]. Studies showed that GM2 could disarm the immune system either by killing the T cells or by causing defective antigen presentation by impairing dendritic cell function [3,5,9,19]. Over-expression of GD3-synthase in a GD3/GD2-negative human osteosarcoma subline caused increased cell migration and invasiveness [20]. On the other hand, GM3 was found to inhibit hepatoma cell motility [21], thereby suggesting complex and differential roles of gangliosides, in tumor growth, progression and metastasis. Anti-ganglioside GM2

Abbreviations: GSL, Glycosphingolipid; MAPK, Mitogen activated protein kinase; FAK, Focal adhesion kinase; RCC, Renal cell carcinoma; GBM, Glioblastoma multiforme; DRGs, Differentially regulated genes; GO, Gene ontology; BiNGO, Biological network gene ontology; RMA, Robust multichip averaging algorithm; PFA, Paraformaldehyde; LSA, Lipid bound sialic acid; CerK, Ceramide kinase.

* Corresponding author at: Division of Molecular Medicine, Bose Institute, Kolkata, P1/12 CIT Scheme VIIM, Kolkata, West Bengal 700054, India.
E-mail address: kbiswas_1@yahoo.com (K. Biswas).

http://dx.doi.org/10.1016/j.bbamcr.2016.04.004
0167-4889/

antibodies have been used in clinical trials, and mostly were associated with better prognosis [12,22,23]. However, it remained unclear whether the anti-tumoral activities observed were in part due to the antibody mediated reversal of GM2's immunosuppressive role on the host immune system or GM2 might actually promote tumor growth through a mechanism independent of its immunosuppressive activity.

Very few studies have addressed the mechanistic details as to how these gangliosides specifically GM2 might modulate tumor growth and progression. Various evidences suggested the involvement of ganglioside GM3 complexed with the integrin receptor and tetraspanin (CD9) inhibiting integrin-dependent signaling and cell motility in non-invasive KK47 human bladder cancer cells versus invasive YTS1 cells [24,25]. GM3 was found to regulate oncogenic transformation through its involvement with MAPK pathway in a study with MEFs isolated from GM3-synthase knockout mice [26]. Tumor-shed ganglioside GD3 enhanced adhesion in melanoma cells by augmenting clustering of integrin receptors in lipid rafts [27] as well as increased invasiveness of gliomas by enhancing the signal of platelet derived growth factor in glycolipid-enriched microdomain (GEM)/raft [28]. Again, neuraminidase (NEU3), a key enzyme involved in ganglioside catabolism was recently identified as a key regulator of β1-integrin recycling pathway and FAK/Akt signaling demonstrating its crucial role in RCC malignancy [29]. Very recently a report from our laboratory have provided the first evidence suggesting a link between GM2 and epithelial–mesenchymal transition in tumors, though the mechanism is yet to be defined [30].

Evidence presented in this study demonstrates a novel role of ganglioside GM2 in mediating tumor cell migration *in vitro* by interacting with the integrin-β1 receptor. Neither silencing or over-expressing GM2-synthase or exogenous addition of GM2 affected tumor cell proliferation suggesting that GM2 did not have any significant role in tumor cell proliferation. However, siRNA mediated silencing of GM2-synthase in GM2 over-expressing tumor cells, CCF52, A549 and SK-RC-26B reduced migration as well as invasion of the cells. Again, over-expression of the same resulted in a significant increase of cellular migration, suggesting a plausible role of GM2 in tumor cell migration *in vitro*. Further, exogenous GM2 treatment caused a dramatic increase in migration as well as invasion of tumor cells confirming the ability of GM2 alone in promoting tumor cell migration as well as invasion. DNA microarray analysis suggests involvement of the integrin-β1 and its signaling machinery, as well as cytoskeletal remodeling in GM2-mediated tumor cell migration. This was validated by real time PCR experiments, western blots of several key members of integrin signaling pathway and related cytoskeletal alterations by confocal microscopy. The role of integrin-β1 in GM2 mediated cell migration was further confirmed by significantly reduced invasion in integrin-β1 silenced tumor cells compared to wild type cells treated with GM2. Again silencing of GM2-synthase caused decreased phosphorylation of key mediators of integrin signaling pathway like FAK, Src, and Erk, while over-expression of GM2 or its exogenous addition increased FAK and Erk phosphorylation respectively. This suggests not only the involvement of integrin-β1 but also the involvement of integrin signaling machinery in GM2 mediated tumor cell migration. That the phosphorylation of Erk in integrin-β1 knockdown SK-RC-45 cells is blocked even in the presence of GM2, confirmed that indeed GM2 mediated tumor cell migration is integrin-β1 dependent and involves modulation of ERK–MAPK pathway. Confocal microscopy demonstrated positive co-localization suggesting a plausible interaction between GM2 and integrin-β1, both at the endogenous cellular level and also after exogenous administration of GM2, which was further confirmed by co-immunoprecipitation studies. Finally, the kinetics of the interaction between GM2 and integrin-β1 was determined by surface plasmon resonance (SPR) analysis. We propose here that over-expression of select gangliosides like GM2 in tumor cells results in enhanced interaction with membrane bound integrin-β1 resulting in activation of the integrin mediated signaling cascades eventually leading to rearrangement of the actin cytoskeleton thereby enhancing migration in tumor cells.

2. Materials and method

2.1. Cell lines and authentication

Human renal cell carcinoma (RCC) cell lines SK-RC-45 and SK-RC-26B were obtained from Dr. Gerd Ritter (Ludwig Institute of Cancer Research, USA) and Dr. James H. Finke (Cleveland Clinic Foundation, USA). Human glioblastoma multiforme (GBM) cell lines CCF52 and CCF4 were obtained from Dr. Vogelbaum (Cleveland Clinic Foundation, Cleveland, Ohio) [9,19]. A549 (human lung adenocarcinoma), H1299 (human nonsmall cell lung carcinoma), HEK 293T (human embryonic kidney 293 T cell) and MCF7 (breast cancer) cells were procured from the central cell repository of the National Center for Cell Science (NCCS), Pune, India and cultured as suggested by the supplier. All the above cell lines except A549, H1299 and HEK 293T cells, were cultured in complete RPMI 1640, containing 10% FBS, 1 mM sodium pyruvate, 2 mM L-glutamine, non-essential amino acids, 100 units/ml penicillin, 100 μg/ml streptomycin and 50 μg/ml gentamycin sulfate at 37 °C with 5% CO_2. The lung cancer cell lines and HEK 293T were cultured in complete DMEM supplemented with 4.5 mg/ml glucose and other ingredients stated above. Cell lines were tested and authenticated periodically and before each experiment both by monitoring cellular morphology at regular intervals by comparative microscopic observation using both high and low culture densities, and evaluating cellular growth analysis by checking proliferation and growth by standard MTT assay.

2.2. Profiling of GM2-synthase and ganglioside GM2 in different tumor cell lines

2.2.1. Quantitative real time PCR

GM2-synthase expression in different tumor cells were compared by quantitative real time PCR (qRT-PCR). In brief, total RNA was extracted from different cancer cell lines like SK-RC-45, SK-RC-26B, CCF52, CCF4, A549 and H1299 with TRIzol reagent (Invitrogen BioServices India Pvt. Ltd), in accordance with the manufacturer's protocol. Concentration and purity of extracted RNA was quantified in a nanodrop spectrophotometer (Eppendorf India Limited) by measuring A260 and A280. The samples having an A260/A280 ratio greater or equivalent to 1.8 were used for cDNA synthesis using a Verso cDNA synthesis kit (Thermo Fisher Scientific). Briefly, 1 μg of RNA and 1 μl of oligo-dT (500 ng) were added and incubated at 65 °C for 10 min following which reverse transcriptase (RT)-enhancer, dNTP mix (0.5 mM final) and Verso enzyme mix including an RNase inhibitor were added to make a final volume of 20 μl. The cDNA synthesis was carried out at 50 °C for 1 h and then 95 °C for 2 min. GM2-synthase gene expression in different cell lines was assessed by qRT-PCR using SYBR green on a 7500 Fast Real-time PCR system (Applied Biosystem). Specific primers used are shown in Supplementary Table S1A. All mRNA quantification data were normalized to the expression of the housekeeping gene, GAPDH and expressed as fold differences of target gene expression relative to SK-RC-45.

2.2.2. Thin layer chromatography (TLC) of isolated gangliosides

Ganglioside profiles of different cancer cell lines were obtained from thin layer chromatograms (TLCs) of ganglioside isolates from tumor cell lines. Gangliosides were extracted from different tumor cell lines using modifications of the method described earlier [31]. Briefly, total lipids were extracted using chloroform:methanol (1:1) for 18 h at 4 °C followed by partitioning in 10 ml of diisopropyl ether/1% butanol/0.1% aqueous NaCl as described previously [9,31]. The lyophilized aqueous phase was passed through a Sephadex G-25 column to get rid of the salts and small molecular weight impurities. Isolated gangliosides were lyophilized and re-dissolved in chloroform–methanol (2:1). TLC analysis was done using precoated silica gel 60 Å TLC plates (Merck, Millipore, India) measuring 10 × 10 cm [9]. Gangliosides were resolved by running the plate in chloroform/methanol/0.25% $CaCl_2$ (60:40:9, v/v/v) and visualized as bands by developing the plates by charring it with 5% concentrated

H_2SO_4. Bovine brain-derived gangliosides (GM3, GM2, GM1, GD1a, and GD3) were run on lanes of the TLC plates as standards. Mass content of GM2 in each cell line was estimated by comparing the pixel density of the bands co-migrating with standard bovine brain derived GM2 in each tumor cell line with the pixel density of a known amount of standard bovine brain derived GM2 as shown in Fig. 1B (table).

2.2.3. Lipid-bound sialic acid (LSA) assay

Lipid-bound sialic acid (LSA) assay was performed to assess the total ganglioside content of tumor cell lines [32,33] using the resorcinol–HCl reagent [9,34]. Briefly, gangliosides from different tumor cell lines were dissolved in 200 μl of cold distilled water and LSA content was quantitated by comparing the absorption at 580 nm with the standard curve generated using known amounts of free sialic acid (NANA or n-acetyl-neuraminic acid, Sigma) [33].

2.2.4. Immunofluorescent staining and microscopy

Immuno-fluorescent staining of the cell lines was done with anti-hamster GM2 antibody (DMF10.167.4, a gift from Dr. Kenneth Rock, University of Massachusetts Medical School, Worcester, MA and Dr. James H. Finke, Cleveland Clinic, Cleveland, USA) [9,23]. Briefly, cells (3×10^4) were grown on a coverslip (diameter, 18 mm) placed in a 12-well plate for 24 h. Cells were washed thrice with 1× PBS and fixed with pre-warmed 3.7% paraformaldehyde (PFA) for 15 min at room temperature.

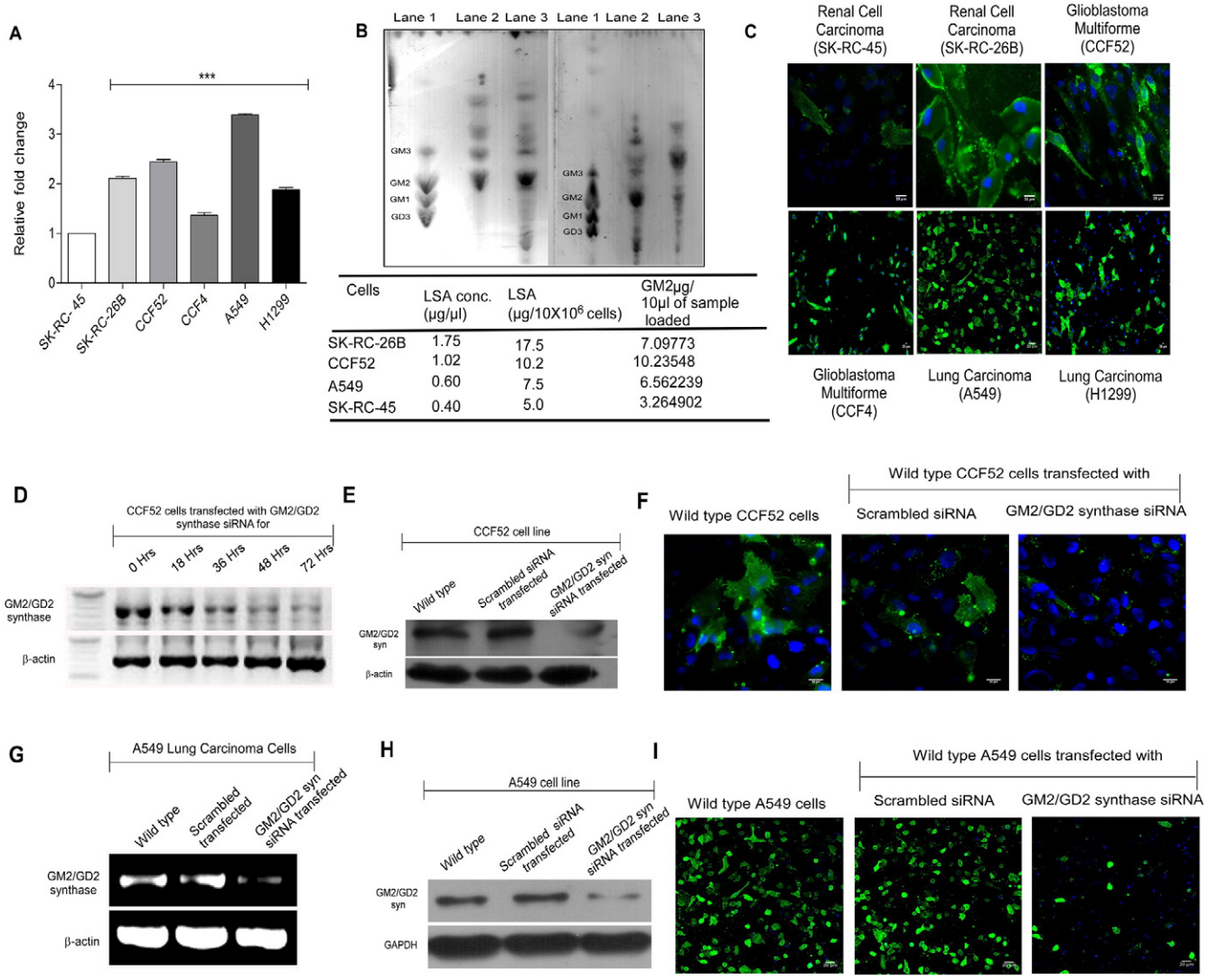

Fig. 1. GM2-synthase mRNA level as well as GM2 is differentially expressed in various cancer cell lines. (A) Quantitative real time PCR of mRNA isolated from SK-RC-45, SK-RC-26B, CCF52, CCF4, A549 and H1299 cells showed significant higher GM2-synthase mRNA expression in all the above tumor cells except SK-RC-45. All mRNA quantification data were normalized to the expression of the housekeeping gene, GAPDH and expressed as fold differences of target gene expression relative to SK-RC-45, $^{***}p < 0.001$ versus SK-RC-45 cells. (B) Representative TLC data of gangliosides isolated from at least 25×10^6 cells of 4 different cancer cell lines as described earlier. Isolated gangliosides were developed in chloroform/methanol/0.25% $CaCl_2$ (60:40:9, v/v/v) and visualized by charring the TLC plate after spraying with 5% H_2SO_4 in ethanol. Left panel: lane 1, mixture of GM3, GM2, GM1 and GD3; lane 2, SK-RC-26B derived gangliosides; lane 3, CCF52 derived gangliosides; right panel: lane 1, mixture of GM3, GM2, GM1 and GD3; lane 2, A549 derived ganglioside and lane 5, SK-RC-45 derived ganglioside. The table represents the lipid bound sialic acid (LSA) concentration and total LSA content in 4 different cancer cell lines. Mass content of GM2 in each cell line was estimated by comparing the pixel density of the bands co-migrating with standard bovine brain derived GM2 in each tumor cell line with the pixel density of a known amount of standard bovine brain derived GM2. (C) Immuno-staining of GM2 in all tumor cell lines with hamster anti-human GM2 antibody. SK-RC-45 cells show a negligible amount of GM2 when compared with SK-RC-26B, CCF52, CCF4, A549 and H1299 cells. (D) Semi-quantitative RT-PCR of RNA isolated from CCF52 cells at 0, 18, 36, 48 and 72 h post-transfection with GM2-synthase siRNA showing time-dependent decrease in GM2-synthase mRNA levels. (E) Western blot analysis showing decrease in protein levels of GM2-synthase in GM2-synthase siRNA transfected CCF52 cells at 48 h post-transfection. (F) Immunofluorescent microscopy in wild type, GM2-synthase and scrambled siRNA transfected CCF52 cells with hamster anti-human GM2 antibody. (G) Semi-quantitative RT-PCR of GM2-synthase in wild type, scrambled and GM2-synthase siRNA treated A549 cells at 48 h post-transfection. (H) Western blot analysis showing a decrease in protein levels of GM2-synthase in GM2 synthase siRNA treated A549 cells at 48 h post-transfection. (I) Immunofluorescent microscopy in wild type, GM2-synthase and scrambled siRNA transfected A549 cells stained with hamster anti-human GM2 antibody.

Fixed cells were incubated in 3% BSA for 1 h. Cells were then incubated with GM2 antibody (anti-hamster) diluted in 1% BSA in a humidified chamber overnight at 4 °C. Cells were then washed thrice with 1× PBS and incubated with anti-hamster Alexa Fluor conjugated 2°Ab. Following washing with 1× PBS thrice, stained cells were mounted on slides with Vectashield mounting medium and images were captured by a fluorescent microscope (Leica DFC450 C, Leica Microsystems India Pvt. Ltd.).

2.3. siRNA transfection to knockdown GM2-synthase message

CCF52, A549 and SK-RC-26B cells were transfected with 75 nM of GM2-synthase siRNA (Santa Cruz Biotechnology Inc., Texas, USA) using Lipofectamine-2000 (Invitrogen BioServices, India) according to the manufacturer's protocol. All experiments were performed at least 48 h post transfection.

2.4. Molecular cloning and over-expression of GM2-synthase in SK-RC-45 cells

GM2-synthase full length coding sequence (CD) CDS was cloned into mammalian expression vector pcDNA3 (Invitrogen, India) to obtain pcDNA3/GM2-synthase construct. Cloning primers are shown in Supplementary Table S1B. SK-RC-45 cells transfected with plasmids (either pcDNA3/GM2-synthase or empty pcDNA3 vector) using Lipofectamine-2000 were selected against G418 (750 μg/ml) to isolate stable GM2 over-expressing clones. GM2 over-expression was confirmed by immunofluorescence microscopy, qRT-PCR and western blotting over empty vector transfected cells.

2.5. Incorporation/accumulation of ganglioside GM2 following exogenous treatment

Following exogenous GM2 administration to tumor cells, GM2 incorporation/accumulation in tumor cells was monitored by measuring the increase in LSA with an increasing dose of added GM2 and also its metabolism into ceramide, the final metabolite in ganglioside metabolism, as described below. SK-RC-45 cells were treated with increasing doses of exogenous GM2 (5 μM, 10 μM, 25 μM), following which LSA content was determined from untreated and treated cells as described before [35]. Briefly, cell pellets from 8×10^5 cells (untreated or treated) were suspended in ice cold water, snap frozen and lyophilized. Lipids from lyophilized cells were first extracted with chloroform/methanol/water 2:1:0.1 (v/v/v) followed by a second extraction with chloroform:methanol (2:1, v/v). Phase partitioning was done by adding water, corresponding to 20% of the total volume of lipid extracted, followed by a centrifugation of 2300 ×*g* for 15 min. The aqueous phase containing gangliosides were dried under nitrogen flow and lyophilized. The lyophilized samples were dissolved in a minimum volume of water and analyzed for LSA as previously mentioned in an LSA assay [9]. For determining the mass amount of GM2, gangliosides were isolated from very few number (5×10^6) of SK-RC-45 cells following exogenous administration of ganglioside GM2 using modifications of methods described earlier [31]. Gangliosides isolated from non-treated as well as treated cells were resolved by TLC and developed as described earlier. A mass amount of GM2 was estimated by comparing the pixel density of the band corresponding to GM2 in SK-RC-45 cells (treated with exogenous GM2) with the pixel density of a known amount of standard bovine brain derived GM2, as described previously in Section 2.2.2.

2.6. Ceramide kinase assay to assess metabolism of administered ganglioside

To ascertain the fate of administered GM2 inside the cell, a ceramide kinase assay was performed as described previously [36]. The principle of the assay was based on monitoring the levels of ceramide with increasing doses of exogenous GM2. This was achieved by measuring the levels of ceramide-1-phosphate generated by an *in vitro* kinase reaction using recombinant human ceramide kinase (CerK), radiolabeled [γ^{32}P] ATP and cellular ceramide as substrate. In brief, cDNA of CerK was first cloned and over-expressed in HEK 293T cells as shown in the schematic representation of the Supplementary Fig. S4. The lysate containing the recombinant CerK and the empty vector were used in an *in vitro* kinase reaction using radio-labeled [γ^{32}P] ATP and incubated with lipid extracts from SK-RC-45 cells treated with different doses of GM2 (5 μM, 10 μM and 25 μM) for 24 h or MCF7 treated with doxorubicin (1 μg/ml) as positive control. The radio-labeled product ceramide-1-phosphate was then extracted and separated by TLC. Radioactive bands were then visualized by a phosphoimager (Typhoon Trio,GE healthcare) with an exposure of 4 h [37].

2.7. MTT assay for cellular proliferation

For cell proliferation assay either wild type, scrambled or GM2-synthase siRNA treated CCF52 and A549 cells, as well as SK-RC-45 cells (wild type, GM2 over-expressing clone) were used. For exogenous addition of GM2, SK-RC-45 cells, either untreated or cells treated with 25 μM of GM2 ganglioside (Alexis, USA) for 12 h, 24 h and 36 h in serum free media were processed for MTT assay. Briefly, MTT (0.5 mg/ml) was added to 4×10^4 cells/well at 24 h, 48 h and 72 h of seeding. 3 h after incubation at 37 °C, cells were washed with 1× PBS, 1 ml of DMSO was added and absorbance was measured at 570 nm.

2.8. In vitro transwell migration assay and matrigel invasion assay

Either wild type, scrambled or GM2-synthase siRNA treated CCF52, A549 or SK-RC-26B cells, as well as SK-RC-45 cells (wild type, GM2 over-expressing clone or integrin-β1 siRNA treated) were used for transwell migration assay and/or matrigel invasion assay. For exogenous ganglioside treatment, SK-RC-45 cells (either wild type or integrin-β1 silenced) were incubated with 25 μM of GM2 ganglioside (Alexis, USA) for 24 h in serum free media. For transwell migration assay, cells (1×10^5) placed in the upper chamber of the cell culture inserts (Cat# 353182, BD Biosciences, NJ, USA) with 400 μl serum free medium were allowed to migrate for 6 h in response to complete medium (700 μl) placed in the bottom chamber of the 12-well transwell plates. Cells that migrated to the lower surface of the membrane were fixed, stained with Giemsa and at least five independent microscopic fields were counted under microscope.

For matrigel invasion assay, cells were serum starved overnight before being harvested. Cells (1×10^5) plated at the top of matrigel precoated 24 well inserts (Corning Biocoat™ 354480) in serum free media were allowed to invade for 22–24 h in response to complete medium placed at the bottom chamber of a 24 well plate. Cells that invaded through matrigel to the lower surface were fixed, stained with Giemsa and at least five different fields were counted under microscope similar to a migration assay.

2.9. DNA microarray to study the alterations in gene expression in response to GM2-synthase knockdown

Total RNA samples were isolated as described before from wild type CCF52 cells and cells transfected with either GM2-synthase siRNA or scramble siRNA (Dharmacon, Thermo Fisher Scientific, India). RNA samples were hybridized to Affymetrix-HG-U133 plus 2.0 gene chips (Affymetrix) which were scanned using the Gene Array scanner (Affymetrix). The CEL files generated by the Affymetrix Microarray Suite (MAS 5.0) were converted into DCP files using the DNA-Chip Analyzer (dChip 1.3, http://biosun1.harvard.edu/complab/dchip/).

2.9.1. Microarray data analysis

Microarray data sets were analyzed using TM4:Microarray Software suite [38]. Raw data were RMA (robust multichip averaging algorithm) normalized and probe sets were filtered by p-value < 0.05 and fold-

change ≥ 2. Hierarchical clustering was performed by complete linkage and un-centered correlation using Cluster 3.0 [39]. Results were visualized using Java Tree View [40].

2.9.2. Enrichment analysis

Functional annotation of the differentially expressed genes was done using BiNGO [41]. Significant gene sets corresponding to cell migration related biological processes obtained from BiNGO results were visualized as an interaction network with Cytoscape and Enrichment Map [42]. The Enrichment Map was created at enrichment p-value = 0.005. Gene interaction network was constructed using Gene MANIA [43]

2.9.3. Quantitative (q) RT-PCR to validate DNA microarray data

RT-PCR was performed with cDNA extracted from CCF52 cells as well as A549 cells (wild type, scrambled or GM2-synthase siRNA) using SYBR green on a 7500 Fast Real-time PCR system (Applied Biosystem). All mRNA quantification data were normalized to the expression of the housekeeping gene, GAPDH and expressed as fold differences of target gene expression relative to wild type. The primers used for selected genes were given in Supplementary Table S2.

2.10. Confocal microscopy for visualizing actin stress fibers in GM2-synthase knockdown cells and studying co-localization of integrin receptor with GM2

For visualizing the actin stress fibers in wild type, GM2-synthase siRNA or scrambled siRNA transfected CCF52 cell type, cells were fixed with PFA, permeabilized and stained with Alexa Fluor tagged phalloidin (green) (Molecular Probes, USA) for 30 min in a humidified chamber. Cells were then mounted by Vectashield and observed under scanning laser microscopy (Leica TCS SP8 STED) and photographed for green and blue channels using Leica Application Suite LAS AF software.

Co-localization of GM2 with the integrin receptor, was studied in CCF52, A549 and SK-RC-45 cells. In brief, CCF52 and A549 cells were fixed with 3.7% PFA and incubated with anti-hamster GM2 and anti-mouse integrin-β1 receptor (Santa Cruz Biotechnology, USA) overnight at 4 °C, washed with 1× PBS and counterstained with secondary (2°) antibodies (anti-hamster AlexaFluor 488 conjugated IgG and anti-mouse AlexFluor 594 conjugated IgG) for studying co-localization of endogenous GM2 with integrin. A similar procedure was used for SK-RC-45 cells following treatment with exogenous GM2 (25 μM) for 12 h and 24 h in serum free media. Cells were mounted on slides with Vectashield mounting media and observed by scanning laser microscopy (Leica TCS SP8 STED) and photographed for blue, red and green channels using Leica Application Suite LAS X software. Co-localization analysis was performed according to [44,45] using Leica Application Suite LAS X which calculated Pearsons correlation coefficient, overlap coefficient (data not shown) and co-localization rate (co-localization area divided by foreground area). For both signals the intensity threshold value of 30% and 20% subtraction was applied. At least three independent experiments were done including five different fields of observation. The scatter plots for correlation analysis of Fig. 8A and B are shown in Supplementary Fig. S5.

2.11. Western immuno-blotting

Cell lysates from CCF52 and A549 cells transfected with either GM2-synthase siRNA or scrambled siRNA and SK-RC-45 cells transfected with either empty vector or with pcDNA3.0/GM2-synthase construct, were probed for GM2-synthase with anti-rabbit GM2-synthase antibody (Abcam) for looking at the expression of GM2-synthase protein level in response to GM2-synthase knockdown or GM2-synthase over-expression. For studying downstream signaling in response to GM2-synthase knockdown, cells following transfection were serum starved for 24 h followed by stimulation with FBS for 30 and 60 min and probed for signaling intermediates (p-FAK, FAK, p-Src, p-Erk, and Erk) (Cell Signaling Technologies, USA) involved in integrin mediated signaling pathway. GM2-synthase over-expressing SK-RC-45 clones (serum starved for 24 h followed by stimulation with FBS for 30 and 60 min) were probed for p-FAK and FAK. Erk phosphorylation in response to exogenous GM2 was studied with SK-RC-45 cells treated with GM2 (25 μM) in serum free medium for 24 h, and stimulated with FBS as described above. For studying integrin dependent Erk phosphorylation in response to GM2, cell lysates from wild type as well as integrin-β1 silenced SK-RC-45 cells with or without exogenously added GM2 were probed for pErk and Erk. Integrin level in GM2-synthase knockdown cells as well as GM2-synthase over-expressed cells were checked by probing them with anti-mouse integrin-β1 receptor antibody (Santa Cruz Biotechnology, USA). GAPDH (Biobharati Life Sciences Pvt. Ltd., India) and β-actin (Santa Cruz Biotechnology, USA) were used as a loading control for all experiments. HRP-coupled anti-rabbit and mouse (Cell Signaling Technologies, USA) was used as 2°Abs.

2.12. Interaction of integrin molecule with GM2 by co-immunoprecipitation in membrane enriched cellular fraction

Interaction of an integrin molecule with GM2 was determined by using membrane enriched fractions isolated from CCF52 and A549 cells as well as SK-RC-45 cell lysates treated with or without exogenous GM2. Briefly, 5×10^5 cells were lyzed using subcellular fractionation buffer containing 250 mM sucrose, 20 mM Hepes (pH 7.4), 10 mM KCl, 1.5 mM $MgCl_2$, 1 mM EDTA, 1 mM EGTA and 1 mM DTT along with protease inhibitor cocktail (Pierce, Thermo Scientific). The suspension was kept on ice for 20 min and passed through a 25 G needle 10 times. The lysate was centrifuged at 3000 rpm for 5 min at 4 °C to remove nuclei and debris. Supernatant was again centrifuged for 8000 rpm to remove mitochondrial fraction. For membrane enriched cellular fraction, the supernatant was further centrifuged in an ultracentrifuge (Himac CP90WX, Hitachi) at 40,000 rpm for 1 h followed by re-centrifugation for 45 min. Finally membrane enriched fraction was re-suspended in Tris–NaCl–EDTA buffer (pH 7.4) containing 1% Triton X-100. Approximately, 50 μg of membrane protein was incubated with or without GM2 (25 μM) in a 300 μl of IP buffer overnight. 15 μg of hamster GM2 antibody was added to the membrane fraction lysates and kept at 4 °C with overnight shaking followed by incubation with 30 μl of the protein G-agarose beads (Abcam) for 4 h at 4 °C. Beads were washed thrice with 1× PBS containing 0.01% Tween-20, then suspended in a final volume of 60 μl of sample buffer containing β-mercaptoethanol, heated to 95 °C for 3 min and centrifuged (1000 × g for 2 min). The supernatants were subjected to SDS-PAGE, transferred to PVDF and probed with anti-mouse integrin-β1 receptor (Santa Cruz Biotechnology, USA). HRP-coupled anti-mouse (Cell Signaling Technologies, USA) was used as secondary antibody. For determining the specificity of the anti-hamster GM2 antibody for immuno-precipitating GM2, the immunoprecipitates were washed and dried using a rotary vacuum evaporator (Operon). Following drying, the beads were suspended in methanol/chloroform (1:1) and ganglioside enriched lipids were extracted using a modified ganglioside isolation procedure as stated before as described in Section 2.2.2 [31]. The extracted gangliosides were dissolved in a minimum volume of chloroform/methanol (1:1) and resolved by TLC.

2.13. Surface plasmon resonance (SPR) to study binding and the kinetics of interaction of GM2 with integrin

SPR was performed to study the interaction of integrin with GM2. The experiment was carried out in a BIAcore X100 instrument (GE Healthcare) by immobilizing full length human α5β1 integrin (Chemicon, Millipore) onto a CM5 sensor chip. Full length human integrin α5β1 (150 μg/ml in 10 mM acetate buffer, pH 4.5 containing 2 mM $MnCl_2$ and 1 mM $MgCl_2$) was immobilized onto a CM5 sensor chip by amine coupling in flow cell 2 at a flow rate of 5 μl/min according

to the manufacturer's protocol (GE Healthcare) with an immobilization level of 20,000 RU. The running buffer used was 10 mM Hepes, pH 7.4, containing 150 mM NaCl, 1 mM $MnCl_2$ and 1 mM $MgCl_2$. Flow cell 1 was kept empty but blocked by the activating carboxymethyl group with an EDC and NHS mixture and consequently deactivated by ethanolamine. Flow cell 1 was used as a blank immobilized reference surface for in-line reference subtraction, providing direct recording and display of blank corrected sensograms. The sensogram from the reference surface reveal non-specific binding. Varying concentrations (1 μM, 5 μM, 10 μM, 25 μM, 50 μM and 100 μM) of ganglioside GM2 were injected at a rate of 30 μl/min at 25 °C followed by dissociation in the same running buffer for 180 s at the same flow rate. The kinetic parameters K_a (association rate constant), K_d (dissociation rate constant) and K_D (binding affinity) were analyzed simultaneously using the BIAeval software.

2.14. Statistical analysis

Statistical analysis was obtained from results of at least three independent experiments and expressed as mean ± SEM. One way ANOVA and one tailed Student's *t*-test were used to evaluate the statistical significance. $p < 0.05$ was considered significant for all tests.

3. Results

3.1. GM2-synthase as well as ganglioside GM2 is differentially expressed in various cancer cell lines

Quantitative RT-PCR shows the relative expression of GM2-synthase mRNA in six different cancer cell lines as shown in Fig. 1A. Most of the cancer cell lines, namely SK-RC-26B, CCF52, CCF4, A549 and H1299 show differential but significantly higher expression of GM2-synthase as compared to the kidney cancer cell line, SK-RC-45 which show moderate levels of GM2-synthase. Whether higher GM2-synthase mRNA corresponds to an elevated expression of ganglioside GM2 was determined by thin layer chromatography (TLC) of gangliosides isolated from different cancer cell lines as described in the Materials and method section. As shown from the TLC chromatogram in Fig. 1B, all of the tumor cell lines show differential levels of ganglioside GM2, as is evident from the band co-migrating with standard bovine brain derived GM2. SK-RC-26B, CCF52 and A549 cells express significantly higher levels of GM2 as compared to the SK-RC-45 cell line. All of the cell lines except SK-RC-45 show similar expression of GM3 as well, although GM3 levels were found to be significantly lower than ganglioside GM2 levels in each of the cells. Interestingly, TLC chromatogram also reveals numerous ganglioside

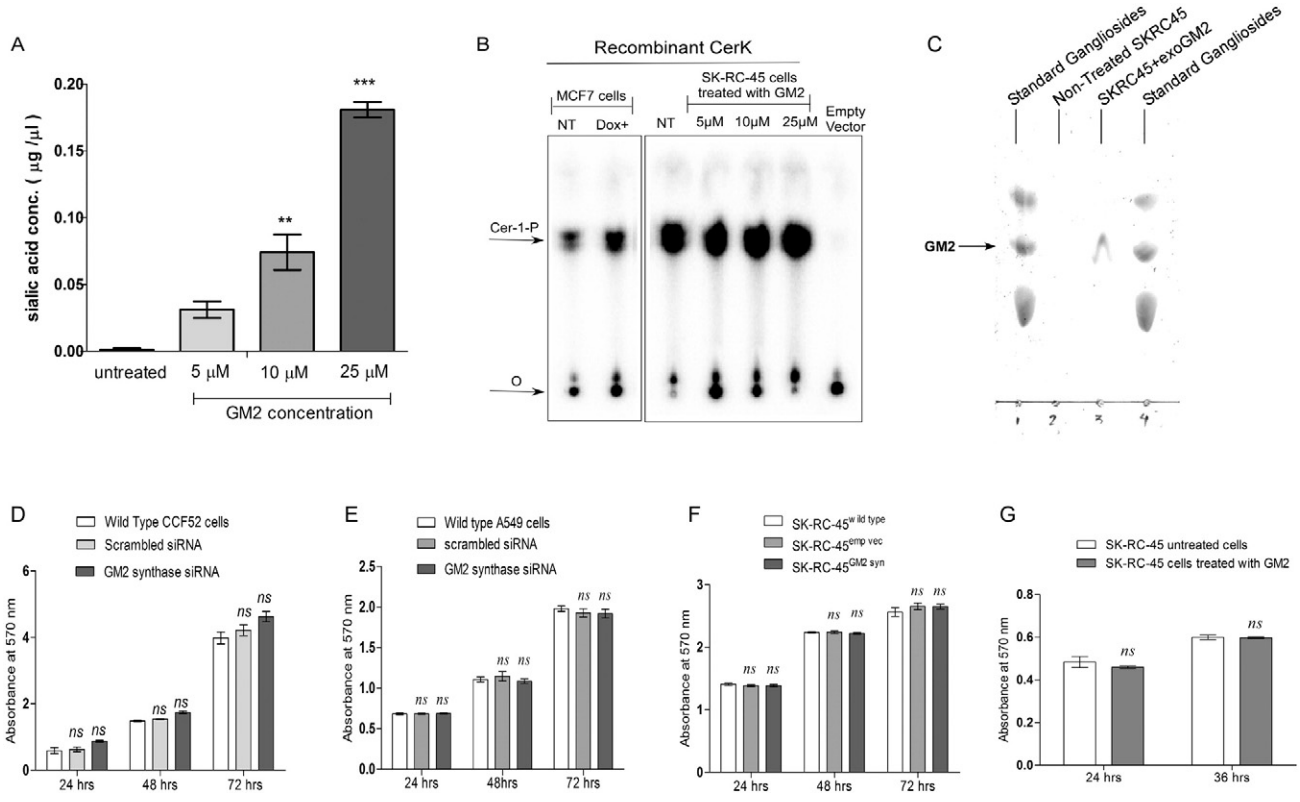

Fig. 2. Ganglioside GM2 has no significant role on tumor cell proliferation. (A) Administration of exogenous GM2 results in an increase of total lipid bound sialic acid content of a cell. 8×10^5 SK-RC-45 cells were treated with increasing doses of exogenous GM2 (5 μM, 10 μM, 25 μM) for 24 h, following which LSA content was determined from untreated and treated cells as described in Materials and method. LSA content was quantitated by comparing the absorption at 580 nm with the standard curve generated using known amounts of free sialic acid. Data were analyzed by one way ANOVA (Turkey's multiple comparison test), $^{**}p < 0.01$ versus sialic acid concentration in 10 μM of GM2 treated; $^{***}p < 0.001$ versus sialic acid concentration in 25 μM of GM2 treated. (B) *In vitro* ceramide kinase (CerK) assay for the measurement of cellular ceramide upon GM2 treatment (5 μM, 10 μM, 25 μM) in SK-RC-45 cells along with MCF7 treated or non-treated with doxorubicin (1 μg/ml). In brief, lipids were extracted from GM2 and doxorubicin treated cells and incubated with recombinant CerK or lysates from cells transfected with empty vector in the presence of [γ^{32}P] ATP. Then radiolabeled ceramides were separated by TLC and visualized in a phosphoimager. "O" indicates the position of origin whereas Cer-1-P indicates migrated radiolabeled ceramide-1-P. "nt" denotes nontreated cells. (C) 5×10^6 SK-RC-45 cells were treated or not with 25 μM exogenous GM2, following which gangliosides were extracted using slight modifications of the Ladisch method [31] described in a previous section. Ganglioside isolated from treated (lane 3) or non-treated cells (lane 2) were resolved on TLC plates along with a mixture of standard bovine brain derived gangliosides (lanes 1 & 4). Pixel density of a standard GM2 band was compared with that of the corresponding GM2 band in lane 3 to calculate the mass amount of GM2. (D–G) *In vitro* cellular proliferation assay by using MTT of wild type, scrambled and GM2-synthase knockdown CCF52 cells (D) and A549 cells (E); empty vector transfected as well as GM2 over-expressed SK-RC-45 cells (F); non-treated SK-RC-45 cells and exogenous GM2 (25 μM) treated SK-RC-45 cells (G). Data were analyzed by Student's "*t*" test; "ns" denotes non-significant.

bands migrating much higher than any of the standard bovine brain derived gangliosides (Fig. 1B). Ganglioside GM2 content was quantified by densitometric analysis described in the Materials and method section, which shows significantly higher levels of GM2 in all of the tumor cell lines except SK-RC-45 cells where there is only moderate levels of GM2 (3.26 μg/10 μl of sample), as depicted in Fig. 1B (table). All of the three tumor cell lines (CCF52, SK-RC-26B and A549) also display significantly higher levels of total lipid bound sialic acid (LSA) compared to SK-RC-45 cells as shown in Fig. 1B (table), which is indicative of the total ganglioside content of the different tumor cell lines. Immunofluorescence microscopy was performed to compare the levels of GM2 expression in various tumor cell lines in order to further confirm the TLC results. Fig. 1C shows significantly elevated expression of ganglioside GM2 in all tumor cell lines except SK-RC-45 as evident from the green fluorescence, which shows a moderate level of GM2 as compared to other tumor cell lines. These results suggest that tumor cells show significantly elevated but variable expression of GM2-synthase as well as GM2 expression. GM2-synthase message was then successfully silenced in CCF52, A549 and SK-RC-26B cell lines using GM2-synthase siRNA. Semi-quantitative RT-PCR shows successful time-dependent silencing of GM2-synthase message between 18 h through 72 h post transfection (Fig. 1D), while western blot confirms the knockdown of GM2-synthase protein expression in CCF52 cells (Fig. 1E) when compared to the non-transfected cells. Effective silencing of GM2-synthase was also obtained in A549 (Fig. 1G and H). A consequent reduction in

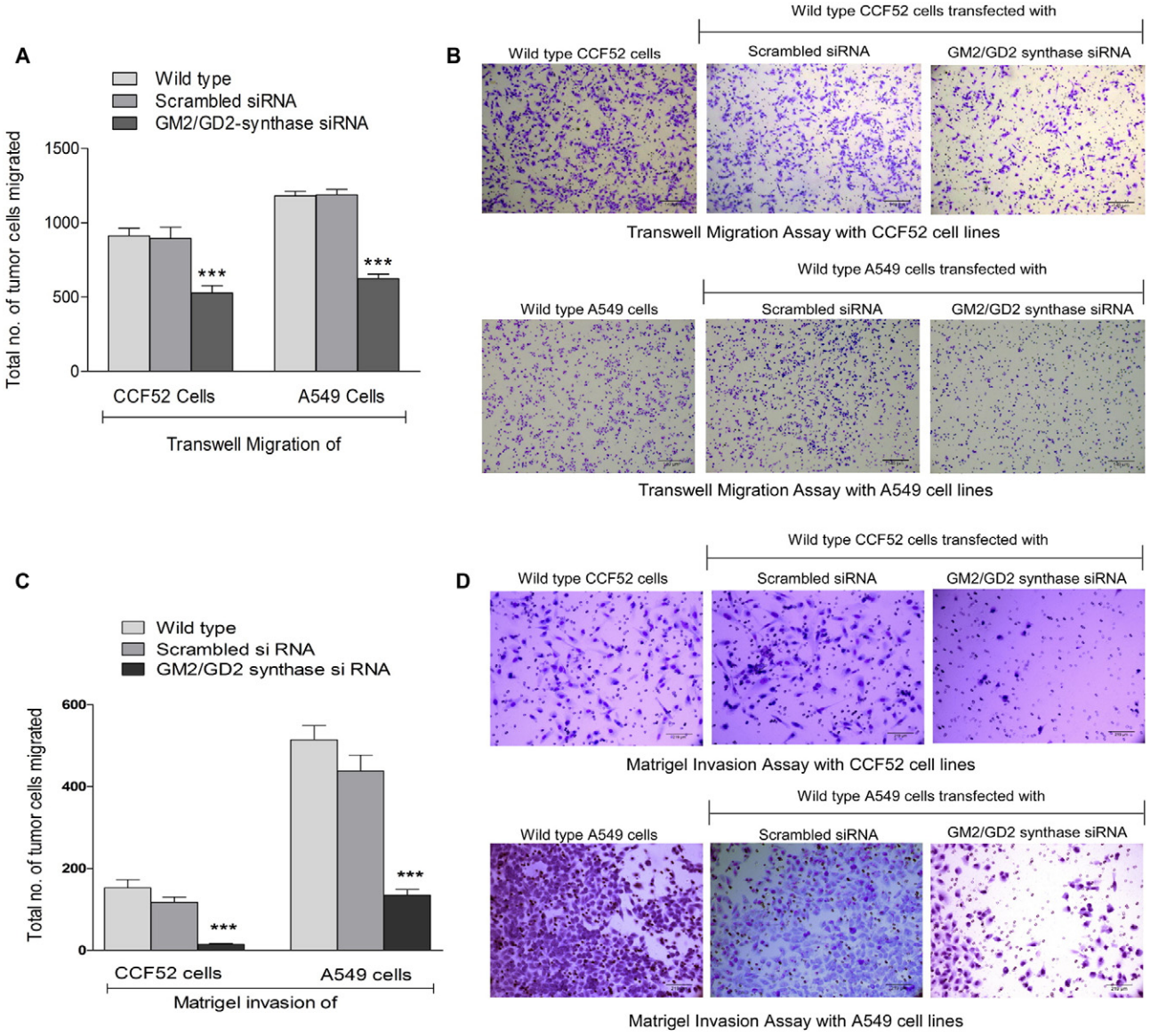

Fig. 3. GM2-synthase knockdown resulted in significant inhibition in tumor cell migration and invasion. (A) *In vitro* transwell migration assay of wild type, scrambled and GM2-synthase knockdown CCF52 cells and A549 cells. Briefly, 6 h after seeding 1×10^5 cells in the upper chamber of the 12-well transwell inserts, cells that migrated through the membrane of the transwell towards 10% FBS were fixed and stained with Giemsa. Migrated cells from 5 random fields were counted under microscope. Data were analyzed by one way ANOVA (Dunnett test), ***$p < 0.001$ versus wild type and scrambled siRNA treated cells. (B) Top panel shows the representative microscopic image of migration in wild type, scrambled and GM2-synthase siRNA transfected CCF52 cells and lower panel represents the microscopic image of migration in wild type, scrambled and GM2-synthase siRNA transfected A549 cells. (C) *In vitro* transwell matrigel invasion assay of wild type, scrambled and GM2-synthase knockdown CCF52 cells and A549 cells. Briefly, 22–24 h after seeding 1×10^5 cells in the upper chamber of the 24-well matrigel inserts, cells that invaded through the matrix of the transwell towards 10% FBS were fixed and stained with Giemsa. Invaded cells from 5 random fields were counted under microscope. Data were analyzed by one way ANOVA (Dunnett test), ***$p < 0.001$ versus wild type and scrambled siRNA treated CCF52 cells and A549 cells. (D) Representative microscopic image of invasion in wild type, scrambled and GM2 synthase siRNA transfected CCF52 (top panel) and A549 (bottom panel) cells.

ganglioside GM2 expression was confirmed by immunofluorescence microscopy which clearly indicates knockdown of GM2 expression in CCF52 (Fig. 1F), A549 (Fig. 1I) and SK-RC-26B (Supplementary Fig. S2) cells at 48 h post-transfection with GM2-synthase siRNA versus cells transfected with scrambled siRNA. This shows that siRNA mediated silencing of GM2-synthase was effective in knocking down GM2 expression in a tumor cell line, thus enabling in determining an optimal time point of GM2 depletion upon GM2-synthase knockdown, which is critical for studying the functional role of GM2 in tumor cell migration.

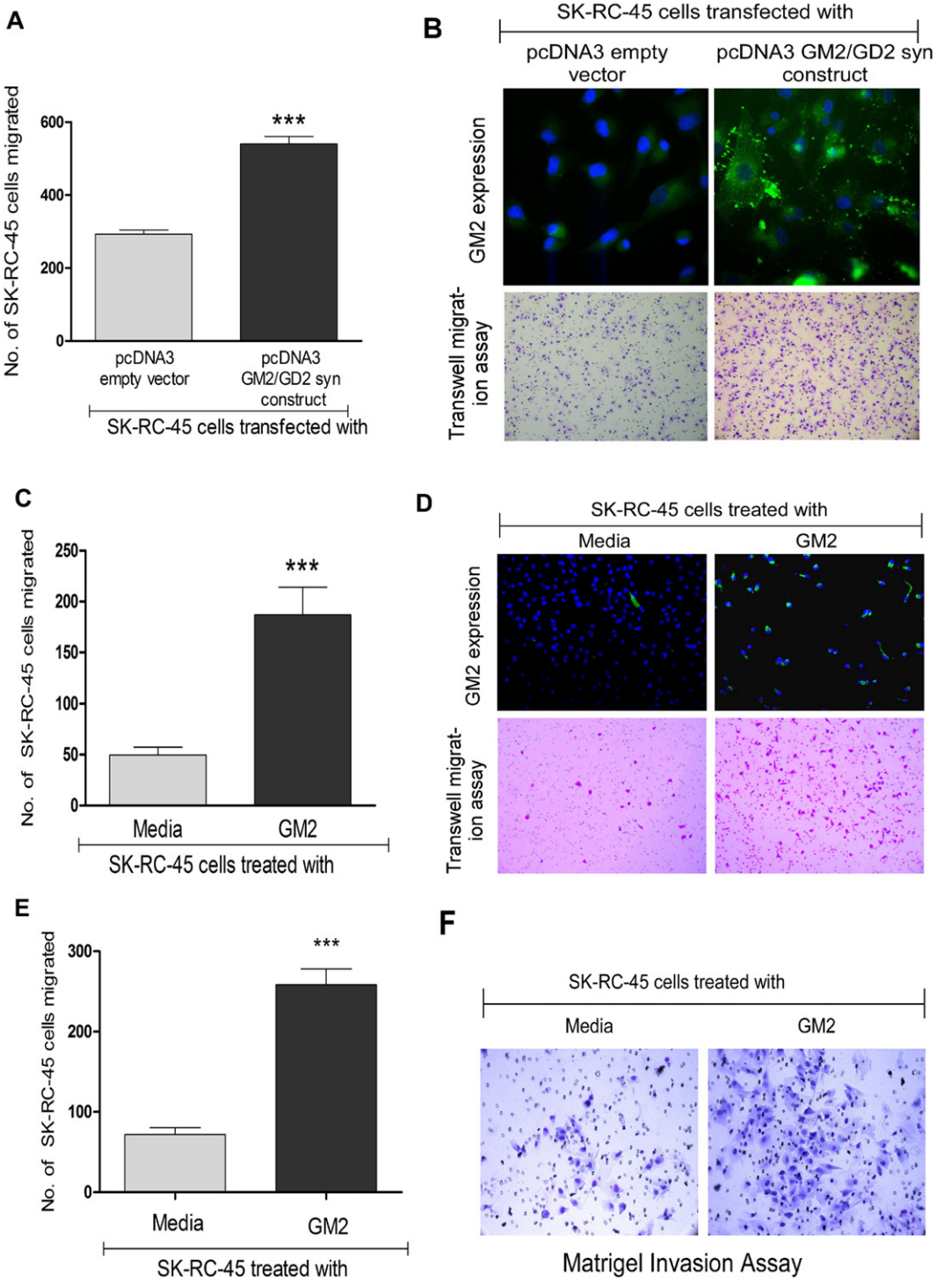

Fig. 4. Ganglioside GM2 is involved in tumor cell migration and invasion. (A) *In vitro* transwell migration assay of empty vector transfected as well as GM2 over-expressed SK-RC-45 cells. Data were analyzed by Student's *t*-test (***$p < 0.001$ versus empty vector transfected SK-RC-45 cells). (B) Upper panels represent GM2 expression in empty vector transfected (left) and GM2 over-expressed (right) SK-RC-45 cells as observed by immuno-fluorescent microscopy. Bottom panel represents microscopic images of chemotactic migration in empty vector transfected versus GM2 over-expressed SK-RC-45 cells. (C) Transwell migration assay with non-treated SK-RC-45 cells and exogenous GM2 (25 μM) treated SK-RC-45 cells. Data were analyzed by Student's *t*-test (***$p < 0.001$ versus non-treated SK-RC-45 cells). (D) Upper panels represent GM2 uptake in non-treated (left) SK-RC-45 cells and GM2 treated (right) SK-RC-45 cells as observed by immunofluorescence microscopy. Bottom panels represent microscopic images showing transwell migration of non-treated SK-RC-45 cells versus GM2 treated SK-RC-45 cells. (E) *In vitro* transwell matrigel invasion assay with non-treated SK-RC-45-cells and exogenous GM2 (25 μM) treated SK-RC-45 cells. Data were analyzed by Student's *t*-test (***$p < 0.001$ versus non-treated SK-RC-45 cells). (F) Representative microscopic images of matrigel invasion in non-treated (left) and GM2 treated SK-RC-45 cells (right).

3.2. Administration of exogenous GM2 results in an increase of total ganglioside bound sialic acid content of a cell with no significant change in its metabolism

Since, 25 μM GM2 was exogenously added in SK-RC-45 cells in many of the experiments performed later, it was important to know whether the exogenously added GM2 was incorporated in the cells, or whether it underwent active metabolism. This was checked by measuring the increase in lipid bound sialic acid (LSA) content as well as the ceramide levels following dose-dependent addition of GM2. As shown in Fig. 2A, increased GM2 uptake actually results in its incorporation in the cells which was observed by the dose dependent increase in total lipid bound sialic acid (LSA) content of SK-RC-45 cells treated with increasing concentrations of exogenously added GM2 (5 μM, 10 μM, 25 μM). Further, to determine how much of this incorporated GM2 is actively metabolized, ceramide levels were measured using an *in vitro* ceramide kinase assay. Ceramide being the ultimate metabolic product of gangliosides it is possible that the incorporated GM2 is metabolized to ceramide by the cell before the assay time (24 h). Metabolic product ceramide was converted to ceramide-1-phosphate [γ^{32}P] by ceramide kinase (CerK) using radio-labeled ATP [γ^{32}P]. Fig. 2B shows a TLC chromatogram of ceramide-1-phosphate by recombinant CerK (overexpressed in HEK 293T cells). No significant changes were observed in the levels of ceramide-1-phosphate in untreated SK-RC-45 cells compared to SK-RC-45 cells treated with varying concentrations of GM2 (5 μM, 10 μM, 25 μM). MCF7 exposed to Doxorubicin (1 μg/ml) for 6 h was used as positive control, which showed a significant increase in the levels of ceramide-1-phosphate. No ceramide phosphorylation was observed with empty vector transfected HEK 293T cells, which was used as a negative control for the assay. A detectable level of GM2

Table 1
Selected differentially regulated gene (DRGs) sets.

Genes downregulated	Fold change
ITGB1	12.89
RHOA	8.42
PTPN11	7.24
RAB8B	5.59
TPM1	3.62
ACTG2	3.59
ARF6	3.09
ARPC4	2.94
TPM2	2.73
VCAN	2.43
CYR61	2.71
ARHGEF6	2.70
CFL2	2.12
VIM	2.12
ROCK1	2.02

List of 15 genes which are significantly downregulated in response to GM2-synthase knockdown by microarray data selected on the basis of existing literature survey demonstrating their pivotal role in integrin signaling.

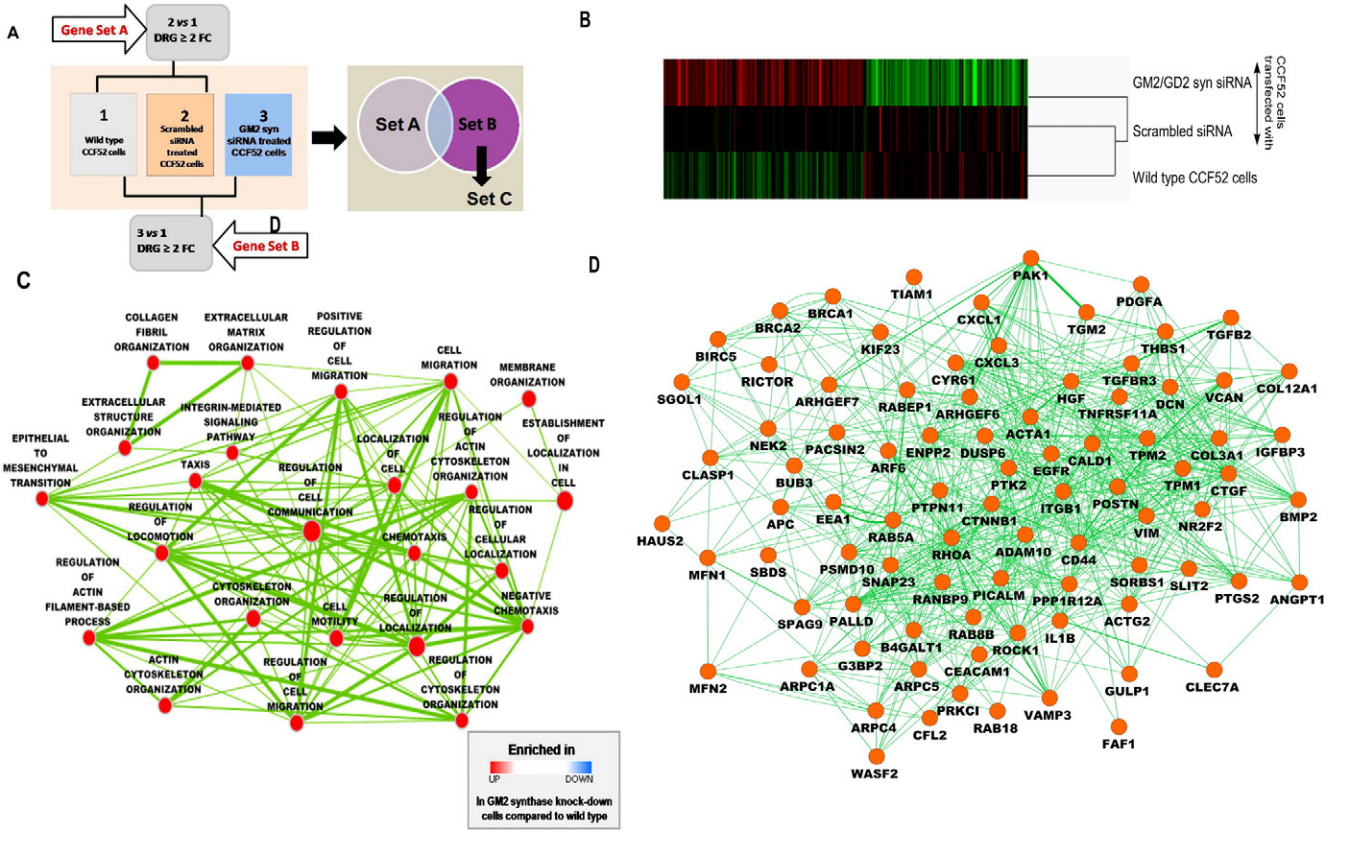

Fig. 5. Microarray analysis with GM2-synthase knockdown cancer cells reveals a distinct gene expression pattern related to cell migration and cytoskeletal remodeling. (A) Schematic workflow for detecting differentially regulated genes in GM2-synthase knockdown CCF52 cells compared to scrambled siRNA treated and wild type CCF52 cells. In the next step, differentially regulated genes (DRGs) with a fold change (FC) of expression ≥2 in scrambled siRNA treated cells *vs* wild type cells (Gene Set A) and in GM2-synthase knockdown cells *vs* wild type cells (Gene Set B) were obtained. Venn diagram between Set A and Set B gave Set C genes, the exclusive set of DRGs in knockdown cells compared to control and wild type. (B) Heatmap showing hierarchical clustering of GM2-synthase knockdown cells, scrambled siRNA (control) and wild type cells. (C) Enrichment map for cell migration and cytoskeleton organization-related gene sets of DRGs in GM2-synthase knockdown CCF52 cells. Red node color represents enrichment in knockdown cells. Color intensity is proportional to enrichment significance. The enrichment map is created at p-value = 0.005. Edge width represents the extent of interconnection between two nodes. (D) Gene interaction network of selected genes from cell migration, cell adhesion and cytoskeleton organization related GO biological processes.

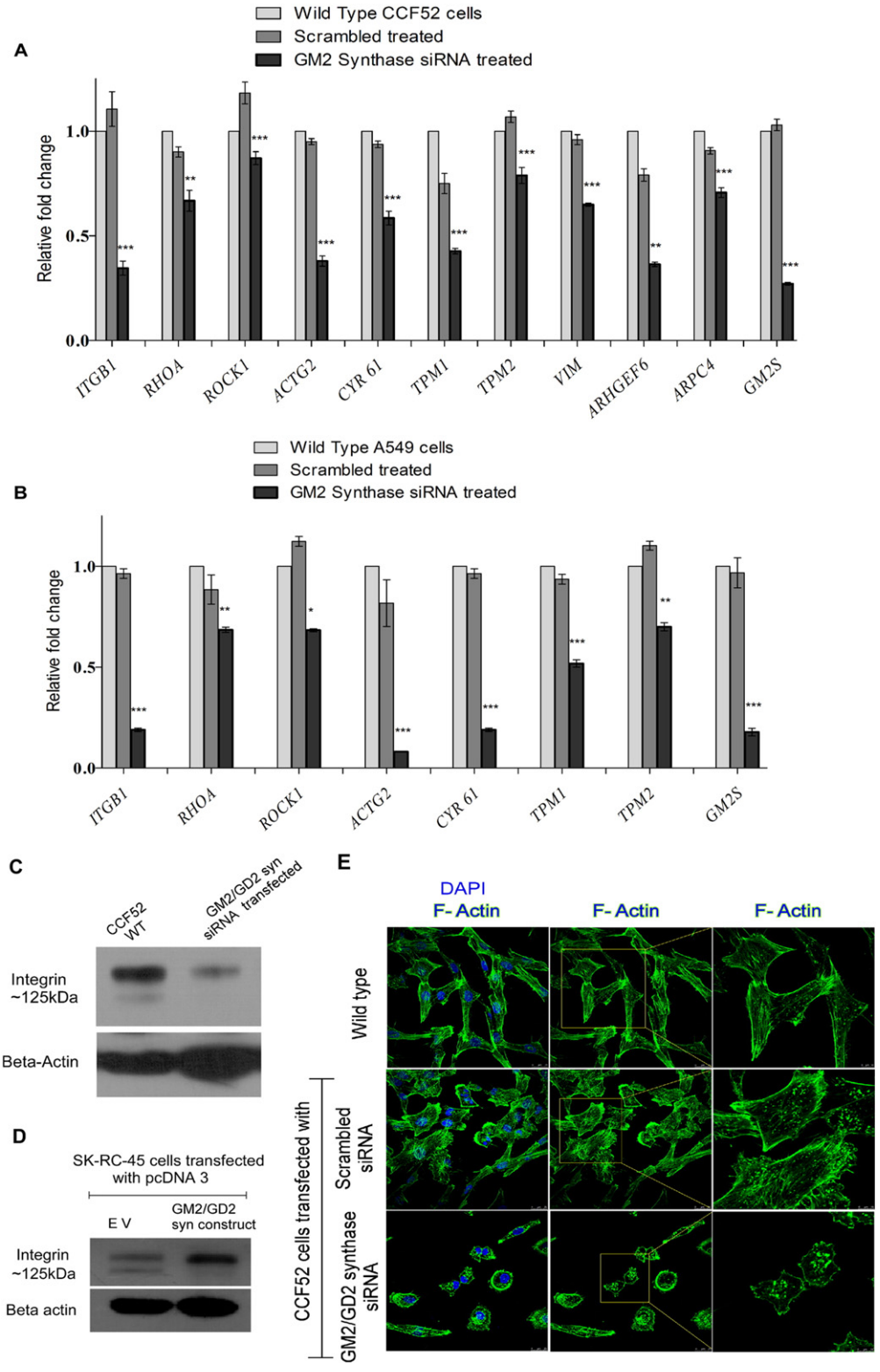

Fig. 6. Validation of the sets of genes significantly downregulated in response to GM2-synthase knockdown in microarray. (A) As shown in Table 1, selected sets of genes in CCF52 cells downregulated in response to GM2-synthase knockdown were validated by quantitative real time PCR. All mRNA quantification data were normalized to the expression of the housekeeping gene, GAPDH and expressed as fold differences of target gene expression relative to wild type. (B) Genes validated in CCF52 cells by RT-PCR were again checked in A549 cells by quantitative real time PCR in response to GM2-synthase knockdown versus scrambled siRNA treated and wild type A549 cells. (C) Expression level of integrin protein in CCF52 wild type and GM2-synthase siRNA treated cells analyzed by western blot. (D) Expression level of integrin protein in empty vector (EV) transfected and GM2 over-expressed SK-RC-45 cells analyzed by western blot. (E) Confocal microscopy demonstrating the reduction in stress fiber in GM2-synthase knockdown CCF52 cells when compared to wild type and scrambled siRNA treated cells after staining with FITC-tagged (green) F-actin antibody. The left panels show the merged image of the cells stained with DAPI and F-actin, the middle panel represents only the F-actin stained image of the same field, and the right panel represents a magnified image of the field as indicated by the box.

was obtained from ganglioside isolates in SK-RC-45 cells treated with exogenous GM2 versus non-treated cells as shown from the thin layer chromatogram (Fig. 2C). By comparing the pixel densities of the GM2 band in the treated lane versus that of the standard bovine brain derived GM2 in Fig. 2C, the mass amount of GM2 actually incorporated was calculated to be 5 μg. These data collectively confirm that exogenously added GM2 is incorporated in the cells, since there is a dose-dependent increase in LSA and no significant alterations were observed in its active metabolism.

3.3. Ganglioside GM2 has no significant role on tumor cell proliferation

MTT assay was performed in GM2-synthase knockdown cells, cells over-expressing GM2-synthase as well as cells treated with exogenous GM2 to measure any change in the mitochondrial activity as an index of cellular proliferation. Although proliferation of both CCF52 and A549 cells (Fig. 2D & E) was found to increase time dependently, however, siRNA mediated GM2-synthase knockdown did not affect proliferation significantly either in the case of CCF52 (Fig. 2D) or A549

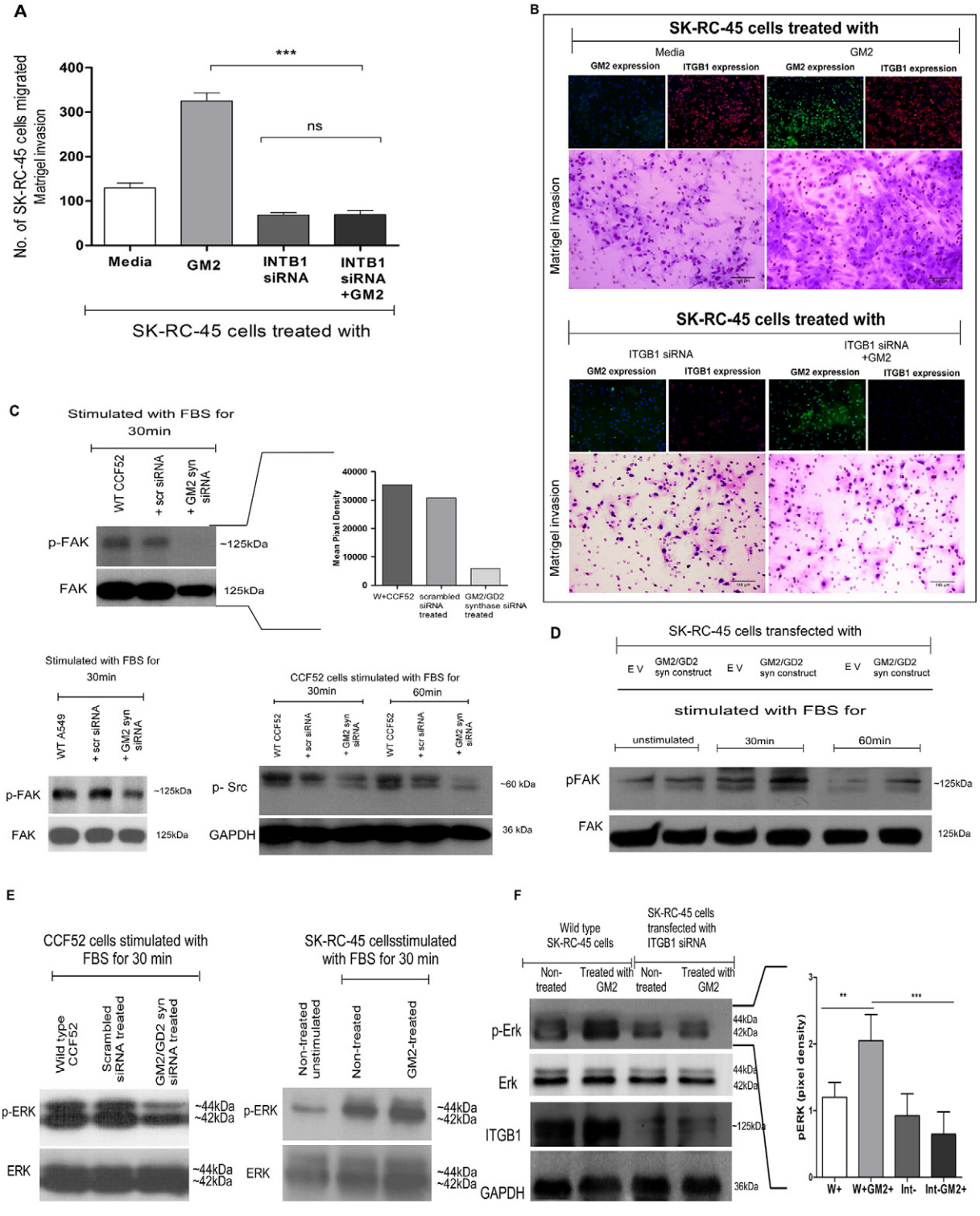

cells (Fig. 2E) when compared to either the scrambled or wild type cells at each time point. Further, proliferation was measured in GM2-overexpressing SK-RC-45 cells and compared with empty vector transfected control cells time dependently. Fig. 2F clearly shows no significant alterations in proliferation of SK-RC-45 cells transfected with GM2-synthase construct as compared to either empty vector transfected cells or wild type SK-RC-45 cells, suggesting that GM2 might not play a role in tumor cell proliferation. Additionally, MTT proliferation was checked in SK-RC-45 cells treated or not with exogenous GM2. As shown in Fig. 2G, there is no significant change in the proliferation of GM2 treated versus non-treated SK-RC-45 cells, which confirmed that GM2 does not play any significant role in proliferative capacity of tumor cells.

3.4. siRNA mediated knockdown of GM2-synthase significantly inhibits tumor cell migration and invasion

Since, beside proliferation migration and invasion of tumor cells constitute one of the important characteristics that govern tumor cell metastasis, we wanted to see if siRNA mediated GM2-synthase knockdown affects tumor cell migration as well as invasion. Migration was measured in GM2-synthase siRNA transfected tumor cells and compared with cells transfected with either scrambled siRNA or wild type cells (Fig. 3A & B) using the transwell migration assay. GM2-synthase silencing resulted in a significant reduction in migration of both CCF52 (Fig. 3A nearly 40% reduction in migration) and A549 cells (Fig. 3A, nearly 45% reduction in migration), thereby suggesting a plausible role of GM2 in tumor cell migration *in vitro*. Fig. 3B represents microscopic images showing significantly less number of cells migrated in response to GM2-synthase knockdown as compared to either wild type CCF52 cells (upper panel) and A549 cells (lower panel) or to their respective scrambled controls. Similar reduction in migration was also observed in SK-RC-26B cells transfected with GM2-synthase siRNA (Supplementary Fig. S3). Tumor cell invasion was assessed in either wild type, scrambled or GM2-synthase siRNA transfected CCF52 and A549 cells (Fig. 3C & D) using the matrigel invasion assay as described earlier. GM2-synthase knockdown caused a significant decrease in tumor cell invasion when compared to either wild type or scrambled tumor cells (Fig. 3C, ~87% reduction in CCF52 and ~70% reduction in A549 cells). Fig. 3D shows photomicrographs of representative fields demonstrating a significantly reduced number of invading cells in GM2-synthase knockdown conditions as compared to either control or scrambled.

3.5. Ganglioside GM2 modulates tumor cell migration

Since, siRNA mediated knockdown of GM2-synthase caused a significant reduction in migration/invasion of at least three different tumor cell lines, we wanted to check whether over-expression of the same results in increased migration of tumor cells. Immunofluorescence data, as shown in Fig. 4B (top panels), qPCR data and western blot (as shown in Supplementary Fig. S1A and B) confirmed GM2 over-expression in cells transfected with GM2-synthase construct versus empty vector transfected cells. Over-expression of GM2-synthase as well as ganglioside GM2 in a lower GM2-expressing tumor cell line SK-RC-45 resulted in a significant increase in tumor cell migration as compared to empty vector transfected cells (Fig. 4A). Photomicrographs of GM2 over-expressed versus empty vector transfected SK-RC-45 cells are represented in Fig. 4B (bottom panels) showing a significantly increased number of migrated GM2 over-expressing clones over empty vector transfected cells. These results confirm a potential role of GM2 in mediating tumor cell migration at least *in vitro*. To conclusively prove the role of GM2 in tumor cell migration, transwell migration and invasion assay was conducted in SK-RC-45 cells exposed to exogenous GM2 treatment. Further, addition of GM2 for 24 h resulted in an increased uptake of the ganglioside as evidenced from the increased fluorescence in GM2 treated versus non-treated cells (Fig. 4D, top panels). Increased GM2 uptake by SK-RC-45 cells resulted in a dramatic increase in tumor cell migration (Fig. 4C) as well as invasion (Fig. 4E) over non-treated cells. Representative photomicrographs clearly show a significant increase in the number of migrated/invaded SK-RC-45 cells in GM2 treated versus non-treated conditions both in migration and invasion assay (Fig. 4D, lower panels & Fig. 4F), hence confirming a vital role of GM2 in tumor cell migration.

3.6. Microarray analysis identifies a distinct gene expression pattern in GM2-synthase knockdown cancer cells as compared to wild type

To elucidate the molecular mechanism, gene expression profiles were compared between wild type cells and scrambled siRNA transfected cells (control) (SetA) and between wild-type cells and GM2-synthase knockdown (SetB) to isolate sets of differentially regulated genes (DRGs) [fold change (FC) ≥ 2]. Between SetA and SetB, the exclusive set of DRGs (SetC) belong to GM2-synthase siRNA treated cells compared to control and WT (Fig. 5A). The heatmap with this exclusive set of genes confirmed the distinct contrast in gene expression signature between the GM2-synthase siRNA treated cells versus corresponding wild type control (Fig. 5B).

3.7. Cell migration related biological processes are significantly associated with GM2-synthase expression in tumor cells

Gene ontology (GO) analysis showed that highly enriched GO biological processes in SetC genes were associated with modulation of cell migration and motility. An enrichment map showed a network of cell migration and motility associated GO biological processes enriched in SetC genes ($p < 0.05$), which were uniquely regulated in GM2-synthase knockdown cells (Fig. 5C). Further investigation into the intercommunication among the participating genes in the enriched GO processes showed a network of gene interaction as depicted in Fig. 5D. Integrin exerts its effect through several key players that act in concert

Fig. 7. GM2 modulates tumor cell migration by involving integrin-dependent phosphorylation of ERK–MAPK pathway. (A) *In vitro* transwell matrigel invasion assay with non-treated SK-RC-45 cells, SK-RC-45 cells treated with exogenous GM2, integrin β1 knockdown SK-RC-45 cells and integrin β1 knockdown cells treated with exogenous GM2. Data was analyzed by one way ANOVA (Tukey's multiple comparison test), ***$p < 0.001$ versus integrin β1 knockdown SK-RC-45 cells treated with exogenous GM2. No significant difference was observed between only integrin β1 knockdown SK-RC-45 cells and integrin knockdown SK-RC-45 cells treated with exogenous GM2. (B) Upper panels represent GM2 uptake (green) and integrin β1 expression (red) by immunofluorescence microscopy and lower panels represent microscopic images showing matrigel invasion in non-treated SK-RC-45 cells, GM2 treated SK-RC-45 cells, integrin β1 knock-down SK-RC-45 cells and integrin β1 knockdown SK-RC-45 cells treated with GM2. (C) Wild type, GM2-synthase and scrambled siRNA treated CCF52 cells (upper panel) and A549 cells (lower left panel) either stimulated with 10% FBS for 30 min or 60 min or both were examined by western blotting using antibodies shown using GAPDH as loading control. Data shows time-dependent decreased phosphorylation of pFAK (upper panel and lower left panel) and pSrc (lower right panel) in GM2-synthase siRNA transfected cells. Inset represents pFAK (pixel densities) normalized to endogenous FAK level. (D) Western-immunoblot showing time dependent increase in pFAK (Y925) level in GM2-synthase over-expressed SK-RC-45 cell lines versus empty vector transfected cells, either stimulated with 10% FBS for 30 min or 60 min. (E) Left panel shows western-immunoblot of decreased phosphorylation of Erk in wild type, GM2-synthase and scrambled siRNA treated CCF52 cells stimulated with 10% FBS for 30 min; right panel shows increased Erk phosphorylation in SK-RC-45 treated exogenously with GM2 (25 μM) versus non-treated cells, stimulated with 10% FBS for 30 min. (F) Western-immunoblot of wild type SK-RC-45 cells either treated (lane 2) with exogenous GM2 (25 μM) or not (lane 1) and SK-RC-45 cells transfected with integrin-β1 siRNA untreated (lane 3) or GM2 treated (lane 4). Inset represents pErk level (pixel densities) normalized to endogenous Erk level (**$p < 0.01$ *vs* wild type and***$p > 0.001$ *vs* GM2 treated integrin β1 knockdown SK-RC-45 cells).

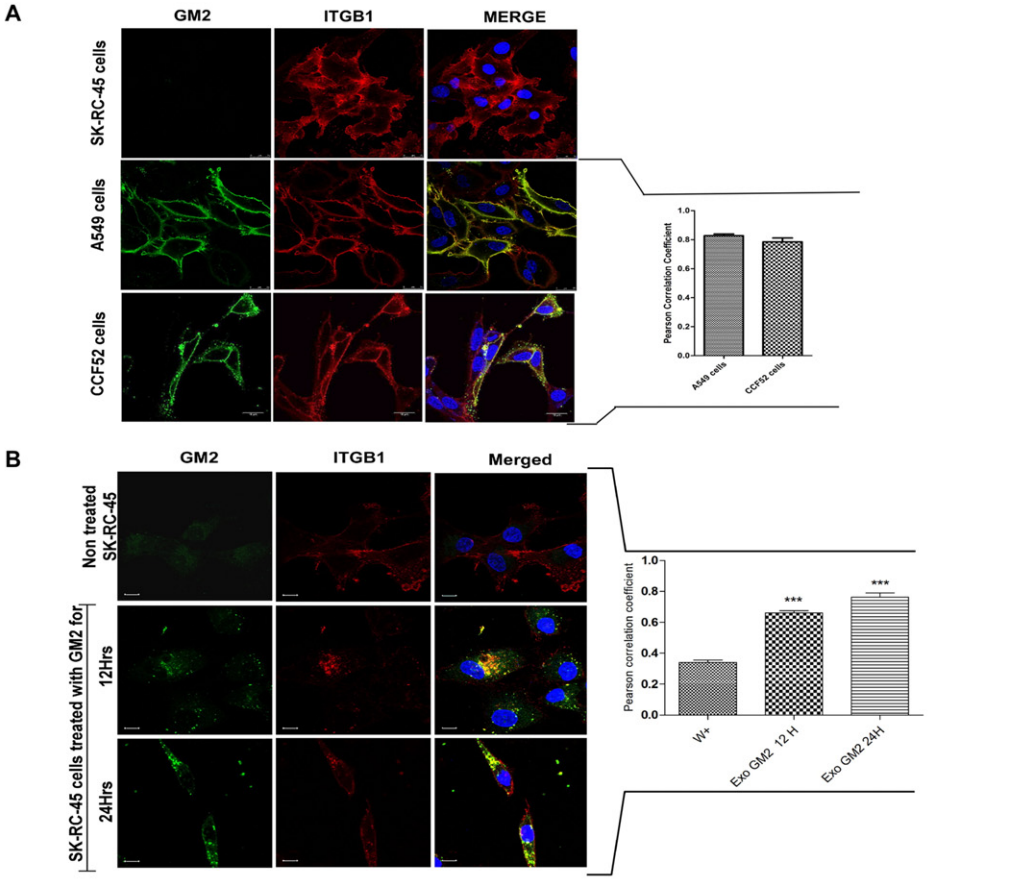

Ligand	Analyte	K_{on} (Ka) ($M^{-1}S^{-1}$)	K_{off} (Kd) (S^{-1})	Affinity (K_D) (M)
GM2	Integrin ($\alpha5\beta1$)	202.1	1.16×10^{-4}	5.7×10^{-7}

to execute the function of cell migration [46]. Since Fig. 5D provides a holistic representation of gene–gene interaction in integrin mediated cytoskeletal organization and cell motility based biological processes, we therefore focused on the key events in the integrin signaling cascade *via* which it modulates cell migration in a GM2-synthase knock-down system. Based on our literature survey and existing information, we found out that the 15 genes mentioned in Table 1 have a crucial role in the perpetration of integrin mediated cell migration. Overall, we found 15 genes (Table 1) which are significantly downregulated in response to GM2-synthase knockdown, that are also important drivers of the integrin mediated signaling cascade that modulate the phenomenon of cytoskeletal organization and cell migration. At least 10 genes out of the 15 genes listed in Table 1 were validated by quantitative real time PCR which shows significant downregulation of mRNA expression of genes (*ITGB1*, *RHOA*, *ROCK1*, *ACTG2*, *CYR61*, *TPM1*, *TPM2*, *VIM*, *ARHGEF6*, *ARPC4*) regulating the integrin dependent signaling, upon GM2-synthase knockdown compared to the scrambled siRNA (Fig. 6A) thereby suggesting the pivotal role GM2 plays in modulating integrin mediated signaling events. Interestingly, 5 out of the 15 genes in Table 1 showed no change in real time PCR following GM2-synthase knockdown (Supplementary Fig. S6). Further, those genes which showed positive validation in CCF52 cells were also validated in the A549 cell line (Fig. 6B), which shows 7 genes in this cell line to be downregulated significantly in response to GM2-synthase knockdown. Additionally, western blot data confirmed significant downregulation in integrin-β1 expression upon GM2-synthase knockdown in CCF52 cells (Fig. 6C), while over-expression of GM2-synthase in SK-RC-45 cells caused a significant upregulation of integrin-β1, as shown in Fig. 6D, thereby further validating the microarray data. Hence, microarray, real time PCR and western blot data suggests a central role of the integrin signaling pathway in GM2-mediated tumor cell migration. Integrin mediated molecular signals ultimately converge to alter cellular migrational characteristics through alterations in cytoskeletal components [47,48]. RhoA-ROCK1 genes downregulated in DNA microarray also suggest cytoskeleton rearrangement, a primary mechanism for cellular motility. Since, RhoA-ROCK1 is known to regulate actin stress fiber formation [49], alterations in an actin cytoskeleton were studied in GM2-synthase knockdown CCF52 cells. Confocal microscopy demonstrates a dramatic decrease in actin stress fiber in CCF52 cells transfected with GM2-synthase siRNA versus that of either scrambled or wild type cells (Fig. 6E), suggesting a pivotal role of GM2 in the remodeling of the actin cytoskeleton which is critical for cell migration.

3.8. GM2 mediated cell migration involves integrin-β1 and integrin-dependent phosphorylation of ERK MAPK pathway

Since, cDNA microarray data and biochemical analysis suggested a plausible role of integrin in GM2 mediated cancer cell migration/invasion, we wanted to confirm whether RNAi mediated silencing of integrin-β1 modulates GM2 mediated migration in cancer cells. siRNA mediated knockdown of integrin-β1 in SK-RC-45 cells clearly caused significant downregulation of integrin-β1 expression as shown in Fig. 7B (bottom panel) and Fig. 7F as compared to wild type SK-RC-45 cells. Data in Fig. 7A shows that while exogenous addition of GM2 in SK-RC-45 (wild type) cells cause a significant increase in the invasion of tumor cells, in the integrin-β1 silenced cells GM2 mediated invasion is significantly blocked confirming that GM2 mediated tumor cell invasion (matrigel) is integrin dependent. Fig. 7B shows representative photomicrographs of wild type SK-RC-45 cells (top panels) and integrin-β1 knockdown cells (bottom panels) in the presence or absence of exogenous GM2. Images clearly show down-regulation of integrin-β1 in SK-RC-45 cells transfected with integrin-β1 siRNA as indicated by a decrease in red fluorescence (Fig. 7B, bottom panels), while exogenous GM2 resulted in an increased uptake of GM2 by the cells as shown by green fluorescence in either wild type or knockdown cells. As integrin recruit and act as a scaffold for many partners like focal adhesion kinase (FAK) and c-Src [50], time-dependent expression and phosphorylation status of FAK and c-Src were analyzed following serum stimulation in CCF52 cells and A549 cells transfected with either GM2-synthase siRNA or scrambled siRNA versus wild type cells (Fig. 7C). Western-immunoblot shows decreased phosphorylation of FAK in CCF52 as well as in A549 cells in response to GM2-synthase knockdown as shown in Fig. 7C, upper panel and Fig. 7C lower left panel. Time-dependent decrease in pSrc levels were also observed in CCF52 cells in response to GM2-synthase knockdown (Fig. 7C, lower right panel). Over-expression of GM2-synthase in SK-RC-45 cells resulted in a time-dependent increase in the phosphorylation of FAK in the GM2 over-expressing clones compared to the empty vector transfected cells (Fig. 7D), thereby confirming the central role of integrin/FAK/Src in mediating GM2 mediated migration of tumor cells. Since phosphorylation of FAK at Y925 is known to cause downstream activation of MAPK pathway [51], Erk1/2 phosphorylation status was monitored in CCF52 cells in response to GM2-synthase knockdown. Marked decrease in the phosphorylation of ERK (pERK1/2) was observed in response to GM2-synthase knockdown at 30 min (Fig. 7E, left panel), while administration of exogenous GM2 increased pERK in SK-RC-45 cells (Fig. 7E, right panel) confirming that Erk phosphorylation is necessary for GM2 mediated migration of tumor cells possibly involving the integrin mediated downstream activation of FAK and Src. This was further confirmed by the fact that, GM2 mediated Erk phosphorylation was blocked in integrin-β1 knockdown (siRNA mediated) SK-RC-45 cells (Fig. 7F), confirming that GM2 mediated Erk phosphorylation is indeed integrin dependent. Hence, these results conclude that GM2 mediates tumor cell migration/invasion in an integrin dependent pathway through involvement of an integrin mediated downstream signaling cascade that involves phosphorylation of Erk.

3.9. GM2 interacts with integrin-β1 to mediate tumor cell migration

In an attempt to elucidate the importance of tumor derived ganglioside GM2 in fine tuning cell signaling by modulating the function of integral membrane proteins, we studied whether GM2 over-expressed in

Fig. 8. GM2 interacts and physically associates with integrin mediating tumor cell migration. (A) Representative image of the confocal microscopy of SK-RC-45, A549 and CCF52 cells with a merged image that shows significantly high interaction between integrin (ITGB1) with GM2 A549 cells and CCF52 cells versus SK-RC-45 cells, which shows low interaction. Right panel graph represents a significant increase in Pearson's correlation coefficient in A549 cells and CCF52 cells *vs* SK-RC-45 cells. The data is a representation of 3 independent experiments of 5 different fields. (B) Representative image of confocal microscopy of SK-RC-45 cells incubated with 25 μM of GM2 for 12 h and 24 h. Data shows a time-dependent increase in co-localization of integrin (ITGB1) (red) and GM2 (green) as shown in the merged images, as well as from the time-dependent increase in Pearson's coefficient (right panel graph). The data is a representation of 3 independent experiments of 5 different observed fields. Pearson's correlation coefficient is analyzed by Leica Application Suite LAS X software as described in the Materials and method section. (C) Direct interaction of endogenous GM2 with integrin-β1 in a CCF52 cell and an A549 cell as shown by a co-immunoprecipitation experiment. Briefly, membrane enriched fraction isolated from CCF52 and A549 cells were immunoprecipitated with an anti-hamster GM2 antibody and isotype control (normal hamster IgG) using protein G-agarose beads. The immunoprecipitates were analyzed by SDS-PAGE and probed for integrin-β1 by western blot with anti-mouse integrin-β1 antibody in both A549 and CCF52 cells and their respective isotype controls. Left panel: protein marker (lane 1), A549 cell membrane enriched fraction (lane 2), A549 cell isotype control (lane 3); middle panel: protein marker (lane 1), CCF52 cell membrane fraction (lane 2) and CCF52 cell isotype control (lane 3); right panel: TLC showing detectable GM2 band in ganglioside isolates from samples IP-ed with anti-hamster GM2 Ab (lane 3) versus that IP-ed with normal hamster IgG (lane 2). Lane 1: standard ganglioside mixture; lane 2: IP with isotype control antibody; lane 3: IP with GM2 antibody. (D) Direct interaction of GM2 with integrin β1 in non-treated SK-RC-45 cell membrane enriched fraction lysates, GM2 treated SK-RC-45 membrane enriched fraction lysate and its isotype control by a co-immunoprecipitation experiment as mentioned above.(E) Sensograms of SPR for GM2 binding to integrin. Various concentrations (1 μM, 5 μM, 10 μM, 25 μM, 50 μM, 100 μM) of GM2 were introduced onto the CM5 sensor chip surface immobilized with α5β1 integrin for 180 s at a flow rate of 30 μl/min. The relative response was determined by subtracting the blank values on the integrin immobilized surface.

tumor cells may be able to interact with its membrane partner integrin, thereby switching on the integrin signaling in tumor cells leading to enhanced cell migration and invasion. Plausible interaction of an integrin receptor with GM2 was studied by confocal microscopy which revealed significantly higher positive co-localization of endogenous GM2 with integrin receptor in A549 cells as well as in CCF52 cells (expressing higher levels of GM2) as compared to SK-RC-45 cells (expressing lower level of GM2) (Fig. 8A) as evident from the Pearsons correlation coefficient (Fig. 8A, right panel graphical representation) and co-localization rate (co-localization area divided by foreground area) (Supplementary Fig. S5A and B). Further we asked whether addition of exogenous GM2 in SK-RC-45 cells causes enhanced co-localization with the integrin receptor. Exogenous administration of GM2 in SK-RC-45 cells caused a time-dependent increase in co-localization of GM2 with the integrin receptor, as evident from confocal microscopy (Fig. 8B) and Pearson's correlation coefficient (Fig. 8B, right panel graphical representation) thereby suggesting a possible interaction of GM2 with the integrin receptor. This was further confirmed by co-immunoprecipitating GM2 with integrin-β1 from membrane enriched cellular fraction obtained from high endogenous GM2 expressing A549 cells and CCF52 cells. As shown in Fig. 8C, GM2 co-immunoprecipitated with integrin in both A549 cells (Fig. 8C, left panel) and CCF52 cells (Fig. 8C, middle panel) whereas no interactions were observed in isotype control (anti-hamster IgG) in both cells. The specificity of the anti-hamster GM2 Ab was ascertained by detecting a GM2 band in TLC with ganglioside isolated from samples immunoprecipitated with either anti-hamster GM2 Ab (Fig, 8C, right panel, lane 3) versus normal hamster IgG (isotype control Ab, Fig. 8C, right panel, lane 2). Next we tested whether we can detect the interaction of GM2 and integrin in SK-RC-45 cell lysates treated with or without exogenous GM2. Fig. 8D clearly shows that GM2 co-immunoprecipitated with integrin-β1 from membrane enriched fraction of SK-RC-45 cell lysates exposed to exogenous GM2 versus the background (non-treated cells) and IgG isotype control, which was detected by western blot using HRP-coupled anti-integrin-β1 antibody. These results confirm that GM2 over-expressed in tumor cells physically interacts with the integrin receptor. Finally, we assessed the ability of ganglioside GM2 to bind directly with integrin molecule, α5β1 by surface plasmon resonance (SPR) using a sensor chip (CM5) immobilized with integrin α5β1. As shown in Supplementary Fig. S7, sensograms from the reference surface show the contribution of nonspecific interaction between the blank surface and the GM2, whereas the sensogram from the active integrin immobilized surface reveals the actual GM2-integrin binding response along with nonspecific binding. A reference subtracted sensogram demonstrates GM2 binding to immobilized integrin α5β1 dose dependently and shows a K_D value (binding affinity) of 5.7×10^{-7} M (0.5 μM) (Fig. 8E). The sensograms were best fitted to a 1:1 binding model of the Langmuir equation, suggesting that one molecule of GM2 might bind to one molecule of integrin.

The results collectively demonstrate a novel role of ganglioside GM2 in mediating tumor cell migration which involves interacting with and regulating the activity of the integrin receptor leading to phosphorylation of key signaling proteins, FAK and Src. This results in downstream activation of the Erk/MAPK causing alterations of cytoskeletal remodeling, which is critical for regulation of cellular motility and migration.

4. Discussion

Several studies have demonstrated the immuno-modulatory roles of ganglioside GM2 in mediating host immune suppression in various tumors [5,9,19,32,52]. Though our group first reported that GM2 has a role in epithelial to mesenchymal transition [30], however, the precise role as well as the mechanism through which GM2 mediates tumor growth, progression and metastasis have not been investigated thoroughly. There have been few reports where anti-ganglioside GM2 antibodies were found to achieve better outcome and prognosis in clinical trials [8,12,22,23,53]. However, it remains unclear whether the observed favorable outcome in these studies stems from antibody mediated reversal of host immune suppression driven by GM2, or GM2 directly modulates tumor growth, progression and metastasis by affecting the tumor cell themselves independent of its effect on the immune system.

In the present study, we propose a novel role of ganglioside GM2 in mediating tumor cell migration/invasion, which is an essential characteristic for determining the aggressiveness and metastatic ability of tumor cells through modulation of the integrin signaling pathway [54]. Although, most of the tumor cell lines exhibited significantly high expression of GM2 levels (Fig. 1B & C), the SK-RC-45 kidney cancer cell line showed relatively lower levels of GM2-synthase as well as lower expression of ganglioside GM2. This is possibly a reflection of limiting substrate (GM3) availability in the SK-RC-45 cell line, since the TLC chromatogram of SK-RC-45 isolated gangliosides show no band corresponding to GM3 (Fig. 1B). Since administration of exogenous GM2 in the SK-RC-45 cell line (having lower expression of GM2) has been used in various experiments to ascertain the role of GM2 specifically, it is important to know whether GM2 gets incorporated into the cells or gets actively metabolized. A dose dependent increase in lipid bound sialic acid with exogenously added GM2 confirms the incorporation of exogenous GM2 within a cell (Fig. 2A), while no significant change in the levels of ceramide-1-phosphate (Fig. 2B) generated by the kinase activity of a recombinant ceramide-1-kinase suggests that not much of the incorporated GM2 is actively metabolized at least at the time point chosen for the assays. Our findings demonstrate a potential role of ganglioside GM2 in tumor cell migration and invasion *in vitro*, either by siRNA mediated knockdown of GM2-synthase (Fig. 3) or stable GM2 over-expression in SK-RC-45 cells (Fig. 4A & B). Previous reports demonstrated the suppression of hepatoma cell motility by ganglioside GM3 [21]. Hence, it is quite possible that the observed reduction in tumor cell migration/invasion in response to GM2-synthase knockdown (Fig. 3) might actually be due to an increase in levels of suppressive GM3 than due to a decrease in GM2. However, the increase in migration observed in GM2 over-expressing SK-RC-45 clones (Fig. 4A) suggests that the observed migration is due to GM2 alone, since SK-RC-45 did not show any appreciable levels of GM3, as evident from the absence of the band corresponding to GM3 (Fig. 1B). To confirm this further, we assessed the migration as well as invasion of tumor cells in response to exogenous GM2 treatment which resulted in a dramatic increase in migratory capacity and invading property of SK-RC-45 cells in response to GM2 treatment (Fig. 4C–F), clearly demonstrating a direct role of GM2 in tumor cell migration. Since immunofluorescence data demonstrated the transfer of exogenous GM2 on the surface of SK-RC-45 cells (Fig. 4D, top panels), this data represents a close mimic of how increased GM2 expression in various tumors may influence motility of the tumor cells.

Although the mechanism by which GM2 promotes tumor induced host immune-suppression have been extensively studied [3,5,9,19], the mechanism through which it might modulate tumor growth and progression was largely unknown. From our microarray data analysis (Fig. 5), we focused and selected certain key players that act as important regulators in integrin mediated cell migration. The selection was based on existing literature regarding their pivotal role and crucial involvement in integrin dependent cytoskeletal alterations and modulation of cellular migration. Overall, we find that these 15 genes (Table 1) are important drivers of the integrin mediated signaling cascade that modulate cytoskeletal organization and cell migration, suggesting a central role of the integrin receptor and its downstream signaling in GM2 mediated migration of tumor cells. Intriguingly, integrin expression was downregulated in GM2-synthase knockdown cell lines (Fig. 6C) and elevated in GM2 over-expressed cell lines (Fig. 6D), thus suggesting regulation of integrin expression by GM2. At least 10 genes were validated by real time PCR (Fig. 6A), which have a

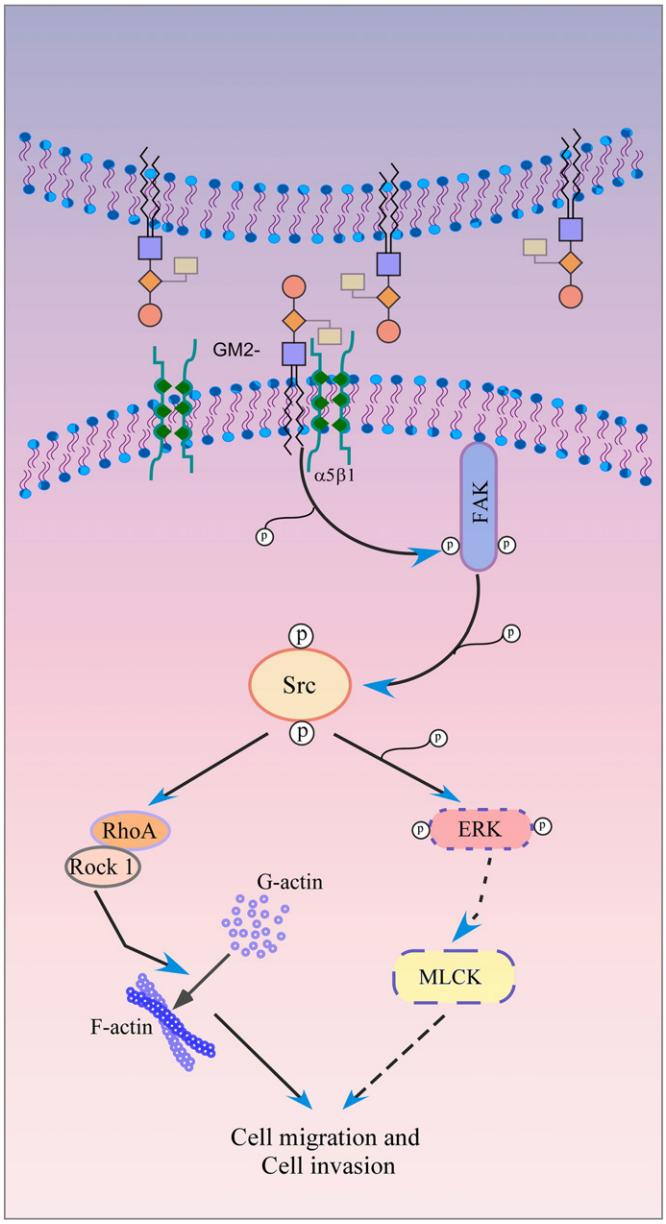

Fig. 9. A hypothetical model proposing how ganglioside GM2 mediates tumor cell migration by interacting with integrin *via* modulation of integrin signaling pathway. Ganglioside GM2, over-expressed in tumor cell lines possibly binds with integrin (α5β1) on the same cells (*cis*) or on different cells (*trans*), thereby switching on the integrin signaling pathway, resulting in further downstream activation of the non-receptor tyrosine kinases like focal adhesion kinase (FAK) and c-Src forming a dual kinase complex. The FAK–Src complex activates and phosphorylates downstream activator proteins like RhoA, ROCK1 and ERK which further enhances F-actin formation thus remodeling the cytoskeleton resulting in enhanced tumor cell migration and invasion.

definitive role in cytoskeleton remodeling and differentiation [55,56]. We do not yet fully understand why GM2-synthase silencing causes reductions in mRNA of adhesion/migration/motility genes, since this is a subject of a separate study currently under active investigation in our laboratory. However, we believe that this may be a consequence of GM2's effect on integrin expression. Since, integrin expression is controlled by GM2 through an unknown mechanism (Fig. 6C & D and Table 1), and since integrin itself regulates expression of several migration/motility related genes [57], it is quite possible that many of the adhesion/migration genes listed in Table 1 or in Fig. 6A & B, may be the consequence of GM2 mediated regulation of integrin expression. However, additional experiments need to be performed to prove this. Additionally, unpublished data from our laboratory shows that GM2 may mediate EMT (epithelial mesenchymal transition) through YAP, a major component of the HIPPO signaling pathway. EMT mediated by YAP involves binding of YAP with TEAD, a transcriptional co-activator. Almost all of the genes listed in Table 1 have TEAD binding sites, which might suggest that GM2 may control expression of many of these genes through modulating the HIPPO signaling pathway. An in-depth study of the molecular signaling mechanisms governing GM2 mediated migration/invasion showed that GM2 mediated invasion is integrin dependent since, exogenous GM2 caused a significant increase in the invasion of wild type SK-RC-45 cells, however siRNA mediated silencing of integrin-β1 in SK-RC-45 cells resulted in an almost 80% block of invasion even in response to GM2 treatment (Fig. 7A–B). Moreover, activation of integrin receptors by GM2 resulted in downstream activation of the MAP kinase (Fig. 7E). That Erk phosphorylation in response to GM2 was indeed integrin dependent was confirmed by a decrease in pErk in integrin knockdown SK-RC-45 cells treated with exogenous GM2 as shown in Fig. 7F.

Tumor associated gangliosides are known to be localized in GEM/rafts and integrin being a membrane protein presents a high possibility that GM2 might interact with membrane bound integrins, switching on its signaling pathway thereby enhancing tumor cell migration. Although, collectively, confocal microscopy (Fig. 8A & B), co-IP data (Fig. 8C & D) as well as the SPR data (Fig. 8E) proves the binding of GM2 with the integrin-β1 receptor, whether GM2 mediates its effect through interacting with integrin on the same cell (*cis*) or on different cells (*trans*) or both simultaneously, needs further investigations. Interestingly, GM2 was earlier reported to inhibit migration by complexing with tetraspanin CD82 membrane protein, a tumor metastasis suppressor [58] in normal bladder cells [11]. Most cancer cells were found to be either CD82 deficient or its expression in cancer cells was found to be significantly low [59], and the absence of CD82 in many cancers have been suggested to be associated with the metastatic ability of tumors [60]. Thus, our study showing the ability of GM2 alone in promoting tumor cell migration/invasion might also suggest a differential role of GM2 in normal versus cancer cells which may be dependent on the availability of the CD82 complex. Hence, it is quite probable that CD82 over-expressed in normal cells might transduce an inhibitory signal towards migration by complexing with GM2, however, in cancer cells lacking CD82, GM2 alone might be pro-migratory, however this needs additional studies.

Hence, our data suggests that the molecular mechanism underlying GM2 mediated cancer cell migration is through a direct interaction of GM2 with integrin in the membrane resulting in the switching on of integrin signaling involving FAK/Src/MAP-K pathway and altering the Rho-ROCK equilibrium in lamellipodia of tumor cells resulting in an altered cytoskeletal modulation ultimately enhancing the migratory behavior of cancer cells. A hypothetical scheme for this mechanism is illustrated in Fig. 9.

5. Conclusion

Our findings presented here show that GM2 mediates tumor cell migration through biophysical interaction of an integrin molecule and activation of the integrin receptor leading to downstream signaling and phosphorylation of Erk–MAPK, which further results in alterations in the actin cytoskeleton leading to increased migration in tumors. This study not only provides the first direct evidence of ganglioside GM2 in tumor cell migration/invasion, but also uncovered a novel pro-tumorigenic mechanism by which a tumor derived glycolipid can bind with integrin to modulate tumor cell behavior, which may eventually help in targeting GM2 and consequently in devising future therapeutic strategies against cancer.

Supplementary data to this article can be found online at http://dx.doi.org/10.1016/j.bbamcr.2016.04.004.

Funding

This work was supported by funds obtained from Bose Institute and the Council of Scientific and Industrial Research (CSIR), India [Sanction No. 27(0246)/11/EMR-II].

Conflict of interest statement

The authors declare that they have no conflicts of interest with the contents of this article.

Author's contribution

M.K., B.M., A.B., S.D. and S.S.R. performed experimental work. S.C. and Z.G. were involved in analyzing the microarray data. K.B. hypothesized, conceptualized and provided overall supervision of the study. K.B., Z.G. and M.K. were involved in drafting the manuscript. K.B. and Z.G. contributed to the final interpretation of the microarray data after analysis. All authors read and approved the manuscript.

Transparency document

The Transparency document associated with this article can be found, in online version.

Acknowledgements

Manjari Kundu (Bose Institute Research Fellowship) thanks Bose Institute and Barun Mahata [09/015(0409)/2011-EMR-1] acknowledges the Council of Scientific and Industrial Research (CSIR), New Delhi, India for providing their Senior Research Fellowship. Avisek Banerjee (P-1133) and Shibjyoti Debnath [F.2-8/2002(SA-1)] acknowledge University Grants Commission (UGC) for providing their Research Fellowship. We also acknowledge Mr. Tarun Mahata (Project Assistant) for assisting in routine laboratory procedures and helping in growing cells for ganglioside isolation.

References

[1] G. van Echten, K. Sandhoff, Ganglioside metabolism. Enzymology, Topology, and regulation, J. Biol. Chem. 268 (1993) 5341–5344.
[2] A. Huwiler, T. Kolter, J. Pfeilschifter, K. Sandhoff, Physiology and pathophysiology of sphingolipid metabolism and signaling, Biochim. Biophys. Acta 1485 (2000) 63–99.
[3] D. Kudo, P. Rayman, C. Horton, M.K. Cathcart, R.M. Bukowski, M. Thornton, C. Tannenbaum, J.H. Finke, Gangliosides expressed by the renal cell carcinoma cell line SK-RC-45 are involved in tumor-induced apoptosis of T cells, Cancer Res. 63 (2003) 1676–1683.
[4] R.G. Uzzo, P. Rayman, V. Kolenko, P.E. Clark, T. Bloom, A.M. Ward, L. Molto, C. Tannenbaum, L.J. Worford, R. Bukowski, R. Tubbs, E.D. Hsi, N.H. Bander, A.C. Novick, J.H. Finke, Mechanisms of apoptosis in T cells from patients with renal cell carcinoma, Clin. Cancer Res. 5 (1999) 1219–1229.
[5] S. Biswas, K. Biswas, A. Richmond, J. Ko, S. Ghosh, M. Simmons, P. Rayman, B. Rini, I. Gill, C.S. Tannenbaum, J.H. Finke, Elevated levels of select gangliosides in T cells from renal cell carcinoma patients is associated with T cell dysfunction, J. Immunol. 183 (2009) 5050–5058.
[6] T. Tsuchida, M.H. Ravindranath, R.E. Saxton, R.F. Irie, Gangliosides of human melanoma: altered expression in vivo and in vitro, Cancer Res. 47 (1987) 1278–1281.
[7] S. Zhang, C. Cordon-Cardo, H.S. Zhang, V.E. Reuter, S. Adluri, W.B. Hamilton, K.O. Lloyd, P.O. Livingston, Selection of tumor antigens as targets for immune attack using immunohistochemistry: I. Focus on gangliosides, Int. J. Cancer 73 (1997) 42–49.
[8] H. Fukumoto, K. Nishio, S. Ohta, N. Hanai, K. Fukuoka, Y. Ohe, K. Sugihara, T. Kodama, N. Saijo, Effect of a chimeric anti-ganglioside GM2 antibody on ganglioside GM2-expressing human solid tumors in vivo, Int. J. Cancer 82 (1999) 759–764.
[9] K. Biswas, A. Richmond, P. Rayman, S. Biswas, M. Thornton, G. Sa, T. Das, R. Zhang, A. Chahlavi, C.S. Tannenbaum, A. Novick, R. Bukowski, J.H. Finke, GM2 expression in renal cell carcinoma: potential role in tumor-induced T-cell dysfunction, Cancer Res. 66 (2006) 6816–6825.
[10] Y. Yuyama, T. Dohi, H. Morita, K. Furukawa, M. Oshima, Enhanced expression of GM2/GD2 synthase mRNA in human gastrointestinal cancer, Cancer 75 (1995) 1273–1280.
[11] A.R. Todeschini, J.N. Dos Santos, K. Handa, S.I. Hakomori, Ganglioside GM2–tetraspanin CD82 complex inhibits met and its cross-talk with integrins, providing a basis for control of cell motility through glycosynapse, J. Biol. Chem. 282 (2007) 8123–8133.
[12] T. Yamada, H. Bando, S. Takeuchi, K. Kita, Q. Li, W. Wang, S. Akinaga, Y. Nishioka, S. Sone, S. Yano, Genetically engineered humanized anti-ganglioside GM2 antibody against multiple organ metastasis produced by GM2-expressing small-cell lung cancer cells, Cancer Sci. 102 (2011) 2157–2163.
[13] S. Hakomori, Glycolipids of tumor cell membrane, Adv. Cancer Res. 18 (1973) 265–315.
[14] S. Ladisch, B. Gillard, C. Wong, L. Ulsh, Shedding and immunoregulatory activity of YAC-1 lymphoma cell gangliosides, Cancer Res. 43 (1983) 3808–3813.
[15] G. Floutsis, L. Ulsh, S. Ladisch, Immunosuppressive activity of human neuroblastoma tumor gangliosides, Int. J. Cancer 43 (1989) 6–9.
[16] R.G. Uzzo, P. Rayman, V. Kolenko, P.E. Clark, M.K. Cathcart, T. Bloom, A.C. Novick, R.M. Bukowski, T. Hamilton, J.H. Finke, Renal cell carcinoma-derived gangliosides suppress nuclear factor-kappaB activation in T cells, J. Clin. Investig. 104 (1999) 769–776.
[17] G.V. Shurin, M.R. Shurin, S. Bykovskaia, J. Shogan, M.T. Lotze, E.M. Barksdale Jr., Neuroblastoma-derived gangliosides inhibit dendritic cell generation and function, Cancer Res. 61 (2001) 363–369.
[18] A. Jales, R. Falahati, E. Mari, E.J. Stemmy, W. Shen, C. Southammakosane, D. Herzog, S. Ladisch, D. Leitenberg, Ganglioside-exposed dendritic cells inhibit T-cell effector function by promoting regulatory cell activity, Immunology 132 (2011) 134–143.
[19] A. Chahlavi, P. Rayman, A.L. Richmond, K. Biswas, R. Zhang, M. Vogelbaum, C. Tannenbaum, G. Barnett, J.H. Finke, Glioblastomas induce T-lymphocyte death by two distinct pathways involving gangliosides and CD70, Cancer Res. 65 (2005) 5428–5438.
[20] K.H. Hidenobu Shibuya, Hiroshi Hotta, Yasuyuki Matsumoto, Yoshihiro Nishida, K.F. Hisashi Hattori, Minoru Ueda, Koichi Furukawa, Enhancement of malignant properties of human osteosarcoma cells with disialyl gangliosides GD2/GD3, Cancer Sci. 103 (2012) (1656-1664).
[21] X. Huang, Y. Li, J. Zhang, Y. Xu, Y. Tian, K. Ma, Ganglioside GM3 inhibits hepatoma cell motility via down-regulating activity of EGFR and PI3K/AKT signaling pathway, J. Cell. Biochem. 114 (2013) 1616–1624.
[22] K. Nakamura, M. Koike, K. Shitara, Y. Kuwana, K. Kiuragi, S. Igarashi, M. Hasegawa, N. Hanai, Chimeric anti-ganglioside GM2 antibody with antitumor activity, Cancer Res. 54 (1994) 1511–1516.
[23] M.W. Retter, J.C. Johnson, D.W. Peckham, J.E. Bannink, C.S. Bangur, K. Dresser, F. Cai, T.M. Foy, N.A. Fanger, G.R. Fanger, B. Woda, K.L. Rock, Characterization of a proapoptotic antiganglioside GM2 monoclonal antibody and evaluation of its therapeutic effect on melanoma and small cell lung carcinoma xenografts, Cancer Res. 65 (2005) 6425–6434.
[24] M. Ono, K. Handa, S. Sonnino, D.A. Withers, H. Nagai, S. Hakomori, GM3 ganglioside inhibits CD9-facilitated haptotactic cell motility: coexpression of GM3 and CD9 is essential in the downregulation of tumor cell motility and malignancy, Biochemistry 40 (2001) 6414–6421.
[25] M.S. Toledo, E. Suzuki, K. Handa, S. Hakomori, Cell growth regulation through GM3-enriched microdomain (glycosynapse) in human lung embryonal fibroblast WI38 and its oncogenic transformant VA13, J. Biol. Chem. 279 (2004) 34655–34664.
[26] A. Hashiramoto, H. Mizukami, T. Yamashita, Ganglioside GM3 promotes cell migration by regulating MAPK and c-Fos/AP-1, Oncogene 25 (2006) 3948–3955.
[27] Y. Ohkawa, S. Miyazaki, K. Hamamura, M. Kambe, M. Miyata, O. Tajima, Y. Ohmi, Y. Yamauchi, K. Furukawa, Ganglioside GD3 enhances adhesion signals and augments malignant properties of melanoma cells by recruiting integrins to glycolipid-enriched microdomains, J. Biol. Chem. 285 (2010) 27213–27223.
[28] Y. Ohkawa, H. Momota, A. Kato, N. Hashimoto, Y. Tsuda, N. Kotani, K. Honke, A. Suzumura, K. Furukawa, Y. Ohmi, A. Natsume, T. Wakabayashi, Ganglioside GD3 enhances invasiveness of gliomas by forming a complex with platelet-derived growth factor receptor alpha and Yes kinase, J. Biol. Chem. 290 (2015) 16043–16058.
[29] C. Tringali, B. Lupo, I. Silvestri, N. Papini, L. Anastasia, G. Tettamanti, B. Venerando, The plasma membrane sialidase NEU3 regulates the malignancy of renal carcinoma cells by controlling beta1 integrin internalization and recycling, J. Biol. Chem. 287 (2012) 42835–42845.
[30] B. Mahata, A. Banerjee, M. Kundu, U. Bandyopadhyay, K. Biswas, TALEN mediated targeted editing of GM2/GD2-synthase gene modulates anchorage independent growth by reducing anoikis resistance in mouse tumor cells, Sci. Rep. 5 (2015) 9048.
[31] S. Ladisch, B. Gillard, A solvent partition method for microscale ganglioside purification, Anal. Biochem. 146 (1985) 220–231.
[32] G. Raval, S. Biswas, P. Rayman, K. Biswas, G. Sa, S. Ghosh, M. Thornton, C. Hilston, T. Das, R. Bukowski, J. Finke, C.S. Tannenbaum, TNF-alpha induction of GM2 expression on renal cell carcinomas promotes T cell dysfunction, J. Immunol. 178 (2007) 6642–6652.
[33] N. Katopodis, C.C. Stock, Improved method to determine lipid bound sialic acid in plasma or serum, Res. Commun. Chem. Pathol. Pharmacol. 30 (1980) 171–180.
[34] L. Svennerholm, Quantitative estimation of sialic acids. II. A colorimetric resorcinol–hydrochloric acid method, Biochim. Biophys. Acta 24 (1957) 604–611.
[35] F. Scandroglio, N. Loberto, M. Valsecchi, V. Chigorno, A. Prinetti, S. Sonnino, Thin layer chromatography of gangliosides, Glycoconj. J. 26 (2009) 961–973.
[36] M. Bektas, P.S. Jolly, S. Milstien, S. Spiegel, A specific ceramide kinase assay to measure cellular levels of ceramide, Anal. Biochem. 320 (2003) 259–265.
[37] D.K. Perry, A. Bielawska, Y.A. Hannun, Quantitative determination of ceramide using diglyceride kinase, Methods Enzymol. 312 (2000) 22–31.
[38] A.I. Saeed, N.K. Bhagabati, J.C. Braisted, W. Liang, V. Sharov, E.A. Howe, J. Li, M. Thiagarajan, J.A. White, J. Quackenbush, TM4 microarray software suite, Methods Enzymol. 411 (2006) 134–193.
[39] M.J. de Hoon, S. Imoto, J. Nolan, S. Miyano, Open source clustering software, Bioinformatics 20 (2004) 1453–1454.
[40] A.J. Saldanha, Java Treeview—extensible visualization of microarray data, Bioinformatics 20 (2004) 3246–3248.
[41] S. Maere, K. Heymans, M. Kuiper, BiNGO: a Cytoscape plugin to assess overrepresentation of gene ontology categories in biological networks, Bioinformatics 21 (2005) 3448–3449.
[42] D. Merico, R. Isserlin, O. Stueker, A. Emili, G.D. Bader, Enrichment map: a network-based method for gene-set enrichment visualization and interpretation, PLoS One 5 (2010) e13984.

[43] D. Warde-Farley, S.L. Donaldson, O. Comes, K. Zuberi, R. Badrawi, P. Chao, M. Franz, C. Grouios, F. Kazi, C.T. Lopes, A. Maitland, S. Mostafavi, J. Montojo, Q. Shao, G. Wright, G.D. Bader, Q. Morris, The GeneMANIA prediction server: biological network integration for gene prioritization and predicting gene function, Nucleic Acids Res. 38 (2010) W214–W220.
[44] M. Kulma, M. Herec, W. Grudzinski, G. Anderluh, W.I. Gruszecki, K. Kwiatkowska, A. Sobota, Sphingomyelin-rich domains are sites of lysenin oligomerization: implications for raft studies, Biochim. Biophys. Acta 1798 (2010) 471–481.
[45] K. Kwiatkowska, E. Marszalek-Sadowska, G. Traczyk, P. Koprowski, M. Musielak, A. Lugowska, M. Kulma, A. Grzelczyk, A. Sobota, Visualization of cholesterol deposits in lysosomes of Niemann–Pick type C fibroblasts using recombinant perfringolysin O, Orphanet J. Rare Dis. 9 (2014) 64.
[46] J.D. Hood, D.A. Cheresh, Role of integrins in cell invasion and migration, Nat. Rev. Cancer 2 (2002) 91–100.
[47] B. Geiger, J.P. Spatz, A.D. Bershadsky, Environmental sensing through focal adhesions, Nat. Rev. Mol. Cell Biol. 10 (2009) 21–33.
[48] M. Vicente-Manzanares, C.K. Choi, A.R. Horwitz, Integrins in cell migration—the actin connection, J. Cell Sci. 122 (2009) 199–206.
[49] S. Pellegrin, H. Mellor, Actin stress fibres, J. Cell Sci. 120 (2007) 3491–3499.
[50] S.K. Mitra, D.D. Schlaepfer, Integrin-regulated FAK-Src signaling in normal and cancer cells, Curr. Opin. Cell Biol. 18 (2006) 516–523.
[51] S.K. Mitra, D. Mikolon, J.E. Molina, D.A. Hsia, D.A. Hanson, A. Chi, S.T. Lim, J.A. Bernard-Trifilo, D. Ilic, D.G. Stupack, D.A. Cheresh, D.D. Schlaepfer, Intrinsic FAK activity and Y925 phosphorylation facilitate an angiogenic switch in tumors, Oncogene 25 (2006) 5969–5984.
[52] M. Wolfl, W.Y. Batten, C. Posovszky, H. Bernhard, F. Berthold, Gangliosides inhibit the development from monocytes to dendritic cells, Clin. Exp. Immunol. 130 (2002) 441–448.
[53] P.O. Livingston, G.Y. Wong, S. Adluri, Y. Tao, M. Padavan, R. Parente, C. Hanlon, M.J. Calves, F. Helling, G. Ritter, et al., Improved survival in stage III melanoma patients with GM2 antibodies: a randomized trial of adjuvant vaccination with GM2 ganglioside, J. Clin. Oncol. 12 (1994) 1036–1044.
[54] J.A. Joyce, J.W. Pollard, Microenvironmental regulation of metastasis, Nat. Rev. Cancer 9 (2009) 239–252.
[55] Z. Wang, J.M. Symons, S.L. Goldstein, A. McDonald, J.H. Miner, J.A. Kreidberg, (Alpha)3(beta)1 integrin regulates epithelial cytoskeletal organization, J. Cell Sci. 112 (Pt 17) (1999) 2925–2935.
[56] E.N. Olson, A. Nordheim, Linking actin dynamics and gene transcription to drive cellular motile functions, Nat. Rev. Mol. Cell Biol., 11 353-365.
[57] M. Chen, M. Sinha, B.A. Luxon, A.R. Bresnick, K.L. O'Connor, Integrin alpha6beta4 controls the expression of genes associated with cell motility, invasion, and metastasis, including S100A4/metastasin, J. Biol. Chem. 284 (2009) 1484–1494.
[58] M.E. Hemler, Tetraspanin proteins promote multiple cancer stages, Nat. Rev. Cancer 14 (2014) 49–60.
[59] Y.C. Tsai, A. Mendoza, J.M. Mariano, M. Zhou, Z. Kostova, B. Chen, T. Veenstra, S.M. Hewitt, L.J. Helman, C. Khanna, A.M. Weissman, The ubiquitin ligase gp78 promotes sarcoma metastasis by targeting KAI1 for degradation, Nat. Med. 13 (2007) 1504–1509.
[60] X.A. Zhang, W.S. Lane, S. Charrin, E. Rubinstein, L. Liu, EWI2/PGRL associates with the metastasis suppressor KAI1/CD82 and inhibits the migration of prostate cancer cells, Cancer Res. 63 (2003) 2665–2674.